Fall 2022

Thermodynamic Assessment of Chromium Corrosion In The Na-K-Mg-U(III, IV) Chloride Salt

Jacob Allen Yingling

THERMODYNAMIC ASSESSMENT OF CHROMIUM CORROSION IN THE NA-K-MG-U(III,IV) CHLORIDE SALT

by

Jacob Allen Yingling

Bachelor of Science
Brigham Young University, 2014

Master of Science
University of South Carolina, 2019

Submitted in Partial Fulfillment of the Requirements

For the Degree of Doctor of Philosophy in

Nuclear Engineering

College of Engineering and Computing

University of South Carolina

2022

Accepted by:

Theodore M. Besmann, Major Professor

Travis W. Knight, Committee Member

Ming Hu, Committee Member

Jake W. McMurray, Committee Member

Cheryl L.Addy, Interim Vice Provost and Dean of the Graduate School

DEDICATION

To my wife Rebecca, for her unrelenting constancy, optimism and creative power. To my children, for teaching me the joy of simple things; may you find bliss in finding your purpose, and peace through right-living. To my parents, grandparents, aunts, uncles, and siblings, you have defined me in incalculable ways. Thank you.

ACKNOWLEDGEMENTS

It has been said, “A city that is set on a hill cannot be hid”, an aphorism I find emblematic of the mountain of support that I have received in the completion of this work. Truly, there have been uncountable encouragements from friends, family, and mentors that constitute the bedrock upon which this small but personally meaningful achievement was able to find sure footing.

I am thankful to my advisor, Dr. Besmann, who is undoubtedly the most well-acquainted person I know. He has a gift for remembering people, and the wisdom to treat them all with respect. I am indebted to his foresight, seeing in me a certain aptitude. His encouragement to pursue a PhD has enabled me access to a field of work that I dearly love.

I feel it necessary to acknowledge Dr. Juliano Schorne-Pinto in his native tongue, pois, seria uma faulta grave se eu não agradesse a meu amigo e mentor. Ele tem o dom de buscar e encontrar rigorosamente as informações mais raras, às quais foram uma grande parte do meu desenvolvimento como scientifico. Considero o envolvimento dele insuperável na minha formação. Certamente, muitos dos característicos de pesquisa mais valerosos eu obtive sob sua influência. Sou profundamente grato ter o conhecido.

Finally, I would be remiss not to mention the role my wife Rebecca has played in this whole matter. Her determination to experience joy in life and to create systems of understanding others, have enabled our family to experience a mutual upward climb amidst great internal and external challenges. You may wonder, dear reader, how it may have been

possible for this work to come forth without financial burden, whilst raising a family of four children. The answer is Rebecca; always and forever, Rebecca.

ABSTRACT

Thermodynamic descriptions of high-order molten chloride salt systems are essential for the development of fast molten salt reactor (MSR) technologies. However, a complete thermodynamic assessment of the essential Na-K-Mg-U(III)-U(IV) molten chloride salt with the most prevalent $CrCl_2$ corrosion product has yet to be provided. This is remedied in the present work through application of the CALculation of PHAse Diagrams (CALPHAD) approach to the available thermodynamic data and new measurements that include differential scanning calorimetry (DSC) observations for previously unexplored two and three component chloride salt systems. Through these efforts, a unique approach was developed for the quantification of uncertainty in phase equilibria obtained from DSC measurements, which provided a distinct advantage in determination of the experimental phase diagrams, and resulted in the apparent discovery of a previously unreported intermediate compound in the NaCl-UCl_3 system.

Throughout the thermodynamic assessments, the heat of mixing ($\Delta_{mix}H$) for some of the needed systems were found to be unavailable. Thus, an improvement upon the Davis' $\Delta_{mix}H$ estimation method was developed to allow $\Delta_{mix}H$ determination at the composition of maximum short-range ordering (SRO) for pseudo-binary systems. The improved approach removes the currently required necessity of arbitrarily selecting the system composition of maximum SRO and successfully reproduces the behavior of the NaCl-UCl_3 and KCl-UCl_3 systems, providing $\Delta_{mix}H$ values that agree well with reported measurements within the propagated uncertainties. In addition to determining the $\Delta_{mix}H$

of the NaCl-$CrCl_2$, and KCl-$CrCl_2$ systems, the methodology was applied to the entirety of the ACl-$PuCl_3$ systems (A = alkali metal) and more than 27 unexplored ACl-$LnCl_3$ systems (Ln = lanthanide), thus opening the door to accurate thermodynamic modeling of many molten chloride salt systems.

Since the formation of corrosion species in molten salt reactor systems is driven by the salt redox condition, indicated primarily by the uranium oxidation ratio (U^{4+}/U^{3+}), assessment of the salt systems including UCl_3-UCl_4 was paramount. To date, no available thermodynamic database models the effect of trivalent and tetravalent uranium chloride on the $CrCl_2$ corrosion potential. Therefore, the chloride salt systems in the Molten Salt Thermal Properties Database – Thermochemical (*MSTDB-TC*) were extended with Gibbs energy models suitable for application to chromium corrosion in fueled chloride molten salt reactor (MSR) coolants. As many thermodynamic data for the alkali systems with UCl_3-UCl_4 are lacking, the work demonstrates a methodology for the development of fully-constrained thermodynamic models in the modified quasi-chemical model quadruplet approximation (MQMQA) that are capable of accurate estimations of thermodynamic properties, even in systems for which very few thermodynamic data are available.

.

TABLE OF CONTENTS

LIST OF TABLES

LIST OF FIGURES

CHAPTER 1: INTRODUCTION

Presently, the nuclear power industry is hindered by the development of an unfavorable late 20th century political environment [1,2], political expediency toward renewables [3], the low cost of combined cycle natural gas power plants [4], and the high (and rising) costs [5] of water cooled nuclear reactor technologies. This latter point is perhaps the most salient reason why the current fleet of operational reactors has, on average, aged to within just a few years of their 40-year operating licenses, with many utilities seeking to extend operations through second license renewals.

Molten Salt Reactors (MSR) are a class of Generation IV nuclear reactor technology designed to address these concerns through a desirable combination of cost [4,6] and safety [7,8] improvements, accomplished through adoption of low pressure containment systems [7], and in the case of chloride fast reactors, extremely high specific burnup through breed-and-burn of heavy metals [9] to reduce fuel cost and long-term spent fuel storage needs. A key advantage of this latter benefit is the ability to reduce waste generated from previous generations of reactors, and meet weapons grade plutonium stockpile reduction commitments [10].

In recognition of these potential advances, the Advanced Reactor Technology (ART) program within the Department of Energy (DOE) has backed MSR development through a revival of research into the technologies that were en vogue during the 60's and 70's. MSR designs are based around a fluoride or chloride salt coolant which also contains the necessary dissolved uranium fuel to sustain the nuclear chain reaction. Due to the

relative mass difference between fluoride and chloride salts, the latter are generally suitable for fast neutron spectrum designs, whereas the former are suited to thermal spectrum operation like much of today's worldwide fleet of civilian power generating nuclear reactors.

To be successful, MSR designs will depend on the availability of reliable thermochemical and thermophysical models to aid design refinement and licensing proposals. Currently, such thermodynamic models are generally unavailable in a publicly available format. In response, the University of South Carolina (UofSC) is developing the Molten Salt Thermal Properties Database – Thermochemical (*MSTDB-TC*) to provide a single location for essential thermodynamic models covering the extent of possible molten salts desired by the MSR community.

Presently, *MSTDB-TC* lacks fluoride and chloride corrosion product descriptions which are of major interest to MSR designers to anticipate the conditions where the corrosion of salt facing materials is thermodynamically restricted. Ultimately, such descriptions will be necessary for licensing of MSRs; but currently, metal compatibility with molten salts is of wide interest, including for nuclear fuel reprocessing [11], concentrating solar power [12], and generally for thermal storage [13]. Modern engineering codes for corrosion in molten salt systems, e.g. the MOOSE based finite-element code YELLOWJACKET, are under development and will require suitable thermodynamic Gibb's energy models of corrosion species in typical molten salts [14].

Although many thermodynamic models for molten fluoride and chloride salts exist in the literature, these are primarily for base salts like LiF, BeF_2, KCl, and NaCl. Few models exist describing the corrosion fluorides and chlorides in combination with uranium

[15,16], and none have described the essential thermodynamics with chromium, with which corrosion in fluoride and chloride salts is most prevalent [17,18]. Since thermodynamic Gibb's energy models are essential to the success of codes like YELLOWJACKET, there is substantial need for a comprehensive database of molten salt corrosion fluorides and chlorides.

The UofSC was awarded funding through the Nuclear Energy University Program (NEUP) to expand the *MSTDB-TC* with thermodynamic descriptions of corrosion fluorides and chlorides typical for structural materials like 316H stainless steel and Hastelloy-N for which Cr, Fe, and Ni are abundant. As part of this NEUP, the *MSTDB-TC* was expanded with a complete thermodynamic description for common chloride salts, including Gibb's energy descriptions of the Na-K-Mg base salt chlorides in conjunction with $CrCl_2$. Additionally, the base salt and $CrCl_2$ were described in the presence of UCl_3, and additional descriptions of the base salt with UCl_4 to allow correct thermodynamic descriptions as a function of the salt redox state, which is expected to require control during MSR operation [19].

To adequately derive these thermodynamic descriptions, suitable Gibb's energy models were developed for each possible pseudo-binary and pseudo-ternary in the Na-K-Mg base salt system, with UCl_3 as having intermediate concentrations, and $CrCl_2$ and UCl_4 each described as minor components. The accomplishment of this goal required a search for any available thermodynamic data including component vapor pressures, electrochemical measurements, phase equilibria, solution calorimetry, and others. New experimental measurements of phase equilibria between the base salts and corrosion species as well as the uranium bearing species were needed to resolve discrepancies in

existing data or to elucidate the thermodynamic system for the first time. Furthermore, strategies for estimating unavailable thermodynamic properties were developed to allow the assessments to be well-informed in terms of enthalpy and specific heat contributions to the Gibbs energy models.

The outlay of the work is as follows: In Chapter 2, a brief overview of the CALPHAD method is provided along with descriptions of the modified quasichemical model. Additionally, the scope of work is described for the pseudo-binary and pseudo-ternary molten chloride salt systems in need of thermodynamic assessment. Chapter 3 contains a publication in which elemental period correlations are developed to allow the unique determination of enthalpy of mixing ($\Delta_{mix}H$), that were necessary for the creation of well specified Gibbs energy models used in the thermodynamic assessments of this work. Chapter 4 is a publication in which a complete thermodynamic description of the Li-Na-K-U(III) chloride molten salt is developed, laying the groundwork for the Na-K-Mg-U(III)-U(IV)-Cr assessment of Chapter 5

CHAPTER 2: BACKGROUND

Salt selection

The Na-K-Mg chloride salt was selected as the base salt system as it is intended to be applied to fast spectrum reactors as conceived by developers like TerraPower and Elysium Industries, who intend to implement chloride salt compositions involving Na, K, and Mg. Some desirable attributes of the chloride salts include lower salt operating temperatures, and much higher solubility of transuranic (TRU) compounds relative to fluoride salts [20]. Chloride salts are also not aggressively corrosive with stainless steels and nickel alloys when adequately purified from oxidant impurities [17,20]. The fast neutron spectrum allows for operation with high buildup of fission products and facilitates the use of waste actinides as fuel [20]. Some disadvantages include more complex chemistry and the production of Cl^{36}, a long-lived isotope that is highly soluble in water [20].

Thermodynamic perspective on corrosion

Corrosion of metals in the presence of chloride salts is only possible when the Gibb's energy of the corrosion reaction is negative relative to the reaction species [17]. Corrosion at the surface of a metal occurs within micro electrochemical cells and depends on the microcell Gibbs energy for the redox reaction. The oxidation and reduction half-cell reactions for chlorine gas oxidant are shown in Equations (2.1) and (2.2), respectively, together forming the overall reaction of Equation (2.3).

$$\mathrm{M(s) + nCl^- \rightarrow MCl_n(s) + ne^-} \tag{2.1}$$

$$0.5nCl_2(g) + ne^- \rightarrow nCl^- \quad (2.2)$$

$$M(s) + 0.5nCl_2(g) \rightarrow MCl_n(s) \quad (2.3)$$

When the standard reduction potentials of Equations (2.1) and (2.2) are known, metal corrosion is thermodynamically possible when $\Delta G < 0$, however, the reduction potentials under the temperature and composition conditions of a MSR are unknown for many chloride salts. The purpose of thermodynamic modeling for corrosion prediction is to determine the species activities of the corrosion product reaction to demonstrate whether formation of corrosion species is thermodynamically favored, as shown in Equation (2.4); a_i is the species activity, $\Delta_r G^o$ is the standard Gibb's energy of reaction, ΔG_c is the cathodic half-reaction in non-standard conditions, and ΔG_a is for the anodic half-reaction.

$$\Delta_r G = \Delta G_c + \Delta G_a = \Delta_r G^o + RT\ln\left(\frac{a_{MCl_n}}{a_M a_{Cl_2}^{0.5n}}\right) \quad (2.4)$$

The spontaneity of metal chloride formation may be predicted since $a_M = 1$ and, at equilibrium, a_{Cl_2}, and a_{MCl_n} may be determined using standard Gibb's energy minimization codes. If a reliable thermodynamic database describing the salt melt is available, this procedure may be used to predict the formation of corrosion products in complex salts and determine the solubility of halide alloy constituents. Of course, these types of calculations may be extended to include additional or alternate oxidizing species, but as the main scope of this work is to define the database necessary for preliminary corrosion evaluation of typical fast reactor molten salts, the corrosion of metals in the presence of hydride and/or oxide impurities is left to future investigators. Olander [21] provides additional examples of how corrosion may be predicted, and even controlled, when related species activities are known.

Corrosion species

Due to the high stability of chromium halides, a primary concern for corrosion of molten chloride salt facing metal alloys is the depletion of chromium [22]. This phenomenon is evident in the SEM-EDS mapping in Figure 2.1 of an Alloy 230 sample, 70Ni-23mol%Cr, explosed to KCl-$MgCl_2$. Since the resulting corrosion products are readily dissolved in the bulk salt, the formation of a passivating layer to prevent continuous material degradation is inhibited. Although low Cr alloys like Hastelloy-N (Ni-16Mo-7Cr-5mass%Fe) may be used to mitigate this mode of corrosive attack, Cr bearing alloys are less expensive and are needed to improve corrosion performance in materials facing the atmosphere.

Review of available thermodynamic data and models

The base salt systems which are of interest to the proposed work are the pseudo-binary and pseudo-ternary chlorides of NaCl, KCl, and $MgCl_2$. Since the alloys that are of primary interest for structural use in contact with molten salts are primarily nickel alloys involving chromium [23], each of these base chloride salts needs to be modeled in combination with $CrCl_2$. Additional descriptions are needed with UCl_3 and UCl_4 to properly describe the molten salt redox condition. To delineate the scope of work necessary to thermodynamically describe this base salt with corrosion chlorides, the state of each necessary subsystem is qualitatively summarized in Table 2.1 and Table 2.2, which generally outlines the present state of the pseudo-binary systems in the literature. In these tables, green systems are fully assessed and already included in the *MSTDB-TC*, orange systems have all endmember Gibbs energy functions available and sufficient phase equilibria to develop a thermodynamic assessment via the CALPHAD method. Red systems will require experimental measurement of phase equilibria.

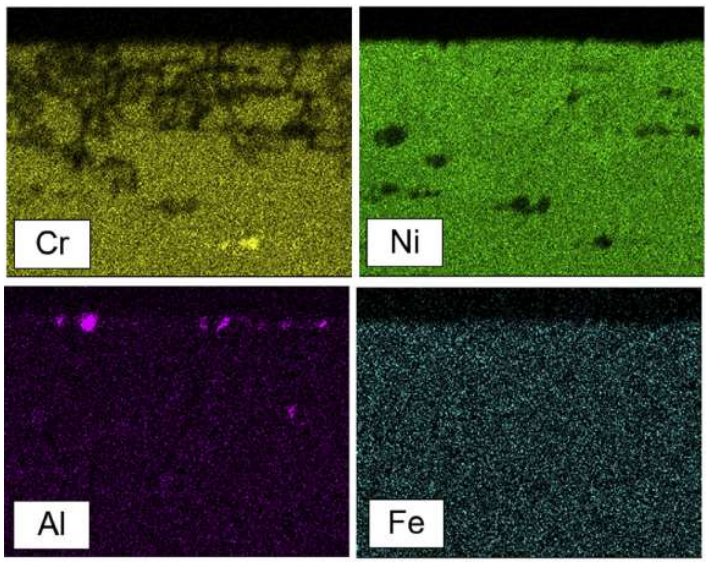

Figure 2.1: Selective Cr depletion of Alloy 230 in KCl-$MgCl_2$ at 750°C for 300 hr. Adapted from [12].

Table 2.1: Availability of phase equilibria for pseudo-binary systems considered in this work.

	KCl	$MgCl_2$	UCl_3	UCl_4	$CrCl_2$
NaCl	[24]	[24]	[25,26]	[26,27]	[28,29]
KCl		[24]	[30,31]	[26,27]	[28,29]
$MgCl_2$			[25,32]	[32,33]	[28]
UCl_3				[28,32]	

Table 2.2: Availability of phase equilibria for pseudo-ternary systems considered in this work.

	$MgCl_2$	UCl_3	UCl_4	$CrCl_2$
NaCl-KCl	[24]	[34]	[35]	[36]
NaCl-$MgCl_2$			[32]	
KCl-$MgCl_2$		[37]		

Role of phase diagrams in thermodynamic model development

The thermodynamic assessment of the systems of Table 2.1 and Table 2.2 will be accomplished through the CALPHAD approach which involves the conceptual connection between phase equilibria and the solid and liquid models describing the Gibb's free energy ($G = H - TS$). Since phase equilibria, such as the liquidus temperature on a phase diagram, occur where the chemical potential of each present species ($\mu_i = \partial G / \partial x_i$) is equal between phases ($\mu_{i,sol} = \mu_{i,liq}$) it is possible to use experimentally determined phase equilibria in the development of thermodynamic models of the Gibb's energy [38]. Consequently, all equilibrium thermodynamic data may be connected to the Gibb's energy, e.g., phase equilibria through differential scanning calorimetry (DSC) or differential thermal analysis (DTA), activity through EMF measurements, and enthalpy of mixing through drop calorimetry, may be used in the development of a well-informed thermodynamic database of models which thoroughly describe a molten salt system. The ensuing models may then be utilized in the calculation of various thermodynamic properties, for example, in the prediction of corrosion product solubility.

When doing this, care must be taken to ensure multiple types of data, e.g. constant temperature enthalpy of mixing ($\Delta_{mix}H$) and liquidus temperature (T_{liq}) throughout the composition range, are used to ensure the resulting Gibb's energy models are not under specified. Guidance in performing assessments using the CALPHAD approach are nicely summarized in Figure 2.2 by Kumar and Wollants [39]. In addition to having the expertise to obtain new thermodynamic data that are unavailable, the CALPHAD practitioner must be broadly informed on many experimental techniques so that they may critically evaluate available experimental and computational information. Certainly, the garbage-in-garbage-

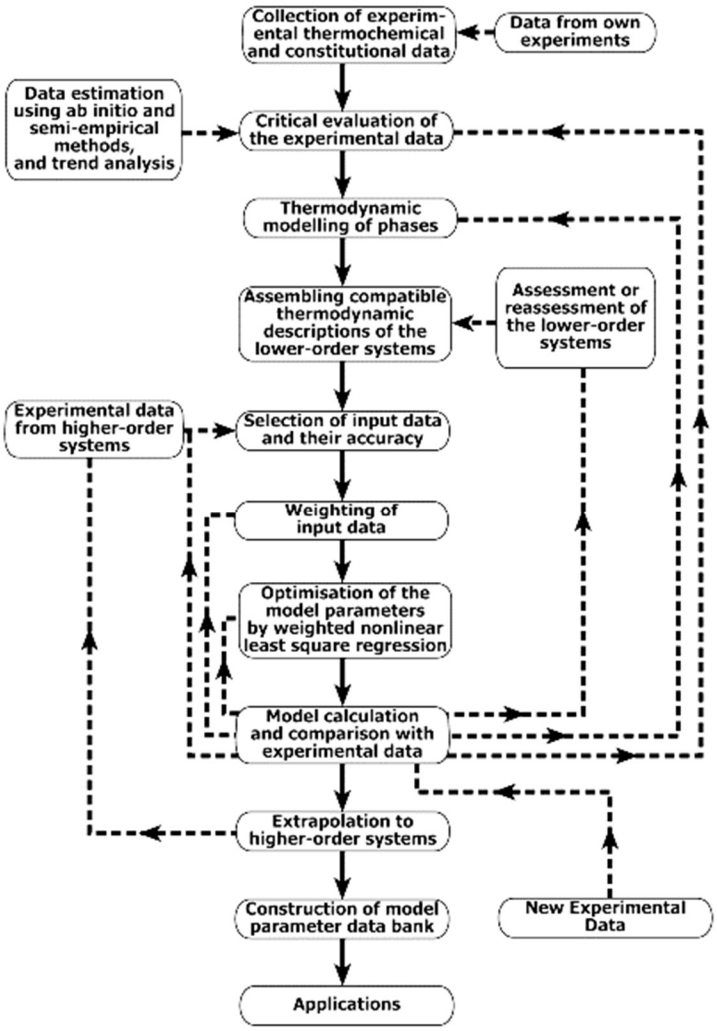

Figure 2.2: Adapted from Kumar and Wollants' CALPHAD guidance flowchart [39].

out (GIGO) adage applies, and careful attention must prevail during the assessment to ensure the reliability of thermodynamic models developed in this manner.

While developing suitable thermodynamic models, practicality must be considered concurrently with the model's ability to represent physical reality. For instance, when considering models suitable to describe molten salts, or any liquid subject to strong first-coordination shell ionic structures (e.g. silicates), the model's ability to capture non-idealities related to coordination structure must be considered. While polynomial models would be convenient to describe the various systems involved in this work, they are empirical only and unable to capture the physical effect of short-range ordering (SRO) as evidenced by the pronounced "V" shaped Gibb's energy of mixing very often found in molten salts (Figure 2.3). Consequently, polynomial and other thermodynamic models that do not account for the SRO evident in molten salts cannot correctly predict thermodynamic properties outside the range of fitted data [40], particularly for application of lower-order system assessments to higher-order calculations.

Thermodynamic models

Liquid solutions

Due to its ability to capture the effect of SRO, the modified quasi-chemical model in quadruplet approximation (MQMQA) is used as the Gibb's energy description of the liquid. The model is described in the papers presented by Pelton et al. [41–43], and as shown in Equations (2.5)-(2.12), it captures the effect of SRO in common anion molten salts by modifying the ideal mixing of the Gibb's energy of each endmember with a pair formation energy, ΔG_{ij}, for each endmember nearest-neighbor pair that has been formed. For instance, as shown in Figure 2.3, a very strongly ordered salt might have $\Delta G_{ij} = -84\ \mathrm{kJ/mol}$.

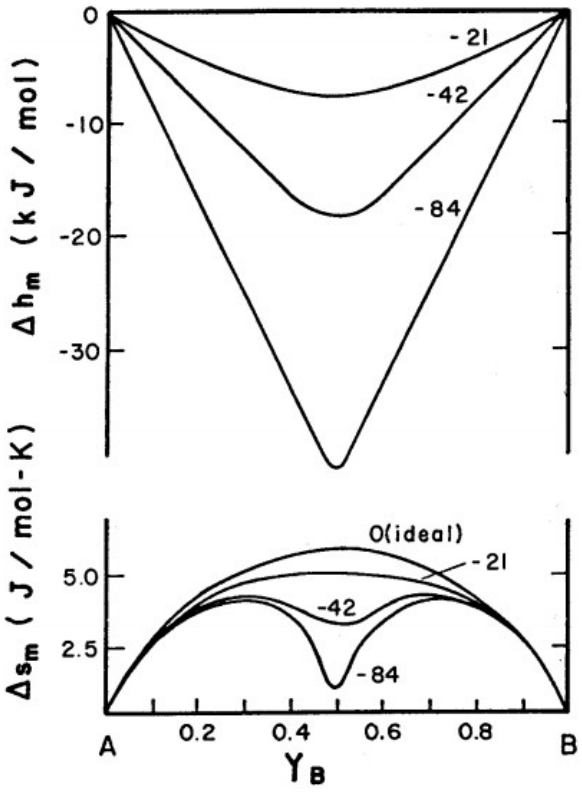

Figure 2.3: Demonstration of pronounced "V" in the Gibb's energy with increasing short-range ordering. Adapted from [41].

$$(i-i)+(j-j)=2(i-j);\Delta G_{ij} \tag{2.5}$$

In the pair approximation of the MQM, which is applicable to common halide salt systems [24], the Gibb's energy of the liquid is given by Equation (2.6). The pure endmember Gibb's energy (G_i^o), enthalpy (H_i^o), and entropy (S_i^o) are provided in Equations (2.7) through (2.9) which must be defined for each endmember liquid in the model. The reader is referred to [42], for a complete description of the model.

$$G=\sum n_i g_i^o - T\Delta S^{config} + \sum_{j>}\sum_{i} n_{ij}\frac{\Delta g_{ij}}{2} \tag{2.6}$$

$$G_i^o = H_i^o - TS_i^o \tag{2.7}$$

$$H_i = H_{i,298K}^o + \int_{298K}^{T} C_{p,i}\ dT \tag{2.8}$$

$$S_i^o = S_{i,298K}^o + \int_{298K}^{T} \frac{C_{p,i}}{T}\ dT \tag{2.9}$$

Solids

Solid phases are treated as a function of their pure component thermodynamic equations. Solid solutions are described using a one lattice polynomial model, which incorporates random mixing described by Equation (2.11) and simple polynomial interaction parameters described by Equation (2.12).

$$G=\sum n_i G_i^o - T\Delta S^{ideal} + G^{ex} \tag{2.10}$$

$$\Delta S^{ideal} = -R\sum X_i \ln(X_i) \tag{2.11}$$

$$G^{ex} = \sum q_{ij}^{mn} X_i^m X_j^n \tag{2.12}$$

Thermodynamic description of endmembers and intermediate compounds

The thermodynamic functions necessary to describe the NaCl, KCl, and $MgCl_2$ endmembers are already available in *MSTDB-TC*. The thermodynamic systems within the scope of this work require additional Gibbs energy functions to describe UCl_3, UCl_4, and

$CrCl_2$ for which reliable sources for these data may be found in Pankratz [44] and the Landolt et al. data series [45].

In the subsequent chapters, the published and submitted manuscripts that describe the specific knowledge gaps and needed experiments for the complete assessment of the Na-K-Mg-U(III)-U(IV)-Cr chloride pseudo-binary and pseudo-ternary systems addressed in this work. In Chapter 3, an enhanced methodology for predicting $\Delta_{mix}H$ is developed, which was essential to the thermodynamic assessments accomplished in successive chapters. Chapter 4 details the model assessments for the Na-K-U(III) systems, and Chapter 5 extends these assessments to include $CrCl_2$, $MgCl_2$ and the UCl_3-UCl_4 systems.

CHAPTER 3: CORRELATIONAL APPROACH TO PREDICTING THE ENTHALPY OF MIXING FOR CHLORIDE MELT SYSTEMS[1]

[1] Reprinted with permission from J. Schorne-Pinto, J.A. Yingling, M.S. Christian, A.M. Mofrad, M.A.A. Aslani, T.M. Besmann, Correlational Approach to Predict the Enthalpy of Mixing for Chloride Melt Systems, ACS Omega. 7 (2022) 362–371. https://doi.org/10.1021/acsomega.1c04755. Copyright 2022 American Chemical Society.

Abstract

A methodology to estimate the heat of mixing ($\Delta_{mix}H$) for salt liquids in unexplored AkCl-AnClx/LnClx (Ak = Alkali, An = Actinide, Ln = Lanthanide) systems has been developed. The improved approach avoids the currently required necessity of arbitrarily selecting the system composition of maximum short-range order, and therefore of most negative $\Delta_{mix}H$, for the estimation. This semiempirical method has computationally reproduced the behavior of NaCl-UCl3 and KCl-UCl3 systems, providing $\Delta_{mix}H$ values that agree well with reported measurements within a propagated 2σ. The capability of the approach is demonstrated in its application to the entirety of the AkCl-UCl3 and AkCl-PuCl3 systems, the results from which have facilitated the accurate thermodynamic modeling of these and other AkCl-AnCl3/LnCl3 systems. The resultant assessed Gibbs energy functions and models have been incorporated in the Molten Salt Thermal Properties Database - Thermochemical (MSTDB-TC).

Introduction

Research in molten salt systems has increased significantly in the last decade due to their application as a solvent for metals, particularly for extraction processes [46,47], recycling and reprocessing of rare-earth elements used in electronics [48–50], permanent magnets in electric motors [51,52] and for nuclear fuels [47,53,54].Salt systems are also being developed as heat transfer media for solar-thermal systems and in molten salt reactors (MSRs), which use salts as a coolant for solid fuel or as a solvent for liquid fuel containing of actinides [55].

New-found interest in MSRs has led a need for molten salt thermodynamic data to aid in modeling of the fuel/coolant, which is a central issue for materials design and system optimization [56,57]. An important thermodynamic value for understanding these systems

is the heat of mixing, or mixing enthalpy ($\Delta_{mix}H$), which represents species interactions and can be used to inform development of thermodynamic descriptions through the CALculation of PHAse Diagram (CALPHAD) approach [58,59]. There is a lack of information on the $\Delta_{mix}H$ for many lanthanide and other important salt systems because of the experimental challenge in measuring these values, and thus, a straight-forward methodology for predicting $\Delta_{mix}H$ would be of great value. In principle, *ab initio* calculations can provide mixing enthalpies, but these are computationally expensive for salt melt systems and resultant values retain significant error. Thus, a more practical approach to predicting $\Delta_{mix}H$ for such salt systems is needed.

This work presents a significantly improved semi-empirical approach to calculating $\Delta_{mix}H$ for an AkCl-$AnCl_3$/$LnCl_3$ salt (Ak = Alkali, An = Actinide, Ln = Lanthanide). It utilizes a unique method for determining the salt composition at maximum short-range order (SRO), which is associated with the most negative mixing enthalpy for the system through correlations of ionic charge and radius among similar (same period) cations. The ultimately goal of this effort is to provide support for the further development of the *Molten Salt Thermal Properties Database-Thermochemical* (*MSTDB-TC*) [60], where the results are key values used in determining overall thermodynamic models for salt systems containing actinides and lanthanides. While the technique finds application with MSR-related salts, the approach is generally applicable to any family of salts and will find utility in many areas where thermodynamic descriptions of molten salts are needed.

Methodology for determining enthalpy of mixing

The enthalpy of mixing is defined as the energy released or absorbed upon mixing of pure components to obtain a single phase in an equilibrium state. From an experimental point-of-view, this intensive (molar) quantity is measured as the change in enthalpy upon

mixing components in the same state, in this case liquid, at constant pressure, temperature, and composition such that

$$\Delta_{\mathrm{mix}}\mathrm{H}\,(\mathrm{T},\mathrm{P},\mathrm{x}) = \mathrm{H}(\mathrm{T},\mathrm{P},\mathrm{x}) - \sum_{\mathrm{i}=1}^{\mathrm{p}} \mathrm{x_i H_i}(\mathrm{T},\mathrm{P}) \tag{3.1}$$

where $\mathrm{H}(\mathrm{T},\mathrm{P},\mathrm{x})$ is the molar enthalpy of the mixture, x_i is the mole fraction of component i in the final mixture, and $\mathrm{H_i}(\mathrm{T},\mathrm{P})$ is the molar enthalpy of pure liquid component i. It should be noted that $\Delta_{\mathrm{mix}}\mathrm{H}$ is generally calculated as the difference between two large quantities so relatively large errors can be introduced if $\mathrm{H_i}$ values are not well known or $\Delta_{\mathrm{mix}}\mathrm{H}$ is small (near ideal mixing), i.e., on the order of a few hundred joules or less.

Influence of alkali ionic radius on $\Delta_{mix}H$

For some alkali salts also containing one or more multi-valent cations, $\Delta_{\mathrm{mix}}\mathrm{H}$ is asymmetric with respect to composition. For example, the most negative $\Delta_{\mathrm{mix}}\mathrm{H}$ for alkali chlorides with $CeCl_3$ is seen at an alkali chloride-rich composition. In isobaric mixtures of constant internal energy this occurs where the structure reaches its most tightly bound structural ordering in the melt ($\mathrm{dH} = \mathrm{dE} + \mathrm{d(PV)}$) and thus represents the maximum SRO, (x symbol in Figure 3.1a), with a minimum $\Delta_{\mathrm{mix}}\mathrm{H}$ at this composition [59]. The minimum value also becomes more negative and the composition where this minimum occurs progresses toward increasingly more alkali-rich compositions with increasing alkali cation radius, where the radii vary as Li < Na < K < Rb < Cs [61]. The systems thus exhibit extensive, increasing SRO in the melt with increasing alkali cation radius similar to alkali-transition metal or -alkaline earth systems [62].

The alkali chloride melts with $CeCl_3$ offer a very good example of the behavior of AkCl-$AnCl_3$/$LnCl_3$ systems. The $\Delta_{\mathrm{mix}}\mathrm{H}$ value is negative, and it becomes more negative with increasing alkali radius (Figure 3.1a), which is a well-understood characteristic

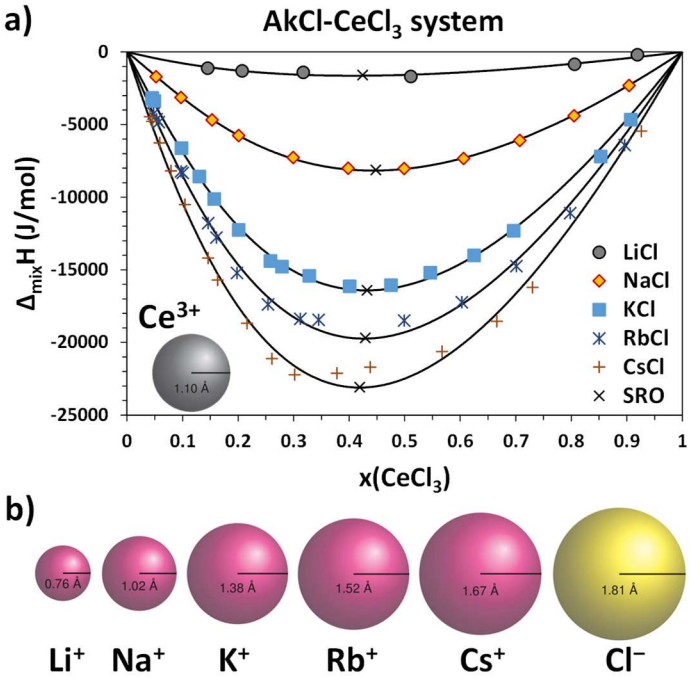

Figure 3.1: a) Δ_mix H for the alkali series with CeCl3 (Ce ionic radius= 1.010 Å) measured by Papatheodorou and Kleppa 16 at 1130 K for LiCl-CeCl3, and at 1118 K for the other systems; b) Ionic radii of the alkali elements and chlorine 18.

of liquids that exhibit extensive SRO with respect to second-nearest-neighbors. Several theories have been developed correlating excess mixing energy with cation radii [62–65], With that of Davis [64,65] appearing to be particularly applicable.Davis [64,65] expanded the conformal solution theory proposed by Reiss, Katz, and Kleppa [66] to, as he termed, "charge-unsymmetrical fused salts," where $\Delta_{\mathrm{mix}}\mathrm{H}$ is described as a function of an interaction parameter λ^{M} that varies linearly with respect to a size parameter Y. In Davis' approach, the underlaying experimental data must be at constant temperature, composition and pressure [67] such that

$$\lambda^{\mathrm{M}} = \frac{\Delta_{\mathrm{mix}}\mathrm{H}}{\mathrm{x}_{\mathrm{AkCl}}\mathrm{x}_{\mathrm{MCl_3}}} = \mathrm{a} + \mathrm{bY} \tag{3.2}$$

Davis [64,65] replaced Y with a size parameter that can account for differing ionic radii, defined as

$$\delta_{12} = \frac{(\mathrm{r}_{\mathrm{Ak}}^{+} + \mathrm{r}_{\mathrm{Cl}}^{-}) - (\mathrm{r}_{\mathrm{M}}^{3+} + \mathrm{r}_{\mathrm{Cl}}^{-})}{(\mathrm{r}_{\mathrm{Ak}}^{+} + \mathrm{r}_{\mathrm{Cl}}^{-}) \cdot (\mathrm{r}_{\mathrm{M}}^{3+} + \mathrm{r}_{\mathrm{Cl}}^{-})} \tag{3.3}$$

where $\mathrm{r}_{\mathrm{Ak}}^{+}$, $\mathrm{r}_{\mathrm{M}}^{3+}$ and $\mathrm{r}_{\mathrm{Cl}}^{-}$ are the ionic radii of the alkali (Figure 3.1b), lanthanide/actinide, and chlorine atom, respectively, which can be found as values in the octahedral geometry in the compendium of Shannon [68]. Measurements on some binary halides carried out by Papatheodorou *et al*. [61,69] and Dienstbach and Blachnik [70] have shown that the λ^{M} description of Davis can be improved by using a quadratic function [63,71] for δ_{12}. In the Flengas and Kucharski [62] theory of $\Delta_{\mathrm{mix}}\mathrm{H}$, the model parameters vary quadratically with δ_{12} within a family of metal dichlorides; suggesting that the physical phenomena responsible for deviations from ideal mixing have a quadratic correlation with δ_{12}.

Reported relations for $\Delta_{\mathrm{mix}}\mathrm{H}$ using Equation (3.2) are understood to represent values normalized to both mixing components and usually fitted to the polynomial, $\lambda^{\mathrm{M}} =$

$a_1 + a_2x + a_3x^2 + a_nx^n$, where x is the mole fraction x_{MCl_3}. This model is adequate for charge symmetric systems that exhibit minima near the equimolar composition. However, the model becomes unsatisfactory with charge asymmetric systems, requiring a higher order polynomial to adequately describe $\Delta_{mix}H$.

Hatem and coworkers [72] developed an improved $\Delta_{mix}H$ relation, referred to as the surrounded ion model (SIM) , Equations (3.4)-(3.5), which takes into account the charge on the ions. In this work, we utilized the SIM of $\Delta_{mix}H$ [73–76], where $p = q = s = 1$ and $r = 3$.

$$\Delta_{mix}H = \big((1-x)pq + xrs\big)x'(1-x')(f_1 + f_2x' + f_3x'^2) \tag{3.4}$$

$$x' = \frac{xrs}{\big((1-x)pq + xrs\big)} \tag{3.5}$$

Temperature dependence of $\Delta_{mix}H$

Papatheodorou and Kleppa [77] used calorimetry to study the influence of temperature on $\Delta_{mix}H$ for the charge-asymmetric systems AkCl-$MnCl_2$ and AkCl-$FeCl_2$ (Ak = Li, Cs) at 1083 K and 963 K with an estimated maximum experimental error of <6%. A later study [78] published data for KCl-YCl_3 at 1143 K and 1053 K as well, although no experimental error was reported; therefore, it is assumed to be 6% based on that for their earlier work. These reported $\Delta_{mix}H$ values for the melts of CsCl-$FeCl_2$ and KCl-YCl_3 are shown in Figure 3.2a,b for two different temperatures with their error limits propagated to obtain the indicated two standard deviations (2σ).

For CsCl-$FeCl_2$ at 1083 K and 963 K for the most negative $\Delta_{mix}H$ values are -23610 ± 425 and -23700 ± 467 J/mol, respectively, for the composition x_{FeCl_2} = 0.43 mol%. Similarly, the KCl-YCl_3 system has a minimum at x_{YCl_3} = 0.35 mol% with values of $\Delta_{mix}H$ of -22770 ± 283 J/mol at 1143 K and -22180 ± 580 J/mol at 1053 K. We note that each set

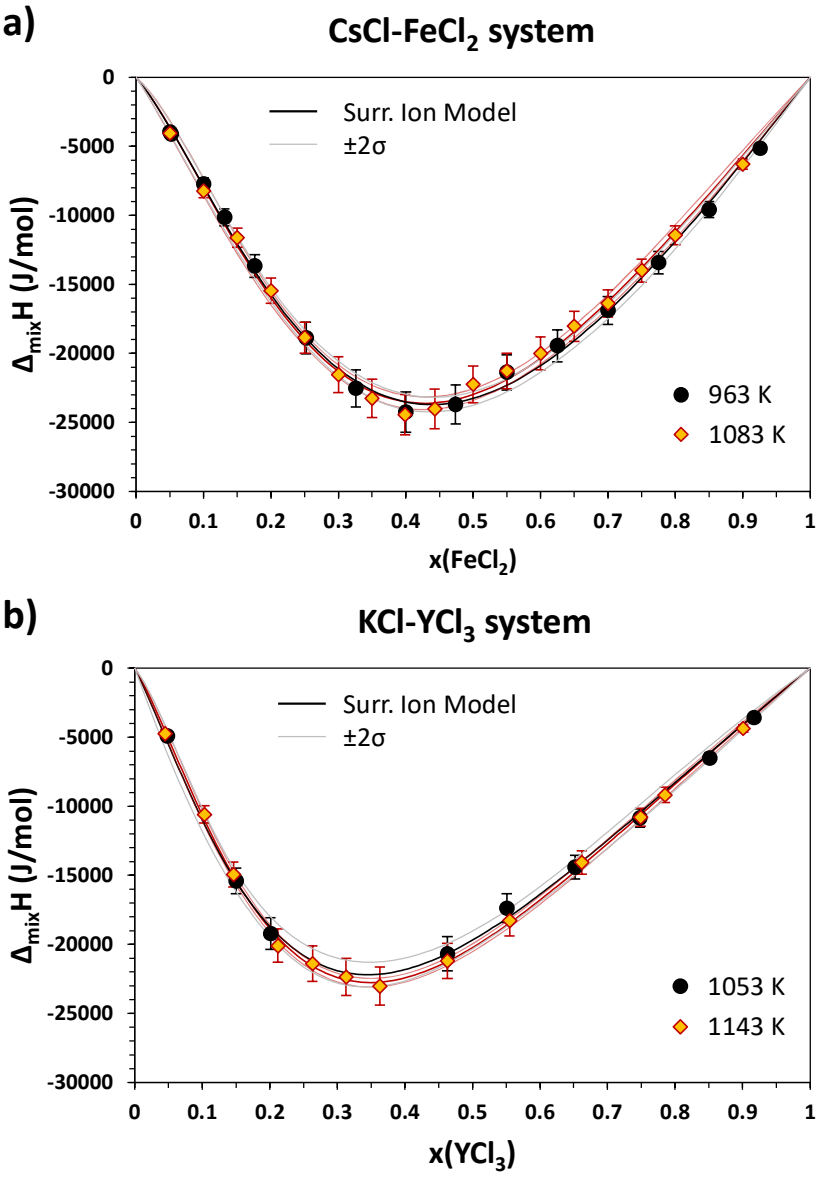

Figure 3.2: a) Values of $\Delta_{mix}H$ for the CsCl-$FeCl_2$ system measured by Papatheodorou and Kleppa [77] at 963 and 1083 K, fitted using the SIM with 2σ intervals; b) values of $\Delta_{mix}H$ KCl-YCl_3 measured by Papatheodorou *et al*. [78] at 1053 and 1143 K.

fall within both 2σ intervals as there is only a maximum difference of 2.6% between the $\Delta_{mix}H$ values, and thus the temperature dependence of $\Delta_{mix}H$ can be disregarded for ΔT £120 K. The result is not surprising as enthalpy is understood to change slowly with temperature as it is defined as the integral of the heat capacity, which for liquids are reported with small or no temperature dependence [79].

Alkali-lanthanide/actinide chloride systems for analysis

The experimental $\Delta_{mix}H$ data for alkali chloride mixtures with lanthanide (and yttrium) trichlorides are abundant in the literature, thanks to extensive work published in the 1960s-1970s by the Kleppa and coworkers [61,63,67,77,80–82], and also in the last few decades by Gaune-Escard's group [71,83–90]. However, work on mixtures of alkali chlorides and actinide trichlorides appears to be nonexistent with the exception of that for the NaCl–UCl_3 and KCl-UCl_3 systems [83,90]. The $\Delta_{mix}H$ of the 48 sets of data available for these systems were extracted for our analysis and listed in Table 3.1.

Other alkali chloride mixtures with trichlorides are available in the literature (e.g., the KCl-$AlCl_3$ [91] system studied at 543 K, the KCl-$FeCl_3$ [92] system studied at 970-1000 K, and the KCl-$BiCl_3$ [89] system studied at 690 K), however, do not contain lanthanides or actinides and are also considered at relatively low temperature compared with the measurements for the systems of this study.

Regression Methodology

In the current work, the relations for $\Delta_{mix}H$ were computed using a Python version 3.8-developed code for regression analysis with calculations carried out using NumPy version 1.19.5 [93]. The Levenberg-Marquardt algorithm (LMA) [94] in SciPy version 1.4.1 [95] was used in a chi-squared minimization to fit the coefficients of the SIM using $\Delta_{mix}H$ values,

Table 3.1: Pseudo-binary systems considered in the current analysis.

System	Ln. & An	Exp. Temp. K	Radius (non-Ak)* Å	x (non-Ak) range Mole fraction	Data points N°	Error %	Reference
LiCl	$LaCl_3$	1173	1.032	[0.196-0.787]	7	5.0	Papatheodorou and Ostvold [69]
	$CeCl_3$	1130	1.010	[0.15-0.92]	6	5.0	Papatheodorou and Kleppa [61]
	$PrCl_3$	1044	0.990	[0.014-0.942]	20	6.0	Rycerz *et al.* [71]
	$NdCl_3$	1044	0.983	[0.031-0.958]	13	6.0	Rycerz *et al.* [71]
	$GdCl_3$	1263	0.938	[0.15-0.68]	6	5.0	Dienstbach and Blachnik [70]
	$TbCl_3$	1109	0.923	[0.0286-0.9017]	15	6.0	Rycerz and Gaune-Escard [84]
	YCl_3	1143	0.900	[0.096-0.907]	6	-	Papatheodorou *et al.* [78]
	$TmCl_3$	1130	0.880	[0.098-0.912]	9	6-8	Chojnacka *et al.* [85]
NaCl	$LaCl_3$	1173	1.032	[0.046-0.852]	10	5.0	Papatheodorou and Ostvold [69]
	$LaCl_3$	1153	1.032	[0.09-0.72]	11	5.0	Dienstbach and Blachnik [70]
	UCl_3	1113	1.025	[0.0048-0.949]	23	6.0	Matsuura *et al.* [83]
	$CeCl_3$	1153	1.010	[0.04-0.81]	9	5.0	Dienstbach and Blachnik [70]
	$CeCl_3$	1118	1.010	[0.05-0.90]	11	5.0	Papatheodorou and Kleppa [61]
	$PrCl_3$	1122	0.990	[0.104-0.953]	14	6.0	Gaune-Escard *et al.* [86]
	$NdCl_3$	1124	0.983	[0.0511-0.9500]	16	6.0	Gaune-Escard *et al.* [87]
	$SmCl_3$	1153	0.958	[0.04-0.80]	9	5.0	Dienstbach and Blachnik [70]
	$GdCl_3$	1263	0.938	[0.08-0.82]	9	5.0	Dienstbach and Blachnik [70]
	$TbCl_3$	1109	0.923	[0.0472-0.9007]	19	6.0	Rycerz and Gaune-Escard [84]
	$DyCl_3$	1153	0.912	[0.03-0.79]	9	5.0	Dienstbach and Blachnik [70]
	$DyCl_3$	1100	0.912	[0.05-0.95]	20	6.0	Gaune-Escard *et al.* [88]
	YCl_3	1143	0.900	[0.047-0.890]	10	-	Papatheodorou *et al.* [78]
	$ErCl_3$	1153	0.890	[0.03-0.79]	9	5.0	Dienstbach and Blachnik [70]
	$TmCl_3$	1130	0.880	[0.020-0.891]	21	6-8	Chojnacka *et al.* [85]
	$YbCl_3$	1153	0.868	[0.10-0.79]	11	5.0	Dienstbach and Blachnik [70]
KCl	$LaCl_3$	1173	1.032	[0.043-0.899]	14	5.0	Papatheodorou and Ostvold [69]
	UCl_3	1113	1.025	[0.0502-0.9048]	12	6-8	Rycerz *et al.* [90]
	$CeCl_3$	1118	1.010	[0.05-0.90]	17	5.0	Papatheodorou and Kleppa [61]
	$PrCl_3$	1122	0.990	[0.0101-0.9470]	20	6.0	Gaune-Escard *et al.* [86]

	$NdCl_3$	1065	0.983	[0.0899-0.9430]	28	6.0	Gaune-Escard *et al.* [87]
	$GdCl_3$	1263	0.938	[0.10-0.79]	8	5.0	Dienstbach and Blachnik [70]
	$TbCl_3$	1109	0.923	[0.0240-0.9532]	28	6.0	Rycerz and Gaune-Escard [84]
	$DyCl_3$	1070	0.912	[0.025-0.946]	23	6.0	Gaune-Escard *et al.* [88]
	YCl_3	1143	0.900	[0.045-0.901]	13	-	Papatheodorou *et al.* [78]
	YCl_3	1053	0.900	[0.048-0.917]	9	-	Papatheodorou *et al.* [78]
	$TmCl_3$	1130	0.880	[0.047-0.928]	20	6-8	Chojnacka *et al.* [85]
RbCl	$LaCl_3$	1173	1.032	[0.046-0.903]	12	5.0	Papatheodorou and Ostvold [69]
	$CeCl_3$	1118	1.010	[0.06-0.90]	16	5.0	Papatheodorou and Kleppa [61]
	$NdCl_3$	1122	0.983	[0.025-0.950]	28	6.0	Gaune-Escard *et al.* [87]
	$GdCl_3$	1263	0.938	[0.10-0.79]	8	5.0	Dienstbach and Blachnik [70]
	$TbCl_3$	1175	0.923	[0.024-0.949]	21	6.0	Rycerz and Gaune-Escard [84]
	YCl_3	1143	0.900	[0.049-0.896]	13	-	Papatheodorou *et al.* [78]
	$TmCl_3$	1130	0.880	[0.050-0.902]	19	6-8	Chojnacka *et al.* [85]
CsCl	$LaCl_3$	1173	1.032	[0.036-0.901]	13	5.0	Papatheodorou and Ostvold [69]
	$CeCl_3$	1118	1.010	[0.045-0.926]	16	5.0	Papatheodorou and Kleppa [61]
	$NdCl_3$	1122	0.983	[0.025-0.941]	29	6.0	Gaune-Escard *et al.* [87]
	$GdCl_3$	1263	0.938	[0.10-0.79]	8	5.0	Dienstbach and Blachnik [70]
	$TbCl_3$	1175	0.923	[0.0239-0.9528]	23	6.0	Rycerz and Gaune-Escard [84]
	YCl_3	1148	0.900	[0.047-0.801]	10	-	Papatheodorou *et al.* [78]

* Ionic radius in the octahedral geometry from Shannon [68]

$$\chi^2 = \sum_i \left(\frac{r_i}{\sigma_i}\right)^2 \tag{3.6}$$

where r_i is the calculated residual and σ_i is the error in the measurement. Experimental errors are usually reported in the form $y = y_o + \delta y$, where y_o is the nominal value and δy is the reported error. In this work, the experimental errors are interpreted as the standard deviation of the measurements. The errors used in Equation (3.6) were taken to be the author reported errors shown in Table 3.1 of the largest reported experimental $\Delta_{mix}H$ for each system. An error of 8% was assumed for systems where no errors were reported by the authors.

Linear error propagation [96] was used to calculate 2σ for the $\Delta_{mix}H$ values determined using Equations (3.4)-(3.5). This method provides an exact description of the variance given that the model is a linear function of the error-prone model parameters, which is naturally the case for the SIM implemented in Equations (3.4)-(3.5). The error propagation relations are Equations (3.7)-(3.8)

$$J = \left[\frac{\partial \Delta_{mix}H}{\partial f_1} \quad \frac{\partial \Delta_{mix}H}{\partial f_2} \quad \frac{\partial \Delta_{mix}H}{\partial f_3}\right] \tag{3.7}$$

$$\sigma^2_{model} = J C_\alpha J^T \tag{3.8}$$

where σ^2_{model} is the variance in $\Delta_{mix}H$, J is the Jacobian for the SIM with respect to the fitting coefficients, J^T is its transpose, and C_α is the variance-covariance matrix of the fitting parameters determined by the regression algorithm.

The optimized coefficients for all 48 systems of Table 3.1 are provided in Table 3.5 through Table 3.9. A set of illustrative experimental and computed values for $\Delta_{mix}H$ are shown in the plots of Figure 3.3 for three pseudo-binary systems**.** Generally, the LiCl-containing systems exhibit greater uncertainty than those for alkali chlorides because of

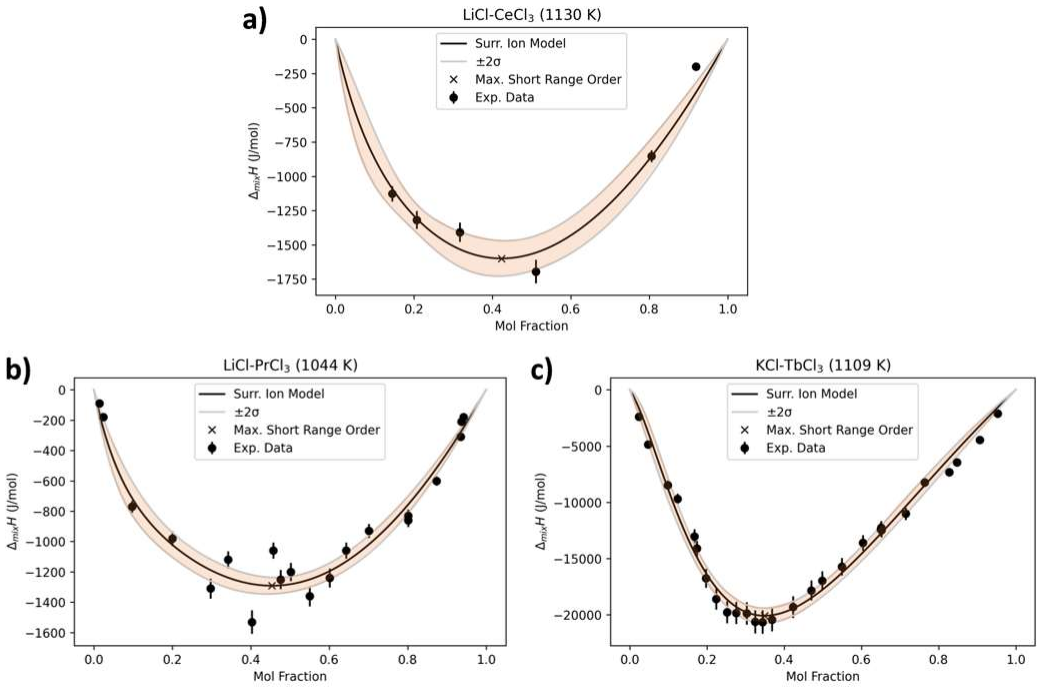

Figure 3.3: Typical pseudo-binary $\Delta_{mix}H$ results from the SIM: a) LiCl-$CeCl_3$ at 1130 K; b) LiCl-$PrCl_3$ at 1044 K and c) KCl-$TbCl_3$ at 1109 K.

the relatively small magnitude of $\Delta_{mix}H$ values for LiCl-containing systems and sparse data. Because of this, they have much larger 2σ relative to a nominal fit of the data. The predicted 2σ bands for the other systems are relatively smaller, as seen in Figure 3.3b,c.

Modeling Alkali-Lanthanide/Actinide Halide Series
Predicting Composition of Maximum SRO:

The method of Davis [64,65] has recently seen increased use [97–101]. Unfortunately, $\Delta_{mix}H$ is often estimated at the equimolar composition, which is incorrect for charge-asymmetric pseudo-binary salt systems as it is not the composition of maximum SRO, as shown in Figure 3.1a for AkCl-$CeCl_3$ systems. In principle, Davis' method could be used for $\Delta_{mix}H$ predictions at every composition. However, for reasons of practicality, a single composition is normally used in estimating $\Delta_{mix}H$. Unfortunately, estimation of $\Delta_{mix}H$ at other than the composition of maximum SRO creates ambiguity (see Figure 3.4). Therefore, an unambiguous application of the Davis' method to charge-asymmetric salt systems requires a means for selecting the composition of maximum SRO [102,103]. We will now address this problem by correlating the composition of maximum SRO with a property of the salt structure, δ_{12}.

The composition at maximum SRO, i.e., where $\Delta_{mix}H$ is most negative, was determined for each system of Table 3.1 by regression of the $\Delta_{mix}H$ functions of Equation (3.4) (Figure 3.5) along with the 2σ values for the linear SRO predictions. Since the experimental composition data errors are much smaller than those for $\Delta_{mix}H$, they are assumed to be error free. Thus, the calculated composition at maximum SRO for each experimental system is assumed to be calculated with no error. The linear behavior seen in Figure 3.5 within a relatively narrow 2σ allows interpolation of the composition at maximum SRO for systems lacking such data. Using the correlations of Figure 3.5, the

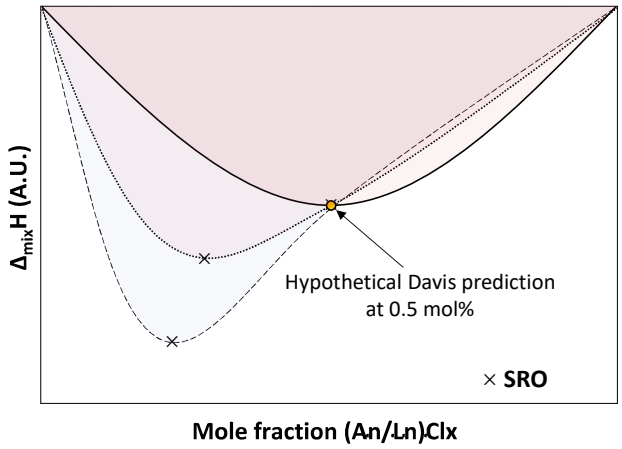

Figure 3.4: Representation of ambiguity in $\Delta_{mix}H$ solutions at the equimolar composition for asymmetric halide salts.

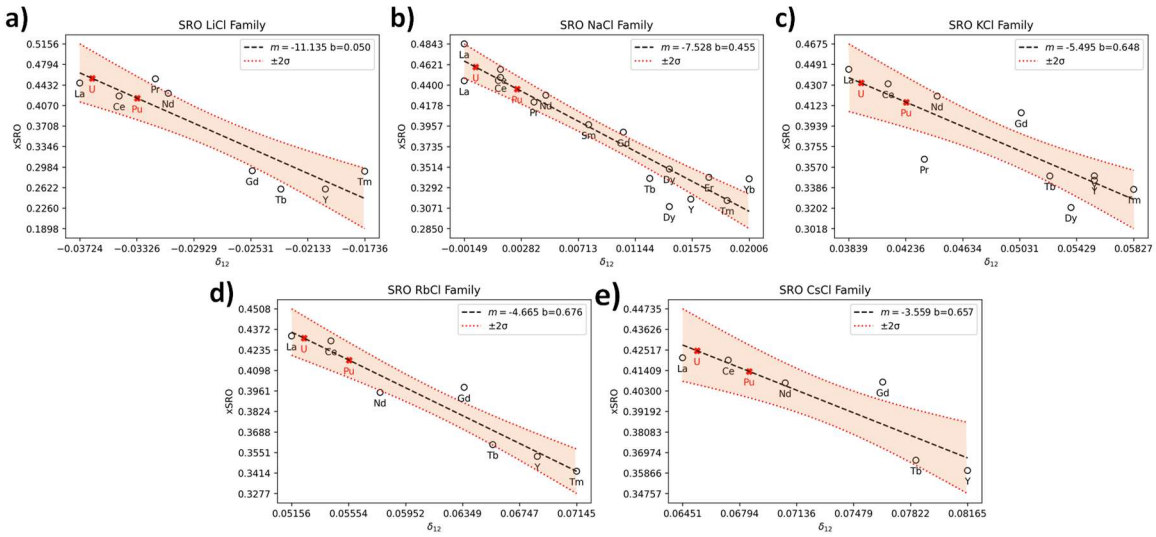

Figure 3.5: Maximum SRO vs. δ_{12} plots with interpolated values for uranium and plutonium alkali chlorides: a) LiCl-MCl_3 series; b) NaCl-MCl_3 series; c) KCl-MCl_3 series; d) RbCl-MCl_3 and e) CsCl-MCl_3 series. The fitted coefficients *b* and *m* were determined from the relation $x_{SRO} = m\delta_{12} + b$.

compositions at maximum SRO were interpolated for the uranium- and plutonium-containing systems and are reported in Table 3.2 along with their respective 2σ values.

Assessment of Methodology via Application to NaCl-UCl_3

There are two alkali–actinide metal chloride systems with available experimental data: The NaCl-UCl_3 system, which was studied by Matsuura *et al.* [83] who measured 23 mixtures at 1113 K; and the KCl-UCl_3 system recently reported by Rycerz *et al.* [90] in which twelve mixtures were studied at 1113 K as well. We used these $\Delta_{mix}H$ values to test our correlational approach, intentionally omitting these data in generating the linear fit of Figure 3.5b. The measurements for NaCl-UCl_3 are seen in Figure 3.6b together with the predicted $\Delta_{mix}H$ values from Figure 3.6a for the composition of maximum SRO of x_{UCl_3}=0.459 mol% interpolated from Figure 3.5b. It is clear that our predictions (x_{UCl_3}=0.459 ± 0.017 mol% and $\Delta_{mix}H$ = 7299 ± 350 J/mol) are in good agreement with Matsuura *et al.* [83] within their reported 6% experimental error (SIM calculated x_{UCl_3} = 0.447 mol% and $\Delta_{mix}H$ = -7290 ± 437 J/mol). Further, our estimation for the KCl-UCl_3 system (x_{UCl_3} = 0.432 ± 0.028 mol% and $\Delta_{mix}H$ = -15851 ± 1003 J/mol) overlap with Rycerz *et al.* [90] $\Delta_{mix}H$ data using their reported 8% uncertainty (SIM calculated x_{UCl_3}= 0.440 mol% and $\Delta_{mix}H$ = -18270 ± 1462 J/mol).

Determining $\Delta_{mix}H$ for UCl_3 or $PuCl_3$ with AkCl

Encouraged by the comparative results for the NaCl-UCl_3 and KCl-UCl_3 systems, our methodology was applied to the remaining alkali-uranium and -plutonium chloride systems. The $\Delta_{mix}H$ calculated for each system at the predicted maximum SRO and with related δ_{12} values were fit to a quadratic polynomial. 2σ intervals for $\Delta_{mix}H$ were produced as previously described by propagating the errors calculated from the $\Delta_{mix}H$ SIM

Table 3.2: Composition at maximum SRO for AkCl-UCl_3 and AkCl-$PuCl_3$ systems with their 2σ values.

Alkali	x_{UCl_3}	2σ Interval	x_{PuCl_3}	2σ Interval
LiCl	0.455	0.503 0.407	0.420	0.458 0.382
NaCl	0.459	0.477 0.442	0.436	0.450 0.422
KCl	0.432	0.461 0.404	0.415	0.440 0.393
RbCl	0.431	0.446 0.417	0.417	0.428 0.405
CsCl	0.425	0.443 0.406	0.414	0.428 0.399

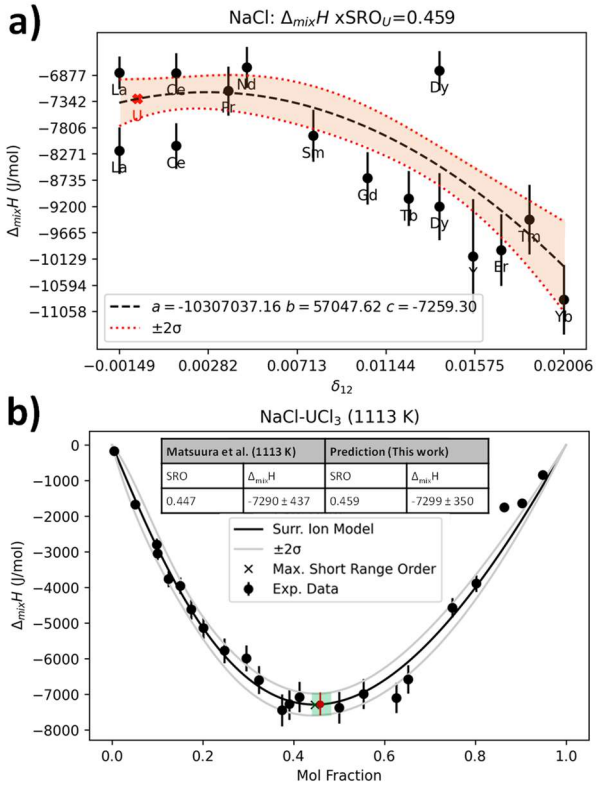

Figure 3.6: a) $\Delta_{mix}H$ at the composition of maximum SRO for NaCl-containing systems; b) Predicted enthalpy of mixing for NaCl-UCl_3 compared with the measured value of Matsuura *et al.* [83] at 1113 K. Red indicates predicted value in both figures.

regression at the composition of maximum SRO (Figure 3.7). Thus, the $\Delta_{mix}H$ predictions incorporate the calculated errors from fitting the experimental $\Delta_{mix}H$ values as well as the relative dispersion around the nominal fit (Figure 3.7 and Table 3.3).

Use of Computed $\Delta_{mix}H$ in CALPHAD Modeling

The methodology for determining $\Delta_{mix}H$ is used in CALPHAD modeling of the NaCl-$PuCl_3$ system to provide an example of its utility. Limited experimental data are available for this system, consisting of only endmember values and phase equilibria (Figure 3.8a) [104]. The excess Gibbs energy for the melt was obtained from our estimation of the $\Delta_{mix}H$ (b) and identification of the composition at maximum SRO. In the development of the set of consistent thermodynamic models of the system, the melt was represented by the modified quasi-chemical model in the quadruplet approximation (MQMQA) [105,106], which takes into account SRO between first- and second-nearest-neighbors on a lattice or sublattice.

For the MQMQA the first-nearest-neighbor (FNN) coordination numbers, z_i, were specified as

$$z^{Na}_{Na_2/Cl_2} = z^{Cl}_{Na_2/Cl_2} = z^{Pu}_{Pu_2/Cl_2} = 6;\ z^{Cl}_{Pu_2/Cl_2} = 2 \tag{3.9}$$

The values of cation-cation second-nearest-neighbor (SNN) coordination numbers, Z_i, that best represent the phase equilibria were found to be

$$Z^{Na}_{NaPu/Cl_2} = 3,\ Z^{Pu}_{NaPu/Cl_2} = 6,\ Z^{Cl}_{NaPu/Cl_2} = 2.4 \tag{3.10}$$

A value of 0.333 was used for the required ratio $Z^{Na}_{NaPu/Cl_2}/(Z^{Na}_{NaPu/Cl_2} + Z^{Pu}_{NaPu/Cl_2})$ to represent the average coordination number of plutonium complex species. This presence of the species $PuCl_6^{3-}$ [107] is seen as the reason why the composition at maximum SRO is skewed toward lower $PuCl_3$ compositions.

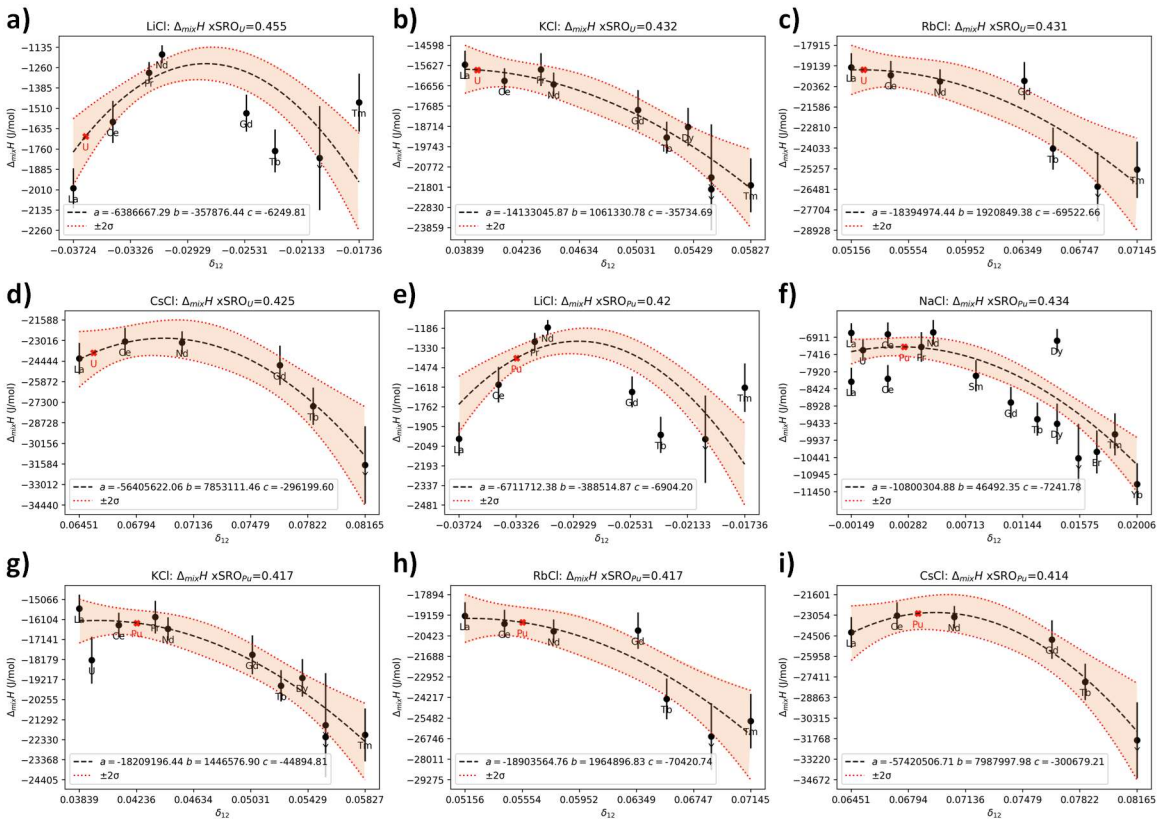

Figure 3.7: Values of $\Delta_{mix}H$ at the composition of maximum SRO for the AkCl-MCl_3 (M = U, Pu), with the exception of NaCl-UCl_3.

Table 3.3: $\Delta_{mix}H$ (J/mol) at the composition of maximum SRO for AkCl-UCl_3 and AkCl-$PuCl_3$ alkali systems with 2σ intervals.

Alkali	$\Delta_{mix}H_{UCl_3}$	2σ Interval	$\Delta_{mix}H_{PuCl_3}$	2σ Interval
LiCl	-1682	-1514 -1850	-1405	-1323 -1488
NaCl	-7299	-6949 -7649	-7193	-6918 -7468
KCl	-15851	-14848 -16854	-16295	-15629 -16961
RbCl	-19379	-18156 -20601	-19606	-18678 -20534
CsCl	-23873	-22330 -25416	-22931	-21792 -24071

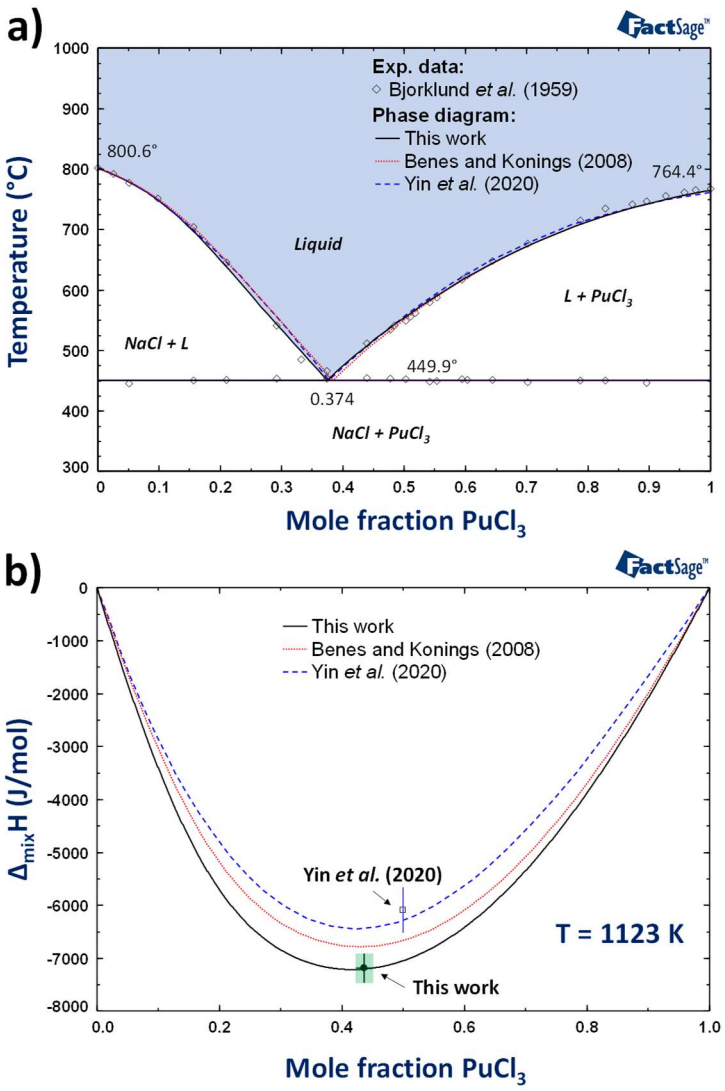

Figure 3.8: a) Computed phase diagram for the NaCl-$PuCl_3$ system using parameters of this work and those of Beneš and Konings [108], and Yin *et al.* [97], together with experimental data [104]. b) $\Delta_{mix}H$ values of this work and those of Beneš and Konings [108], and Yin *et al.* [97].

The excess Gibbs free energy for NaCl-$PuCl_3$ melts was determined by optimizing the known system phase equilibria, the predicted $\Delta_{mix}H$, and the thermodynamic values for the compounds in Table 3.4, and found to be expressed as

$$\Delta g_{NaPu/Cl}\ (J/mol) = -8685.7 - 0.993T - 4079.8\chi_{NaPu} - 6004.6\chi_{PuNa} \quad (3.11)$$

where χ_{NaPu} and χ_{PuNa} represent the cation pair fractions as defined in the MQMQA. The NaCl-$PuCl_3$ is an eutectic system, and it was previously described by Beneš and Konings [108] and Yin *et al.* [97]. Both models have similar calculated phase diagrams, differing by $\Delta_{mix}H$ (Figure 3.8b). Yin *et al.* [97] predicted $\Delta_{mix}H$ for this system, however, they have used an equimolar composition and no lanthanide- or actinide-like systems. Consequently, our predicted $\Delta_{mix}H$ is over 10% more negative than Yin *et al.* [97] value (Figure 3.8b).

Conclusions

In this work we have developed a correlational approach to estimate the composition of maximum SRO at which $\Delta_{mix}H$ is most negative. Additionally, the correlation captures the errors of available experimental data and propagates them to predicted values. As experimental measurements of $\Delta_{mix}H$ are often unavailable or difficult to obtain, the demonstrated relations and developed methodology meet a critical need for efficiently generating thermodynamic properties of molten salts.

Our analysis of 48 charge asymmetric actinide/lanthanide systems indicates that the previously observed quadratic (or nearly linear) relationship of δ_{12} to $\Delta_{mix}H$ applies within families of alkali chlorides with lanthanide and actinide trichloride salts. We have uniquely observed that there appears to be a linear correlation between δ_{12} and the pseudo-binary composition at the most negative $\Delta_{mix}H$ values. This correlation has allowed the development of a novel, simple, and yet accurate method to predict the pseudo-binary

Table 3.4: Thermodynamic properties of compounds used in the NaCl-$PuCl_3$ optimization.

	T range (K)	$H^{\circ}_{298.15}$ (J/mol)	$S^{\circ}_{298.15}$ (J/mol.K)	c_p(J/mol.K)	Ref.
NaCl (s)	298.15 to 1500	-411120	72.132	45.94 + 0.016318(T/K)	[109]
NaCl (l)	298.15 to 1500 1500 to 2000	-394956	76.076	77.7638 - 0.0075312 (T/K) 66.944	[109]
$PuCl_3$ (s)	298.15 to 2000	-959600	161.4	91.412 + 0.03716(T/K) - 27400$(T/K)^{-2}$	[108]
$PuCl_3$ (l)	298.15 to 2000	-931116	170.463	144	[108]

composition at the most negative $\Delta_{mix}H$ for these salts. When coupled to the Davis [64,65] approach, it provides a new means for well-predicting $\Delta_{mix}H$ at the composition of maximum SRO, the value for which no longer needs to be assumed *a priori*.

Along with propagated errors from the underlying experimental data, our method provides valuable information for the development of unambiguous thermodynamic models for halide salts. Hence, we have produced a complete set of heretofore unknown values for the thermodynamic properties of the AkCl-UCl_3 and AkCl-$PuCl_3$ salt systems at potential MSR temperatures. The results reported here are being integrated into the *Molten Salt Thermal Properties Database – Thermochemical (MSTDB-TC)* [60] that serves as a resource for the MSR and related communities. Although we focused on the application of molten salt melts for MSRs, the approach to determine solution $\Delta_{mix}H$ can be used for a wide variety of technologically interesting halide salt systems that require thermodynamic models for their effective implementation. Additional $\Delta_{mix}H$ predictions of unmeasured AkCl-$LnCl_3$ systems are provided in the supplementary material.

Author Contributions

J.S.P‡ and J.A.Y.‡ are responsible for writing and development of ideas for the manuscript with feedback given by all authors. J.S.P.‡ compiled and critically evaluated the available data, J.A.Y.‡ performed the statistical analysis and error propagation. M.S.C., M.A.A.A. and A.M.M. advised J.S.P.‡ and J.A.Y.‡ in various matters including graphical design, document structure, methodology, and statistical analysis. T.M.B directed the research.

Supplementary material

Regression analysis of lanthanides/actines systems

We fitted the extracted experimental points from the systems listed in Table 3.1 (main manuscript) using the surrounded ion model, where the f_1, f_2, and f_3 coefficients from this regression (see Equation (3.5) in the main manuscript).

LiCl-MCl_3 systems

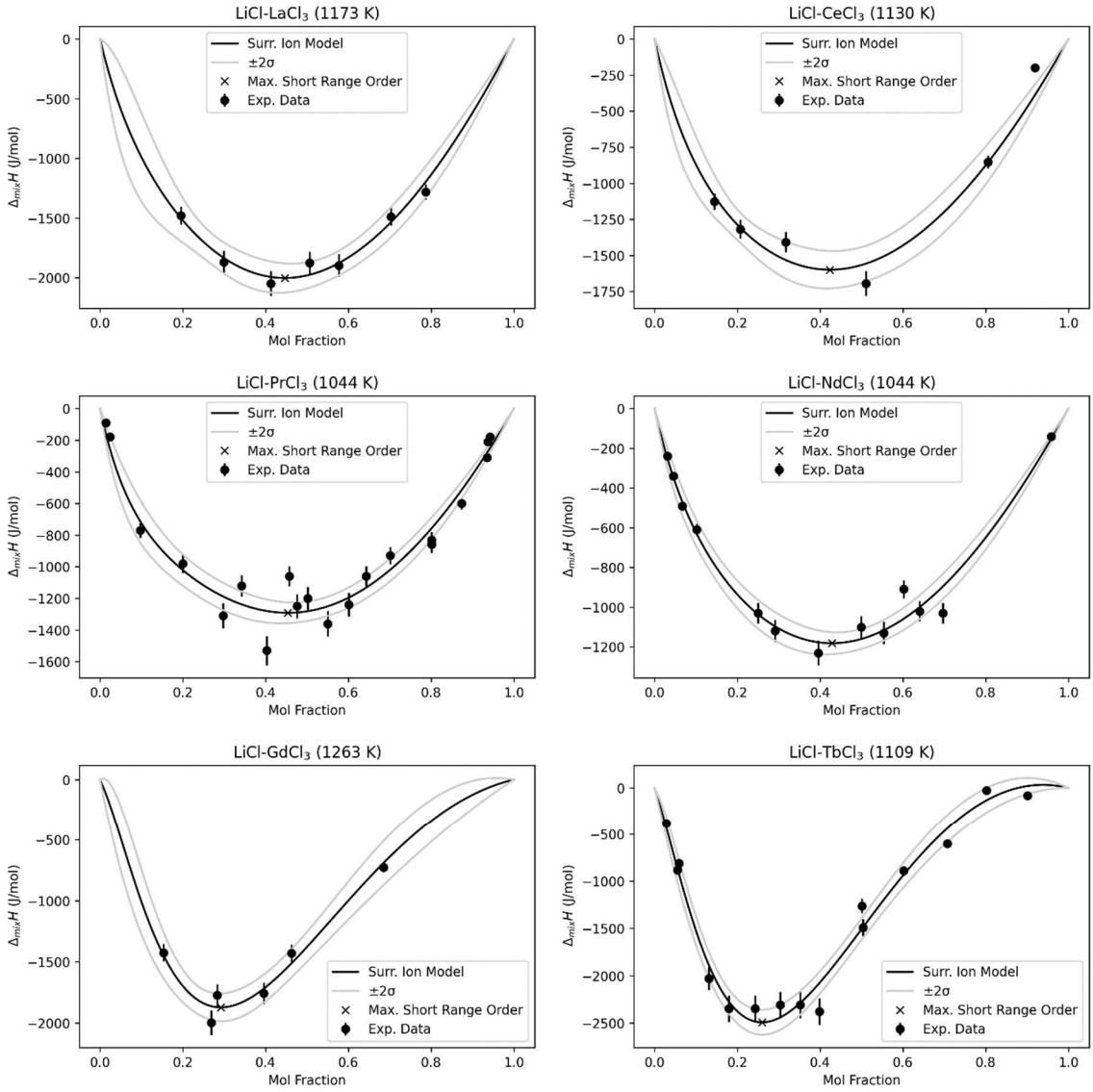

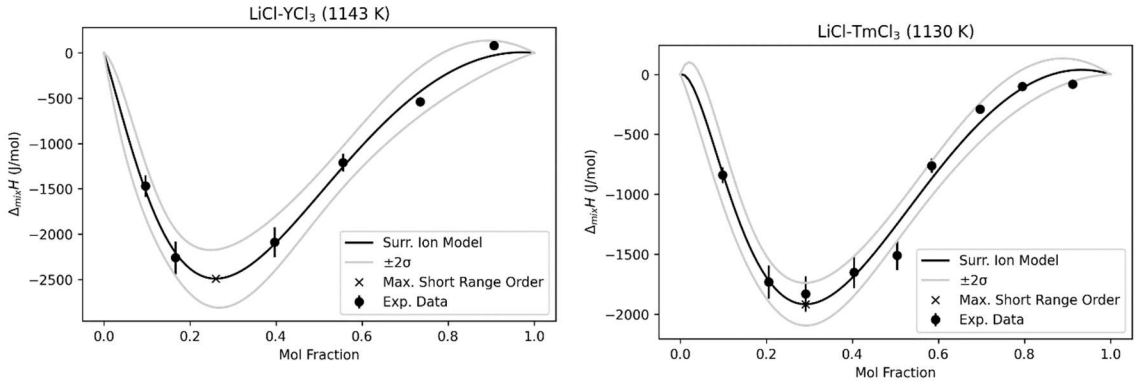

Figure 3.9: Pseudo-binary $\Delta_{mix}H$ values computed using a surrounded ion model-based approach for LiCl-MCl_3 series.

Table 3.5: Fitted coefficients f_1, f_2, and f_3 for LiCl-MCl_3 series.

System	Ln. & An	Exp. Temp. K	f_1	f_2	f_3
LiCl	$LaCl_3$	1173	-2393.1	-11655.1	13257.6
	$CeCl_3$	1130	-3123.2	2085.7	-2727.3
	$PrCl_3$	1044	392.9	-22287.5	23010.0
	$NdCl_3$	1044	-4872.9	3134.9	-4906.1
	$GdCl_3$	1263	-4390.9	-14501.6	19988.9
	$TbCl_3$	1109	-4458.1	3332.8	-3946.4
	YCl_3 [1]	1143	-4143.2	5045.8	-5440.0
	$TmCl_3$	1130	-5123.1	-11631.3	17187.8

NaCl-MCl_3 systems

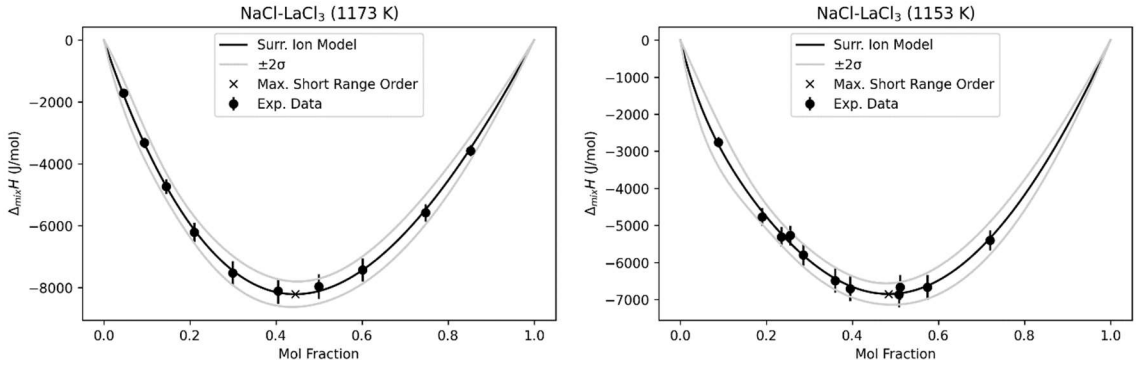

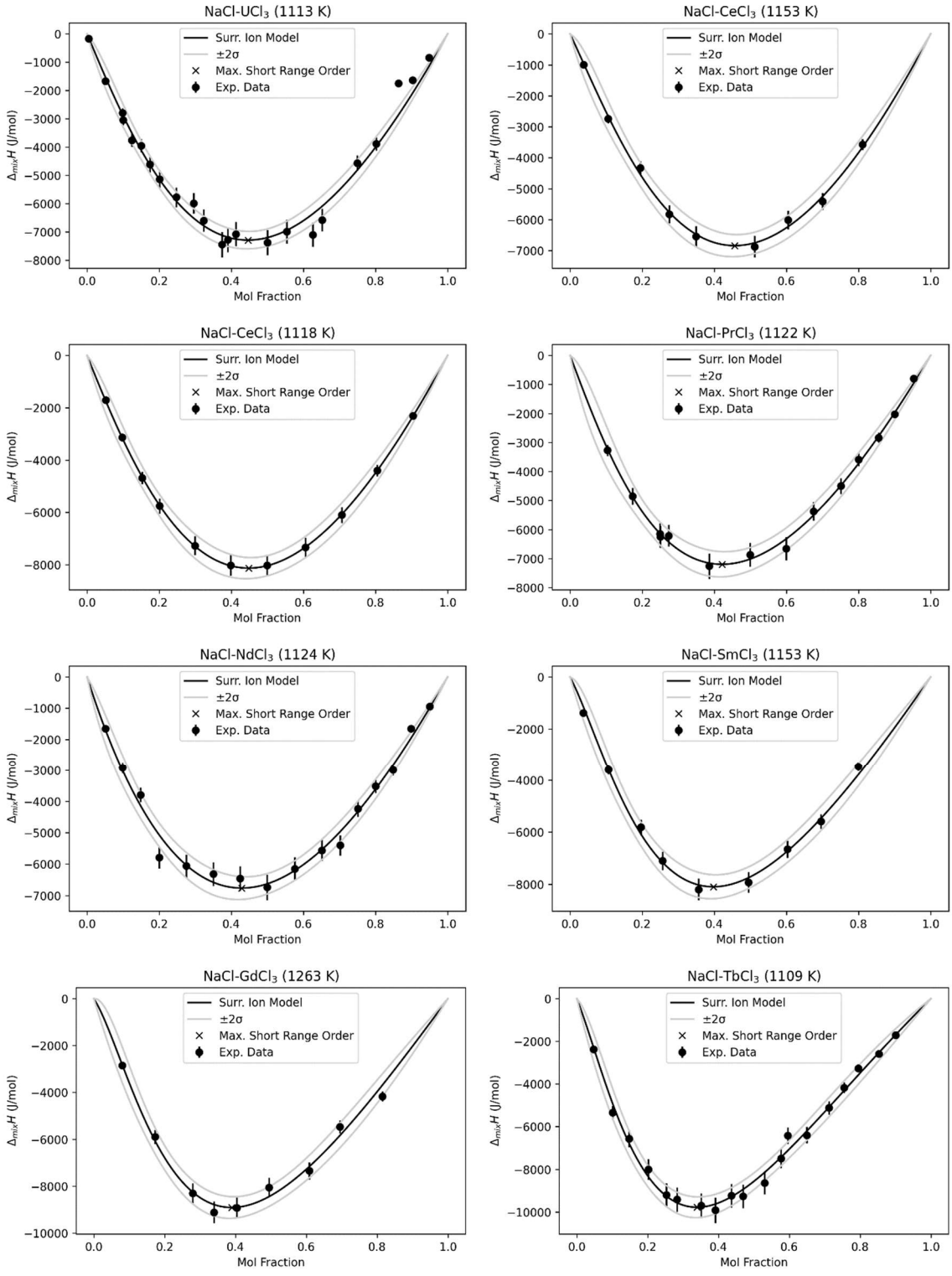
NaCl-UCl$_3$ (1113 K)
NaCl-CeCl$_3$ (1153 K)
NaCl-CeCl$_3$ (1118 K)
NaCl-PrCl$_3$ (1122 K)
NaCl-NdCl$_3$ (1124 K)
NaCl-SmCl$_3$ (1153 K)
NaCl-GdCl$_3$ (1263 K)
NaCl-TbCl$_3$ (1109 K)
Surr. Ion Model
±2σ
Max. Short Range Order
Exp. Data
$\Delta_{mix}H$ (J/mol)
Mol Fraction

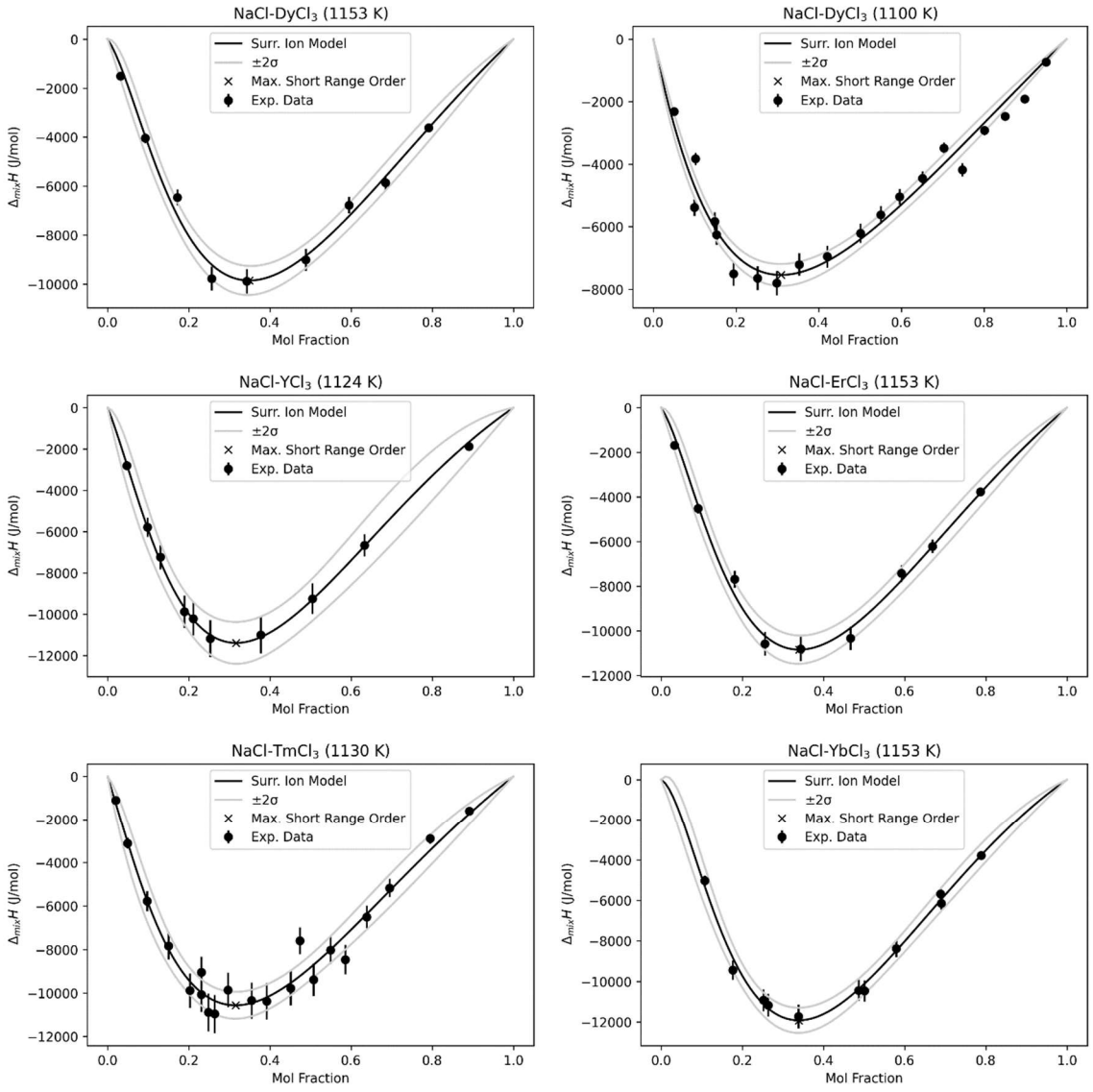

Figure 3.10: Pseudobinary Δ_{mix}H values computed using a surrounded ion model-based approach for NaCl-MCl_3 series.

Table 3.6: Fitted coefficients f_1, f_2, and f_3 for NaCl-MCl_3 series

System	Ln. & An	Exp. Temp. K	f_1	f_2	f_3
NaCl	$LaCl_3$	1173	-21047.0	-2345.8	10122.9
	$LaCl_3$	1153	-7744.5	-58045.4	49906.1
	UCl_3	1113	-8323.2	-10907.7	-2826.5
	$CeCl_3$	1153	-12177.8	-4460.7	-3829.2
	$CeCl_3$	1118	-16047.9	-55338.1	57831.0

$PrCl_3$	1122	-11508.8	-10360.4	-3846.2
$NdCl_3$	1124	-7729.2	-39697.6	26818.5
$SmCl_3$	1153	-15827.2	14807.6	-24066.4
$GdCl_3$	1263	-8774.5	-28948.4	17623.4
$TbCl_3$	1109	-11149.7	-11294.8	1618.3
$DyCl_3$	1153	-20170.9	-33646.6	38856.5
$DyCl_3$	1100	-8888.0	-65776.0	59029.7
YCl_3 [1]	1143	-3322.6	-94243.6	83493.6
$ErCl_3$	1153	-14079.7	-4308.0	-7708.8
$TmCl_3$	1130	-14064.4	-39761.5	37401.5
$YbCl_3$	1153	-10193.9	-9986.8	-2720.9

KCl-MCl_3 systems

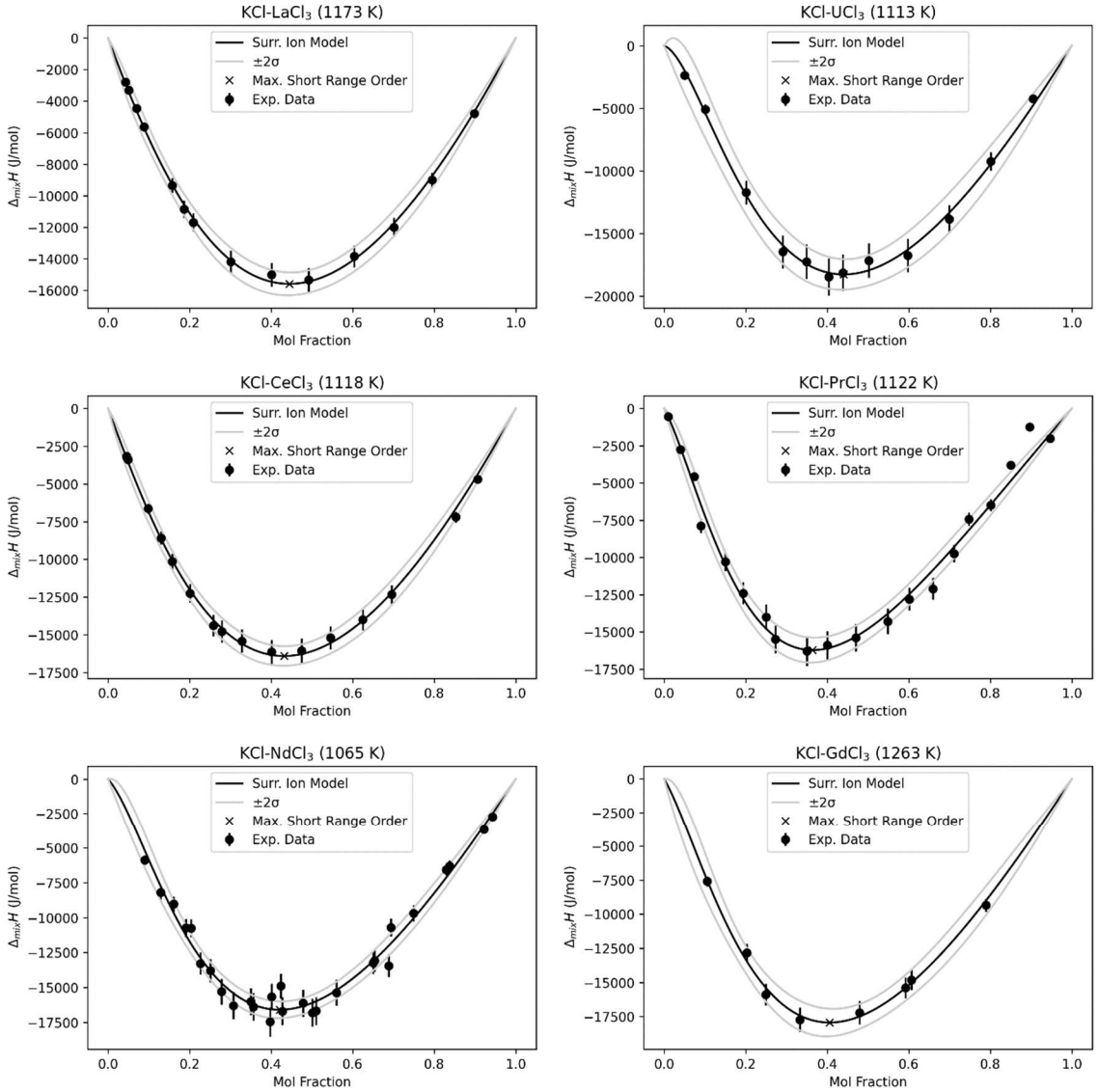

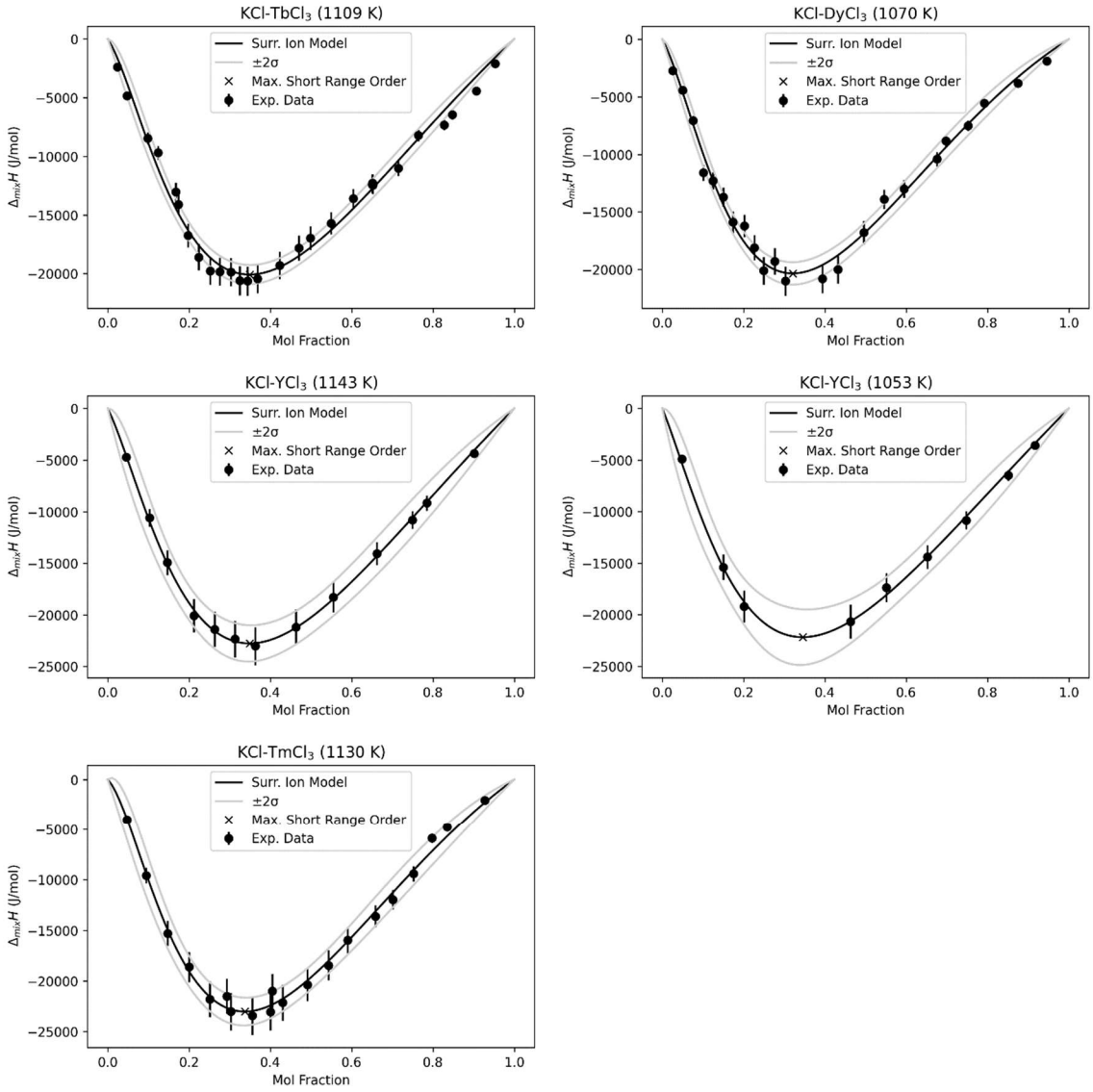

Figure 3.11: Pseudobinary Δ_{mix}H values computed using a surrounded ion model-based approach for KCl-MCl_3 series.

Table 3.7: Fitted coefficients f_1, f_2, and f_3 for KCl-MCl_3 series.

System	Ln. & An	Exp. Temp. K	f_1	f_2	f_3
KCl	$LaCl_3$	1173	-23556.7	-17042.7	-8399.5
	UCl_3	1113	-17374.0	-113160.2	97643.0
	$CeCl_3$	1118	-13921.3	-158449.3	142897.8
	$PrCl_3$	1122	-21239.7	-121418.0	120282.4
	$NdCl_3$	1065	-10909.4	-69583.5	35755.7
	$GdCl_3$	1263	-26683.3	-105596.0	92246.2
	$TbCl_3$	1109	-17448.0	-65969.0	37297.5

$DyCl_3$	1070	-17255.8	-73844.5	58959.7
YCl_3 ǂ	1143	-32530.1	-84203.1	76747.9
YCl_3 ǂ	1053	-24711.3	-23606.6	-896.2
$TmCl_3$	1130	-3853.1	-89497.6	41025.5

RbCl-MCl_3 systems

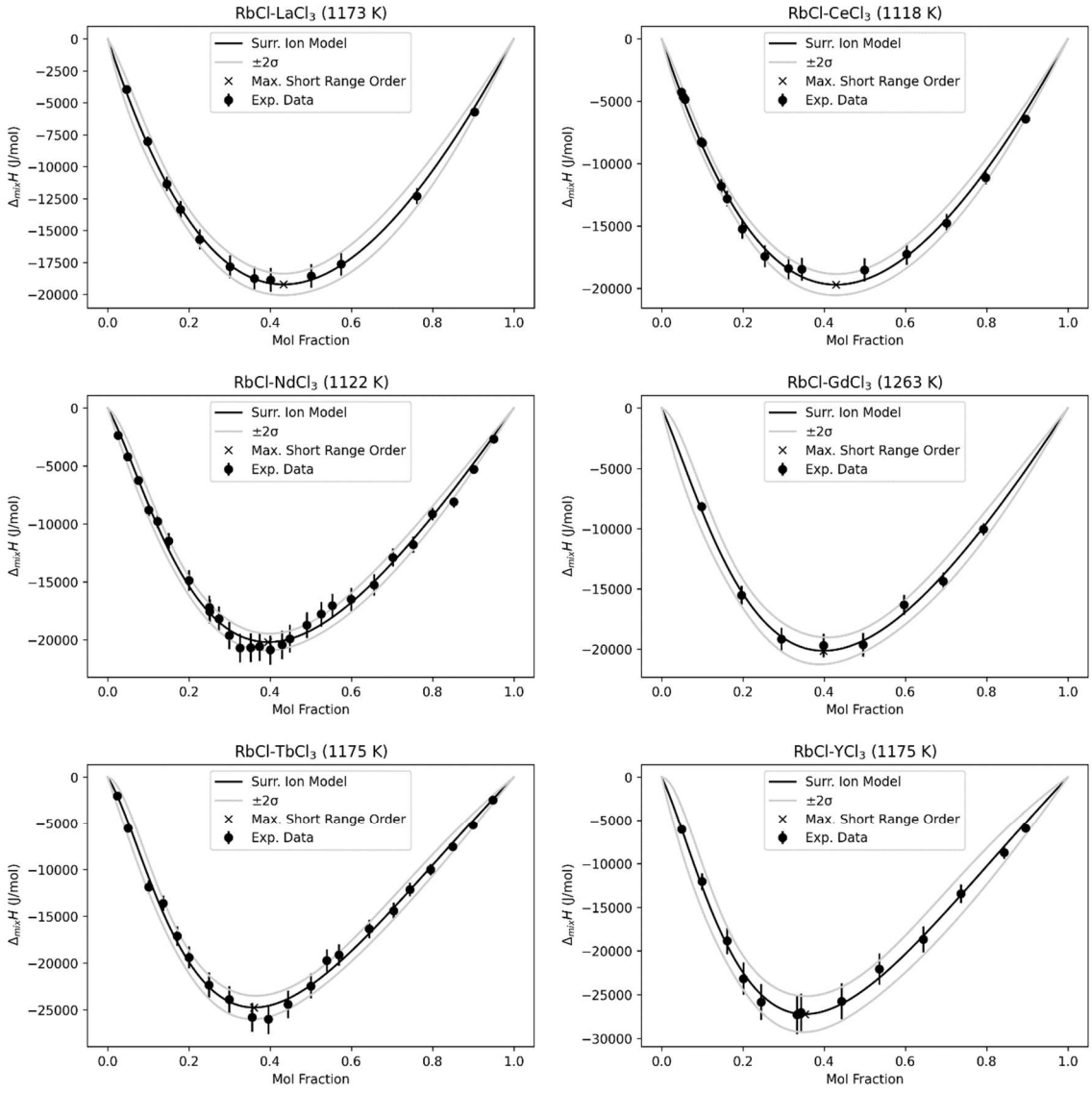

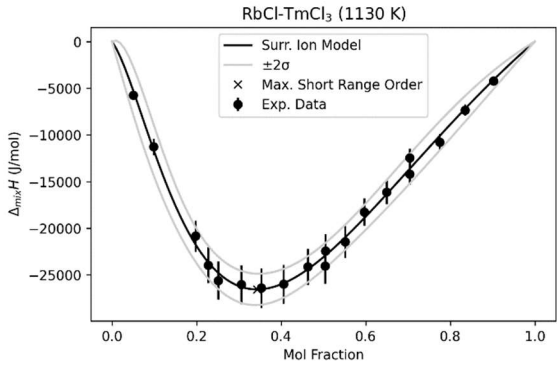

Figure 3.12: Pseudobinary Δ_{mix}H values computed using a surrounded ion model-based approach for KCl-MCl_3 series.

Table 3.8: Fitted coefficients f_1, f_2, and f_3 for RbCl-MCl_3 series.

System	Ln. & An	Exp. Temp. K	f_1	f_2	f_3
RbCl	$LaCl_3$	1173	-25201.2	-61083.7	35075.6
	$CeCl_3$	1118	-21956.2	-129085.2	105126.9
	$NdCl_3$	1122	-32422.4	-21447.2	-5214.0
	$GdCl_3$	1263	-32347.8	-17385.1	-8782.7
	$TbCl_3$	1175	-32788.0	-120761.9	103694.7
	YCl_3 [‡]	1143	-20745.5	-76765.3	48224.8
	$TmCl_3$	1130	-21321.0	-160464.3	142387.1

CsCl-MCl_3 systems

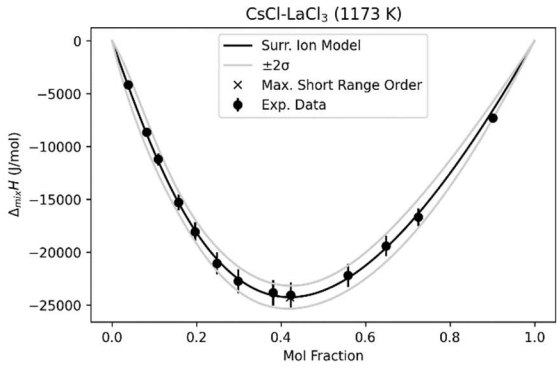

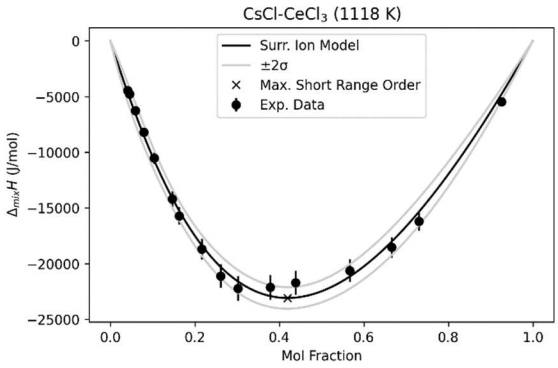

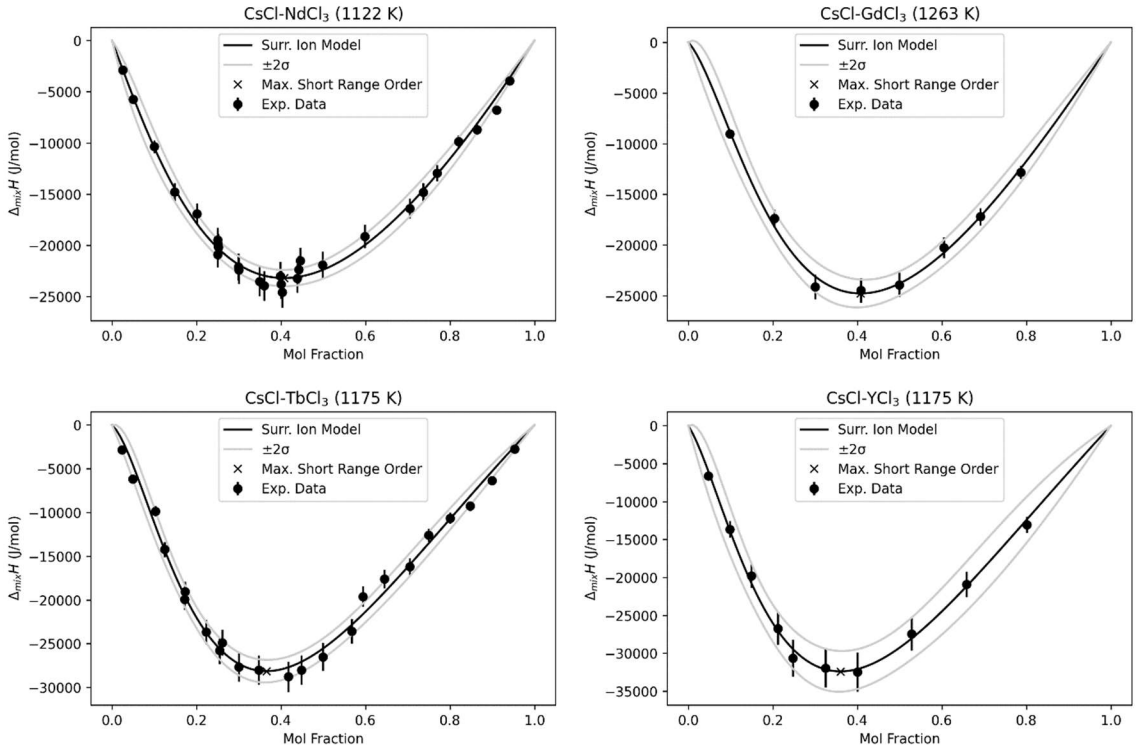

Figure 3.13: Pseudobinary Δ_{mix}H values computed using a surrounded ion model-based approach for KCl-MCl_3 series.

Table 3.9: Fitted coefficients f_1, f_2, and f_3 for CsCl-MCl_3 series

System	Ln. & An	Exp. Temp. K	f_1	f_2	f_3
CsCl	$LaCl_3$	1173	-15126.8	-116346.3	69233.6
	$CeCl_3$	1118	-14348.5	-176006.4	139127.0
	$NdCl_3$	1122	-37540.5	-38617.8	6141.0
	$GdCl_3$	1263	-29031.6	-168506.0	137505.9
	$TbCl_3$	1175	-37094.2	-41099.1	14686.4
	YCl_3 [1]	1148	-39682.4	-25912.7	-1528.9

CHAPTER 4: THERMODYNAMIC MEASUREMENTS AND ASSESSMENTS FOR LICL-NACL-KCL-UCL_3 SYSTEMS[2]

[2] J.A. Yingling, J. Schorne-Pinto, M. Aziziha, J.C. Ard, A.M. Mofrad, M.S. Christian, C.M. Dixon, T.M. Besmann. Article submitted to the Journal of Chemical Thermodynamics 7/16/2022.

Abstract

Thermodynamic descriptions of higher-order molten salt systems are essential for the effective application of molten salt technologies. However, for pyroprocessing and molten salt reactor development, a complete description of the key Li-Na-K-U(III) chloride system has yet to be provided. To remedy this, we applied the CALculation of PHAse Diagrams (CALPHAD) approach to all available phase equilibria and related thermodynamic measurements that include new differential scanning calorimetry (DSC) observations for pseudo-binary and pseudo-ternary systems to obtain consistent and accurate sets of thermodynamic properties. An outcome of that effort was the apparent discovery of a previously unreported intermediate compound in the NaCl-UCl_3 system. In this effort, we adopted a unique approach to the quantification of uncertainty in phase equilibria obtained from DSC measurements, which can provide distinct advantages in phase diagram analysis. The methodology indicates that reported values of uncertainty are often underestimated. The assessed systems of the current effort were incorporated in the publicly available *Molten Salt Thermal Properties Database - Thermochemical*.

Introduction

The *Molten Salt Thermal Properties Database - Thermochemical* (*MSTDB-TC*)[110,111] effort seeks to provide useful thermodynamic models within a convenient database for global equilibrium applications relevant to molten salt reactor (MSR) coolant and fuel systems [112] and also to pyroprocessing [113], and the use of salts in non-nuclear applications. As part of this effort, this work has sought to evaluate and develop thermodynamic models and values for the LiCl-NaCl-KCl-UCl_3 system. The LiCl-KCl-UCl_3 subsystem is important to pyroprocessing and electrorefining technologies for nuclear fuel reprocessing [114–116], whereas the NaCl-KCl-UCl_3 subsystem is important to MSR

developers [117]. The pseudo-binary subsystems of these pseudo-ternary salts were previously investigated, though not all use common thermodynamic reference values. Additionally, no current work describes the pseudo-ternary subsystems using liquid solution models that are compatible with the *MSTDB-TC* other than via interpolations from the pseudo-binary descriptions.

Differential scanning calorimetry (DSC) measurements of the subsystems in the LiCl-NaCl-KCl-UCl_3 pseudo-quaternary salt system were performed, mainly focusing on resolving disagreements between existing data and developing a reliable thermodynamic assessment in regions of highest compositional interest to MSRs. In addition to those measurements and assessments, a methodology is demonstrated for the measurement of molten salt phase equilibria via DSC that appropriately addresses the uncertainty in the results.

This work is distinct from previous approaches in that it ensures that the developed liquid Gibbs energy solution models are consistent with the excess heat capacity ($\Delta_{\mathrm{mix}}C_{\mathrm{p}}$) values of the melt solutions as well as the phase equilibria, liquid enthalpy of mixing ($\Delta_{\mathrm{mix}}H$), and electromotive force (EMF) measurements. The result is an accurate thermodynamic representation of the pseudo-quaternary LiCl-NaCl-KCl-UCl_3 molten salt developed using existing high-order equilibria and original DSC measurements.

Thermodynamic modeling

Liquid solution

The melt is modeled in the manner adopted by the MSTDB-TC [110,111,118], utilizing the calculation of phase diagrams (CALPHAD) [119] method and Factsage™ software [120] to develop solution descriptions using the modified quasi-chemical model in the quadruplet approximation (MQMQA) [121].

For common anion systems, the MQMQA accounts for short-range ordering (SRO) between second nearest neighbors (SNN) in a pair exchange reaction of Equation (4.1), which gives rise to the Gibbs energy contribution of Equation (4.2),

$$(A-X-A)+(B-X-B)=2(A-X-B);\ \Delta G_{AB/X} \tag{4.1}$$

$$\Delta G_{AB/X}=\sum_{i,j} G^{i,j}_{AB/X}\,\chi^{i}_{AB/X}\chi^{j}_{BA/X}\ (i\geq 0, j\geq 0) \tag{4.2}$$

$$\chi_{AB/X}=\frac{n_{AB/X}}{n_{AB/X}+n_{AA/X}+n_{BB/X}+\cdots} \tag{4.3}$$

where A, and B, represent all combinations of cations A and B, X represents the common anion, $\chi_{AB/X}$ are the quadruplet fractions defined in Equation (4.3), and $n_{AB/X}$ are the moles of $(A-X-B)$. Further details on the MQMQA are provided by Pelton et al. [121].

For reciprocal salt descriptions, the first nearest-neighbor (FNN) to SNN correlation factor, $\zeta_{A/Cl}$, is defined by Wang et al. [122] as Equation (4.4). Equations (4.5) and (4.6) are the alkali and uranium values, respectively. The cation coordination numbers ($Z^{A}_{A/X}$) are given in Table 4.1, and those of the anions ($Z^{X}_{A/X}$) are determined to satisfy the requisite change-neutrality condition of the melt [121].

$$\zeta_{A/X}=\frac{2Z^{A}_{A/X}Z^{X}_{A/X}}{Z^{A}_{A/X}+Z^{X}_{A/X}} \tag{4.4}$$

$$\zeta_{Li/Cl}=\zeta_{Na/Cl}=\zeta_{K/Cl}=6 \tag{4.5}$$

$$\zeta_{U/Cl}=3;\ \zeta_{U_2/Cl}=1.714286 \tag{4.6}$$

Components that exhibit complex anion formation in the presence of stabilizing cations [123] will sometimes require multiple species to properly describe their thermodynamics, and in particular, their phase equilibria [124]. It has been demonstrated

Table 4.1: SNN coordination numbers of the liquid solution.

A	B	$Z^{A}_{AB/Cl}$	$Z^{B}_{AB/Cl}$
Li^{+}	Li^{+}	6	6
Na^{+}	Na^{+}	6	6
K^{+}	K^{+}	6	6
U^{3+}	U^{3+}	6	6
U_2^{6+}	U_2^{6+}	6	6
Li^{+}	Na^{+}	6	6
Li^{+}	K^{+}	6	6
Li^{+}	U^{3+}	2	6
Li^{+}	U_2^{6+}	2.2	6
Na^{+}	K^{+}	6	6
Na^{+}	U^{3+}	2	6
Na^{+}	U_2^{6+}	1.2	6
K^{+}	U^{3+}	2	6
K^{+}	U_2^{6+}	2	6
U^{3+}	U_2^{6+}	6	6

that a complexing endmember may be modeled in the liquid with any number of constituent species [125,126]. In the development of *MSTDB-TC*, such treatment is necessary for the description of UCl_3 since MSR-relevant salt systems include several highly stabilizing alkali cations such as K^+ and Cs^+. Therefore, as indicated in Table 4.1, the liquid solution model of pure UCl_3 incorporates two endmembers, a monomer (U^{3+}), and a dimer (U_2^{6+}).

Pelton et al. [121] indicated that SNN coordination numbers do not need to precisely correspond to observed values as long as the SNN ratios represent known compositions at maximum SRO. Therefore, we adopted a practice for MQMQA descriptions that implements the use of multiple endmember species to describe a pure component. In the current effort, for N species representing a pure endmember, $N-1$ SNN coordination numbers were selected to represent the stoichiometric compositions of all proposed complexes. The remaining endmember SNN CN value should be selected to best complete the representation of the overall system. This approach to modeling the salt melt accommodates any necessary complex species while allowing a practical MQMQA description.

Solid solutions

The Gibbs energy of the solid solutions is represented with the single sublattice polynomial model [127] described by Equation (4.7), where G^o is the stoichiometric sum of the endmember Gibbs energies, G^{id} is the ideal mixing entropy, and G^{xs} is the excess Gibbs energy term defined by Equation (4.8), where Y is the equivalent site fraction defined by Equation (4.9), x is the molar fraction, Z is the endmember coordination number, and L_{ij} is an interaction parameter that can be a function of temperature.

$$G = G^o + G^{id} + G^{xs} \tag{4.7}$$

$$G^{xs} = \sum_{i\geq 0}\sum_{j\geq 0} Y_A^i Y_B^j L_{ij} \tag{4.8}$$

$$Y_A = \frac{Z_A x_A}{Z_A x_A + Z_B x_B + \cdots} \tag{4.9}$$

Materials and Experimental methods

Anhydrous lithium chloride (LiCl), sodium chloride (NaCl), and potassium chloride (KCl) were obtained with a supplier-reported cation mass fraction purity of >99.9%, while uranium trichloride (UCl_3) was obtained without a purity specification. In Table 4.2, the purity of the alkali chlorides and UCl_3 were estimated by evaluation of the DSC-determined melting point and peak shape, as well as through confirmation of structure by room temperature powder X-ray diffraction (XRD). The associated XRD patterns and DSC scans are provided in the supplemental material Figure 4.28 through Figure 4.31 and Figure 4.32 through Figure 4.35, respectively.

LiCl and NaCl exhibited smooth DSC profiles with a single sharp peak, though the DSC of KCl showed evidence of a small impurity (Figure 4.34). The melting points of LiCl, NaCl, and KCl were determined as 879.8±1.4K, 1075.2±0.9K, and 1044.5±1.7, respectively, where temperature uncertainties are expanded uncertainties U(*T*) [128] determined by the method described in the supplemental material with a 95% confidence interval (CI) of approximately 2σ. UCl_3 also had a single peak, though broader than those of the alkali chlorides, at 1105.2±4.9K. The much higher uncertainty in the UCl_3 measurement is due to a higher measured extrapolated onset temperature at a DSC scan rate of 2K min^{-1} relative to other scan rates (Figure 4.35). A discussion of these melting

Table 4.2: Sample materials used in DSC measurements in this work.

Formula	Source	State	Mole fraction purity[a]
LiCl	BeanTown Chemical	Powder	0.97±0.01
NaCl	BeanTown Chemical	Powder	0.99±0.01
KCl	BeanTown Chemical	Beads	0.98±0.01
UCl_3	TerraPower	Powder	0.96±0.03

[a] Uncertainties are the standard uncertainties u(x) [128] estimated from DSC and XRD analyses.

points relative to those in the review by Parker et al. [129] is given in the supplementary material along with a rationale for the determined purities of Table 4.2.

DSC and XRD sample preparation

Samples were prepared within an MBraun Unilab Pro glovebox under high purity argon with H_2O and O_2 concentrations maintained below 3ppm and 10ppm, respectively. Salts were weighed on an Ohaus PA84C scale with ±0.3mg precision, where all reported mass uncertainties are the expanded uncertainty U(*m*) (95% CI ~2σ) into a total mixed mass of at least 100mg to minimize uncertainties in composition. To ensure a homogeneous mixture, the samples were manually ground in an agate mortar and pestle for 15 minutes, then sealed within Netzsch 100 µl stainless steel crucibles containing a custom nickel metal liner as described by Piro et al. [130].

Powder XRD

Transmission mode powder XRD measurements were made with a Rigaku Smartlab X-ray Diffractometer with Mo source ($K\alpha_1$ = 0.70932 Å, $K\alpha_2$ = 0.71316Å). Room temperature measurements used a 0.01° step at 5° min^{-1} during a 10-minute acquisition. Samples were loaded within the glovebox into Pyrex capillaries (OD= 1 mm) for room temperature measurements of LiCl, NaCl, and KCl. A fused silica capillary (OD= 0.3 mm) was used for UCl_3 samples. The exposed capillary end was stoppered with clay. Rietveld refinement was performed using SmartLab Studio II software.

High-temperature XRD measurements used a 0.02° step at 1.5° min^{-1} during a 30-minute acquisition and were performed on a mixture of NaCl-33mol%UCl_3. Before making the measurements, the sample material was held above the melting point (873.2±2K) in an agitated muffle furnace for two hours to assure homogeneity. The sample was then annealed below the likely solidus temperature at 723.2±2K for 17 hours. XRD patterns

were obtained at room temperature, 373, 473, 573, 673, and 723, with an assumed ±2K using a heating rate of 2 K min^{-1}. Upon reaching 723±2K, three patterns were obtained after one hour of isothermal holds.

DSC calibrations, measurements, and determination of uncertainty

The instruments used in this work include a Netzsch Pegasus 404F3 and Netzsch Jupiter STA409 heat-flux type DSC equipped with an S-type thermocouple and a SiC or graphite furnace. During measurements, high-purity argon (70mL min^{-1}) purge and protective gas (20mL min^{-1}) flows were used along with a tantalum ring getter below the sample holder to minimize crucible oxidation. The Netzsch Pegasus 404F3 was heated to 1773K for 15 minutes after which a temperature calibration under heating and cooling was conducted following the zero K min^{-1} extrapolation procedure of Della Gatta et al. [131]. The Netzch Jupiter STA409 was calibrated at 2 K min^{-1}. Details of each calibration are available in the supplementary material.

A unique method of uncertainty determination was applied for the pseudo-binary phase equilibria measurements which were coupled to the calibrations and rely on well-known methods of error propagation for equations that are linear with respect to fitting parameters [96]. Under the reasonable assumption that the random errors in DSC-determined transition temperatures are normally distributed, this approach may be used to propagate the random uncertainty of the calibration as well as the uncertainties of the calibrant reference transition temperatures to determine the uncertainty in the calibration-corrected DSC measurements. This approach to determining uncertainties is further discussed in the supplementary material.

Results

Structure in UCl_3-containing melts

A complex network of interlinking polyhedra can develop in pseudo-binary salt systems where strongly polarized anions are mixed with low-valent, large intermediary cations [132]. An extreme example of this is BeF_2, which can self-polymerize in its pure state without additional intermediary cations [132,133], though the effect becomes more pronounced with the addition of large alkali cations [134,135]. Hence, the pure BeF_2 endmember required two species for the liquid (BeF_2 and Be_2F_4) to properly describe the KF-BeF_2 melt using the MQMQA [122]. As U^{3+} is a highly valent cation, and since Cl^- ions are more polarizable than F^- ions, UCl_3 may also require a multiple species description in the development of the UCl_3 systems involving heavy alkali chlorides.

UCl_3 has been observed with either a FNN coordination of 6 [136] or 7 [137], and as no interlinking polyhedra were experimentally observed, Adya [138] suggested that UCl_3 is a regular ionic liquid. Coordination 6 and 7 structures were obtained from molecular dynamics (MD) calculations which exhibit a change in first shell coordination preference from 6 to 7 as the concentration of UCl_3 in alkali chlorides increases [139,140]. More recently, MD has shown coordination up to 8 [140] and 9 [126], but the major first shell contributors remain the FNN CN 6 and 7 at low and moderate mole fractions of UCl_3 [126], respectively. More recently, polarizable ion model MD studies [126,140] suggested polymeric linking occurs in NaCl-UCl_3.

Thus, non-fixed CN values must be accommodated in melts of an alkali halide with UCl_3. In the current work, these are described in the liquid solution model using two endmembers: the U_2Cl_6 dimer representing the polymeric nature of the liquid, and a 6-coordinated monomer to describe the UCl_6^{3-} complex anion. The latter complex was used in the description of the monomer since alkali uranium hexachloride compounds with KCl,

RbCl, and CsCl are observed [31], implying the existence of the complex anion UCl_6^{3-}. $DyCl_3$ similarly displays strong octahedral complexing with the same charge [138], and spectrophotometry indicates octahedral complexes form at low concentrations of UCl_3 in a LiCl-KCl eutectic [141]. As a result, to correspond with the formation of UCl_6^{3-} complex anions, the U monomer is represented in the liquid by a 3:1 A^+ to U^{3+} SNN CN ratio to allow maximum ordering for the 6-coordinated UCl_3 endmember to occur near 25mol% UCl_3 for the various alkali chloride-UCl_3 systems.

Binary systems

Obtaining $\Delta_{mix}H$ and $\Delta_{mix}C_p$

We used experimental and predictive data for $\Delta_{\mathrm{mix}}H$ and $\Delta_{\mathrm{mix}}\mathrm{C_P}$ in the development of pseudo-binary assessments. In the absence of experimental measurements, the previously developed correlations of Schorne-Pinto et al. [142] and Redkin et al. [143] were used to obtain $\Delta_{\mathrm{mix}}H$ and $\Delta_{\mathrm{mix}}C_{\mathrm{P}}$. The $\Delta_{\mathrm{mix}}H$ has been measured for the LiCl-NaCl [144], LiCl-KCl [144], NaCl-KCl [144], NaCl-UCl_3 [145], and KCl-UCl_3 [146] systems. The value for LiCl-UCl_3 is from the correlation of Schorne-Pinto et al. [142]. The $\Delta_{\mathrm{mix}}H$ of the symmetric alkali chloride systems are well-described in the thermodynamic descriptions of Lu et al. [147] and thus utilized here. Estimated values for the ACl-UCl_3 systems are shown in Figure 4.1.

In contrast to $\Delta_{\mathrm{mix}}H$, there are significantly fewer measurements of $\Delta_{\mathrm{mix}}C_{\mathrm{P}}$. Redkin et al. [148] established that $\Delta_{\mathrm{mix}}C_{\mathrm{p}}$ is linearly correlated with $\Delta_{\mathrm{mix}}H$ in a dataset of molten salt eutectics, thus allowing $\Delta_{\mathrm{mix}}H$ values to be used to estimate$\Delta_{\mathrm{mix}}C_{\mathrm{p}}$. However, since using a linear correlation with this dataset is problematic as it results in positive $\Delta_{\mathrm{mix}}C_{\mathrm{P}}$ at $\Delta_{\mathrm{mix}}H = 0$, we adopted an exponential relation that is approximately linear at large $\Delta_{\mathrm{mix}}H$,

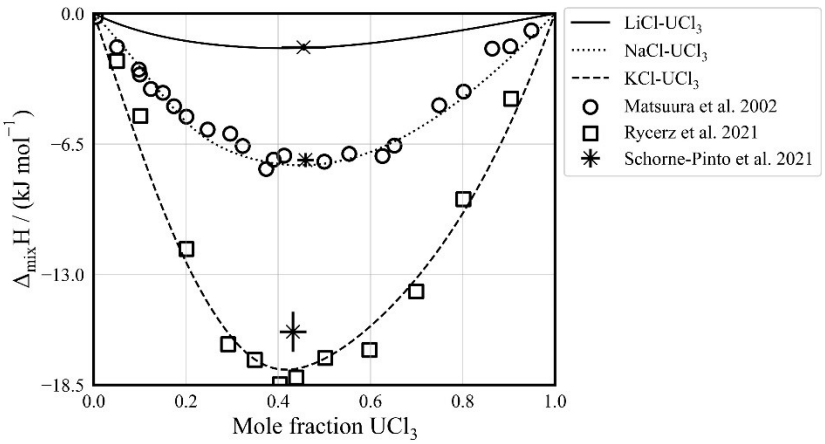

Figure 4.1: Experimental and liquid solution model calculated $\Delta_{mix}H$ for the LiCl-UCl_3, NaCl-UCl_3, and KCl-UCl_3 systems at 1113K and those from the correlation of Schorne-Pinto et al. [142], with their associated reported uncertainties.

well-representing the results of Redkin et al. [148] and appropriately passes through the origin such that $\Delta_{\mathrm{mix}}C_{\mathrm{P}} = 0$ in unmixed systems. An orthogonal distance regression of this relation is seen in Figure 4.2 and uses a 6% $\Delta_{\mathrm{mix}}H$ and 4 J mol^{-1}K^{-1} $\Delta_{\mathrm{mix}}C_{\mathrm{P}}$ uncertainty from the values of Redkin et al. [148] and provides $\Delta_{\mathrm{mix}}C_{\mathrm{p}}$ values for the LiCl-NaCl, LiCl-UCl_3, NaCl-UCl_3, and KCl-UCl_3 systems of 1.9, 2.5, 6.1, and 9.8 J mol^{-1}K^{-1}, respectively. These values are shown in Figure 4.3, and since the experimental uncertainty of $\Delta_{\mathrm{mix}}C_{\mathrm{P}}$ values are often greater than 50% of the nominal values [149], we assumed a 4 J mol^{-1}K^{-1} uncertainty interval for the correlation.

We used the values of $\Delta_{\mathrm{f}}H^{\mathrm{o}}$, and S^{o} at 298.15 K, and C_{p} for the solid and the liquid from a previous thermodynamic assessment by Beneš and Konings [25,150]. However, the liquid Gibbs energy of formation function for liquid UCl_3 is described as estimated with a value of 150 J mol^{-1}K^{-1} likely stemming from the lack of experimental C_{p} measurements for the liquid and comes from correlations with the lanthanide trichlorides [151]. Capelli and Konings [152] most recent recommendation is 129.7 J mol^{-1}K^{-1} which is in the range of very recent ab initio MD calculations [153] which predicted values of 128.5 and 141.4 J mol^{-1}K^{-1} [153]. The latter of these MD calculated values uses a functional that more accurately reproduces the $C_{\mathrm{p}}$of NaCl, however, and there is no indication that the methodology is suitable for UCl_3. As a more definitive resource for the liquid C_{p} is not yet available, the present work continues with the estimated value of 150 J mol^{-1}K^{-1} as it is in reasonable agreement with the recent MD as well as the lanthanide trichloride correlations.

We developed our liquid UCl_3 Gibbs function using the $\Delta_{\mathrm{f}}H^{\mathrm{o}}$, S^{o} and C_{p} of the solid phase [154], and using third-law analysis, we determined the liquid Gibbs energy

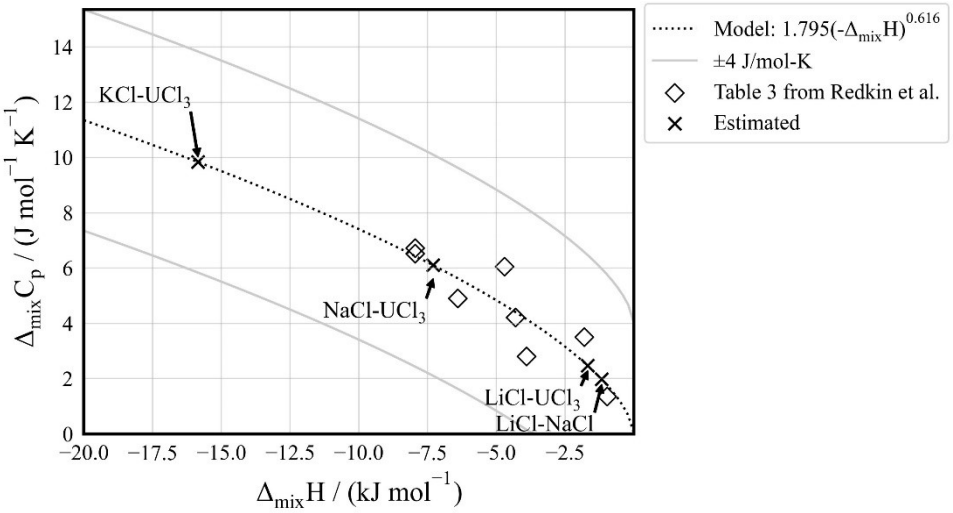

Figure 4.2: Experimental and estimated $\Delta_{\mathrm{mix}}C_{\mathrm{p}}$ of mixed chloride molten salts at the lowest eutectic from Redkin et al.[148].

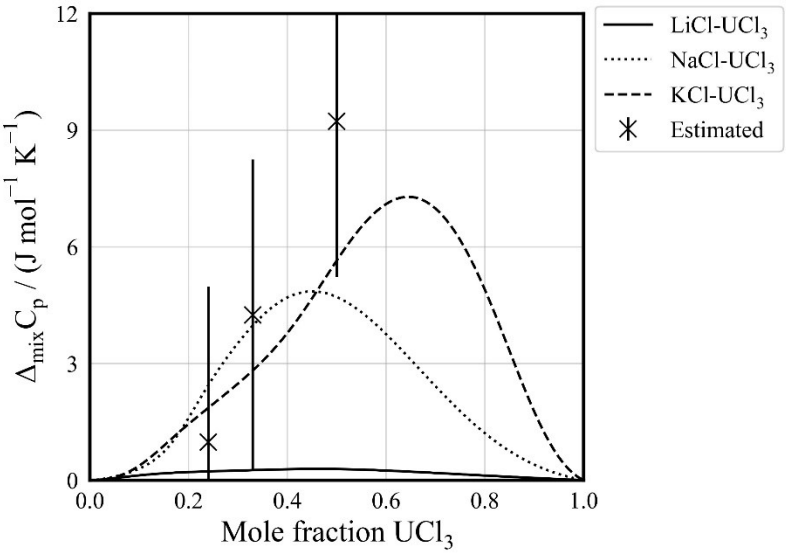

Figure 4.3: Calculated $\Delta_{\mathrm{mix}}C_{\mathrm{p}}$ at 1113K compared to the estimated values from Figure 4.2 at the lowest eutectic for each system. The estimated uncertainty is ±4 J mol^{-1}K^{-1}.

function from that of the solid using the enthalpy of fusion determined by Kovács et al. [155] of 49.0 kJ mol^{-1}, an estimated C_p of 150 J $mol^{-1}K^{-1}$, and the lower of the commonly reported melting points of 1110 K, which agrees well with the value of Parker et al. [129] within the usual thermal measurement expanded uncertainty of about ±1-3K (95% CI ~2σ) for molten salts [30,155–158]. The resulting function is shown against an experimental function provided by Martinot [159] in Figure 4.4.

It is evident in Figure 4.4 that our estimated Gibbs energy of formation ($\Delta_f G$) function for liquid UCl_3 agrees at low temperature with the function provided by Martinot [159] and is nearly identical to that of Beneš [25]. To arrive at this result, care was needed to ensure comparison against the same reference state. In this case, Martinot's [159] function is based on a particular $\Delta_f G$ for liquid AgCl which we adjusted to correspond with the function within Factsage's FactPS database [120]. No details are given by Martinot [159] as to the source of his function except an indication that the details would be made available in another publication. To our knowledge, this publication never eventuated. Martinot's [159] function is ~3kJ $mol^{-1}K^{-1}$ more stable at high temperatures than our estimated function which suggests that the liquid C_p of UCl_3 is higher than previously estimated values. First-time measurements are needed to establish the C_p of liquid UCl_3.

Endmember, compound, and vapor species thermodynamic values are provided in Table 4.3, noting that the gas phase is modeled as ideal. An asterisk indicates estimated values that were determined as adjustable parameters in the CALPHAD assessment.

LiCl-NaCl

The LiCl-NaCl system was previously reported [24,147,160] and that representation was evaluated to be adequate and used in the current assessments. The

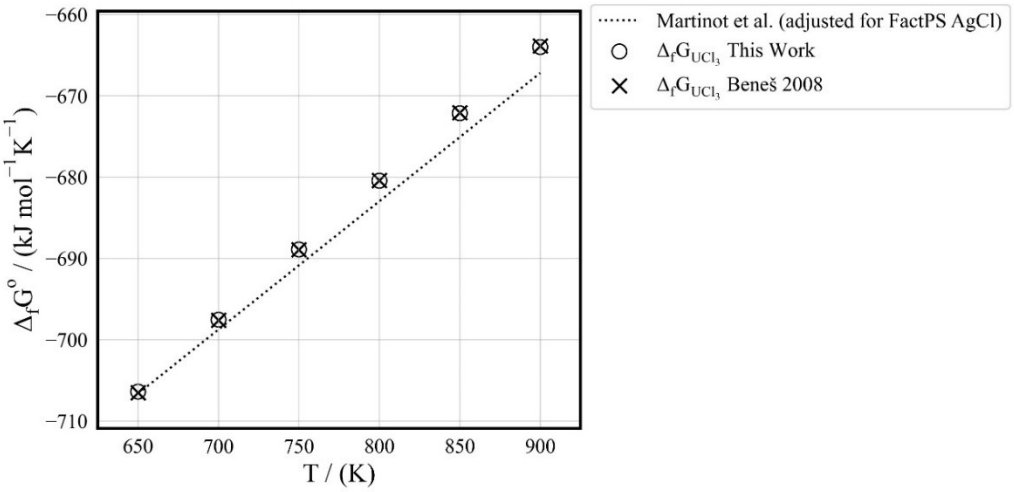

Figure 4.4: Calculated subcooled liquid UCl_3 Gibbs energy of formation compared to previously reported functions [25,159].

Table 4.3: Thermodynamic values for endmember and intermediate compounds. * indicates estimated through thermodynamic assessment.

Comp.	$\Delta_f H^o(298.15)$ / (kJ mol^{-1})	$\Delta S^o(298.15)$ / (J mol^{-1} K^{-1})	C_p / (J mol^{-1} K^{-1})	Reference
LiCl(s)	-408.266	59.3	41.4174 + 0.0233969·T	[24]
LiCl(l)	-395.776	66.277	73.3832 - 0.0094726·T	[24]
LiCl(g)	-195.719	212.924	36.802464 + 0.000891192·T - 349364·T^{-2}	[24]
NaCl(s)	-411.120	72.132	45.94 + 0.016318·T	[24]
NaCl(l)	-394.956	76.076	77.7638 - 0.0075312·T	[24]
NaCl(g)	-181.42	229.793	37.364 + 0.00071·T - 163206.1·T^{-2}	[161]
KCl(s)	-436.684	82.550	40.015776 + 0.025468·T + 364844.8·T^{-2}	[24]
KCl(l)	-421.825	86.523	73.59656	[24]
KCl(g)	-214.681	238.990	37.145552 + 0.000949768·T - 84098.4·T^{-2}	[24]
UCl_3(s)	-863.7	163.9	106.967 - 0.0208595 T - 129994·T^{-2} + 3.6389·10^{-5}·T^2	[154]
UCl_3(l)[a, b]	-845.611	154.663	150	This work
UCl_3(g)	-523	380.409	84.018 - 0.0034732·T - 79890·T^{-2} + 3.613 10^{-6}·T^2	[154]
NaU_2Cl_7(s)	-2113.6 *	436.2 *	259.874-0.025401·T - 259988·T^{-2} + 7.2778·10^{-5}·T^2*	This work
KU_2Cl_7(s)	-2136.4 *	470.7 *	253.9498 - 0.01625·T +104856.8·T^{-2} + 7.27781·10^{-5} T^2*	This work
K_3UCl_6(s)	-2174.4*	464 *	207.827 + 0.1·T + 1552834.4·T^{-2}*	This work
K_2UCl_5(s)	-1793.4	311 *	167.812 + 0.082056·T + 1187989.6·T^{-2}*	This work, [162]

[a] Solution model for monomer species representing UCl_6^{3-} is $G^o(UCl_6^{3-}) = G^o(UCl_{3(l)}) + 50000 - 7.5\ T$ (J mol^{-1}).

[b] Solution model for dimer species is $G^o(U_2Cl_{6(l)}) = 2\ G^o(UCl_{3(l)}) + 273.6 + 0.2147\ T - 0.45\ T \ln(T)$ (J mol^{-1}).

model parameters to describe the liquid and solid solutions are given in Equations (4.10) and (4.11), respectively.

$$\Delta G_{LiNa/Cl} = -1562 + 0.2T \tag{4.10}$$

$$G^{xs}_{LiNa} = 7500 Y_{Li} Y_{Na} + 4600 Y_{Li} Y_{Na} (Y_{Li} - Y_{Na}) \tag{4.11}$$

The computed phase equilibria agree well with observations but the calculated value for liquid $\Delta_{mix} C_p = 0$ J mol^{-1}K^{-1} since the liquid model does not use a $T\ln(T)$ term. However, this agrees with the estimated $\Delta_{mix} C_p$ value of 1.9 J mol^{-1}K^{-1} within the expected ±4 J mol^{-1}K^{-1} uncertainty of Figure 4.2. The calculated liquid $\Delta_{mix} H$ well-reproduces the measurements of Hersh and Kleppa [144].

LiCl-KCl

The LiCl-KCl system has been extensively studied including several thermodynamic assessments [30,163–167], as well as an assessment by Chartrand and Pelton [24] which we utilized for the description of the liquid. We added a limited range of solid solubility near the endmembers, as described by Ghosh et al. [30]. The resulting interaction parameters for the liquid and solid solution are provided in Equations (4.12) and (4.13), respectively.

$$\begin{aligned} \Delta G_{LiK/Cl} = -4884.6 + 1.1T + (-1147.3 + 1.5416T)\chi_{KLi} \\ + (-864.7 - 0.3805T)\chi_{LiK} \end{aligned} \tag{4.12}$$

$$G^{xs}_{LiK} = 24700 Y_{Li} Y_{K} \tag{4.13}$$

The calculated phase diagram is given in Figure 4.5 which well reproduces the LiCl-KCl liquidus. The experimental $\Delta_{mix} H$ of Hersh and Kleppa [144] is similarly well-reproduced. The halite and sylvite solubility are limited to 0.95mol% of either endmember to conform with our interpretation of Ghosh's [30] measurements at 3 and 5mol%.%. Since

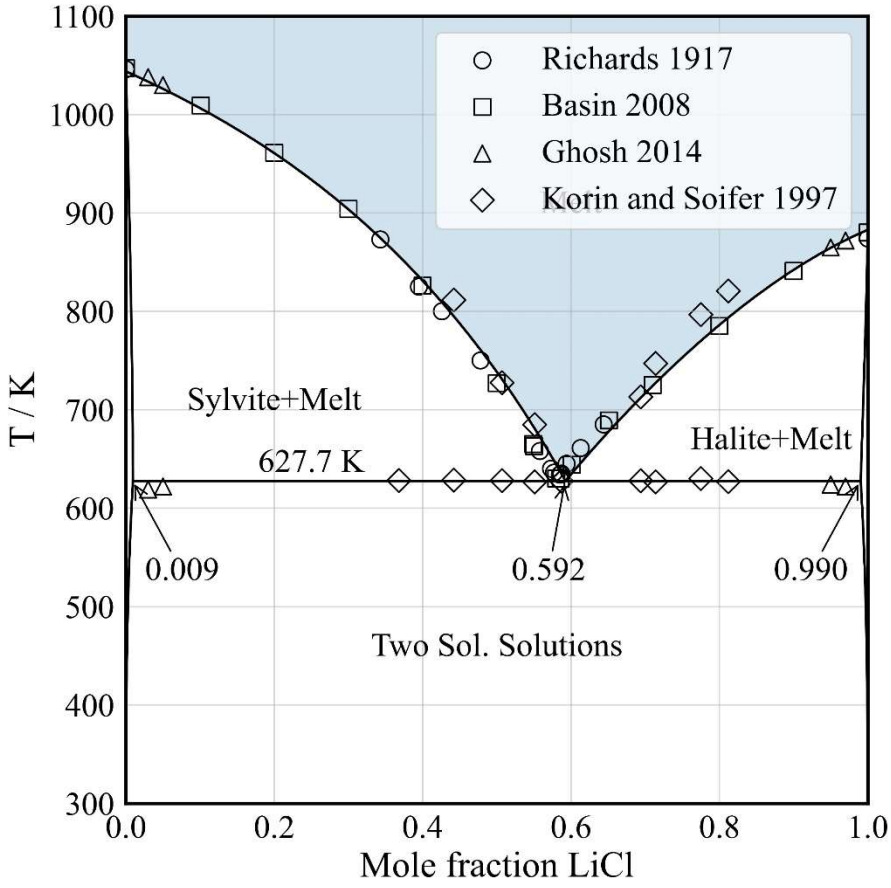

Figure 4.5: Computed phase diagram and experimental phase equilibria [30,163,164,166]of the LiCl-KCl system.

the liquid solution does not use a $T\ln(T)$ term, calculated $\Delta_{\mathrm{mix}}C_{\mathrm{p}}$ is very small and does not agree with the average experimental value of 5.75 J mol^{-1}K^{-1} as measured by Korin and Soifer [166].

NaCl-KCl

The system was previously well assessed by Chartrand and Pelton [24,160,168] and we use their endmember values and solution models as they are compatible with *MSTDB-TC*. Their parameters are reproduced in Equations (4.14) and (4.15), which well reproduce the known phase equilibria and $\Delta_{\mathrm{mix}}H$. The calculated liquid $\Delta_{\mathrm{mix}}C_{\mathrm{p}}$ is very small due to the near-ideal solid solution in this system [144] and agrees with the measurements of Sergeev et al. [169] within the uncertainty limits in the temperature range of interest (750-930K).

$$\Delta \mathrm{G}_{\mathrm{NaK/Cl}} = -695.5 - 67\chi_{\mathrm{NaK}} \tag{4.14}$$

$$\mathrm{G}^{\mathrm{xs}}_{\mathrm{NaK}} = \mathrm{Y}_{\mathrm{KCl}}\mathrm{Y}_{\mathrm{NaCl}}\big(14333 + 3278\mathrm{Y}_{\mathrm{NaCl}} + 32.796T - 5.598T\ln(T)\big) \tag{4.15}$$

LiCl-UCl₃

The phase equilibria of the LiCl-UCl_3 system were extensively studied [26,114,170,171]. Additionally, a thermodynamic assessment of this simple eutectic system was produced by Ghosh et al. [30], however, it is not compatible with MSTDB-*TC* and thus requires a reassessment. Disagreement about the measured liquidus temperatures between Desyatnik et al. [170] and Barton [26] is seen at moderate to high concentrations of UCl_3. The disagreement between data sets creates doubt as to the true composition of the eutectic, which is important for accurately representing the higher-order systems LiCl-NaCl-UCl_3 and LiCl-KCl-UCl_3.

Table 4.4: DSC events of the LiCl-UCl_3 system.

Mole fraction UCl_3	Equilibrium reaction	Type of equilibrium	DSC thermal events / K[a]	
			Heating	Cooling
0.101	$LiCl(s) + UCl_3(s) \leftrightarrow L$	Eutectic	768.8±1.6	765.0±2.0
	$LiCl(s) + L \leftrightarrow L'$	Liquidus	844.9±1.5	841.7±1.3
0.184	$LiCl(s) + UCl_3(s) \leftrightarrow L$	Eutectic	766.6±2.3	762.5±1.7
	$LiCl(s) + L \leftrightarrow L'$	Liquidus	806.2±3.6	800.8±2.6
0.254	$LiCl(s) + UCl_3(s) \leftrightarrow L$	Eutectic	770.2±7.4	760.5±3.0
0.391	$LiCl(s) + UCl_3(s) \leftrightarrow L$	Eutectic	770.0±1.7	765.4±1.4
	$UCl_3(s) + L \leftrightarrow L'$	Liquidus	883.6±8.4	884.6±4.4
0.495	$LiCl(s) + UCl_3(s) \leftrightarrow L$	Eutectic	769.4±1.4	761.4±2.5
	$UCl_3(s) + L \leftrightarrow L'$	Liquidus	947.6±1.4	937.1±3.3

[a] Expanded uncertainties, U(*T*) (95% CI ~2σ).

To resolve the eutectic composition for this system, we performed DSC measurements at compositions of 0.10, 0.254, 0.391, and 0.495mol% UCl_3, (Table 4.4). Reported uncertainties result from calibration and error propagation using the method described in the supplemental material. The phase transitions on heating were determined using an extrapolated onset for the eutectic and the DSC peak for the liquidus.

The liquid model parameters, which were determined from these and previous [26,114,170] measurements, were evaluated as Equations (4.16) and (4.17). In Figure 4.6, a Tammann analysis technique discussed by Rycerz et al. [172] is used to exclude the eutectic determined by Desyatnik et al. [170] of 26.5mol% UCl_3. The SNN CN ratio of 2:6 selected for Li^+:U_2^{6+} allowed simultaneous reproduction of the eutectic composition at 25.4mol% UCl_3 as well as the composition at the minimum in $\Delta_{\mathrm{mix}}H$ at 45.5mol% UCl_3 to agree with that of the correlation in Figure 4.1.

$$\Delta \mathrm{G}_{\mathrm{LiU_2/Cl}} = -4150 - 5T \tag{4.16}$$

$$\Delta \mathrm{G}_{\mathrm{LiU/Cl}} = -20500 - 1.6T \tag{4.17}$$

The phase equilibria for this system are well-represented by the computed diagram (Figure 4.7) that results from our assessment. Although no experimental $\Delta_{\mathrm{mix}}H$ values are available, the computed minimum closely matches the value obtained by the correlation in Figure 4.1. Similarly, as seen in Figure 4.3, the computed $\Delta_{\mathrm{mix}}C_{\mathrm{p}}$ agrees well with the value obtained from the correlation in Figure 4.2 within the uncertainty limits.

NaCl-UCl_3

In addition to the reported phase equilibria studies [26,27,158,173,174], we performed DSC measurements at compositions of 2.5-74.3mol% (Table 4.5). In those

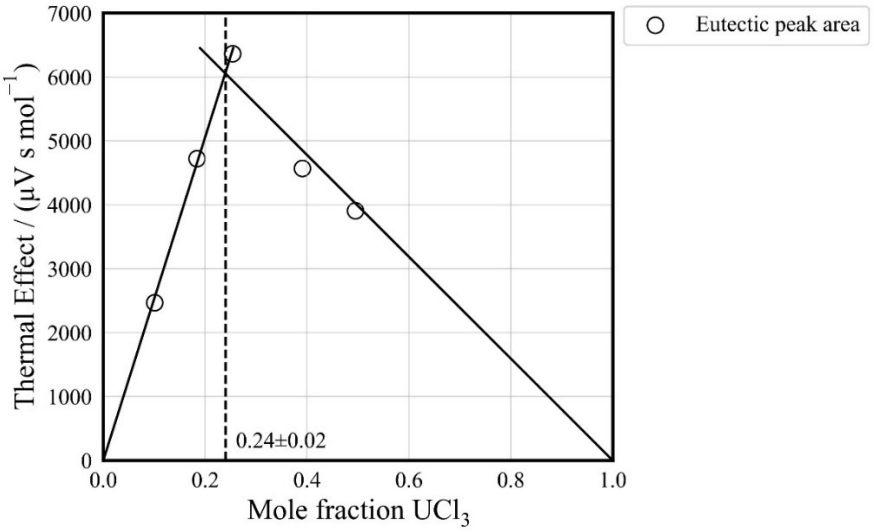

Figure 4.6: Tammann analysis [172] of thermal effect for samples of LiCl-UCl_3 evaluated upon cooling at 5 K min^{-1}.

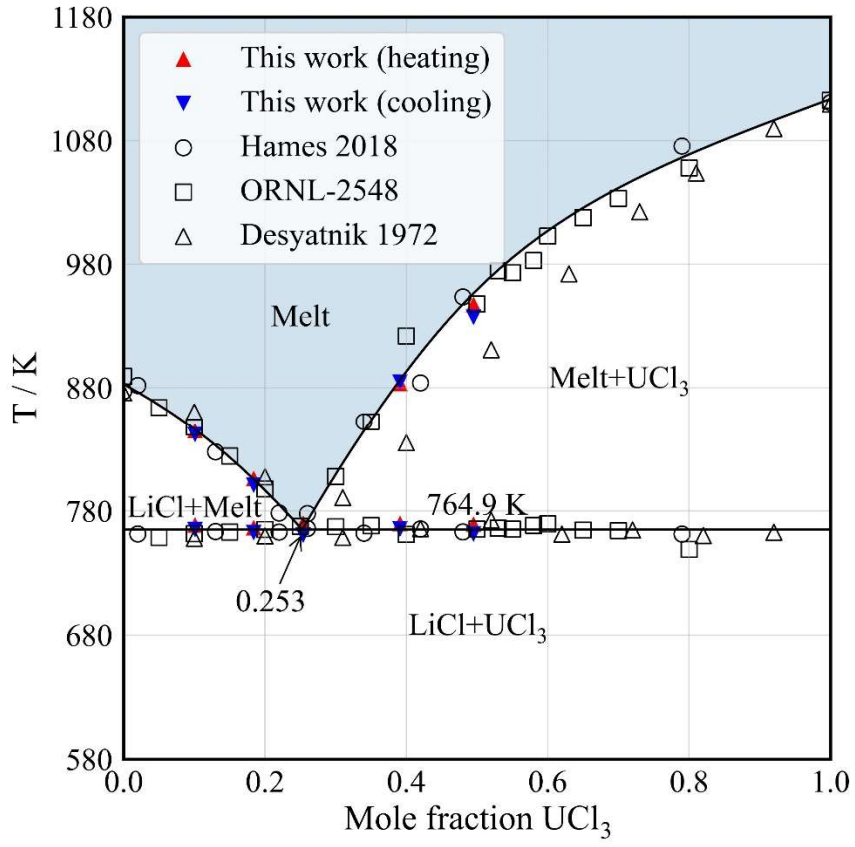

Figure 4.7: Computed phase diagram of the LiCl-UCl_3 system together with phase equilibria measurements [26,114,170].

Table 4.5: DSC events of the NaCl-UCl3 system.

Mole fraction UCl_3	Equilibrium reaction	Type of equilibrium	DSC thermal events / K[a]	
			Heating	Cooling
0.025	$NaCl(s) + NaU_2Cl_7(s) \leftrightarrow L$	Eutectic	779.5±3.4	773.1±6.1
	$NaCl(s) + L \leftrightarrow L'$	Liquidus	1060.1±1.6	1062.7±1.5
0.053	$NaCl(s) + NaU_2Cl_7(s) \leftrightarrow L$	Eutectic	785.6±1.8	784.5±2.8
	$NaCl(s) + L \leftrightarrow L'$	Liquidus	1059.9±1.4	1054.0±1.6
0.103	$NaCl(s) + NaU_2Cl_7(s) \leftrightarrow L$	Eutectic	785.9±1.5	786.0±1.6
	$NaCl(s) + L \leftrightarrow L'$	Liquidus	1034.6±1.6	1027.2±4.8
0.150	$NaCl(s) + NaU_2Cl_7(s) \leftrightarrow L$	Eutectic	785.3±2.7	786.7±2.0
	$NaCl(s) + L \leftrightarrow L'$	Liquidus	1001.6±3.7	995.7±3.0
0.212	$NaCl(s) + UCl_3(s) \leftrightarrow NaU_2Cl_7(s)$	Peritectoid	695.3±1.7	672.9±14.5
	$NaCl(s) + NaU_2Cl_7(s) \leftrightarrow L$	Eutectic	794.3±2.9	792.3±0.8
	$NaCl(s) + L \leftrightarrow L'$	Liquidus	934.1±15.9	930.3±4.9
0.221[c]	$NaCl(s) + NaU_2Cl_7(s) \leftrightarrow L$	Eutectic	793.9±1.6	770.8±1.2
	$NaCl(s) + L \leftrightarrow L'$	Liquidus	914.9±2.8	911.5±2.5
0.314[c]	$NaCl(s) + NaU_2Cl_7(s) \leftrightarrow L$	Eutectic	768.4±2.3	780.7±1.3
	$NaCl(s) + L \leftrightarrow L'$	Liquidus	787.8±1.3	802.7±2.3
0.334	$NaCl(s) + UCl_3(s) \leftrightarrow NaU_2Cl_7(s)$	Peritectoid	688.8±1.4	674.0±1.6
	$NaCl(s) + NaU_2Cl_7(s) \leftrightarrow L$	Eutectic	769.5±1.8	778.2±21.3
0.408	$NaCl(s) + UCl_3(s) \leftrightarrow NaU_2Cl_7(s)$	Peritectoid	691.8±2.1	674.1±2.3
	$NaCl(s) + NaU_2Cl_7(s) \leftrightarrow L$	Eutectic	774.5±4.4	777.7±1.9
	$NaU_2Cl_7(s) + L \leftrightarrow L'$	Liquidus	854.0±7.2	844.7±1.3
0.425	$NaCl(s) + UCl_3(s) \leftrightarrow NaU_2Cl_7(s)$	Peritectoid	669.5±1.7	656.6±6.9
	$NaCl(s) + NaU_2Cl_7(s) \leftrightarrow L$	Eutectic	781.6±1.6	782.9±2.7
	$NaU_2Cl_7(s) + L \leftrightarrow L'$	Liquidus	854.3±3.6	850.9±11.5
0.431	$NaCl(s) + UCl_3(s) \leftrightarrow NaU_2Cl_7(s)$	Peritectoid	687.8±1.5	666.3±0.9
	$NaCl(s) + NaU_2Cl_7(s) \leftrightarrow L$	Eutectic	779.8±3.0	781.8±2.6
	$NaU_2Cl_7(s) + L \leftrightarrow L'$	Liquidus	859.3±2.8	856.4±4.5
	[d]		908.7±14.6	[b]
0.506	$NaCl(s) + UCl_3(s) \leftrightarrow NaU_2Cl_7(s)$	Peritectoid	692.6±1.2	661.7±5.4
	$NaCl(s) + NaU_2Cl_7(s) \leftrightarrow L$	Eutectic	776.3±1.5	775.1±2.3
	$NaU_2Cl_7(s) + L \leftrightarrow L'$	Liquidus	902.4±3.2	899.9±2.9
0.559	$NaCl(s) + UCl_3(s) \leftrightarrow NaU_2Cl_7(s)$	Peritectoid	668.2±1.3	654.6±0.8
	$NaCl(s) + NaU_2Cl_7(s) \leftrightarrow L$	Eutectic	774.7±2.3	778.2±1.1
	$NaU_2Cl_7(s) \leftrightarrow L + UCl_3(s)$	Peritectic	909.1±6.1	907.6±2.6
0.646	$NaCl(s) + UCl_3(s) \leftrightarrow NaU_2Cl_7(s)$	Peritectoid	678.3±4.0	647.1±15.9
	$NaU_2Cl_7(s) \leftrightarrow L + UCl_3(s)$	Peritectic	925.4±3.1	942.5±17.1
	$L + UCl_3(s) \leftrightarrow L'$	Liquidus	996.4±3.8	990.3±12.1
0.743	$NaU_2Cl_7(s) \leftrightarrow L + UCl_3(s)$	Peritectic	924.8±5.0	971.9±33.8
	$L + UCl_3(s) \leftrightarrow L'$	Liquidus	1039.0±11.4	1025.8±22.1

[a] Expanded uncertainties, U(T) (95% CI ~2σ).
[b] Thermal effect not detected on heating and cooling.
[c] Scanning range was insufficient to detect compound formation.
[d] Additional peak likely due to failure to reach equilibrium

measurements, we identified transitions that involve the formation and decomposition of a heretofore unidentified compound, as indicated by a Tammann analysis in Figure 4.8, which clearly shows the stoichiometry of a compound near ~66mol% UCl_3 and the presence of a DSC thermal event near 688K seen in Figure 4.9 for the 33.4mol% UCl_3 measurement.

The possibility of an intermediate compound is also indicated by the ionic potential ratio, computed using Equation (4.18), where z and r are the cation charge and ionic radius respectively, and which has been used to predict the presence of compounds in mixed salt systems [175]. Using the 6-coordinated Shannon ionic radii [176], we calculated the ionic potential ratio for NaCl-UCl_3 in the manner of Gaune-Escard et al. [177], where IP_{Na+}/IP_{U3+} = 0.335, and found the ionic potential ratio to correspond with those for alkali-lanthanide chloride systems with one intermediate compound [177] (Note: the compound $Na_3Nd_5Cl_{18}$, as determined by Seifert et al. [178] having IP_{Na+}/IP_{Nd3+} = 0.321, was incorrectly reported by Gaune-Escarde et al. [177] as Na_3NdCl_6 [178]). Sato and Ogawa also confirmed the existence of $Na_3Nd_5Cl_{18}$ [179].

$$\frac{IP_1}{IP_2} = \frac{z_1/r_1}{z_2/r_2} \tag{4.18}$$

As Seifert et al. [180] and Gaune-Escard et al. [177] observed many compounds with the ALn_2Cl_7 stoichiometry (A=Alkali, Ln=Lanthanide) and the similar stoichiometry intermediate compound, $Na_3Nd_5Cl_{18}$ is also stable [178], we propose the existence of a NaU_2Cl_7 or $Na_3U_5Cl_{18}$ phase in the NaCl-UCl_3 system. For thermodynamic modeling purposes, we selected the NaU_2Cl_7 stoichiometry consistent with the assessment of Sun et al. [181] for the ACl-$NdCl_3$ systems that include ANd_2Cl_7 compounds.

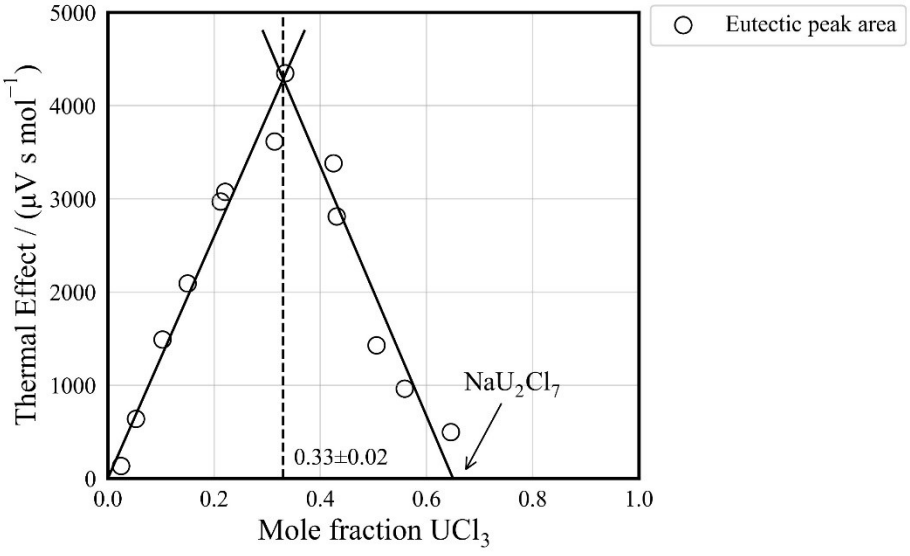

Figure 4.8: Tammann diagram showing the thermal effect for samples of NaCl-UCl_3 evaluated upon cooling at 5 K min^{-1}.

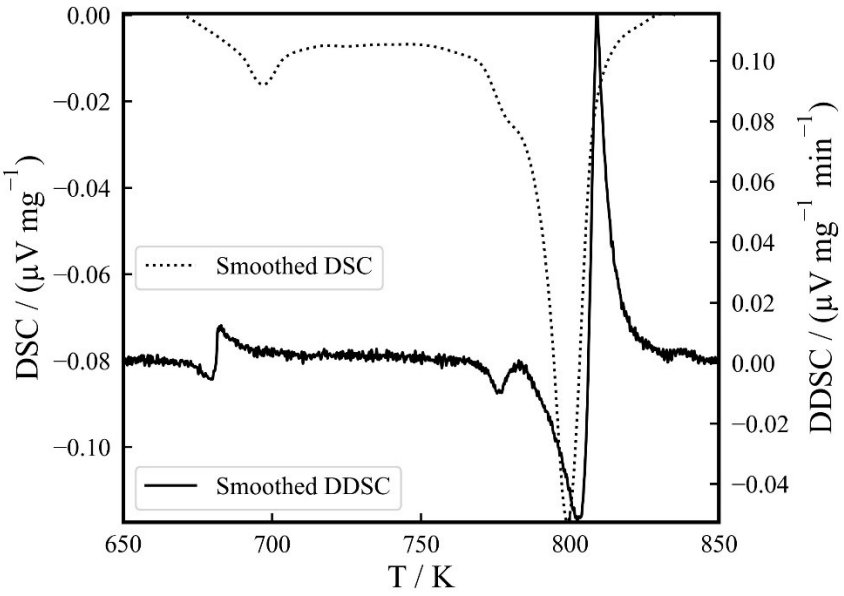

Figure 4.9: DSC and differential of DSC measurements on heating at 5 K min^{-1} of a 33.4mol% mixture of UCl_3 in NaCl.

We further investigated the possibility of an intermediate compound in the NaCl-UCl_3 system by characterizing a previously equilibrated 33mol% UCl_3 sample using high-temperature powder XRD. The patterns were taken at 300, 573, and 723K (Figure 4.10) and indicate the presence of NaCl (peaks at 2θ = 14.25°and 20.20°), at least one unidentified phase associated with 2θ values of 6.2°, 6.9°, and 10.8° and the absence of peaks for UCl_3, implying an intermediate phase lies between the endmembers at higher NaCl concentrations. As NaU_2Cl_7 represents the more frequently observed alkali lanthanide double chloride stoichiometry and agrees well with the composition inferred from the DSC measurements in Figure 4.8, an intermediate phase of this stoichiometry is likely to exist in the system. In Figure 4.10, the peaks associated with the unknown compound are present after the high-temperature XRD measurement on cooling to room temperature. We attribute these peaks to the persistence of a metastable phase below the peritectoid decomposition temperature.

Although a model utilizing the MQMQA was produced by Rose and Thomas [182], a reassessment was necessary to include the liquid $\Delta_{\mathrm{mix}}H$ values from Matsuura et al [145], the additional measurements of Table 4.5, and the proposed high temperature intermediate compound NaU_2Cl_7. Liquid interaction parameters are given in Equations (4.19) through (4.23). The SNN CN ratio of 1.2:3 between the Na^+ and U_2^{6+} cations was selected to allow the eutectic to form near 34mol% UCl_3. The calculated phase diagram in Figure 4.11 conforms well to the known phase equilibria. Figure 4.1 shows very good agreement between the calculated and experimental liquid $\Delta_{\mathrm{mix}}H$. The estimated liquid $\Delta_{\mathrm{mix}}C_{\mathrm{p}}$ shown in Figure 4.3 also agrees well with the calculated value in Figure 4.2.

$$\Delta \mathrm{G}_{\mathrm{NaU_2/Cl}} = -23650 + 2T + 0.9T\ln(T) \tag{4.19}$$

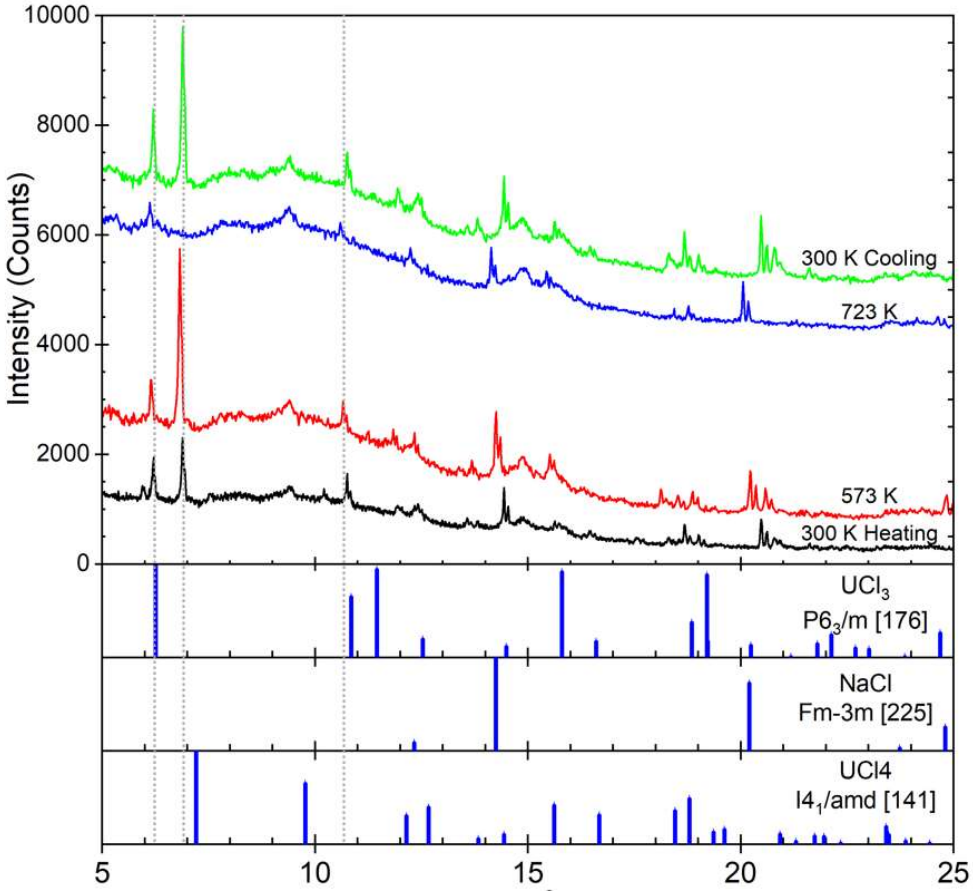

Figure 4.10: High-temperature powder XRD of NaCl-33mol%UCl_3. Dotted lines indicate peaks associated with an unidentified phase.

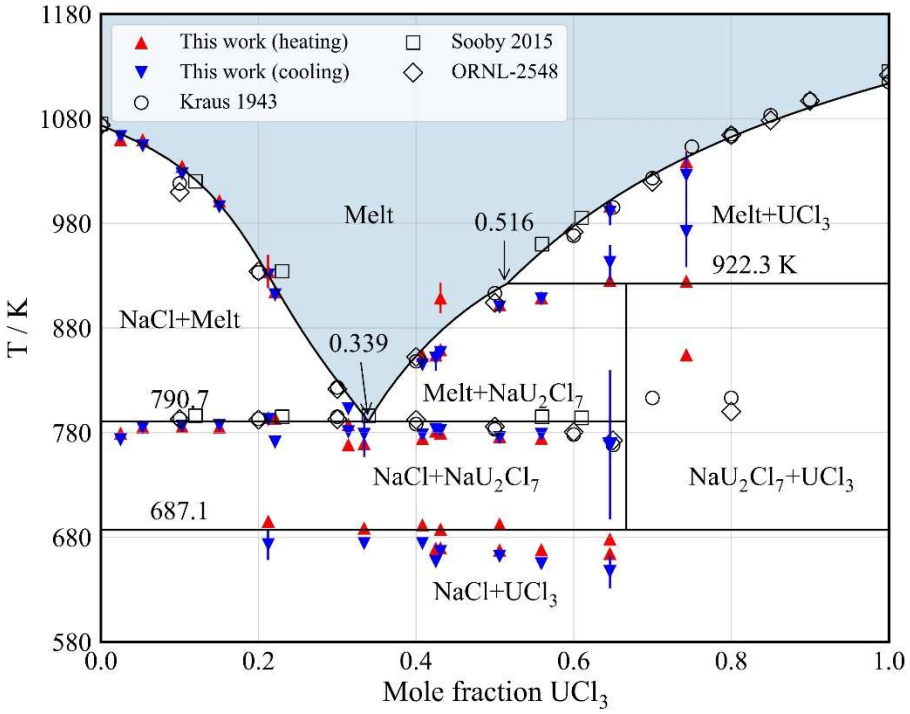

Figure 4.11: Calculated phase diagram of the NaCl-UCl_3 system with phase equilibria measurements. Expanded uncertainty intervals are shown for measurements with U(*T*)>10K.

$$\Delta G_{NaU_2/Cl} = -15850\chi_{U_2Na} \quad (4.20)$$

$$\Delta G_{NaU_2/Cl} = (4500 - 9T)\chi_{NaU_2} \quad (4.21)$$

$$\Delta G_{NaU/Cl} = -24500 - 2T \quad (4.22)$$

$$\Delta G_{NaU/Cl} = -3T\ln(T)\chi_{UNa} \quad (4.23)$$

KCl-UCl_3

There is some uncertainty regarding the intermediate compounds in the KCl-UCl_3 system. The K_2UCl_5 phase is uniformly accepted with disagreement about the presence of the high-temperature compound K_3UCl_6 which is absent from the reports of Kraus [27], and Hames et al. [114], however, it is included in Rycerz et al. [146] thermodynamic assessment, and in the experimental phase diagram of Suglobova et al. [31]. The ionic potential ratio ($IP_{K+}/IP_{U3+} = 0.248$) correlation for the KCl-UCl_3 system indicates that three compounds are likely to exist, with at least one melting incongruently [177]. This together with the observed thermal events at temperatures below the well-established eutectic temperature near 20mol% UCl_3 [31,146], provide a substantial argument for the presence of the high-temperature compound K_3UCl_6, which we included in our assessment of the system.

An additional intermediate compound is possible based on an analysis like that which identified NaU_2Cl_7. The existence of an intermediate compound with stoichiometry near 66% UCl_3 is suggested by the stability of the analogous KNd_2Cl_7 phase [178]. Finally, a similar stoichiometry compound, $K_3U_5Cl_{18}$, was found by Lexa et al.[183] in powder XRD studies of LiCl-KCl-UCl_3 eutectic compositions. While there is substantial support for of the presence of another intermediate phase, current information is inadequate to allow its identification.

The phase equilibria studies of this system [27,31,114] are in poor agreement, except with regard to the temperatures and compositions of the liquidus and eutectic below 20mol% UCl_3. We performed additional DSC measurements to help resolve some of the disparities in the reported phase equilibria above 20mol% UCl_3, and in these measurements, we observed kinetic effects in the K_2UCl_5 liquidus measurements which complicated the identification of the liquidus. Figure 4.12 shows the progressive development of the liquidus near 861K as the DSC scan heating rate is reduced, which signals the system has not equilibrated.

Further insight into the intermediate compound formation in the system KCl-UCl_3 is found in the two endothermic peaks of Figure 4.12 near the eutectic temperature of 812K. As can be seen from Figure 4.12, what can be interpreted as a single eutectic peak at a heat rate of 10 K min^{-1} reveals a likely intermediate phase at a heat rate of 5 or 2 K min^{-1}. Thus, the use of disparate scan rates can be a source of the disparity in the reported eutectic temperatures for compositions >33mol% UCl_3.

Using a DSC calibrated at 2 K min^{-1}, we measured five samples of the compositions in Table 4.6. Each sample was subjected to mechanical agitation for 30 min at 100K above the expected liquidus temperature, followed by rapid quenching to room temperature, and subsequent annealing at 723K for six hours. However, this procedure proved to be insufficient to fully equilibrate the mixtures, although there was some improvement in detecting the liquidus. The measurements in Table 4.6 confirm the liquidus identified by the cooling measurements of Suglobova and Chirkst [31].

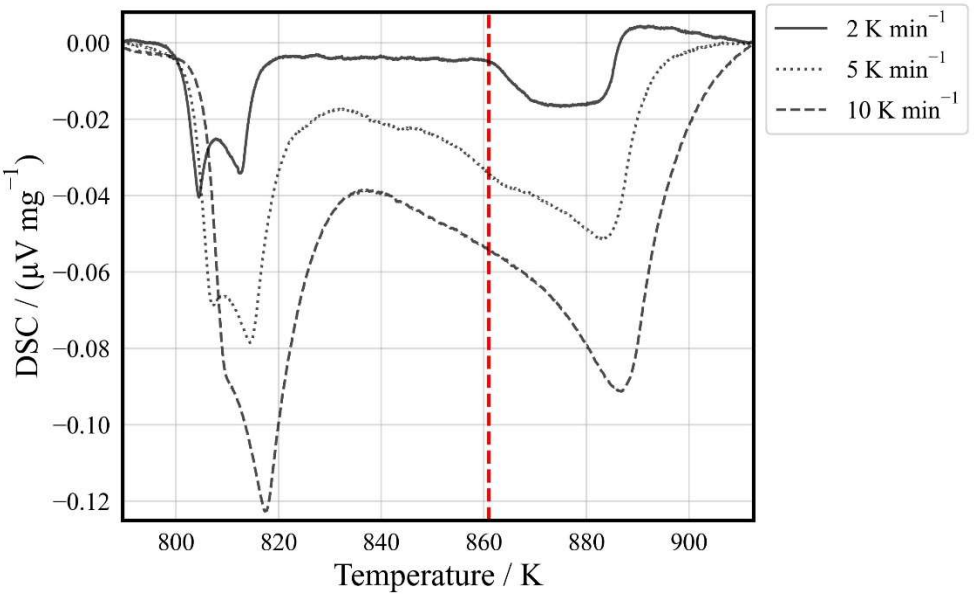

Figure 4.12: Uncalibrated DSC traces generated at 2, 5, and 10 K min^{-1} heat rates for KCl-42mol% UCl_3.The vertical line indicates the temperature of the liquidus.

Table 4.6: DSC measurements of the KCl-UCl_3 system. Samples annealed for 6 hours at 723K.

Mole fraction UCl_3	Equilibrium reaction	Type of equilibrium	Heating / K[a]
0.051	$KCl(s) + K_3UCl_6(s) \leftrightarrow L$	Eutectic	866.6
	$KCl(s) + L \leftrightarrow L'$	Liquidus	1022.7
0.329	$K_3UCl_6(s) + K_2UCl_5(s) \leftrightarrow L$	Eutectic	860.8
	$K_2UCl_5(s) + L \leftrightarrow L'$	Liquidus	885.5
0.419	$K_2UCl_5(s) + UCl_3(s) \leftrightarrow KU_2Cl_7(s)$	Peritectoid	800.5
	$K_2UCl_5(s) + KU_2Cl_7(s) \leftrightarrow L$	Eutectic	808.6
	$K_2UCl_5(s) + L \leftrightarrow L'$	Liquidus	854.1
0.498	$K_2UCl_5(s) + UCl_3(s) \leftrightarrow KU_2Cl_7(s)$	Peritectoid	796.5
	$K_2UCl_5(s) + KU_2Cl_7(s) \leftrightarrow L$	Eutectic	809.6
0.575	$K_2UCl_5(s) + UCl_3(s) \leftrightarrow KU_2Cl_7(s)$	Peritectoid	798.5
	$K_2UCl_5(s) + KU_2Cl_7(s) \leftrightarrow L$	Eutectic	818.9
	$KU_2Cl_7(s) \leftrightarrow UCl_3(s) + L$	Peritectic	886.4

[a] U(T)=2 K (95% CI ~2σ)

While the phase equilibria for the KCl-UCl_3 system have been thoroughly studied [27,31,114,184], and assessments performed by Ghosh et al. [30] and later by Rose and Thomas [182], a reassessment was required since the earlier works did not consider the $\Delta_{\mathrm{mix}}H$ measurements of Rycerz et al. [146] as these were previously unavailable. In the reassessment, the computed values of $\Delta_{\mathrm{mix}}H$ agree within the experimental uncertainty. The calculated liquid $\Delta_{\mathrm{mix}}C_{\mathrm{p}}$ also agrees with the Figure 4.3 predicted value within the expected uncertainty interval. The MQMQA parameters are listed in Equations (4.24)-(4.28), together with the Gibbs energy relations for the phases, yielding the computed phase diagram of Figure 4.13 which well describes the collective phase equilibria.

$$\Delta \mathrm{G}_{\mathrm{KU_2/Cl}} = -34432 + 0.5T \tag{4.24}$$

$$\Delta \mathrm{G}_{\mathrm{KU_2/Cl}} = -22000 + 2.5T\ln(T)\chi_{\mathrm{U_2K}} \tag{4.25}$$

$$\Delta \mathrm{G}_{\mathrm{KU_2/Cl}} = -5000\chi^2_{\mathrm{KU_2}} \tag{4.26}$$

$$\Delta \mathrm{G}_{\mathrm{KU/Cl}} = -39600 \tag{4.27}$$

$$\Delta \mathrm{G}_{\mathrm{KU/Cl}} = -4.5T\ln(T)\chi_{\mathrm{UK}} \tag{4.28}$$

Ternary systems

We used the Kohler-Toop method of ternary extrapolation [127] with the pseudo-binary system interaction parameters of Equation (4.2) to obtain interpolated pseudo-ternary systems. In doing so, we considered endmembers of similar cation oxidation state as symmetric and those with dissimilar oxidation state as asymmetric, which is an accepted approach [25,185]. Pseudo-ternary parameters, $\Delta \mathrm{G}_{\mathrm{AB(C)/Cl}}$, are included as necessary to improve the representation of the phase equilibria and the available electrochemical measurements.

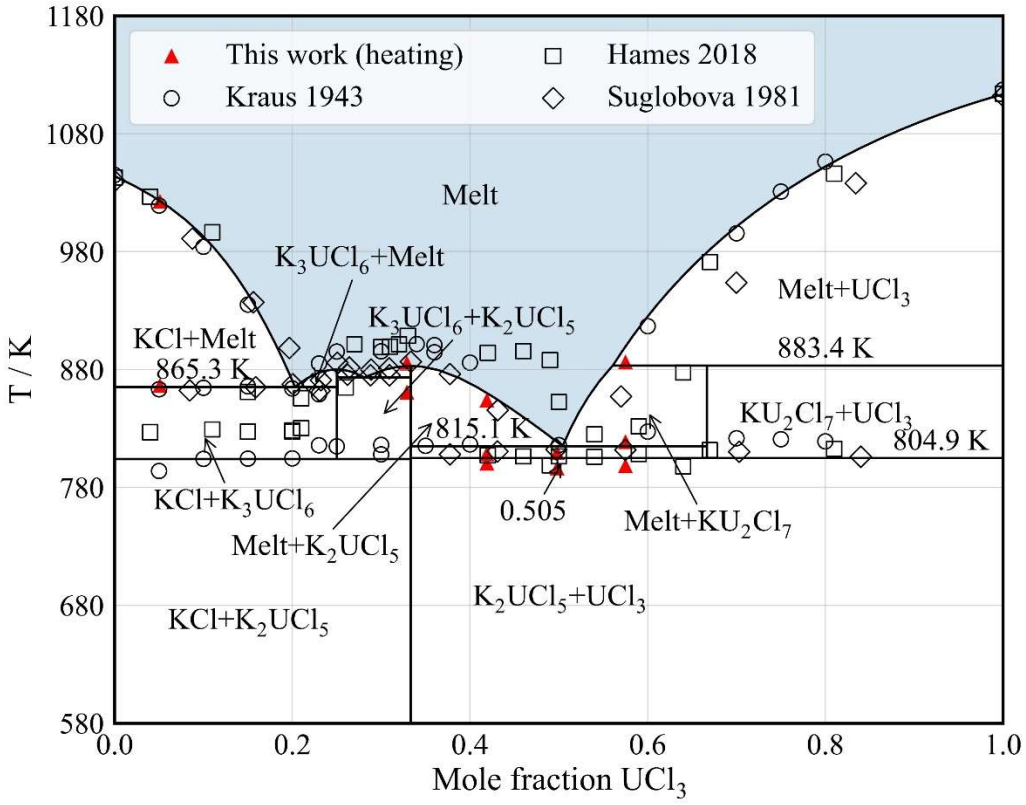

Figure 4.13: Calculated phase diagram and experimental phase equilibria [27,114,162] of the KCl-UCl_3 system

LiCl-NaCl-KCl

The system was investigated by DTA and reassessed by Lu et al. [147] using a single ternary interaction parameter for the melt, provided in Equation (4.29). The pseudo-binary subsystem excess Gibbs energy parameters for the LiCl-NaCl-KCl solid solution were given previously for the pseudo-binary subsystems in Equations (4.11), (4.13), and (4.15) and only differ from those of Lu et al. [147] in that the LiCl-KCl solid solution has a slightly expanded solubility limit. The calculated phase diagram in Figure 4.14 is in excellent agreement with the measurements of Lu et al. [147].

$$\Delta G^{001}_{KNa(Li)/Cl} = -2900 \quad (4.29)$$

LiCl-NaCl-UCl_3

This system is assessed for the first time using the only set of experimental phase equilibria which is from Desyatnik and Dubinin [186]. We performed DSC measurements at two additional compositions (Table 4.7), however, the second measurement at 26.3mol% UCl_3 was less certain in composition due to reusing the 18.2mol% sample through direct addition of a small amount of UCl_3. The single ternary interaction parameter determined in the assessment is provided in Equation (4.30).

As the representation of the LiCl-NaCl solid solution provides too negative a Gibbs energy to allow a proper description of the phase equilibria, the LiCl-NaCl-UCl_3 invariant temperature and composition were calculated without the LiCl-NaCl solid solution as 656.2K at 43.1LiCl-36.5NaCl-20.3mol%UCl_3, which differ from the value of 638K at 46LiCl-25.5NaCl-28.5mol% UCl_3 determined by Desyatnik and Dubinin [186]. However, the assessment calculated value agrees well with our measurements which indicate an invariant temperature of 653.6±2K. The discrepancy with the stability of the LiCl-NaCl solid solution remains unresolved since corrections to the LiCl-NaCl solid solution are

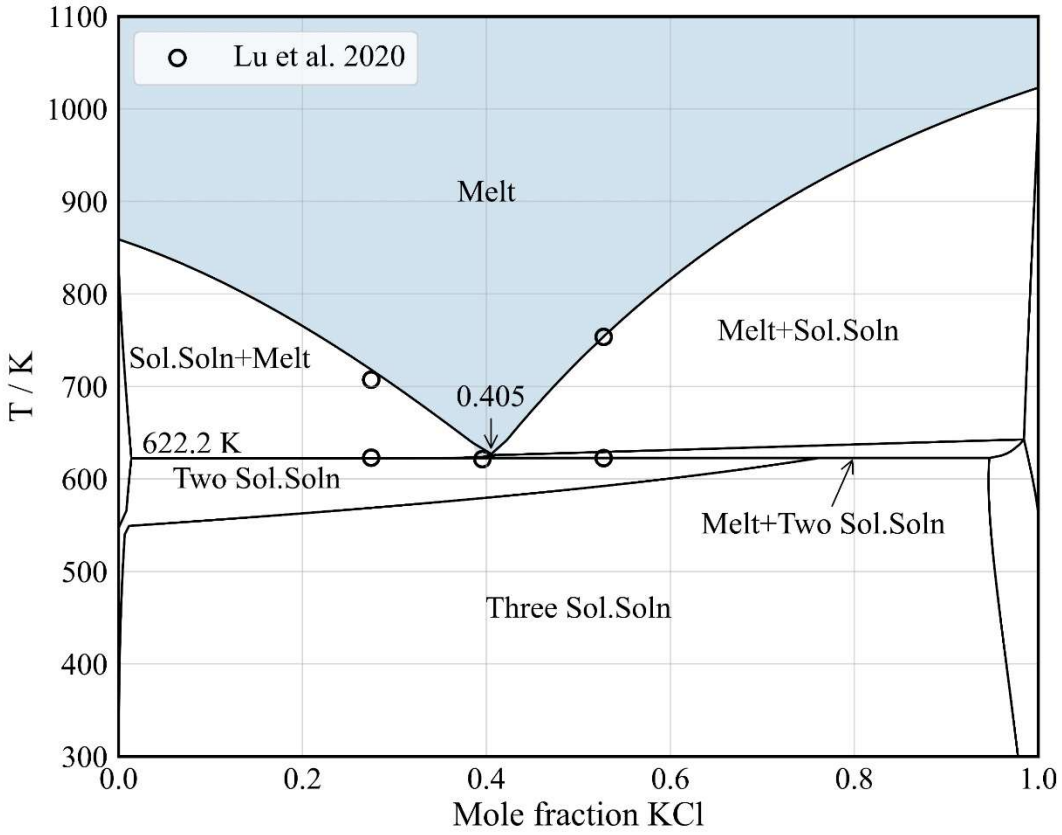

Figure 4.14: Calculated phase diagram and experimental phase equilibria [147] of the LiCl-KCl section with constant 9mol% NaCl.

Table 4.7: DSC events of the LiCl-NaCl-UCl_3 system.

Mole fraction			Equilibrium reaction	Type of equilibrium	Heating / K[a]
LiCl	NaCl	UCl_3			
0.402	0.416	0.182	Sol.Soln + UCl_3(s) ↔ L	Eutectic	653.4
			UCl_3(s) ↔ Solid Soln. + L	Peritectic	718.1
			Sol.Soln + L ↔ L'	Liquidus	784.0
0.362	0.375	0.263	Sol.Soln + UCl_3(s) ↔ L	Eutectic	653.7
			Sol.Soln↔UCl_3(s) + L	Peritectic	717.5
			UCl_3 + L ↔ L'	Liquidus	768.4

[a] U(*T*) = 2 K (95% CI ~2σ)

avoided as they would require the reassessment of several related systems, which are currently well-represented. The phase diagram of Figure 4.15 is calculated from Equation (4.30).

$$\Delta G^{101}_{NaU(Li)/Cl} = -6000 \quad (4.30)$$

LiCl-KCl-UCl_3

This pseudo-ternary system was assessed by Ghosh et al. [30] who considered the measurements of Thamer [37], Nakakyoshi [171], and Desyatnik and Dubinin [187], however, the system required reassessment here as the solution models are not compatible *MSTDB-TC*. In the reassessment, we also included the more recent measurements of Hames et al. [114] which describe the LiCl-KCl-UCl_3 system as two single eutectic subsystems, namely LiCl-KCl-K_2UCl_6, and LiCl-K_2UCl_6-UCl_3.

The pseudo-ternary diagram of

Figure 4.16 is calculated using the interaction parameters of Equations (4.31) through (4.34) and reproduces the experimental measurements of Nakayoshi et al. [171] very well. The measurements of Desyatnik and Dubinin [187] were not utilized due to very poor agreement with the other datasets. In total, 32 experimental liquidus data points were considered in the reassessment. The resulting computed pseudo-ternary liquidus projection, in Figure 4.17, has an average calculated temperature deviation of 12.2K, and of these, only 3 points deviate by more than 25K.

$$\Delta G^{001}_{LiU_2(K)/Cl} = -7700 \quad (4.31)$$

$$\Delta G^{102}_{KU_2(Li)/Cl} = -22000 \quad (4.32)$$

$$\Delta G^{101}_{KU(Li)/Cl} = 17000 \quad (4.33)$$

$$\Delta G^{001}_{KU(Li)/Cl} = -17500 \quad (4.34)$$

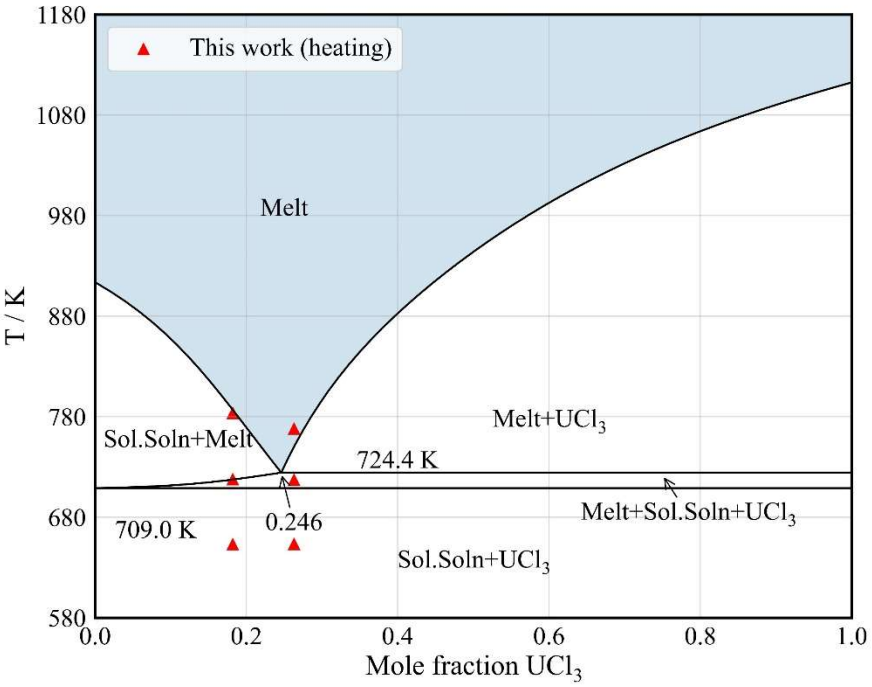

Figure 4.15: Pseudo-ternary phase diagram for the LiCl-NaCl-UCl_3 system with a fixed 50.9mol%NaCl-49.1mol%LiCl relative content. The measurement at 26.3mol% UCl_3 has an estimated ±3% composition expanded uncertainty (95% CI ~2σ).

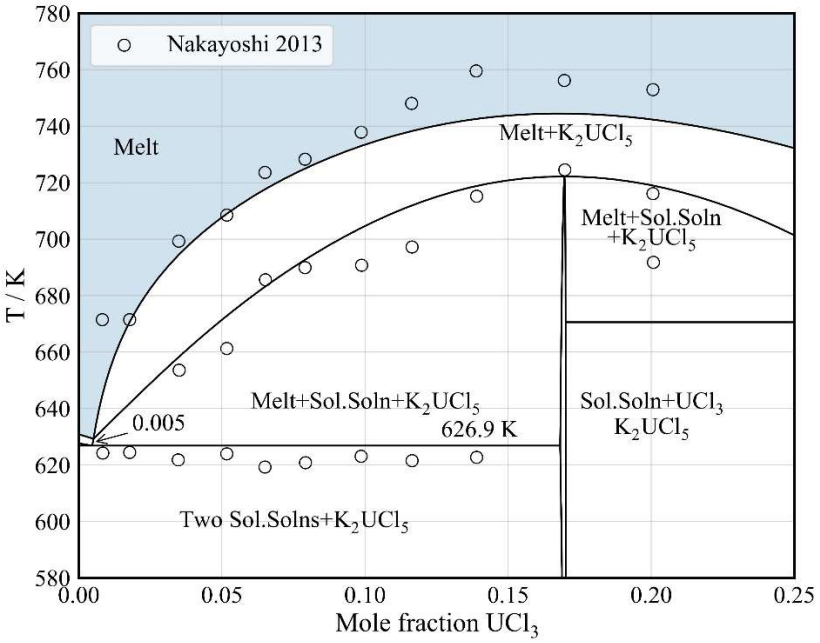

Figure 4.16: Isopleth of UCl_3 in 59:41 molar LiCl-KCl eutectic.

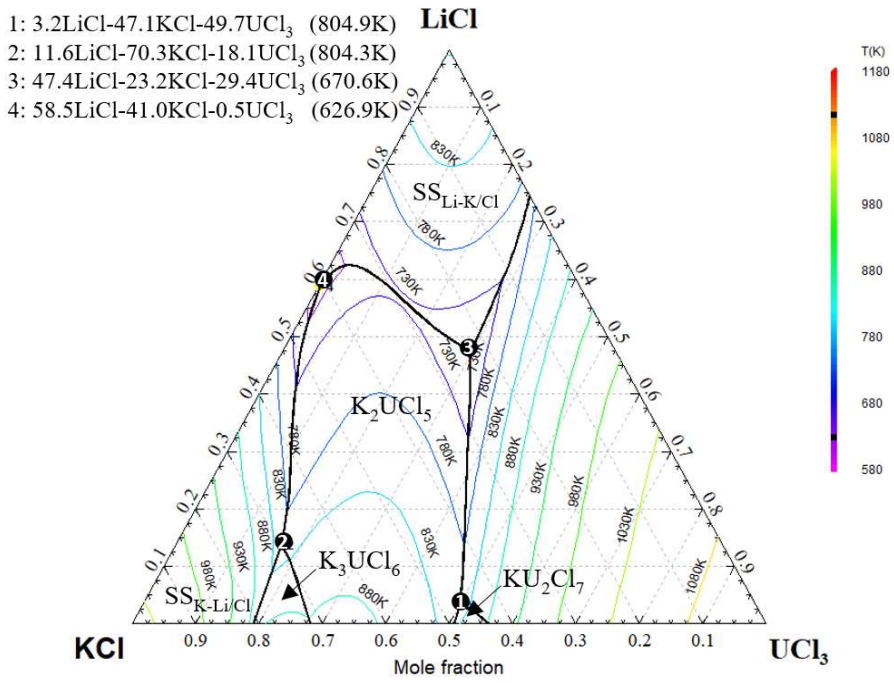

Figure 4.17:Liquidus projection of the LiCl-KCl-UCl_3 system.

The LiCl-KCl eutectic is a common electrolyte for electromotive force measurements (EMF) and several studies involving UCl_3 were reviewed by Caligara et al [188]. Ghosh et al. [30] also measured the EMF of the $U^{3+}|U$ redox couple, although the values do not well fit the theoretical Nernst slope [189]. Using the method described by Caligara et al. [188], a consistent means was used to calculate activity coefficients from the measurements of Knacke et al. [190] and Caligara et al. [188] near 0.2mol% UCl_3 and were found to agree well.

To compare the EMF-determined activity coefficient for UCl_3 with that computed from the assessed liquid model, we applied Equations (4.35) and (4.36) where μ_i° is the standard state chemical potential, a_{liq} and γ_{liq} are the activity and activity coefficient, respectively, of UCl_3 in the melt, and P is the partial pressure of UCl_3 vapor above the melt. The results are given in Figure 4.18 and agree well with the γ_{liq} calculated from the EMF measurements of Caligara et al. [188] and Knacke et al. [190].

$$\mu_{liq}^{\circ}(T) + RT\ln(a_{liq}) = \mu_{gas}^{\circ}(T) + RT\ln(P / Pa) \quad (4.35)$$

$$a_{liq} = \gamma_{liq} x_{liq} \quad (4.36)$$

NaCl-KCl-UCl_3

Although this pseudo-ternary system was already assessed by Yin et al. [168] and Rose and Thomas [182] a reassessment was required since their thermodynamic assessment did not consider the available equilibria measurements of Desyatnik et al. [34] or Thamer [37]. To complement the available phase equilibria measurements, we performed an additional five measurements, Table 4.8, along two isopleths, with the first two along the NaCl-KCl eutectic toward the UCl_3 vertex (Figure 4.19) and three from K_2UCl_5 toward the NaCl vertex (Figure 4.20).

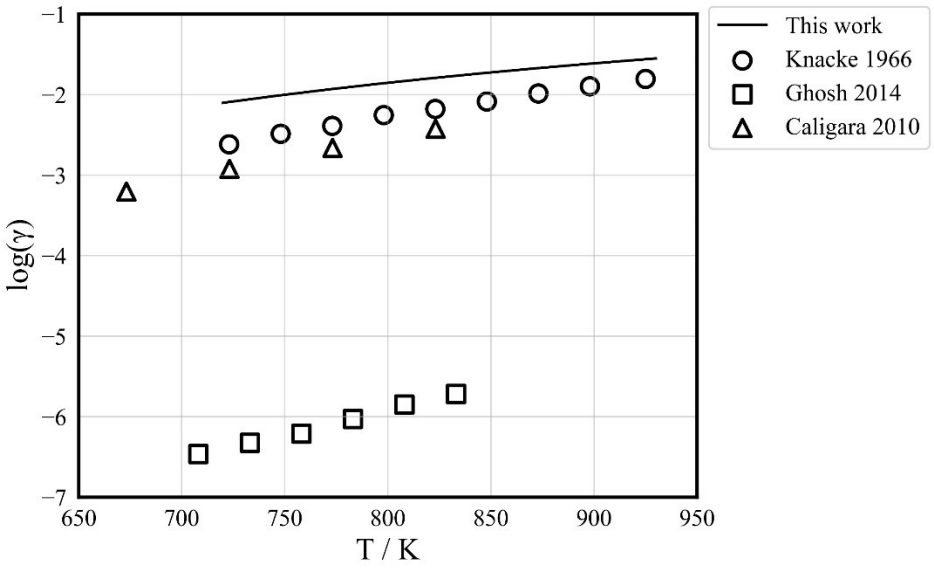

Figure 4.18: Liquid UCl_3 activity coefficient (relative to liquid reference state) at infinite dilution in LiCl-KCl eutectic solvent. The EMF values [30,190,191] were recalculated for consistency using the $Cl_2|Cl^-$ reference electrode as defined by Caligara et al.[188].

Table 4.8: DSC measurements of the NaCl-KCl-UCl_3 system.

Mole fraction			Equilibrium reaction	Type of equilibrium	Heating / K[a]
NaCl	KCl	UCl_3			
0.475	0.475	0.05	Sol. Soln + L ↔ L’	Liquidus	919.4
0.437	0.437	0.126	Sol. Soln + K_2UCl_5(s) ↔ L Sol. Soln + L ↔ L’	Eutectic Liquidus	787.3 885.7
0.148	0.566	0.286	Sol. Soln + K_2UCl_5(s) ↔ L K_2UCl_5(s) + L ↔ L’	Eutectic Liquidus	787.5 851.2
0.285	0.478	0.237	K_2UCl_5(s) ↔ Sol.Soln + L Sol.Soln + L ↔ L’	Peritectic Liquidus	786.4 805.3
0.546	0.302	0.152	K_2UCl_5 ↔ K_2UCl_5’ + L K_2UCl_5 ↔ Sol. Sol + Melt Sol. Sol + L ↔ L’	Solidus Peritectic Liquidus	782.9 807.7 928.2

[a] U(*T*)=2 K (95% CI ~2σ)

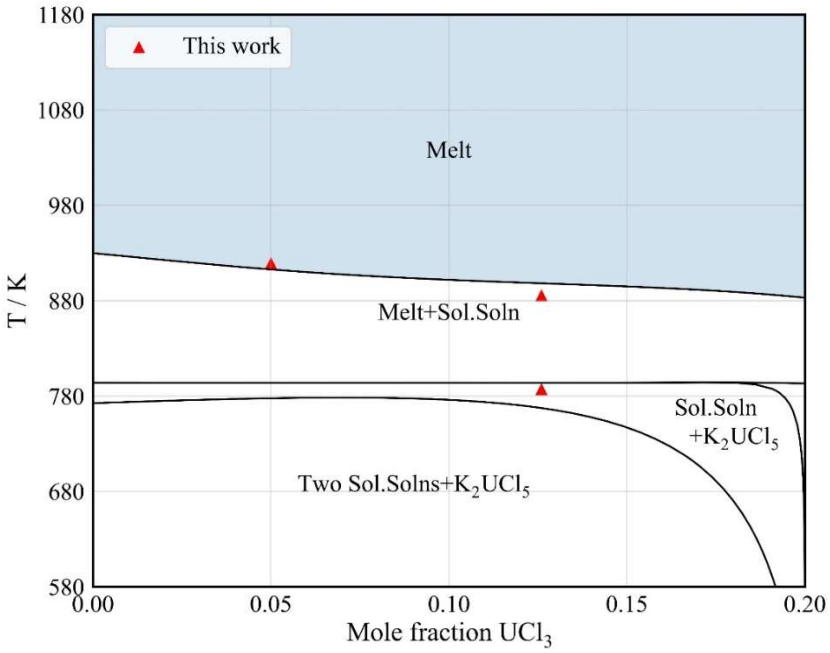

Figure 4.19: Isopleth of UCl_3 in 1:1 molar NaCl-KCl and the measurements of this work

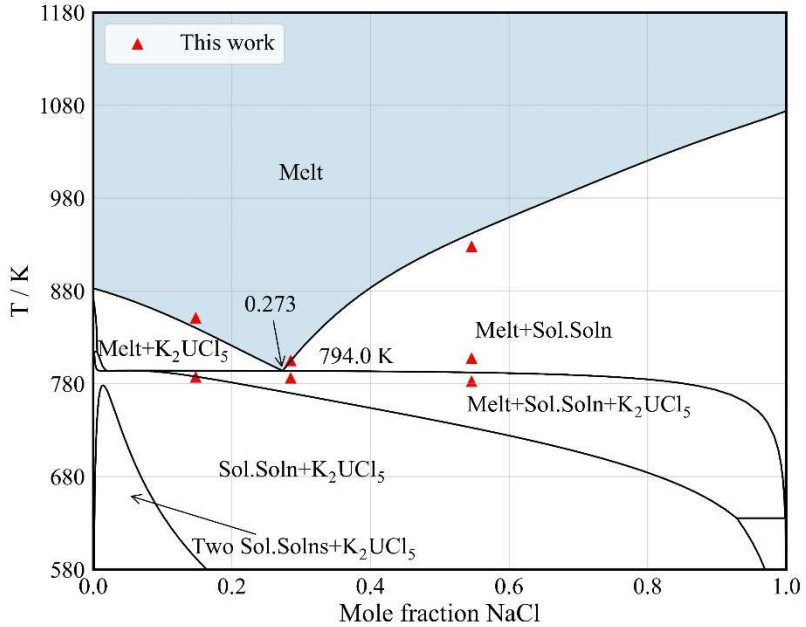

Figure 4.20: Isopleth of UCl_3 in K_2UCl_5. Data points from Desyatnik et al. [34] were extracted graphically..

NaCl-KCl is not commonly used as an electrolyte in UCl_3 EMF studies with only the measurements of Smirnov and Skiba [192] and those of Flengas et al. [193] available. In the review by Caligara et al. [188], the reported $U^{3+}|U$ potentials of Smirnov and Skiba [192] and Flengas et al. [193] differ from each other by 49mV. We recalculated their liquid UCl_3 activity coefficients for comparison with those derived from our representation of the melt using Equations (4.35) and (4.36), and found good agreement among the measured and calculated values (Figure 4.21).

The pseudo-ternary MQMQA interaction parameters resulting from the assessment are given in Equations (4.37) through (4.40), with the resulting calculated liquidus projection (Figure 4.22) being in good agreement with the experimental phase diagram of Desyatnik et al. [34]. The measurements of Thamer [37] could not be adequately represented by the assessment as they are too high in temperature and fail to agree with the determined eutectic temperature of the KCl-UCl_3 system.

$$\Delta G^{103}_{KU(Na)/Cl} = -15000 \quad (4.37)$$

$$\Delta G^{001}_{NaU_2(K)/Cl} = -18000 \quad (4.38)$$

$$\Delta G^{001}_{KU_2(Na)/Cl} = -3000 \quad (4.39)$$

$$\Delta G^{001}_{KU_2(U)/Cl} = -3000 \quad (4.40)$$

Discussion

In the summary of phase equilibria for pseudo-binary salt systems presented by Sangster and Pelton [160], there are many that use values and models compatible with *MSTDB-TC* [24]. Lu et al. [147] refined the solid solution in the LiCl-NaCl-KCl pseudo-ternary, resulting in an assessment that suitably represents the phase equilibria and liquid $\Delta_{mix}H$. We adopted this assessment since it is used in many systems already described in

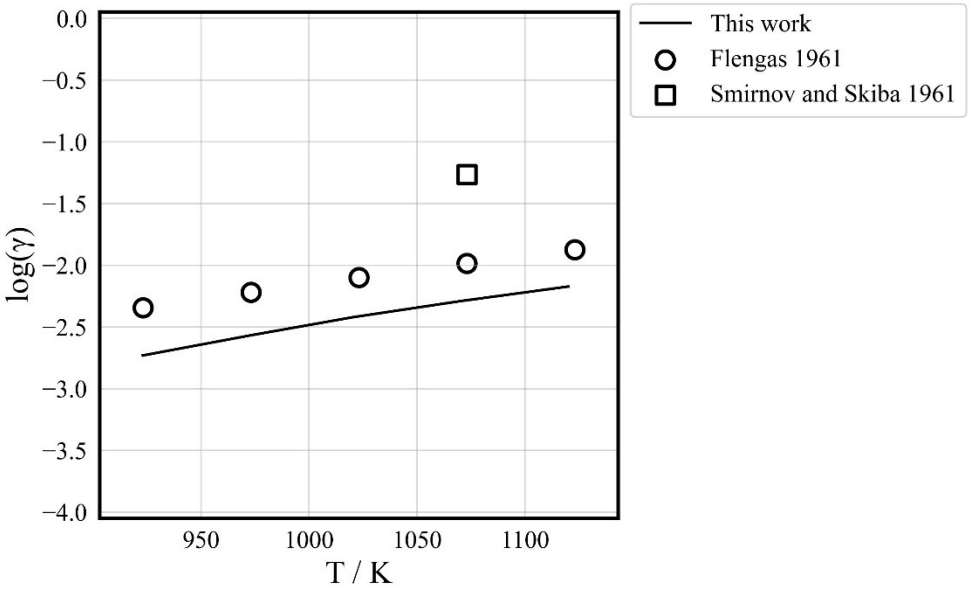

Figure 4.21: Liquid UCl_3 activity coefficient (relative to liquid reference) at infinite dilution in NaCl-KCl eutectic solvent. The EMF data [192,193] were recalculated for consistency using the $Cl_2|Cl^-$ reference electrode defined by Flengas et al.[193].

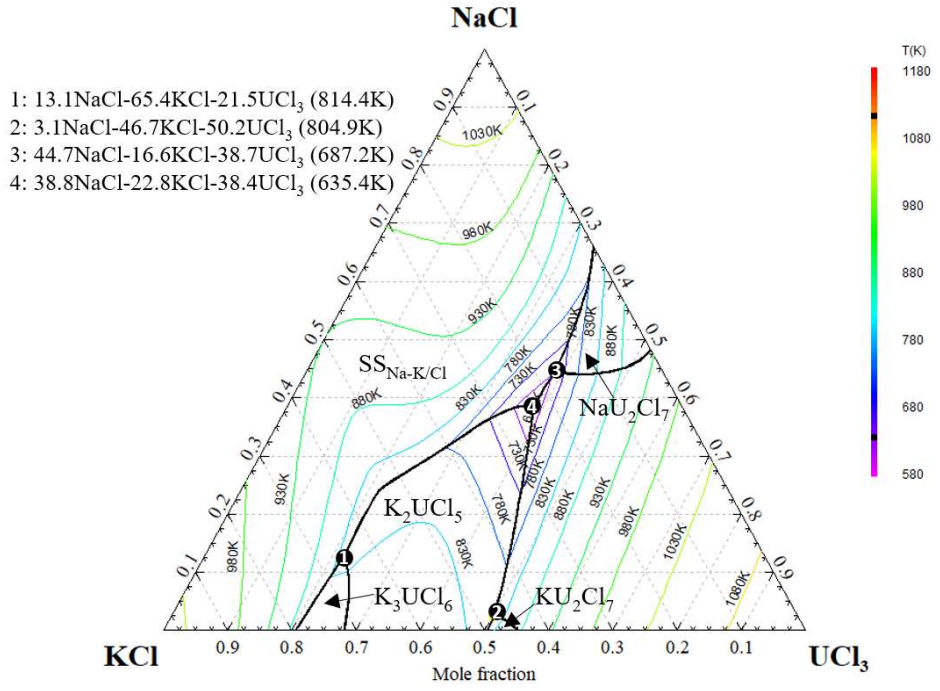

Figure 4.22: Liquidus projection of the NaCl-KCl-UCl_3 system.

our database. However, their present description of the solid solution cannot adequately represent the related phase transitions in our assessments for LiCl-NaCl-UCl_3 and NaCl-KCl-UCl_3. Additionally, Lu's liquid model does not include an interaction parameter for describing $\Delta_{\mathrm{mix}}C_{\mathrm{p}}$, as it does not include a $T\ln(T)$ term. This is an issue for the LiCl-KCl eutectic as it has an average liquid $\Delta_{\mathrm{mix}}C_{\mathrm{p}}$ of 5.75 J $mol^{-1}K^{-1}$ as measured by Korin and Soifer [166], which is not well represented by the present model's calculated value of only 0.46 J $mol^{-1}K^{-1}$ at 1000K for the eutectic composition.

Ghosh et al. [30] examined the LiCl-KCl system at 3, 5, 95, and 97mol% LiCl and determined a solid solubility limit of 5mol% for either endmember. Our reinterpretation of the results, however, indicates the solubility should be somewhat less. Since measurement of the eutectic transition enthalpy at the extremes of pseudo-binary phase diagrams will have very small values there is much larger uncertainty than at higher molar contents, and so it is unlikely that Ghosh et al. [30] could reliably distinguish between the eutectic and solvus based on only four measurements. As the liquid fraction is zero at the limit of solid solubility, we think it more likely that their measurements at 3, and 97mol% represented the eutectic, and thus, the solubility limit must be <1mol%. Our conclusion agrees well with that of Sangster and Pelton [160], who exclude any solid solubility based on the limiting slope of the liquidus.

In the NaCl-UCl_3 system (Figure 4.11), there are three DSC events for the compositions 43.1, 50.6, and 74.3mol% UCl_3 to which we were not able to attribute the cause to the presence of any known phases. They are the low-temperature transitions on heating of 699.8±1.6K, 667.8±1.3K, and 854.4±12.9K, and are in poor agreement with the cooling measurements of 666.3±0.9K, 661.7±5.4K, and 902.7±3.7K, respectively. The

lack of formation or decomposition of the NaU_2Cl_7 compound in the 74.3mol% measurement is particularly important as it suggests that our description of the high uranium-containing phases is incomplete. The measurements may be related to compound formation kinetics, but regardless, they indicate the need to further investigate the NaCl-UCl_3 system at UCl_3 contents >60mol%.

In contrast to this work, Barton [26] and Krause [27] do not observe AU_2Cl_7 intermediate compounds and instead note eutectic transitions at concentrations above 66mol% UCl_3 in the NaCl-UCl_3 and KCl-UCl_3 systems. Their measurements relied upon the EMF response from an immersed thermocouple which requires detection of thermal arrests upon cooling, a technique that is insensitive to compound formation as kinetic factors can prevent phase formation at a sufficiently rapid cooling rate. The tendency to observe an apparent eutectic instead of compound formation is commonly observed in DTA/DSC measurements performed on cooling. Rycerz et al. [172] reported such phenomena in their DSC measurements on cooling in the RbBr-$DyBr_3$ system, in which the incomplete formation of the incongruently melting $RbDy_2Br_7$ allowed some solid $DyBr_3$ to coexist with the melt. Thus, upon continued cooling, the eutectic between the melt and $DyBr_3$ was also observed. Similarly, the large temperature difference between the melting point of UCl_3 and incongruent melting point of AU_2Cl_7 allows reaction kinetics to limit the formation of AU_2Cl_7 during cooling. The result is the analogous observation of UCl_3 present with the melt, and thus, all lower temperature thermal events associated with UCl_3, such as the NaCl-UCl_3 eutectic reaction, are observed during cooling.

Desyatnik and Dubinin [186], determined LiCl-NaCl-UCl_3 to contain a single eutectic system with a low melting point of 638±2K at 46LiCl-28.5NaCl-25.5UCl_3mol%.

While our measurements indicate reasonable agreement with an invariant point temperature of 653.6±2K, our representation of the system does not allow the calculation of an invariant point composition due to the relative stability of the LiCl-NaCl solid solution To address this issue will require additional measurements in the low UCl_3 composition region as well as a reassessment of the LiCl-NaCl pseudo-binary solid solution considering additional equilibria information for the LiCl-NaCl-UCl_3 and NaCl-KCl-UCl_3 systems.

In the LiCl-KCl-UCl_3 system, the phase equilibria of Desyatnik et al. [187] could not be reasonably included in our assessments due to their disagreement with all other sets of values. In Table 4.9, the pseudo-ternary invariant temperatures and compositions of Desyatnik and Dubinin [186], Hames et al. [114], and Ghosh et al. [30] are compared with our calculated values. Our calculated invariant temperature and composition agree with those of Ghosh et al. [30] for invariant 4 of Figure 4.17. Our calculated invariant 3 composition also agrees with that of Ghosh et al. [30], however, the temperatures do not. In the range of compositions of the highest interest, the present assessment provides a good description of the known measurements.

An experimental phase diagram for the NaCl-KCl-UCl_3 system is available from Desyatnik [34], however, the data for only a single isopleth were provided in the publication. Two invariant points are given with temperatures of 713.2±2K and 691.2±2K and compositions of 24NaCl-60KCl-15UCl_3mol% and 47NaCl-30KCl-33UCl_3mol%, respectively. Using our representation of the system, we were unable to obtain the lower melting invariant point due to the relative stability of the NaCl-KCl solid solution. This indicates that the system interaction parameters will need to be revised based on a

Table 4.9: Composition and temperatures of invariants in the LiCl-KCl-UCl_3 system (Figure 4.17).

Invariant 4				Invariant 3				
LiCl	KCl	UCl_3	Temperature / K	LiCl	KCl	UCl_3	Temperature / K	Reference
29.5	58.5	12.0	608.2±2	38	30.5	31.5	668.2±2	[186]
50	42	8	619±1	42	25	33	681±6	[114]
58.5	41.0	0.5	626.9	47.4	23.2	29.4	670.6	This work[b]
57.6	41.9	0.005	625	45.6	21.3	33.1	702	[30][a]

[a] author reported uncertainties, assumed to be U(*T*) (95% CI ~2σ).
[b] Calculated.

reassessment of the NaCl-KCl system informed by higher-order phase equilibria involving UCl_3.

The phase equilibria determination for the NaCl-KCl-UCl_3 system of Thamer et al. [37] could not be satisfactorily reproduced using our representation, yet it exhibited good agreement with other experimentally determined values. The highest temperature DTA measurements were determined by Thamer et al. [37] for the isopleth ratio of 48:52 molar UCl_3 to KCl containing 20.4, 20.9, and 30.3mol% NaCl are 840K, 828K, and 808K respectively. Considering the liquidus temperature at 48mol% UCl_3 in the KCl-UCl_3 pseudo-binary is only 825.8K, our representation fails to reproduce these values without somehow increasing the KCl-UCl_3 eutectic temperature by ~14K, which would disagree with the current measurements for the pseudo-binary system.

Conclusions

In this work, LiCl-NaCl-KCl-UCl_3 salt system thermodynamic assessments were developed using classic CALPHAD techniques. These are the product of the first-time thermodynamic assessment of the LiCl-NaCl-UCl_3 system in addition to the reassessments of the LiCl-UCl_3, NaCl-UCl_3, KCl-UCl_3, LiCl-KCl-UCl_3, and NaCl-KCl-UCl_3 systems. Measurements of pseudo-binary and pseudo-ternary phase equilibria, $\Delta_{\mathrm{mix}}H$, $\Delta_{\mathrm{mix}}C_{\mathrm{p}}$, and EMF were used to generate the Gibbs energy representations of the phases. Previously developed correlations were applied to better inform liquid solution model development for systems lacking $\Delta_{\mathrm{mix}}H$ and $\Delta_{\mathrm{mix}}C_{\mathrm{p}}$ values. The liquid solution model employs two endmembers to represent UCl_3 to allow the mixing of their two distinct coordination behaviors and thus to represent observed variation in second nearest-neighbor coordination numbers as a function of temperature and composition, and so simulate the short-range ordering. The resulting assessed systems are seen to well-reproduce available solid-liquid

equilibria, advancing the understanding of these salt systems and providing an essential resource for thermodynamic calculations for pyrochemical and MSR applications.

It was noted that for the pseudo-quaternary assessment it was essential to use multiple scan rates for DSC measurements and their extrapolation to 0 K min^{-1} to resolve disagreements among disparate data sets for the pseudo-binary and pseudo-ternary subsystems. The measurements employed a unique uncertainty determination that exposed important issues regarding reported uncertainties for typical DSC measurements. As shown in the supplemental material, it was our experience that single scan rate calibrations are unable to capture at least 0.5K of random error for single scan rate measurements performed at ≥5 K min^{-1}. Extrapolation of DSC measurements to 0 K min^{-1} was found to minimize uncertainty due to random effects and can reveal kinetic effects which are not apparent from single scan rate measurements. The use of this method allowed a critical evaluation of likely non-equilibrium DSC thermal events that resulted in improvements to the KCl-UCl_3 phase diagram. The measurements also suggested two new compounds, NaU_2Cl_7 and KU_2Cl_7, may be stable in these systems.

The thermochemical properties calculated for the pseudo-binary salt systems investigated here should be highly reliable, with some reservation with respect to computing C_p values due to limitations in available experimental data. The properties of the pseudo-ternary melt at <33mol% UCl_3 well reproduce accepted values and thus can be considered highly reliable. The system assessments, therefore, represent a significant resource for applications of these molten salt systems, allowing for dependable property determinations and confidence in projecting system behavior. The assessed models and values in thermodynamic database form are available within *MSTDB-TC* Ver. 2.0 and

higher, which can be accessed via the Oak Ridge National Laboratory GitHub site following the instructions in the supplementary material.

Author Contributions

J.A.Y. and J.S.P. were equally responsible for the development of ideas for the manuscript, DSC analysis, and thermodynamic assessment. J.A.Y drafted the manuscript with feedback given by all authors. J.A.Y compiled and critically evaluated electrochemical data. J.S.P. performed thermal treatment of DSC samples. J.S.P. and J.A.Y compiled and critically evaluated phase equilibria, C_{p} and excess enthalpy data. J.A.Y. performed the DSC uncertainty model. M.A performed XRD sample preparation, measurement, and analysis. M.A, J.C.A., M.S.C., A.M.M., C.M.D, and T.M.B advised J.S.P. and J.A.Y. in various matters including graphical design, document structure, methodology, and statistical analysis. T.M.B. directed the research.

Acknowledgments

This research was supported by the U.S. Department of Energy Office of Nuclear Energy, Nuclear Energy Advanced Modeling and Simulation Program and administered by Oak Ridge National Laboratory, which is operated by UT-Battelle, LLC, for the U.S. Department of Energy, and funded at the University of South Carolina under subcontract no. CW21750.

The authors are grateful to Prof. Hans-Conrad zur Loye for use of the XRD facilities, Hunter Tisdale for assistance in performing the XRD measurements, and Dr. Gregory Morrison for assistance in preparing XRD specimens.

Supplementary material

DSC Calibration and Uncertainty Assessment

The metal standards and molten salt transitions listed in Table 4.10 were used to define the reference transition temperature of the calibration materials on heating and

Table 4.10: Calibration materials.

Material	Transition	Temp./°C	Reference
Indium	S → L	156.5985	[194]
Lead	S → L	327.462	[194]
Ag	S → L	961.78	[194]
CsCl	S → S	476.85	[195]
CsCl	S → L	646.0	[196]
K_2SO_4	S → S	583.65	[195]
NaF	S → L	995.85	[197]

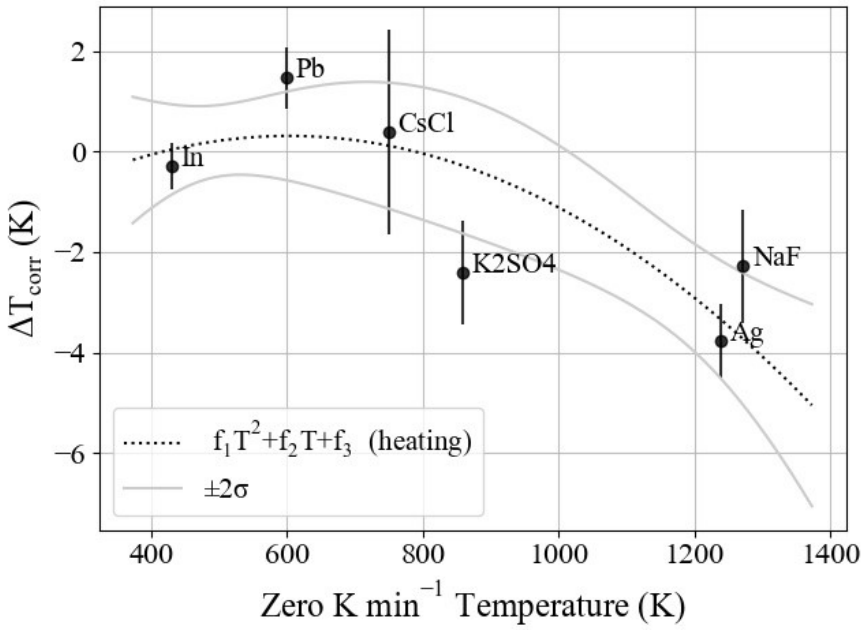

Figure 4.23: Heating calibration of Netzsch Pegasus 404F.

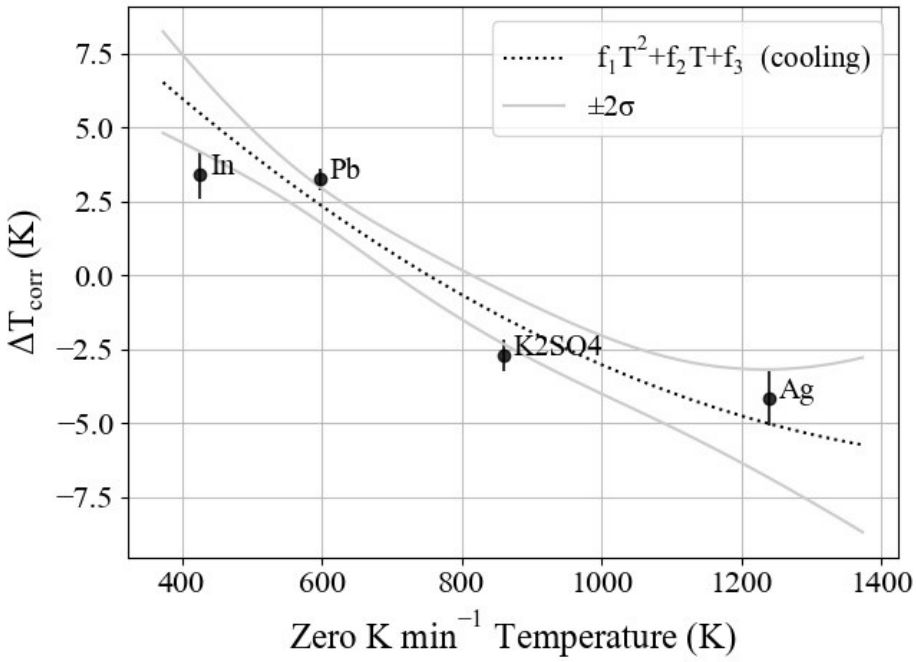

Figure 4.24: Cooling calibration of Netzsch Pegasus 404F.

cooling. Using molten salt calibrants in the temperature range of interest allows the calibration to better represent the molten salt sample measurement errors as the transition peaks of molten salts are generally less certain than for those of metals. Calibration material transition temperatures were determined as extrapolated onset of DSC for solid to liquid [131]and solid-solid [195] transitions.

Using the same symbol notation as Della Gatta et al [131], Equations (4.41)-(4.43) describe the Netzsch Pegasus 404F temperature calibration model shown in Figure 4.23. T_{tr} is the calibration corrected temperature, T_{meas} is the zero K min^{-1} sample temperature taken from extrapolations of measurements at 20,10,5, and 2 K/min, ΔT_{corr} is the temperature correction, $T_{trs,i}$ is the calibrant reference transition temperatures, and $T_{e,i}$ are the zero K/min linearly extrapolated temperatures of each calibrant. The regression parameters are f_1, f_2, and f_3, and were optimized using SciPy's optimize.curve_fit() (version 1.7.1). The calibration functions for the Netzsch Jupiter STA409 are the same, however, T_{meas} and $T_{e,i}$ are the average temperatures of the latter three of four measurements at 2 K/min.

$$T_{tr} = T_{meas} + \Delta T_{corr} \tag{4.41}$$

$$\Delta T_{corr,i} = T_{trs,i} - T_{e,i} \tag{4.42}$$

$$\Delta T_{corr} = f_1 T_{meas}^2 + f_2 T_{meas} + f_3 \tag{4.43}$$

The general law of error propagation [96,128] was used to determine measurement uncertainties for the Netzsch Pegasus 404F calibration (Figure 4.23 and Figure 4.24). Model variances are given by Equations (4.44)-(4.47) where $\sigma_{T_{tr}}^2$ is the variance of the

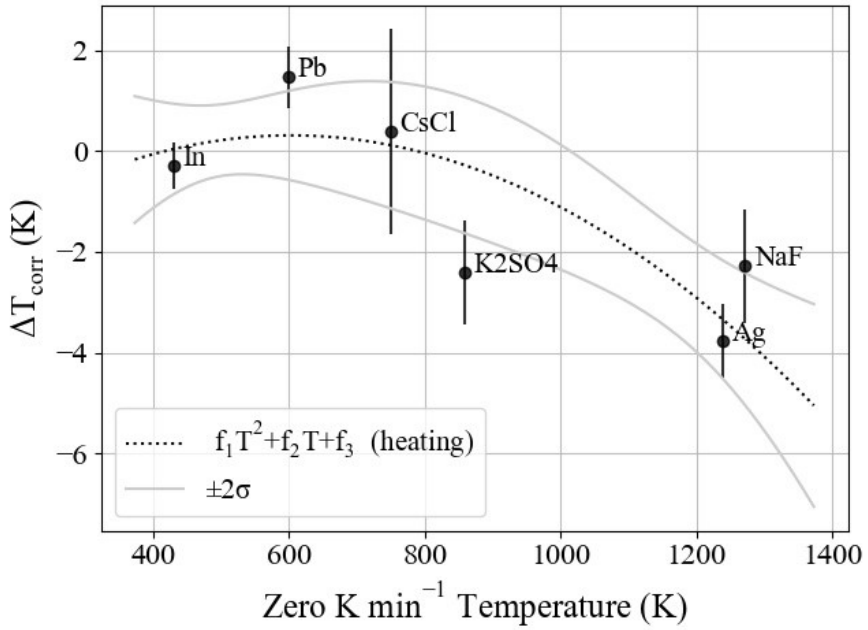

Figure 4.23: Heating calibration of Netzsch Pegasus 404F.

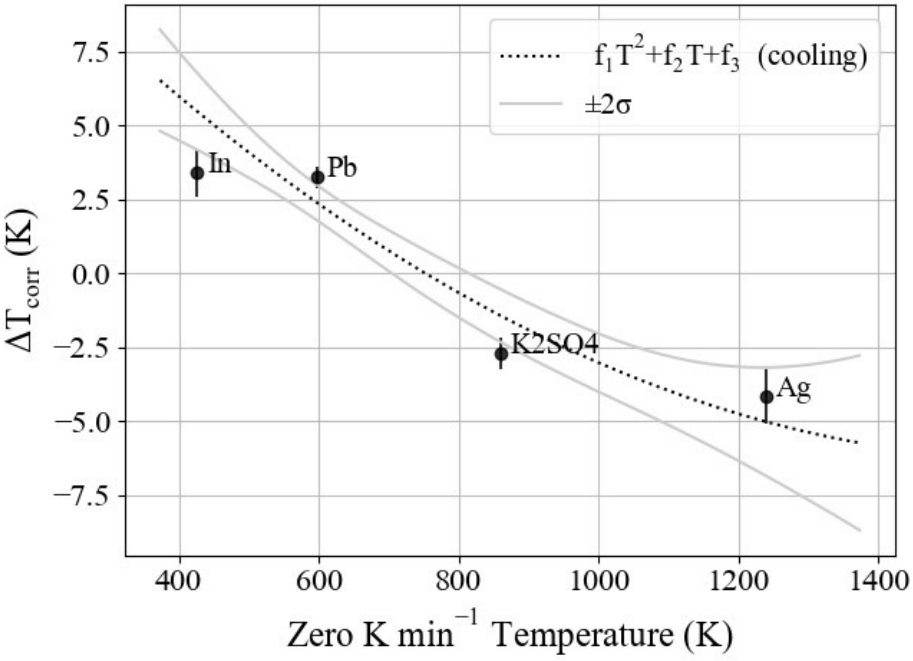

Figure 4.24: Cooling calibration of Netzsch Pegasus 404F.

calibration corrected temperature, $\sigma^2_{T_{meas}}$ is the variance of the zero K min^{-1} linearly extrapolated sample temperature, $\sigma^2_{\Delta T_{corr}}$ is the variance of the calibration correction which includes $\sigma_{T_{meas}}$ (i.e. 'absolute_sigma'=True in the optimize.curve_fit() package), $\sigma^2_{T_{trs,i}}$, are the variances of the author reported material transition temperatures, $\sigma^2_{T_{e,i}}$ are the variances of the zero K min^{-1} linearly extrapolated onset temperatures of each calibrant, and $C_{\Delta T_{corr}}$ is the covariance matrix of the fitting parameters f_1, f_2, and f_3. S^T, is the transpose of the sensitivity vector which is composed of the partial derivatives of Equation (4.43) with respect to each fitting parameter. The Netzsch Jupiter STA409 heating calibration uncertainty (Figure 4.25) was evaluated subjectively via a Type B uncertainty assessment [128] as is typical practice for DSC measurements.

$$\sigma^2_{T_{tr}} = \sigma^2_{T_{meas}} + \sigma^2_{\Delta T_{corr}} \tag{4.44}$$

$$\sigma^2_{\Delta T_{corr,i}} = \sigma^2_{T_{trs,i}} + \sigma^2_{T_{e,i}} \tag{4.45}$$

$$\sigma^2_{\Delta T_{corr}} = S^T C_{\Delta T_{corr}} S \tag{4.46}$$

$$S^T = [T^2_{meas} \quad T_{meas} \quad 1] \tag{4.47}$$

Uncertainty of DSC measurements

The scan rate dependence of DSC measurements is well known [131,198–200] and depends on the physical properties of the sample, primarily with respect to thermal conductivity [201]. As shown in Figure 4.26, extrapolated onset temperatures vary at finite heating rates for samples that are identical in material type and total mass.

For these measurements, three Pb samples with masses 48.3, 48.0, and 47.7mg were prepared using Ni liners of mass 185.5, 185.4, and 185.4mg. The purpose of these measurements was to observe DSC variations under conditions of normal use at finite scan

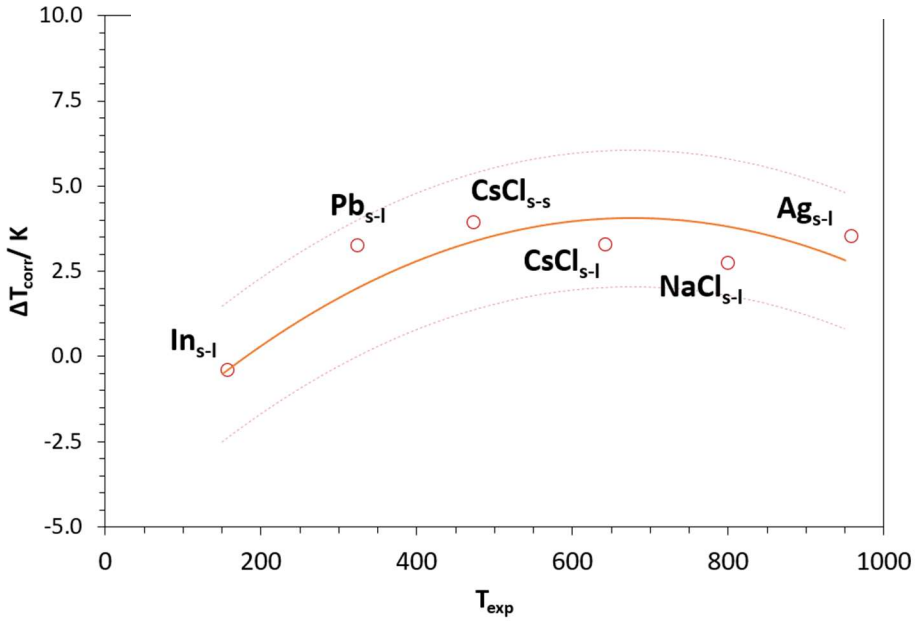

Figure 4.25: Heating calibration of Netzsch Jupiter STA409. Additional lines are ±2K estimated uncertainty.

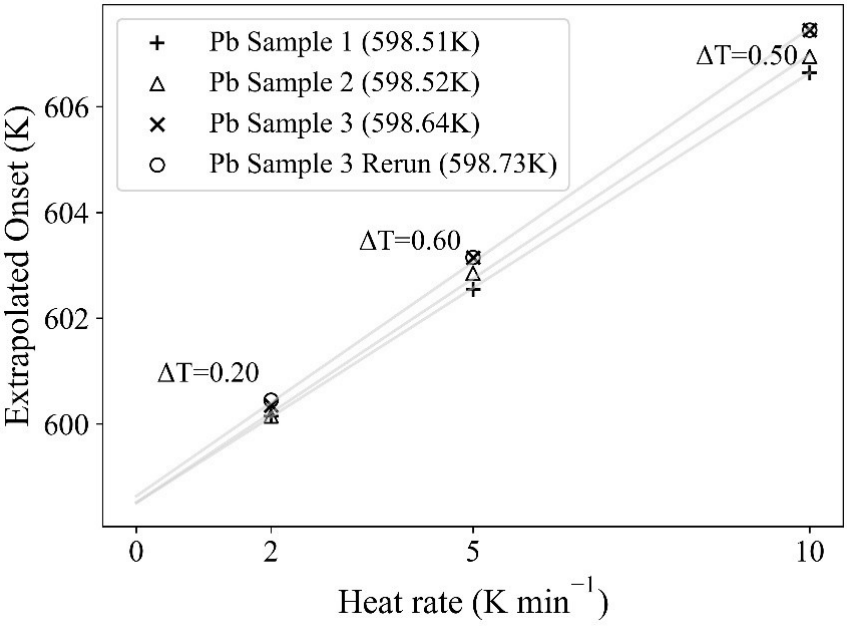

Figure 4.26: Variation in heat rate temperature dependence for Pb samples of similar mass. Zero K min^{-1} extrapolated measurement in parenthesis. 20 K min^{-1} scan rate discarded from dataset due to nonlinearity.

rates and compare these to the measurement after extrapolation to zero K min^{-1}. The reference crucible was removed and repositioned between each sample's measurement. Sample 3 was rerun without breaking contact between the sample and DSC thermocouple to demonstrate the instrument's repeatability under best-case circumstances.

DSC scans are usually repeated on a sample without breaking sample contact with the DSC thermocouple. As shown in Figure 4.26, this is a condition where the scan rate dependence is almost perfectly repeatable, and so, any uncertainty determination made on the basis of these measurements will greatly underestimate actual uncertainties [129]. The measurements of Figure 4.26 also indicate that DSC measurements vary under normal usage for any particular scan rate, even when the sample material type and mass are identical. For instance, at 10 K $min^{-1}$the range of temperature values is equal to 0.50K. Therefore, unless calibration samples are adjusted between measurements to mimic normal DSC use, this error will be unaccounted for in single heat rate calibrations. Because of this, we regard 0.50K as near the minimum possible error for calibrations at 10 K min^{-1} in our instrument and crucible arrangement.

Since extrapolation to zero K min^{-1} represents the sample in equilibrium, it is the preferred choice for measurement of phase equilibria. This was tested by preparing two samples each of In and $NaAlCl_4$. These materials are similar in melting point, 156.5985°C [194] and 152.85°C [202] respectively, yet are different in their physical properties. The two samples of each material differed in sample mass at least by a factor of three, typically between 10-50mg. In addition, the reference crucible position was readjusted between the measurement of each sample.

In Figure 4.27, the measurement variation at 10 K min^{-1} is 1.20K and 2.70K, for In and $NaAlCl_4$ respectively. This variation is reduced to 0.04K and 0.21K, respectively, when the measurement trend is extrapolated to 0 K min^{-1}. Based on the differences between Figure 4.26 and Figure 4.27 for the temperature variations at a given scan rate, it appears that sample type and normal variation in sample mass add an additional 0.7-1.2K of measurement error over those of the same type and mass. The commonly reported [30,155–158] molten salt measurement uncertainty of about ±1-3K agrees well with this result for constant scan rates $\leq$10 K min^{-1}.

Endmember characterization

Powder XRD patterns and DSC of the endmembers LiCl, NaCl, KCl, and UCl_3 are provided in Figure 4.28 through Figure 4.35. No detectable impurities were present in each XRD measurement. The DSC peaks for LiCl and NaCl are sharp and smooth with good agreement between heating and cooling. A small impurity is present in KCl and its cooling measurements have a small, but predictable, subcooling effect. The DSC of UCl_3 is smooth but much less sharp. In addition, the subcooling behavior is unpredictable and substantial.

The melting points of the substances of this study are compared to those reviewed by Parker et al. [129] in Figure 4.36. Our measurement of the melting point of LiCl (879.8±1.4K) may be depressed by approximately 3K from that of the most commonly reported value of 883±2K and so we have estimated the purity as 97±1mol% (standard uncertainty u(x)). NaCl melted at 1075.2±0.9K which is high in the range of values reported by Parker et al. [129] but corresponds very well with the international temperature scale value (ITS-90) of 1075.168±0.011K [194] from which we estimate 99±1mol% purity.

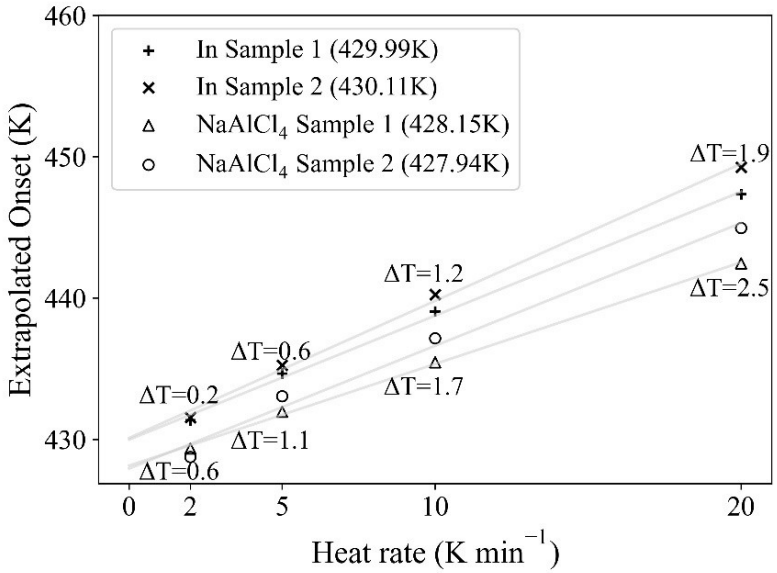

Figure 4.27: Variation in heat rate temperature dependence for In and $NaAlCl_4$ samples with material mass variation. Zero K min^{-1} extrapolated measurement in parenthesis.

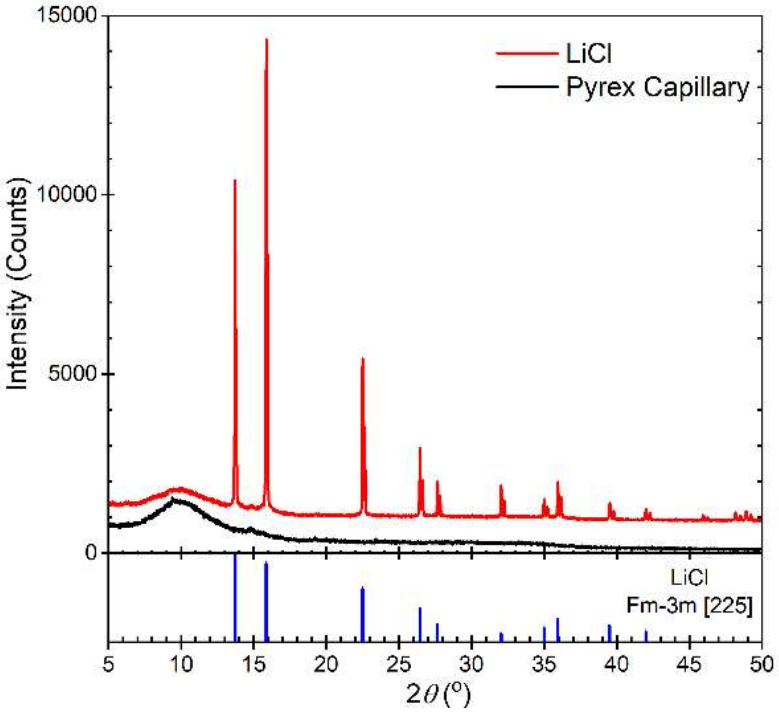

Figure 4.28: Room temperature powder XRD pattern of LiCl.

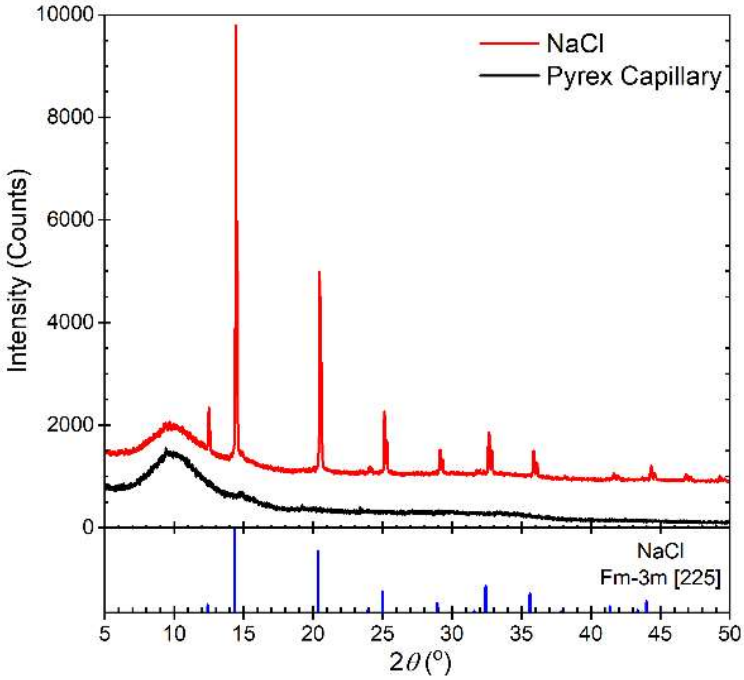

Figure 4.29: Room temperature powder XRD pattern of NaCl.

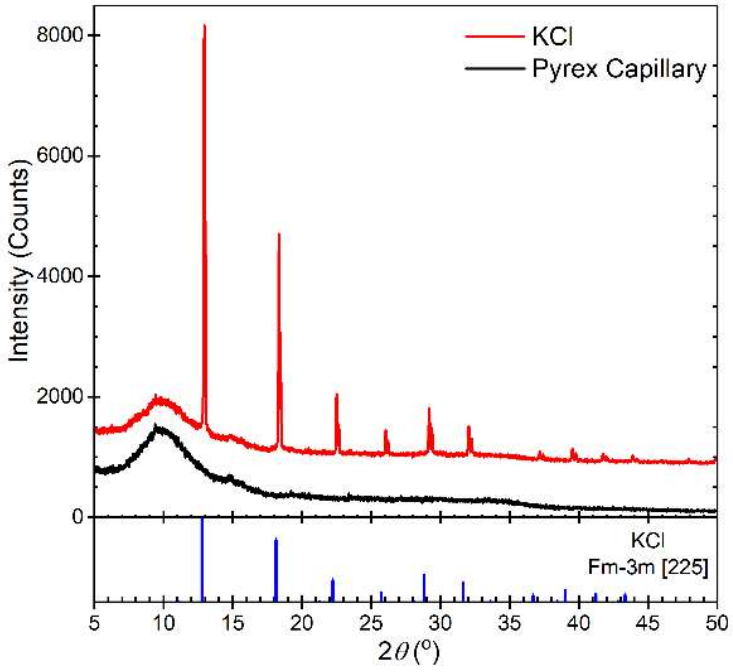

Figure 4.30: Room temperature powder XRD pattern of KCl.

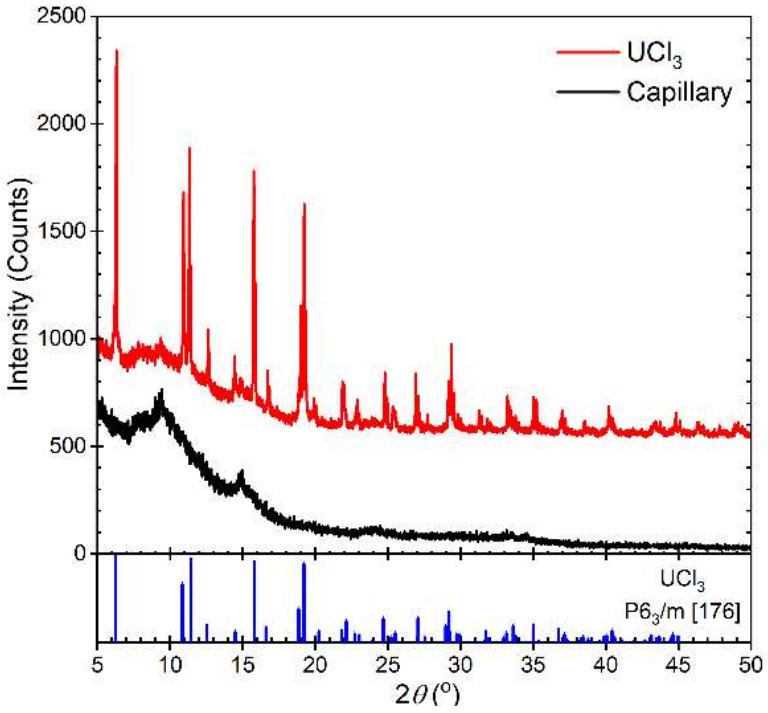

Figure 4.31: Room temperature powder XRD of UCl_3.

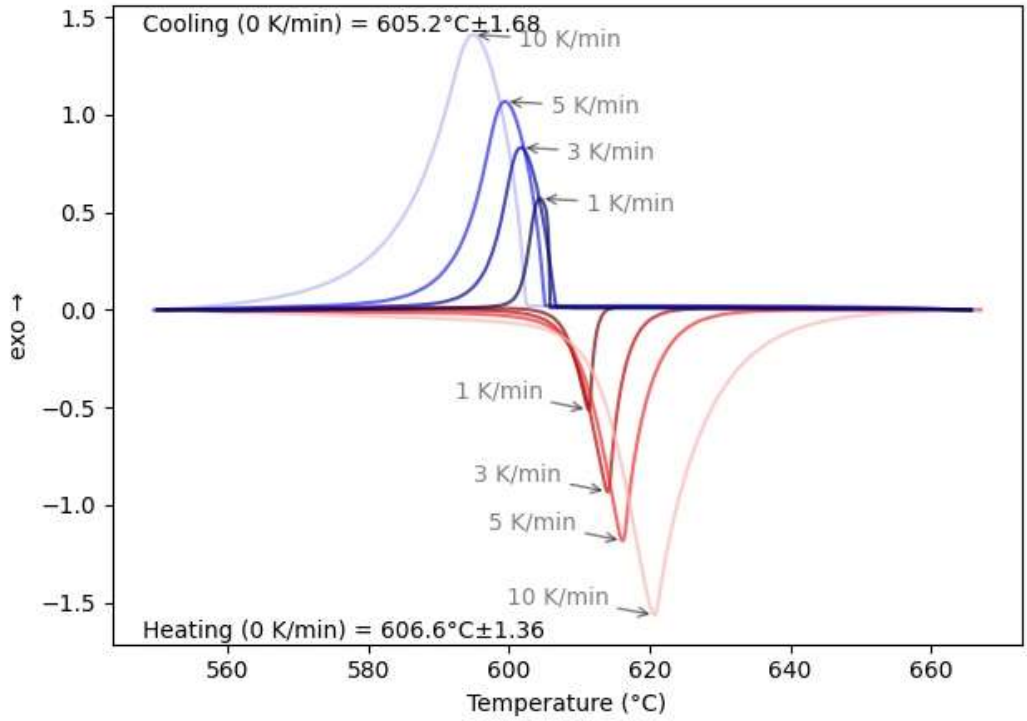

Figure 4.32: Heating and cooling DSC scans of LiCl.

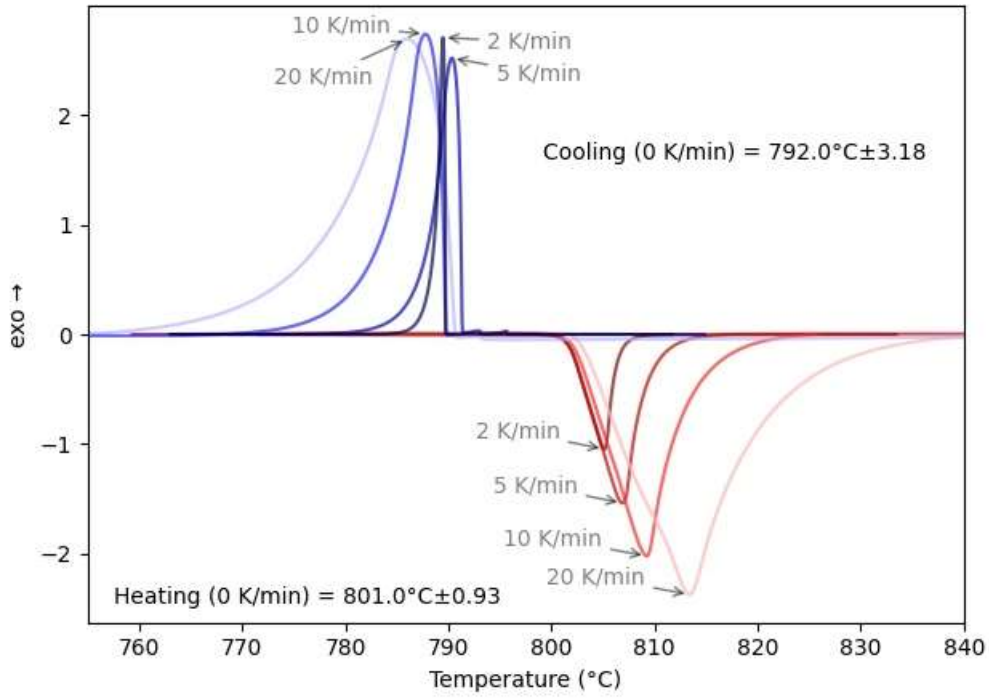

Figure 4.33: Heating and cooling DSC scans of NaCl.

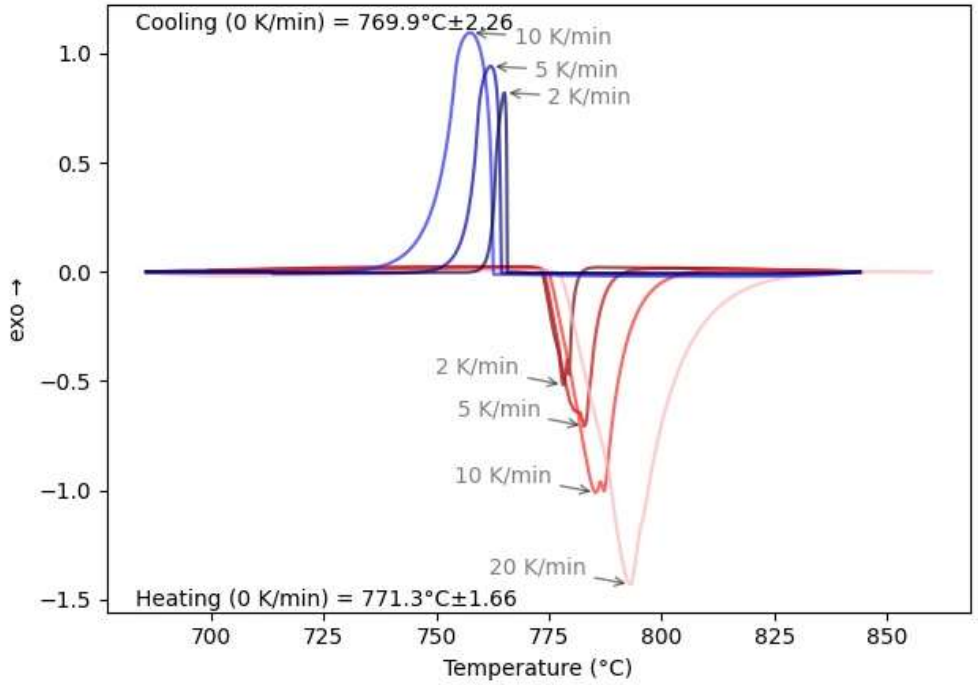

Figure 4.34: Heating and cooling DSC scans of KCl.

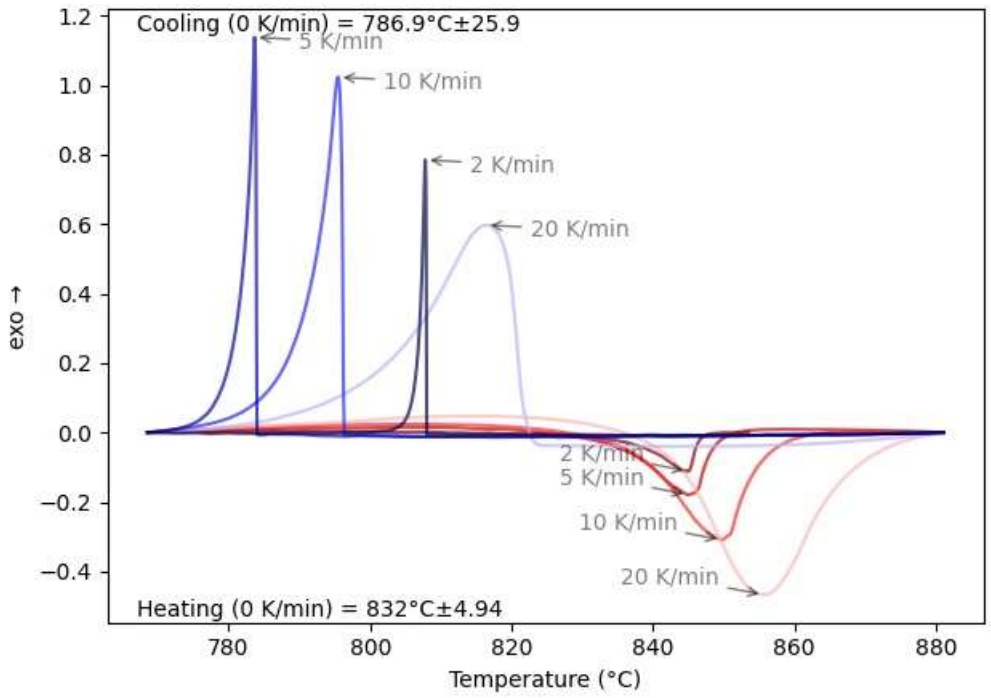

Figure 4.35: Heating and cooling DSC scans of UCl_3.

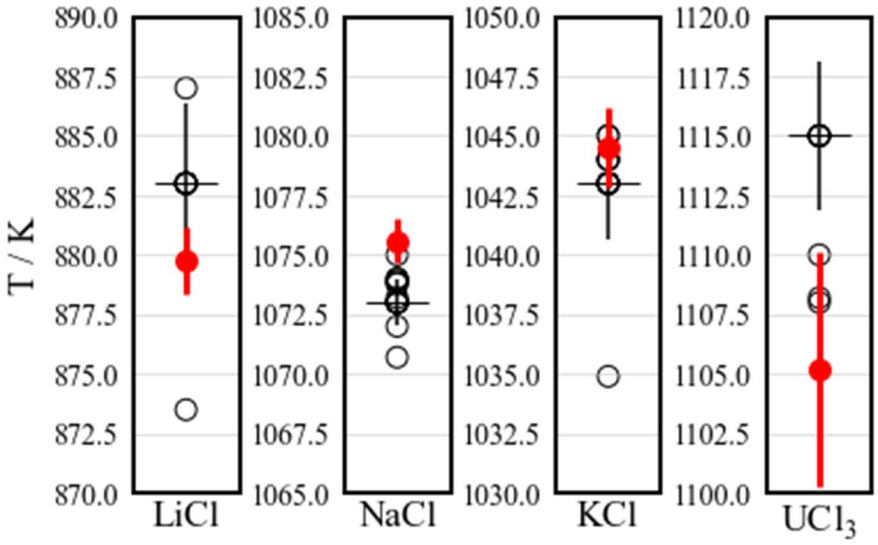

Figure 4.36: Comparison of the pure substance melting points in this study (red markers and bars) to those of the dataset found in Table 1 of Parker et al. [129]. Open circles are the dataset values, the median is indicated by a horizontal line, and the standard deviation as a vertical line.

KCl melted at 1044.5±1.7K which is well matched by the values reported by Parker et al. [129], but we estimate the purity to be 98±1mol% due to a small aberration in the DSC curve. We determined a melting point of 1105.2±4.9K for UCl_3 which is lower than all previously reported values. The broadness and lack of steady baseline prior to the peak in Figure 4.35 suggests that some impurities are present, however, these were not detected by XRD which indicates a purity of approximately 96±3mol%

MSTDB-TC Access

The databases and associated documents are hosted on a publicly accessible, permission-protected server at Oak Ridge National Laboratory (ORNL): https://code.ornl.gov/neams/mstdb/. Access requires an ORNL XCAMS account and an MSTDB membership, which once granted will allow downloading of all files.

- Go to https://xcams.ornl.gov
- Select "I need an account."
- Read and acknowledge the User Agreement
- Enter your email address and username following the guidelines on the page.
- Enter "Personal Information" and "Contact Information" per the guidelines
- Create an XCAMS password according to the guidelines provided on the page.
- On the final step, note the activation sequence box at mid-page. Wait until each action item turns green and the box heading reads "Transactions Complete"
- Log into https://code.ornl.gov using your new XCAMS username and password
- Request MSTDB membership
- Send an email to mstdb@ornl.gov with “MSTDB Access Request” as subject
- Include your XCAMS ID and brief summary of the purpose for your request MSTDB-TC is a copyrighted database available license-free, and cannot be sold all or in part.

Contacts: Ted Besmann (besmann@sc.edu)

CHAPTER 5: THERMODYNAMIC ASSESSMENT OF CR CORROSION IN NACL-KCL-$MGCL_2$-UCL_3-UCL_4 SALT FOR MOLTEN CHLORIDE REACTOR APPLICATIONS[3]

[3] J.A. Yingling, M. Aziziha, J. Schorne-Pinto, J.P.S Palma, J.C. Ard, R.E. Booth, C.M. Dixon, T.M Besmann. To be submitted to the Journal of Molecular Liquids.

Abstract

The formation of corrosion species in molten salt reactor systems is driven by the salt redox condition, indicated primarily by the uranium oxidation state ratio (U^{4+}/U^{3+}). In chloride salts, chromium is well known to have the highest tendency to deplete from alloy surfaces, however, no available thermodynamic database suitably models the effect of trivalent and tetravalent uranium chloride on the $CrCl_2$ corrosion potential. In this work, we extend the Molten Salt Thermal Properties Database – Thermochemical (*MSTDB-TC*) with Gibbs energy models suitable for application to chromium corrosion in chloride molten salt fueled nuclear reactors. The work requires the development of fully-constrained thermodynamic models, utilizing the modified quasi-chemical model in the quadruplet approximation for the melt and a single sublattice model for the solid solution phases, such that accurate estimations of thermodynamic properties may be possible, even in systems for which very few thermodynamic data are available. In so doing, it was necessary to use elemental period correlations in the estimation of thermodynamic values of the NaCl-$CrCl_2$ and KCl-$CrCl_2$ systems allowing a well-informed description of $CrCl_2$ behavior in the compositions of technical interest for the Na-K-Mg-U^{3+}-U^{4+} chloride salt.

Introduction

Corrosion control is important for molten salt reactor (MSR) systems and depends in part on the chemical potential relationship between the oxidative species in the melt and the solid phases of the structural materials [17,21]. Similar to the issue of corrosion product formation and deposition (CRUD) in water-cooled reactors [203], the degradation of salt-facing materials and the transport and deposition of corrosion products are essential to well-informed MSR design. Corrosion product migration is driven by Gibbs energy gradients, that is, from regions of high to low chemical potential [204], primarily due to differences

in temperature [205]. As a result, thermodynamic descriptions are required for understanding fundamental corrosion driving forces in MSRs as well as other phenomena, necessitating the inclusion of well-described thermodynamic models in multi-physics reactor simulation codes [14].

Previous thermodynamic assessments have described the Na-K-U(III) chloride salt [206] which is extended in this work to include $CrCl_2$ and UCl_4 at relatively low concentrations. $MgCl_2$ is additionally modeled as it may be used as a part of a redox control program [207] and is a constituent in investigations of MSR salt compositions [208], thermodynamics [25], corrosion studies [22], and fast spectrum reactor analysis [209,210].

The highest concentration base salts for MSR systems are NaCl and KCl, with $MgCl_2$ and UCl_3 intermediate in content, and UCl_4 and $CrCl_2$ as minor salt constituents. Table 5.1 lists the pseudo-binary, pseudo-ternary, and pseudo-quaternary systems developed in this work, with the assessed systems included in *MSTDB-TC*.

Of the pseudo-binary systems shown in Table 5.1, only the KCl-$CrCl_2$ system has thermodynamic data available other than phase equilibria. Phase equilibria alone may be used to develop thermodynamic models via the calculation of phase diagrams (CALPHAD); however, enthalpy, entropy, and heat capacity cannot be uniquely determined solely from Gibbs energy values. For instance, at a particular temperature and composition, two thermodynamic assessments with drastically different interaction parameters can have identical excess Gibbs energy of mixing while having large differences in excess values of enthalpy ($\Delta_{\mathrm{mix}}H$), entropy (ΔS^{ex}), and/or isobaric heat capacity ($\Delta_{\mathrm{mix}}C_{\mathrm{p}}$). Thus, models that are developed without independent specification of

Table 5.1: Thermodynamic assessments and reassessments in this work, where bolded systems indicate first-time assessments.

Endmembers	UCl_3	UCl_4	$CrCl_2$
UCl_3		**Phase diagram (PD)** [32]	**PD**
NaCl	[206]	**PD** [26,211,212]	**PD** [29,213–215]
KCl	[206])	**PD** [26,211,212]	**PD**[29,216]**, EMF** [217]
$MgCl_2$	PD[32,33,218]	**PD** [32,33]	**PD** [28]
NaCl-KCl	[206]	**PD** [35]**, EMF** [159,193]	**EMF** [217]
NaCl-$MgCl_2$	*	*	**EMF** [219]
KCl-$MgCl_2$	*	*	**EMF** [220]
NaCl-KCl-$MgCl_2$	*	*	**EMF** [221]

excess thermodynamic values may properly reproduce the system phase equilibria, but not necessarily the thermodynamic properties of the mixed systems.

As the primary objective of this work is to provide valid thermodynamic descriptions of corrosion driving forces in chloride MSRs, the phase equilibria above 20mol% of either $CrCl_2$ or UCl_4 are of secondary concern as these components will be present at generally low concentrations. Instead of prioritizing good agreement with every aspect of the phase diagram, this work focuses on ensuring well-informed thermodynamic models that correctly represent $\Delta_{\mathrm{mix}}H$ and thermodynamic activity at every composition as well as providing the best possible fit to the phase equilibria. This is accomplished by constraining the parameters of the thermodynamic assessments such that the phase models and values can well-predict pseudo-binary $\Delta_{\mathrm{mix}}H$ and liquid species thermodynamic activity using only phase equilibria. The technique involves reconciling experimental phase equilibria and calculated values to obtain a MQMQA parameterization that is justified by the quantity and quality of available thermodynamic data. This can be especially important for melts involving endmembers with highly polarizing cations like U^{4+}, for which localized structural ordering effects can result in phase diagram features that are not broadly representative of the melt at every composition. The approach to the assessments is given in the supplementary material.

Materials and experimental methods

The salts obtained for this study include high-purity (>99.9mass%) anhydrous $MgCl_2$ (Alfa Aesar), and $CrCl_2$ (Strem Chemicals). The purity of UCl_3 (Terra Power, LLC) was not specified but was previously evaluated by us to be 96±3mass% [206], where the indicated uncertainty is the estimated standard uncertainty [128]. Samples were prepared within an MBraun Unilab Pro glovebox under high purity argon with H_2O and O_2

concentrations maintained below 3ppm and 10ppm, respectively. Salts were weighed on an Ohaus PA84C scale with ±0.3mg precision into a total mixed mass of about 100mg (expanded uncertainty U(m) [128], 95% confidence approximately 2σ). The samples were manually ground with an agate mortar and pestle for 15 minutes and sealed within Netzsch 100 µl stainless steel crucibles containing a custom nickel metal liner as described by Piro et al. [130].

Salt structures and the purity of the salts were verified via room temperature transmission mode powder x-ray diffraction (XRD) measurements using a Rigaku Smartlab X-ray Diffractometer with Mo source ($K\alpha_1$ = 0.70932 Å, $K\alpha_2$ = 0.71316Å). Corning Pyrex capillaries were used for $MgCl_2$ and fused silica for $CrCl_2$ with OD=1 mm and were loaded within the glovebox and the open ends were stoppered with clay. Rietveld refinement was performed using SmartLab Studio II software.

Thermal measurements were made with a Netzsch Pegasus 404F3 heat-flux type differential scanning calorimeter (DSC) equipped with an S-type thermocouple and a SiC furnace. During the measurements, high-purity argon (70mL min^{-1}) and protective gas (20mL min^{-1}) purges were used along with a tantalum ring getter to minimize crucible oxidation. The DSC was heated to 1773K for 15 minutes after which temperature calibrations under heating and cooling were conducted following the zero K min^{-1} extrapolation procedure of Della Gatta et al. [131]. The calibration incorporates a unique method for uncertainty quantification previously described [206].

The purity of $MgCl_2$ is estimated to be 0.99±0.01, and $CrCl_2$ is estimated at 0.98±0.02 mole fraction basis from the powder XRD analysis and shape of the DSC scans. DSC confirmed the melting point (T_m) of the pure salts of 986.8±2.0K and 1090.5±2.1K,

which are reported as 987.2K [194] and 1097.2K [194], respectively (expanded uncertainty U(*T*) [128], 95% confidence approximately 2σ). The characterization of the UCl_3 was previously reported [206]. The XRD pattern and DSC scans of $MgCl_2$ and $CrCl_2$ are provided in the supplemental material (Figure 5.24 - Figure 5.27).

Thermodynamic modeling

The assessments are done via the calculation of phase diagrams (CALPHAD) [119] using Factsage™ software [120] to develop thermodynamic models that relate the system Gibbs energy to experimental and computational data [39]. The NaCl-KCl-$MgCl_2$ system was previously assessed by Chartrand and Pelton [24] and we have continued with the parameters resulting from that assessment. The NaCl-KCl-UCl_3 was also previously assessed [206], the models of which are extended in the current work to include the $MgCl_2$, $CrCl_2$, and UCl_4 endmembers.

Liquids

The melt phase is described with the modified quasi-chemical model in the quadruplet approximation (MQMQA) [121]. For common anion systems, the MQMQA accounts for short-range ordering (SRO) between second nearest neighbor (SNN) atoms in a pair exchange reaction Equation (5.1)which gives rise to the pair exchange reaction Gibbs energy of Equation (5.2), where A, and B, represent all combinations of cations, X represents the common anion, and. $\chi_{AB/X}$ are the quadruplet fractions as defined by Pelton et al. [121].

$$(A-X-A)+(B-X-B)=2(A-X-B);\ \Delta G_{AB/X} \tag{5.1}$$

$$\Delta G_{AB/X}=\sum_{i,j} G^{i,j}_{AB/X}\,\chi^{i}_{AB/X}\chi^{j}_{AB/X}\ (i\geq 0, j\geq 0) \tag{5.2}$$

The first nearest-neighbor (FNN) to SNN correlation factor, $\zeta_{A/Cl}$ (Equation (5.3)), is defined by Wang et al. [122] based on the endmember cation ($Z^{A}_{A/X}$) and anion ($Z^{X}_{A/X}$) coordination numbers. The values for the alkali chlorides with MgCl2 [24] and UCl3 [206] were determined previously, and Equations (5.4)-(5.5) contain the values for the divalent chlorides and UCl4, respectively, determined from $Z^{A}_{A/X} = 6$ and $Z^{X}_{A/X} = Z^{A}_{A/X}/n$, where n is the cation valence.

$$\zeta_{A/X} = \frac{2Z^{A}_{A/X} Z^{X}_{A/X}}{Z^{A}_{A/X} + Z^{X}_{A/X}} \tag{5.3}$$

$$\zeta_{Mg/Cl} = \zeta_{Cr/Cl} = 4 \tag{5.4}$$

$$\zeta_{U^{IV}/Cl} = 2.4 \tag{5.5}$$

The liquid models were assessed following the approach described in the supplemental material, which constrains the fit of MQMQA adjustable parameters according to the quantity and quality of available thermodynamic data. The cation-cation coordination numbers, $Z^{A}_{AB/X}$ and $Z^{B}_{AB/X}$ of the resulting liquid models, are given in Table 5.2 where $Z^{B}_{AB/X} = 6$ is fixed and the SNN coordination number ratio fit from the experimental invariant compositions as a function of $Z^{A}_{AB/X}$.

Solid solutions

The Gibb's energy of solid solutions is modeled using a single sublattice polynomial model [127] Equation (5.6), where G^{o} is the stoichiometric sum of the endmember Gibbs energies, G^{id} is the contribution of the ideal mixing configurational entropy, and G^{xs} is the excess Gibbs energy term defined by Equation (5.7), where Y in Equation (5.8) is the equivalent site fraction, x is the molar fraction, Z is the endmember coordination number, and L_{ij} can be temperature-dependent interaction parameters.

Table 5.2: SNN coordination numbers of the liquid solution.

A	B	$Z^{A}_{AB/Cl}$
Cr^{2+}	Cr^{2+}	6
U^{4+}	U^{4+}	6
Na^{+}	Cr^{2+}	4.2
Na^{+}	U^{4+}	3.9
K^{+}	Cr^{2+}	3
K^{+}	U^{4+}	4.9
Cr^{2+}	U^{3+}	6
Cr^{2+}	U_2^{6+}	3
Mg^{2+}	Cr^{2+}	6
Mg^{2+}	U^{3+}	6
Mg^{2+}	U_2^{6+}	3
Mg^{2+}	U^{4+}	3
U^{3+}	U^{4+}	6
U^{4+}	U_2^{6+}	2

$$G = G^{o} + G^{id} + G^{xs} \tag{5.6}$$

$$G^{xs} = \sum_{i\geq 0}\sum_{j\geq 0} Y_A^i Y_B^j L_{ij} \tag{5.7}$$

$$Y_A = \frac{Z_A x_A}{Z_A x_A + Z_B x_B} \tag{5.8}$$

Results

The endmember functions and solution models were described previously for the NaCl-KCl-UCl_3 [206] and NaCl-KCl-$MgCl_2$ [185] systems and are expanded here to include $MgCl_2$, UCl_4, and $CrCl_2$ endmember functions and solution models for the pseudo-binary, pseudo-ternary, and pseudo-quaternary systems indicated in Table 5.1. The Gibbs energy functions not previously described by Chartrand and Pelton [185] and Yingling et al. [206] are provided in Table 5.3.

The UCl_4 solid has well-known values of C_p from the reviews of Grenthe et al. [154], and enthalpy of fusion (ΔH_{fus}) and melting point (T_m) from Konings et al. [150]. To simplify the UCl_4 endmember description, we describe the two solid-solid transitions [222,223], and the melting of UCl_4 as a single event. The liquid C_p was considered a constant from the values measured by Popov et al. [224], rather than the steeply increasing linear function of Barin [225]. Gas-phase C_p, S_{298}, and $\Delta_f H_{298}$ are from Grenthe et al. [154] and were used to compute the vapor pressure above pure liquid and solid UCl_4 which well-reproduces the observations in Figure 5.1a. The values of $\Delta_f G$ reported by Martinot [159], agree well with our function as shown in Figure 5.1b.

The high temperature C_p is unknown for $CrCl_2$, however T_m and ΔH_{fus} [226] are known, from which Pankratz [44] estimated the C_p function from the low temperature C_p,

Table 5.3: Endmember and intermediate compound thermodynamic data. Bolded values were determined as part of the constrained CALPHAD assessment.

Comp.	$\Delta_f H^o$/ (kJ mol^{-1})	ΔS^o/ (J mol^{-1} K^{-1})	C_p / (J mol^{-1} K^{-1})	Reference
UCl_4(s)	-1018.8	197.2	$116.32 + 0.03108 \cdot T - 340402 \cdot T^{-2}$	[150,154]
UCl_4(l)	-985.5[a]	221.9[a]	162.3225	[197,224]
UCl_4(g)	-815.4	409.2	$110.634 + 0.00324 - 715600 \cdot T^{-2} - 3.12\ 10^{-7} \cdot T^2$	[154]
Na_2UCl_6(s)	-1879.9	**323.3**	$208.2 + 0.06372 \cdot T - 340402 \cdot T^{-2}$	[227]
$KUCl_5$(s)	-1510.0	**270.4**	$156.336 + 0.0566 \cdot T + 24443 \cdot T^{-2}$	[227]
K_2UCl_6(s)	-1962.3	**378.1**	$196.352 + 0.0820 \cdot T + 389288 \cdot T^{-2}$	[227]
$CrCl_2$(s)	-395.4	115.3	$73.245 + 0.013 \cdot T - 528835 \cdot T^{-2}$	[44,228]
$CrCl_2$(l)	-378.9	116.9	100.416	[44]
$CrCl_2$(g)	-117.6	319.4	$59.654 - 0.0013 \cdot T - 272700 \cdot T^{-2} + 3.22 \cdot 10^7 \cdot T^2$	[229]
Na_2CrCl_4(s)	-1216.6	**266.7**	$165.125 + 0.0456 \cdot T - 528834 \cdot T^{-2}$	This work
$KCrCl_3$(s)	-856.0	**192.8**	$114.248 + 0.0440 \cdot T - 381964 \cdot T^{-2}$	[197]
K_2CrCl_4(s)	-1274.8	**306.8**	$154.264 + 0.0694 \cdot T - 17119 \cdot T^{-2}$	[197]

[a] Determined via third law.

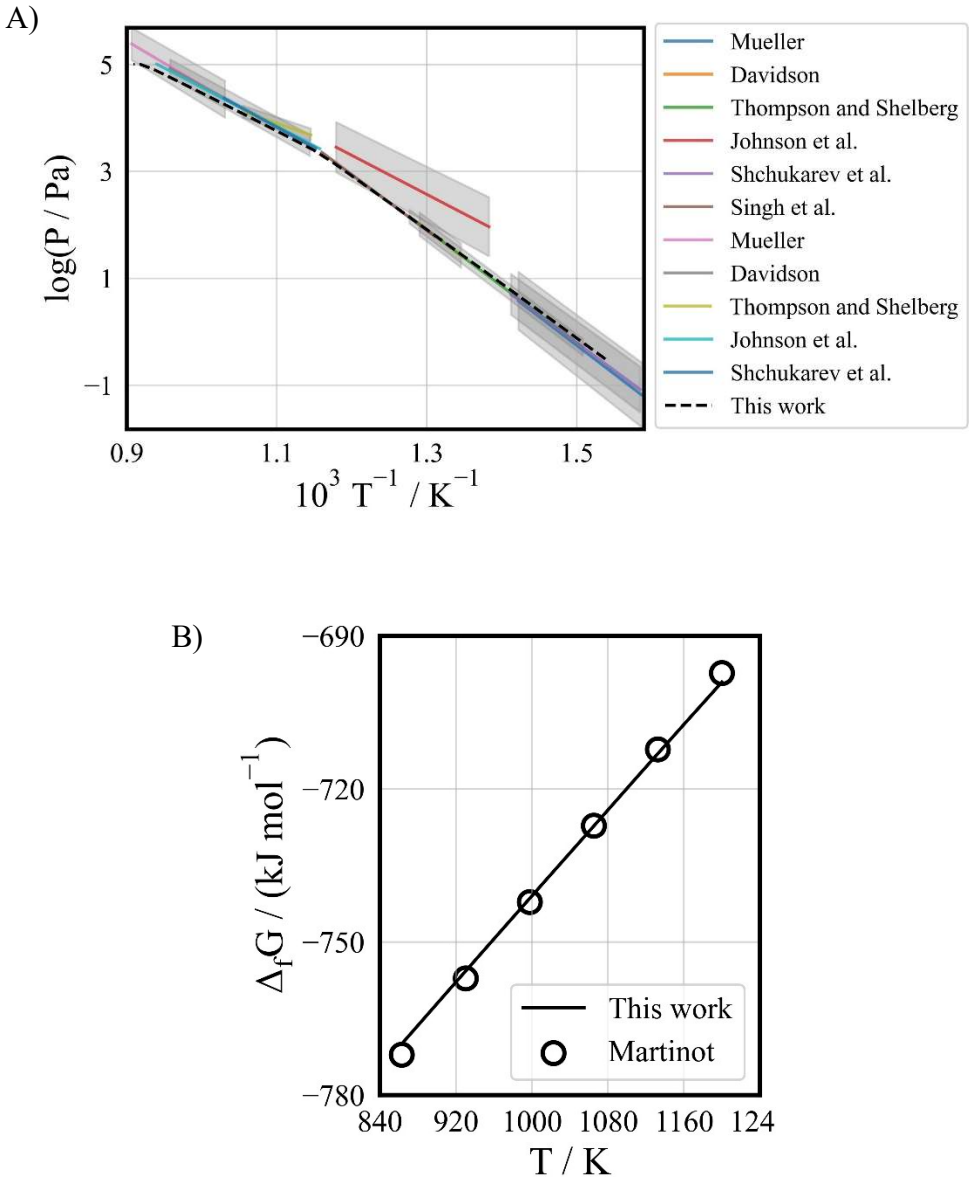

Figure 5.1: a) Calculated UCl_4 vapor pressure above solid and liquid UCl_4 under standard conditions. Functions of experimental data and uncertainties are from Table 1 of [230] b) Calculated $\Delta_f G$ for UCl_4(l) compared to the function values reported by Martinot [159].

$\Delta_f H_{298}$, and S_{298} data of Stout and Chisholm [228]. Figure 5.2a compares the low temperature experimental data of Stout and Chisholm [228] and Anderson [231], to Pankratz's [44] estimated function which smoothly connects to the experimental data of Stout and Chisholm [228], although not to that of Anderson [231]. The high-temperature C_p estimation is reasonable since the slope matches the NIST C_p temperature dependence of an equilibrated 1:1 molar mixture of Cr(s) and Cl_2(g) [232]. The computed liquid-vapor equilibrium of Figure 5.2b closely matches the measurements of Doerner [233] and Schoonmaker et al. [234].

MgCl2-UCl3

The $MgCl_2$-UCl_3 system was previously assessed by Beneš and Konings [25] as a simple eutectic using the sole phase equilibria measurements of Desyatnik et al. [32]. We obtained DSC measurements of two additional compositions to confirm the experimental phase diagram, with the eutectic and liquidus temperatures in good agreement (Table 5.4). Since the UCl_3 description in *MSTDB-TC* is incompatible with that of the previous assessment of Benes and Konings [25], we have reassessed this system using the constrained approach described in the supplemental material.

As the $MgCl_2$-UCl_3 is a simple eutectic system, under the condition that the endmember Gibbs energy functions are well-described, the simplest MQMQA contains two degrees of freedom (DOF) which are the liquid SNN coordination number ratio and a temperature and composition independent interaction parameter. These two DOF were specified by fixing the experimental eutectic composition and temperature, respectively.

The solution model parameter of Equation (5.9) produces the calculated phase diagram of Figure 5.3 which very well reproduces both reported and our experimental phase

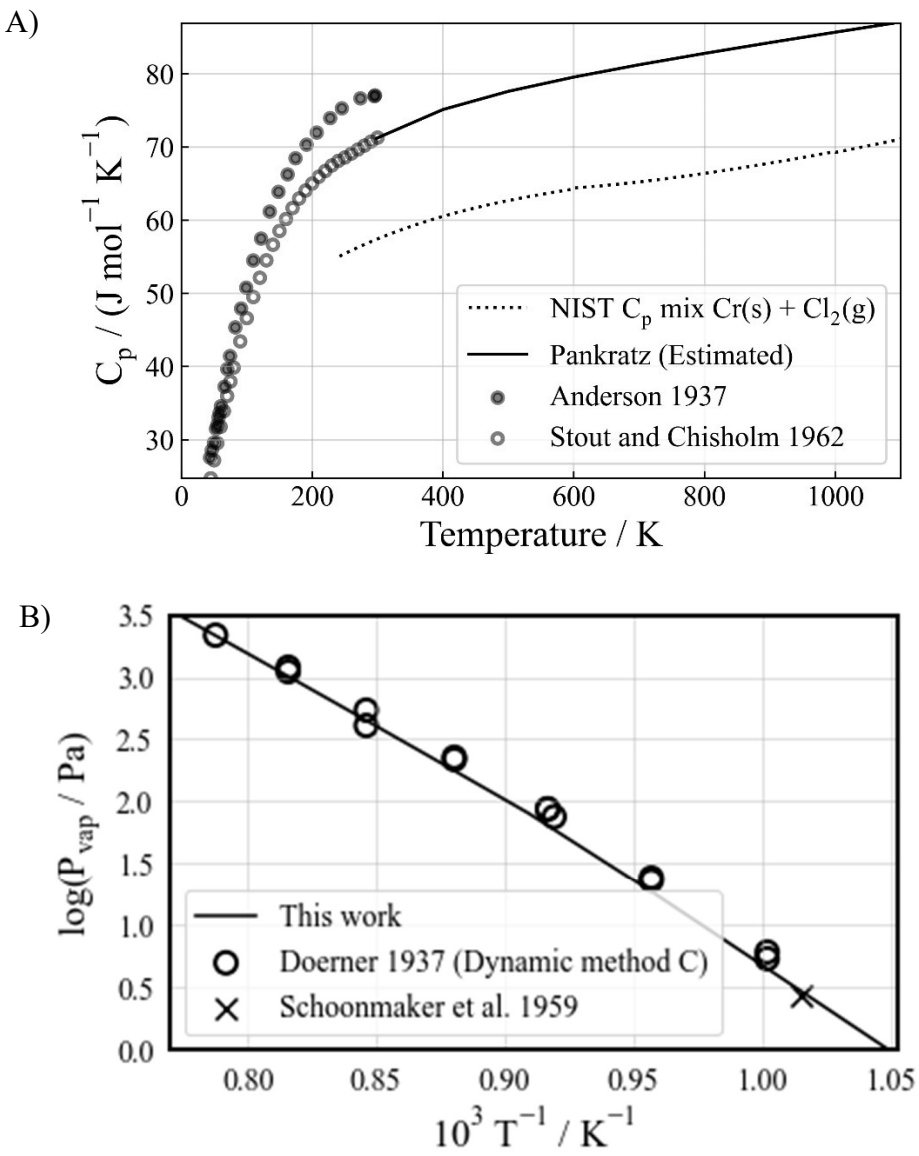

Figure 5.2: a) Experimental and estimated C_p as a function of temperature. b) Comuputed $CrCl_2$ vapor pressure over $CrCl_2$(l) compared to measured values.

Table 5.4: Results of DSC measurements in the $MgCl_2$-UCl_3 system.

Mole fraction UCl_3	Equilibrium reaction	Type of equilibrium	DSC thermal events / K[a]	
			Heating	Cooling
0.15	$MgCl_2$(s) + UCl_3(s) ↔ L	Eutectic	949.2±1.8	951.3±10.9
	$MgCl_2$(s) + L ↔ L'	Liquidus	965.9±1.2	969.4±4.1
0.49	$MgCl_2$(s) + UCl_3(s) ↔ L	Eutectic	944.6±1.5	955.1±4.2
	UCl_3(s) + L ↔ L'	Liquidus	1012.0±6.6	999.6±11.3

[a] Expanded uncertainties, U(T) (95% confidence interval approximately 2σ).

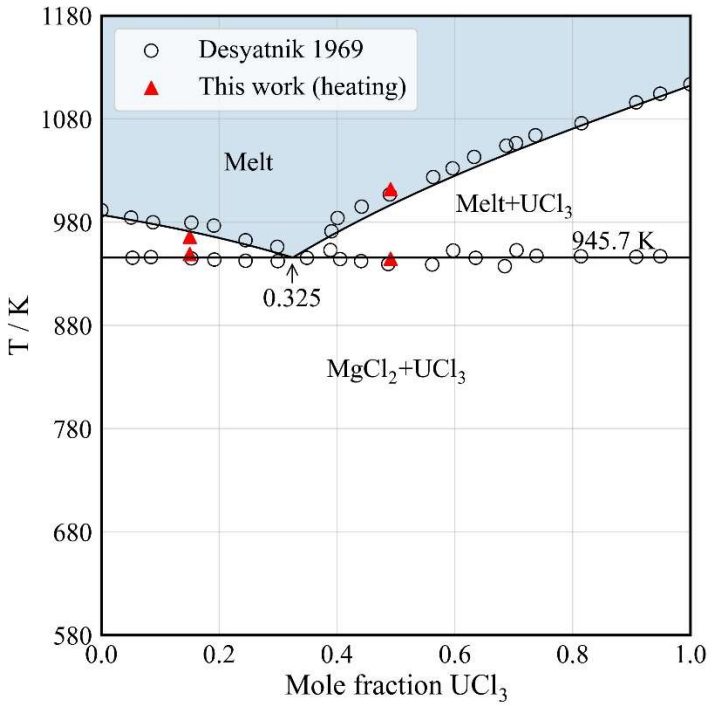

Figure 5.3: Calculated phase diagram of the $MgCl_2$-UCl_3 system well representing the observed system values.

equilibria measurements. Moreover, as discussed in the supplementary material, by limiting Equation (5.2) to a single temperature and composition independent value, we have taken maximum advantage of the model's ability to describe ordering within the melt. The models and values should thus provide reasonable representations of $\Delta_{mix}H$ and species activities.

$$\Delta G_{MgU^{4+}/Cl} = -700 \quad (5.9)$$

$CrCl_2$-UCl3

As no reported phase equilibria are available for the $CrCl_2$-UCl_3 system, we performed DSC measurements on five compositions (Table 5.5). The measurements indicate the existence of a eutectic, however, use of a solely eutectic solution model was unable to properly describe the liquidus near the $CrCl_2$ and UCl_3 endmembers. This is a common problem in CALPHAD thermodynamic assessments [160,185] whereby the Van't Hoff relation requires that additional equilibria are needed to properly describe the limiting slope of a system near the endmembers [235].

We identified a likely additional phase in the system using cationic potential trends as described by Gaune-Escard et al. [177] and Gawel [175], in which we evaluated the number and type of phases present and calculated the cationic potential ratio (Equation (5.10)) for each experimentally known system involving $CrCl_2$ [28,29,214,216,236] (Table 5.6),

$$\frac{IP_A}{IP_{Cr}} = \frac{z_A/r_A}{z_{Cr}/r_{Cr}} \quad (5.10)$$

where z is the cation charge and r is the 6-coordinated Shannon ionic radius [176]. As indicated in Table 5.6, the system $CrCl_2$-UCl_3 is suggested to have solid solutions by its ionic potential ratio ($IP_{U^{3+}}/IP_{Cr}$= 1.17).

Table 5.5: Results of DSC measurements of the $CrCl_2$-UCl_3 system.

Mole fraction UCl_3	Equilibrium reaction	Type of equilibrium	DSC thermal events / K[a]	
			Heating	Cooling
0.19	Sol.Soln#1 + SolSoln#2 ↔ L	Eutectic	966.2±1.5	943.9±14.6
	Sol.Soln + L ↔ L'	Liquidus	1054.3±1.0	1024.8±5.7
0.31	Sol.Soln#1 + SolSoln#2 ↔ L	Eutectic	972.4±1.1	977.8±15.7
	Sol.Soln + L ↔ L'	Liquidus	1021.4±5.4	1022.5±4.6
0.53	Sol.Soln#1 + SolSoln#2 ↔ L	Eutectic	971.4±5.0	979.1±11.5
	Sol.Soln + L ↔ L'	Liquidus	1005.0±1.0	985.8±9.9
0.76	Sol.Soln#1 + SolSoln#2 ↔ L	Eutectic	958.6±1.1	965.2±4.6
	Sol.Soln + L ↔ L'	Liquidus	1062.7±3.1	1051.5±13.9
0.84	Sol.Soln#1 + SolSoln#2 ↔ L	Eutectic	959.5±3.2	953.2±9.4
	Sol.Soln + L ↔ L'	Liquidus	1092.7±1.0	1091.9±16.1

[a] Expanded uncertainties $U(T)$

Table 5.6: Cationic potential trend of various pseudo-binary systems involving $CrCl_2$.

Cation (A)	IP_A/IP_{Cr}	# of Compounds	Reference
Cs(+)	0.24	2	[29,216,236]
Rb(+)	0.26	2	[29]
K(+)	0.29	2	[29,216]
Na(+)	0.39	1	[29,214]
Li(+)	0.53	1+ Sol. Soln.	[29]
Mn(2+)	0.96	Two Sol. Soln.	[28]
Fe(2+)	1.03	Two Sol. Soln.	[28]
Mg(2+)	1.11	Two Sol. Soln.	[28]

To determine the extent of mutual solid solubility, we evaluated the thermal effect of the eutectic transformation in our DSC measurements via the Tammann method [172], which employs basic phase fraction relations to determine the compositional limits of liquid formation. As shown in Figure 5.4, the observed thermal effects of our measurements on cooling suggest a eutectic composition of 45mol% and a limit of a solid solubility between 12-18mol% of either endmember.

Consistent with our constrained assessment approach, the presence of the solid solution adds an additional solution parameter which results in three DOF to be constrained. Thus, (i) the liquid interaction parameter of Equation (5.11) was fit to reproduce the eutectic temperature, (ii) the solid solution interaction parameter of Equation (5.12) was fit to ensure that the maximum endmember solid solubility is equal to the lower value of the expected solid solubility limit, and (iii) the composition of the eutectic informed the choice of the liquid SNN coordination number ratio. The resulting calculated phase diagram in Figure 5.5 reproduces our heating measurements very well.

$$\Delta G_{CrU_2^{6+}/Cl} = -3580 \quad (5.11)$$

$$G^{xs}_{CrU_2^{6+}} = 21180\, Y_{CrCl_2} Y_{UCl_3} \quad (5.12)$$

NaCl-UCl4

The phase equilibria of the NaCl-UCl_4 system were investigated by Barton [26], Kraus [27], Kuroda [212], Bogacz [211], and Desyatnik et al. [237], and each of these authors reports a Na_2UCl_6 intermediate compound. The $\Delta_f H_{298}$ of Na_2UCl_6 is available from Martynova [238], C_p may be estimated via proportional mixing of the NaCl and UCl_4 endmember values using the Neumann-Kopp (NK) rule [239], and S^{298} is unknown. The $\Delta_{mix} H$ of the liquid is also unknown, and a suitable dataset for its estimation is not available. Thus, the liquid interaction parameter, unknown S^{298} of Na_2UCl_6, and liquid SNN coordination number ratio are considered three DOF in the NaCl-UCl_4 assessment.

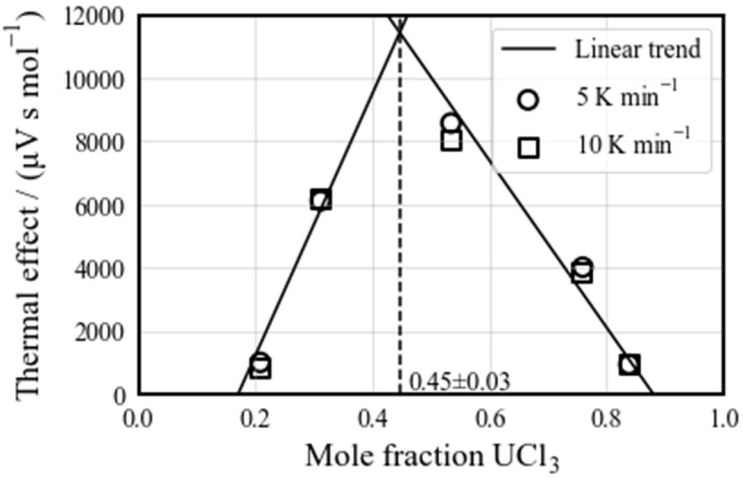

Figure 5.4: Trend of DSC eutectic reaction peak size on cooling.

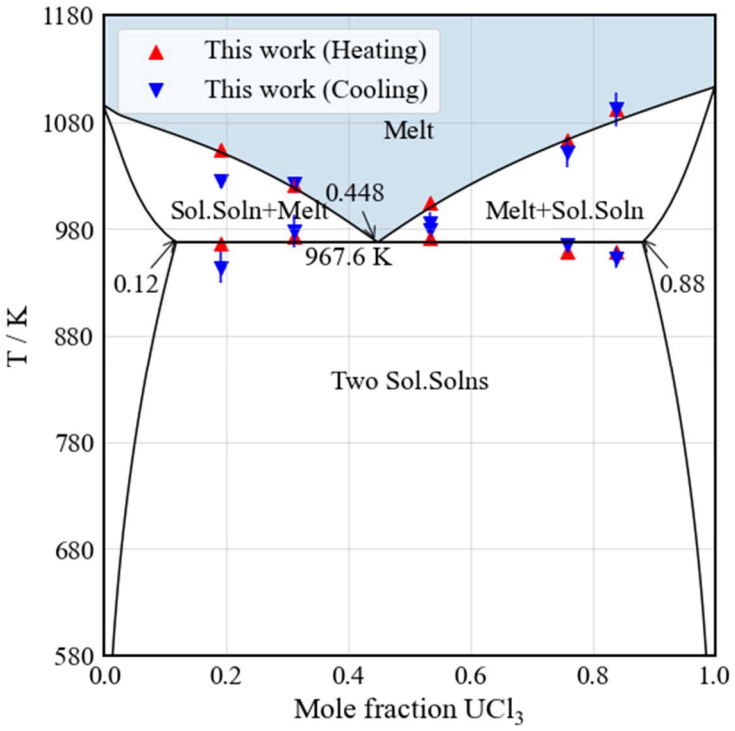

Figure 5.5: Calculated phase diagram for the $CrCl_2$-UCl_3 system together with measured values. Uncertainty intervals are shown for $2\sigma \geq 5$K.

The pseudo-binary assessment prioritizes the phase equilibria of compositions <20mol% UCl_4 since these are important to MSRs. Because of this, correctly reproducing the eutectic composition and temperature between NaCl and Na_2UCl_6 was emphasized. Nevertheless, to ensure that the calculated liquid activities and $\Delta_{\mathrm{mix}}H$ are accurate, the essential phase equilibria ≥20mol% UCl_4 must be adequately represented and therefore, the eutectic temperature between Na_2UCl_6 and UCl_4 must also be considered. Thus, the three DOF of the system assessment are constrained by ensuring that these regions of the phase diagram are well-fit, resulting in Equation (5.13), from which the phase equilibria of Figure 5.6 are obtained.

$$\Delta \mathrm{G}_{\mathrm{NaU^{4+}/Cl}} = -17650 \tag{5.13}$$

The calculated phase equilibria in Figure 5.6 are in excellent agreement with those measured for compositions >20mol% UCl_4, as well as the eutectic temperature and composition at higher UCl_4 content and the Bogacz and Trzebiatowski [211] measurements of the UCl_4 liquidus.

KCl-UCl4

The phase equilibria of the KCl-UCl_4 system were studied by Barton [26], Kuroda and Suzuki [212], Kraus [27], Martynova et al. [240], and Bogacz and Trzebiatowski [211], whom each include the congruently melting compound K_2UCl_6 for which $\Delta_{\mathrm{f}}H^{\mathrm{o}}_{298}$ is available from Martynova et al. [238]. They also determined the $\Delta_{\mathrm{f}}H^{\mathrm{o}}_{298}$ for the congruently melting compound $KUCl_5$. The additional phases KU_2Cl_9 and KU_3Cl_{13} were reported by Bogacz and Trzebiatowski [211], however, these were excluded from the thermodynamic assessment as they lack known values of $\Delta_{\mathrm{f}}H^{\mathrm{o}}_{298}$. Given the available information, the liquid interaction parameter, S^{298} of K_2UCl_6 and of $KUCl_5$, and liquid SNN coordination number ratio represent four DOF in the KCl-UCl_4 assessment.

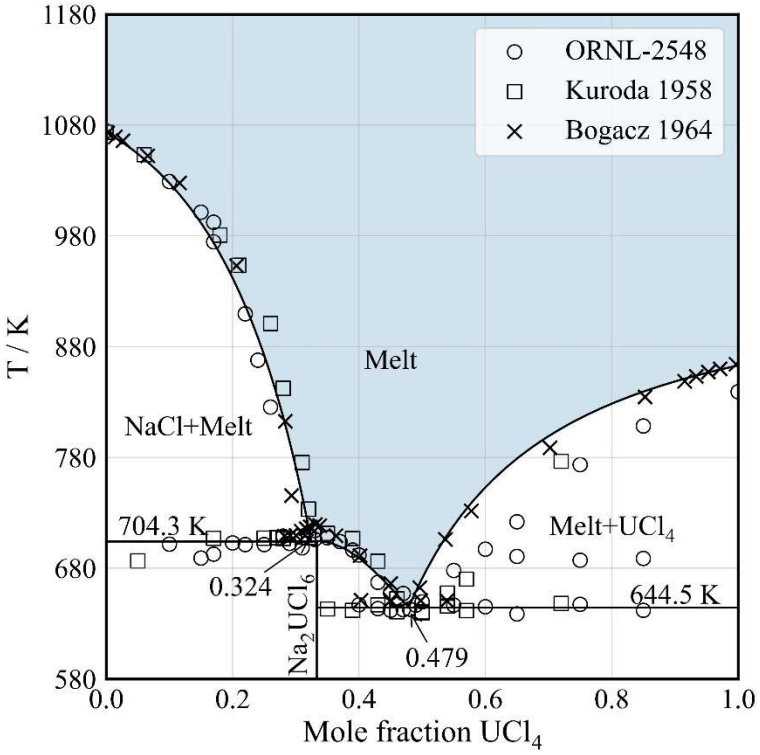

Figure 5.6: Calculated phase diagram and experimental phase equilibria [26,211,212] for the NaCl-UCl_4 system.

We prioritized the phase equilibria of compositions <20mol% UCl_4 to focus the accuracy of the assessment on compositions of greatest importance. To assure a correct description of the liquid $\Delta_{mix}H$, the eutectic temperature between K_2UCl_6 and $KUCl_5$ as well as between $KUCl_5$ and UCl_4 must also be well represented. However, the range of temperatures reported for these eutectics varies considerably [26,27,211,212,241] which prevents them from being used to constrain the DOF in the assessment. Because of this, the fit of the liquid SNN coordination number, liquid interaction parameter, and S^{298} values for K_2UCl_5 and $KUCl_5$ are not unique, and consequently, the KCl-UCl_4 phase diagram alone is insufficient to constrain the system assessment.

To address the issue of insufficient variables to constrain the system, the phase equilibria of the NaCl-KCl-UCl_4 pseudo-ternary system was enlisted utilizing the relevant liquidus values and eutectic composition and temperature determined by Desyatnik et al. [35]. The pseudo-ternary measurements of Martynova et al. [241] were not used in the assessment as the reported equilibria have UCl_4 contents higher than the applicable composition range of the present effort. Thus, the essential features of the pseudo-binary and pseudo-ternary phase equilibria were used to obtain the interaction paramenter of Equation (5.14) as well as the intermediate compound S^{o}_{298} values for K_2UCl_6 and $KUCl_5$. The calculated phase equilibria of the pseudo-binary system in Figure 5.7 agree very well with experimental values except for the liquidus reaction involving K_2UCl_6, which is outside of the composition range of interest. The calculated liquidus in the pseudo-ternary sections of Figure 5.8 and Figure 5.9, at 10 and 20mol% UCl_4 respectively, very well reproduce the experimental phase diagram of Desyatnik et al. [35].

$$\Delta G_{KU^{4+}/Cl} = -31000 \quad (5.14)$$

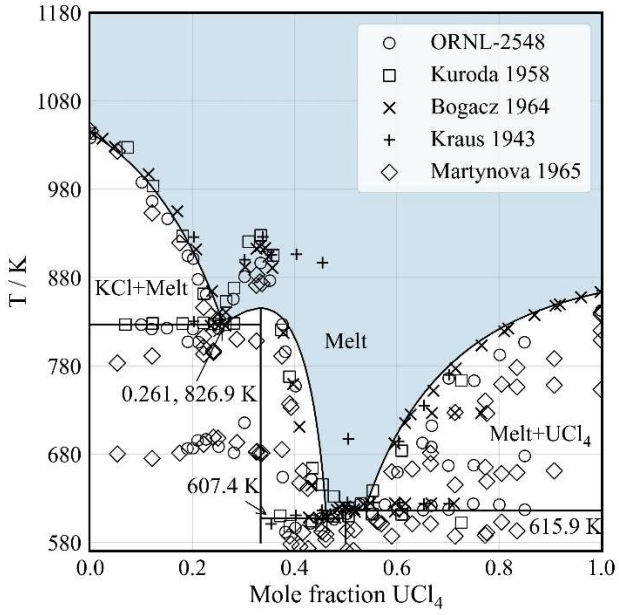

Figure 5.7: Calculated phase diagram and experimental phase equilibria [26,27,211,212,240] of the KCl-UCl_4 system.

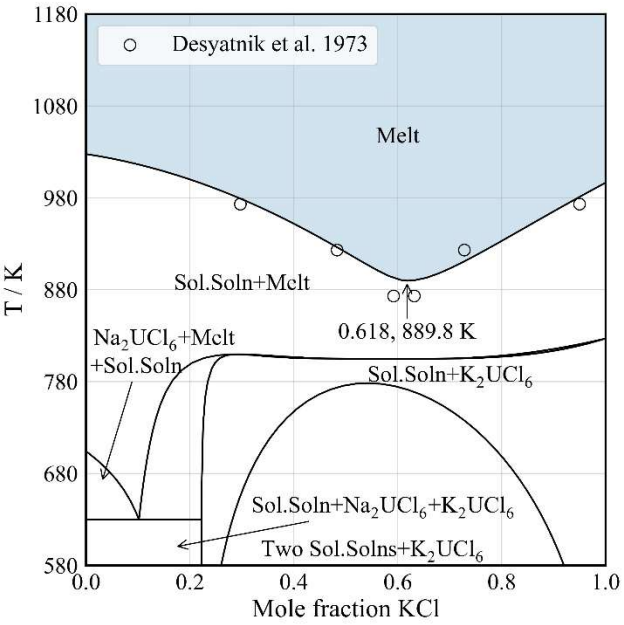

Figure 5.8: Calculated NaCl-KCl pseudo-ternary system with a constant 10mol% UCl_4 content including the NaCl-KCl solid solution. Experimental points [35] were extracted graphically.

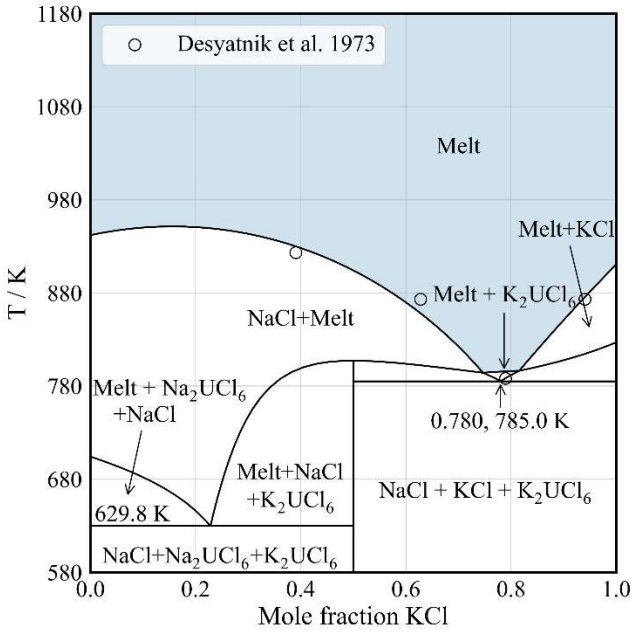

Figure 5.9: Calculated NaCl-KCl pseudo-ternary system with a constant 20mol% UCl_4 calculated excluding the NaCl-KCl solid solution. Experimental points [35] were extracted graphically.

The activity coefficient of dilute UCl_4 ($\gamma_{U^{4+}}$) in NaCl-KCl eutectic was recalculated from the measurements of Flengas [193] using Equation (5.15) for comparison against model-determined values. The apparent potential (E^*) was determined from the standard reduction potential of the anode ($E^{o}_{U^{4+\rightarrow 3+}}$), which was derived from the standard Gibbs energy of reaction ($\Delta_r G^o$) for the reduction of the tetrachloride via $UCl_4(l) \rightarrow UCl_3(l)+0.5Cl_2(g)$ (Equation (5.16)), and the standard reduction potential of the cathode ($E^{o}_{Ag^+}$). $\gamma_{U^{3+}}$ which is also available from the measurements of Flengas [193], with $\gamma_{Ag^+} = 1$ for a NaCl-KCl eutectic electrolyte [193]. E^* and m are the intercept and slope of a linear regression of the experimental cell potential (E_{cell}) using Equation (5.17).

The calculated results for the dilute activity coefficient of liquid UCl_4 are in very good agreement with experimental values but do not precisely reproduce the temperature dependence (Figure 5.10). Overall, the values are in the range of experimental uncertainty for open circuit potentiometric measurements of uranium chlorides [188], and since the calculated $\gamma_{U^{4+}}$ values were measured relative to those previously determined for $\gamma_{U^{3+}}$ [193], they are expected to have a larger uncertainty due to the compounding of errors from the experimentally determined $\gamma_{U^{3+}}$ values.

$$E^* = E^{o}_{Ag^+} - E^{o}_{U^{4+\rightarrow 3+}} + \frac{RT}{F}\ln\left(\frac{\gamma_{Ag^+}\,\gamma_{U^{3+}}}{\gamma_{U^{4+}}}\right) \quad (5.15)$$

$$E^{o}_{U^{4+\rightarrow 3+}} = 3E^{o}_{U^{3+}} - 4E^{o}_{U^{4+}} \quad (5.16)$$

$$E_{cell} = E^* + m\ln\left(\frac{x_{Ag^+}\,x_{U^{3+}}}{x_{U^{4+}}}\right) \quad (5.17)$$

UCl_3-UCl_4

Kraus [27] determined that UCl_3 and UCl_4 have only limited liquid miscibility, albeit from only a small number of phase equilibria experiments. This contradicts

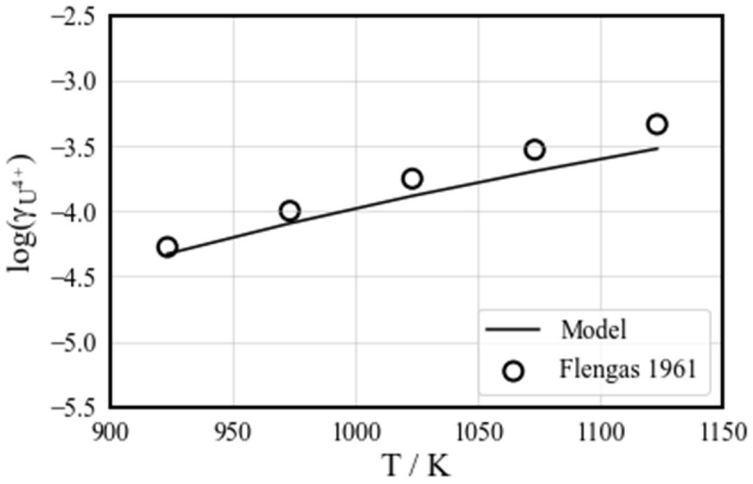

Figure 5.10: Calculated and experimental [193] infinitely dilute activity coefficient of liquid UCl_4 in 1:1 molar NaCl-KCl.

Desyatnik et al. [32] whose measurements indicate a eutectic and significant solubility of UCl_4 in UCl_3 up to ~45mol% UCl_4. Considering only phase diagram data are available, our attempts to model the solid solution were unable to produce a satisfactory description capable of representing the solidus and solvus without an unjustifiably large number of parameters. Also, the limiting slope of the UCl_3-rich liquidus agrees well with a solely eutectic description. Thus, the system is described as a simple eutectic to avoid the uncertainty of an excessively parameterized Gibbs energy description of the solid solution, with the determined interaction parameter of Equation (5.18) which allowed the computing of the phase diagram of Figure 5.11 that very well represents liquidus values. The eutectic temperature is reported by Desyatnik et al [32] as 818.2K, but this is likely too low as this eutectic temperature cannot be reconciled with the temperatures of the liquidus, and moreover, it coincides with the solid-transition temperature of 821K reported by Fouque et al. [222].

$$\Delta G_{U_2^{6+}U^{4+}/Cl} = -4500 \tag{5.18}$$

$MgCl_2$-UCl_4

Phase equilibria for the $MgCl_2$-UCl_4 system were measured by Sterlin and Artamonov [33] and Desyatnik et al. [32] who report the same eutectic temperature of 813.2K, however, their reported liquidus temperatures and eutectic compositions are significantly different. The measurements of Desyatnik et al. [32] are more reliable as they are from differential thermal analysis (DTA) rather than the surface temperature technique of Sterlin and Artamonov [33]. Ideal mixing of the liquid $MgCl_2$ and UCl_4 endmembers yields liquidus temperatures that are much lower than observed, implying the need for a positive liquid interaction parameter.

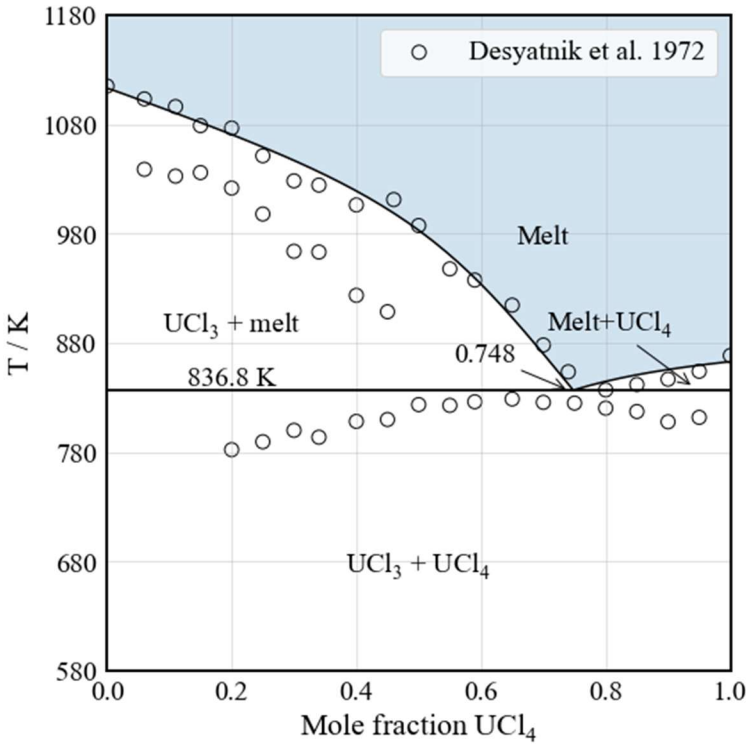

Figure 5.11: Calculated phase diagram and experimental [32] phase equilibria of the UCl_3-UCl_4 system.

Since $MgCl_2$ is known to form complex anions of type $MgCl_4^{2-}$ [242] and UCl_4 forms UCl_6^{2-} complexes [243], the need for a positive Gibbs interaction may be explained by competition between complexes formed by the endmembers, which would be similar to the positive values observed for the BeF_2-ZrF_4 system [244], but to a lesser extent due to Mg^{2+} and U^{4+} being less strongly polarizing than are Be^{2+} and Zr^{4+}. Our assessment uses a liquid SNN coordination number ratio and liquid interaction parameter that best reproduces the eutectic composition. The use of the MQMQA interaction parameter of Equation (5.19) produces the calculated phase diagram in Figure 5.12 which very well describes the liquidus. As in the case of the UCl_3-UCl_4 system, the calculated eutectic temperature of the resultant model is higher than that observed, likely caused by the difficulty of distinguishing the eutectic reaction from the solid-solid transitions of UCl_4 which occur just below that temperature.

$$\Delta G_{Mg U^{IV}/Cl} = 1500 \tag{5.19}$$

NaCl-KCl-CrCl₂

We have created a first-time thermodynamic assessment of this pseudo-ternary system from the available phase equilibria of Seifert and Klatyk [29], Shiloff [214], Kanno et al. [215], Gut and Gnehm [216], and Belorukova et al. [36] and EMF data for dilute $CrCl_2$ in KCl and NaCl-KCl eutectic from Tumidajski and Flengas [245]. The experimental data are used together with our estimations of $\Delta_{mix}H$ for the NaCl-$CrCl_2$ and KCl-$CrCl_2$ systems which follow the method described by Shorne-Pinto et al. [142].

The pseudo-binary subsystems contain the intermediate compounds Na_2CrCl_4 [215,246], K_2CrCl_4 [29], and KCrCl3 [29] for which S^{298} is not available, nor is $\Delta_f H_{298}$ available for Na_2CrCl_4. Thus, the pseudo-ternary model has a minimum of eight DOF,

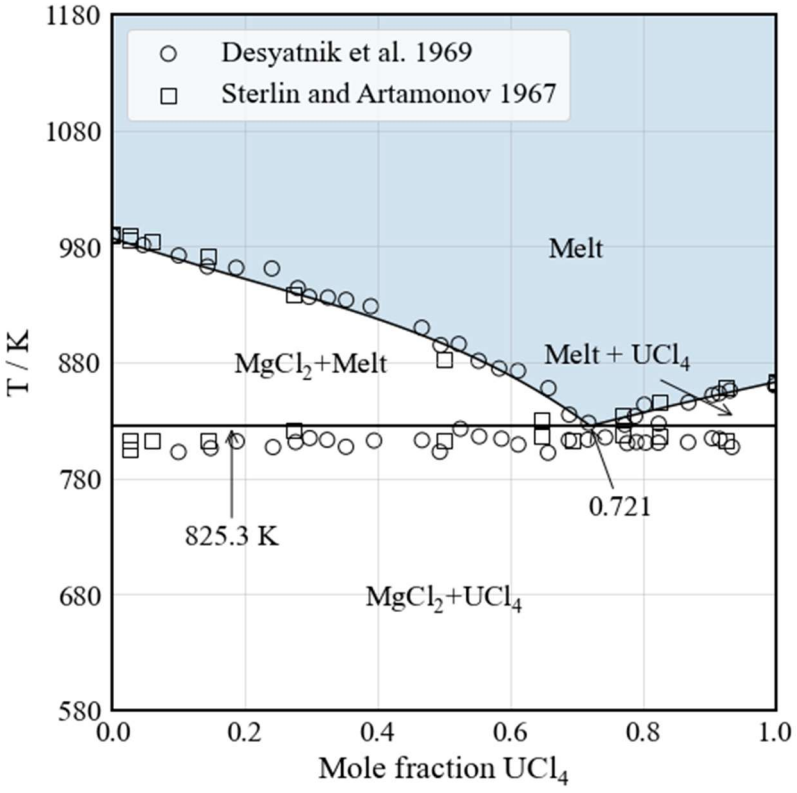

Figure 5.12: Calculated phase diagram and experimental phase equilibria of the $MgCl_2$-UCl_4 system [32,33].

represented by the liquid interaction parameters and liquid SNN coordination number ratio of each pseudo-binary system, S^{298} of the three intermediate compounds, and $\Delta_f H_{298}$ of Na_2CrCl_4. As demonstrated in the previous system assessments, 7 DOF may be constrained through the use of the constituent pseudo-binary phase equilibria. The final DOF may be constrained using a cationic potential correlation that allows relatively accuate estimatation of the $\Delta_f H_{298}$ of Na_2CrCl_4.

As noted, we used a correlational approach between elemental periods [107] to estimate the $\Delta_f H_{298}$ of the Na_2CrCl_4 compound. A suitable dataset exists in the tabulated values of Glushko [197] including those for K_2CoCl_4, Rb_2CoCl_4, Cs_2CoCl_4, Na_2MnCl_4, Rb_2MnCl_4, Cs_2MnCl_4, K_2FeCl_4, Rb_2FeCl_4, and Cs_2FeCl_4. We determined a clear linear relationship between $\Delta_f H_{298}$ and IP_A/IP_M for the alkali series of fixed transition metal chloride, varying A with constant M in A_2MCl_4. For constant A and varying M, the trend is quadratic between Co, Fe, and Mn, in agreement with our earlier results for constant alkali $\Delta_{mix} H$ trends [142]. The experimental $\Delta_f H_{298}$ values and correlations are shown in Figure 5.13 and the resultant predicted values for both linear and quadratic correlations are given in Table 5.7.

Additional $\Delta_f H_{298}$ data are available for alkali transition metal double chlorides of the type A_2MCl_4, including the intermediate compounds Rb_2TiCl_4, Cs_2TiCl_4, Rb_2CuCl_4, Cs_2CuCl_4, Rb_2VCl_4, and the alkali series of A_2ZnCl_4 [197]. As shown in Figure 5.13, however, these values were not included in the correlations as they do not conform to the observed trend between Co, Fe, Cr, and Mn that we also observed in available $\Delta_{mix} H$ values.

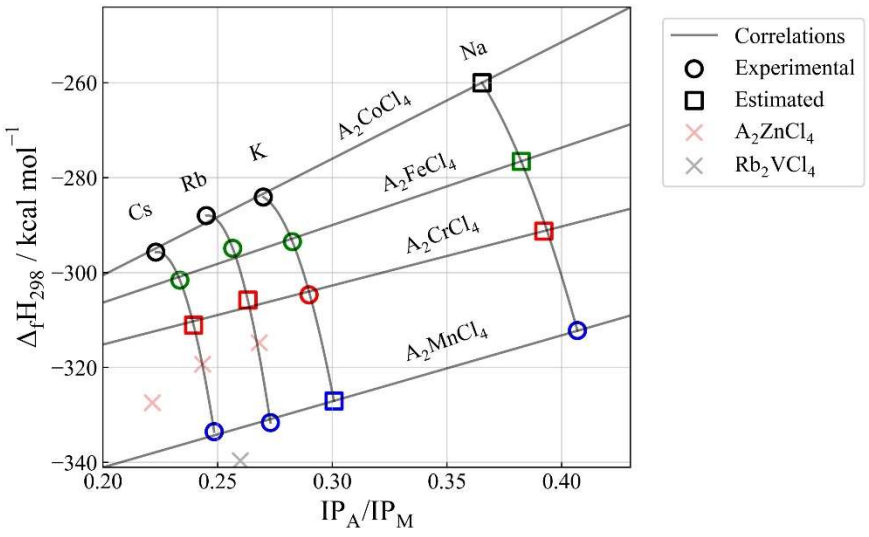

Figure 5.13: Experimental and estimated 298K formation enthalpy for A_2MCl_4 compounds [197].

Table 5.7: Estimated compound values of this work.

Compound	$\Delta_f H_{298}$ / kJ mol^{-1} [a]
Na_2CoCl_4	-1088±28
Na_2FeCl_4	-1157±31
Na_2CrCl_4	-1217±28[b]
K_2MnCl_4	-1368.3±2.4
Rb_2CrCl_4	-1279.4±2.0
Cs_2CrCl_4	-1301.4±1.7

[a] Expanded uncertainties U(H) of 95% confidence. Caution: confidence intervals should not be interpreted as a 95% probability that the estimated interval contains the true value [247].
[b] Extrapolated from the A_2CrCl_4 set using interpolated estimations of Rb_2CrCl_4 and Cs_2CrCl_4

We also estimated the liquid $\Delta_{mix}H$ for NaCl-$CrCl_2$ and KCl-$CrCl_2$ from the available $\Delta_{mix}H$ data [248] for the ACl-$MnCl_2$, ACl-$FeCl_2$, and ACl-$CoCl_2$ systems, so that together with the EMF measurements of Tumidajski and Flengas [245] and the pseudo-ternary phase equilibria of Belorukova et al. [36], an additional four liquid interaction parameters may be included in the solution models without underspecifying the Gibbs energy description. We again assumed a linear relationship between the molar compositions of maximum SRO (x_{SRO}) in the self-same alkali chloride systems (Figure 5.14), calculated $\Delta_{mix}H$ at the ACl-$CrCl_2$ x_{SRO} for each system in the dataset, and finally, used a quadratic correlation between these to estimate the unknown $\Delta_{mix}H$ (Figure 5.15).

The resultant values of x_{SRO} for the NaCl-$CrCl_2$ and KCl-$CrCl_2$ systems are 0.42±0.01 and 0.43±0.02, respectively, and the most negative values of $\Delta_{mix}H$ are -7093±363 and -15757±804 J mol^{-1}, respectively. As shown in Figure 5.16, the available experimental data and estimations of this work yielded Equations (5.20)-(5.23) which are used to very well describe all available pseudo-binary phase equilibria. The pseudo-ternary phase equilibria measurements shown in Figure 5.17 are also very well represented without the use of pseudo-ternary liquid interaction parameters. The estimated values of $\Delta_{mix}H$ and resultant calculated values are shown in Figure 5.18a, and the calculated and experimental values of γ_{CrCl2} in 1:1 molar NaCl-KCl are provided in Figure 5.18b, all showing very good agreement.

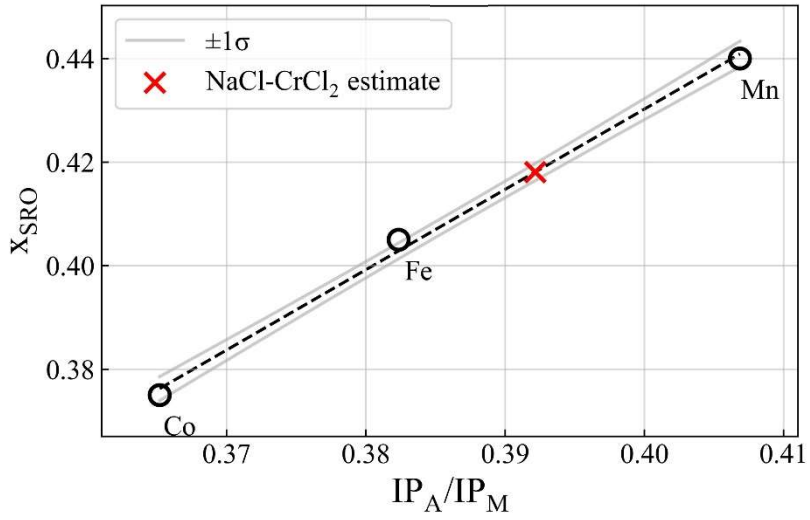

.

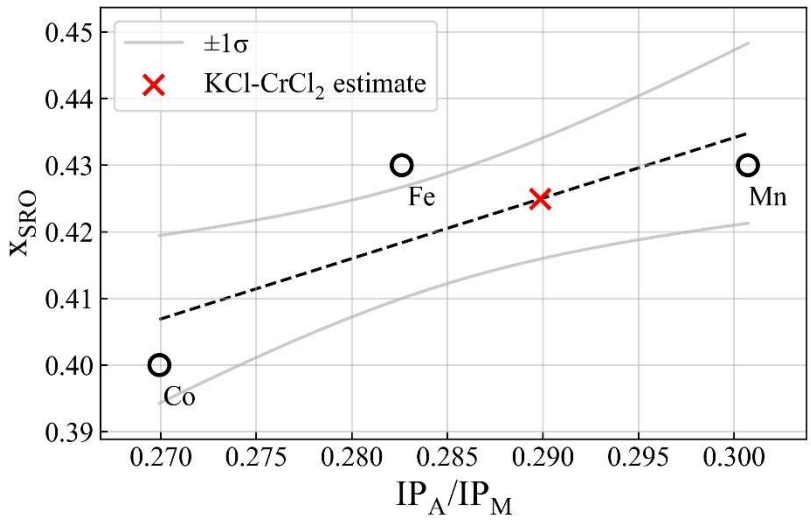

Figure 5.14: Estimated composition of maximum short-range ordering, a) $NaCl\text{-}CrCl_2$ (, b) $KCl\text{-}CrCl_2$.

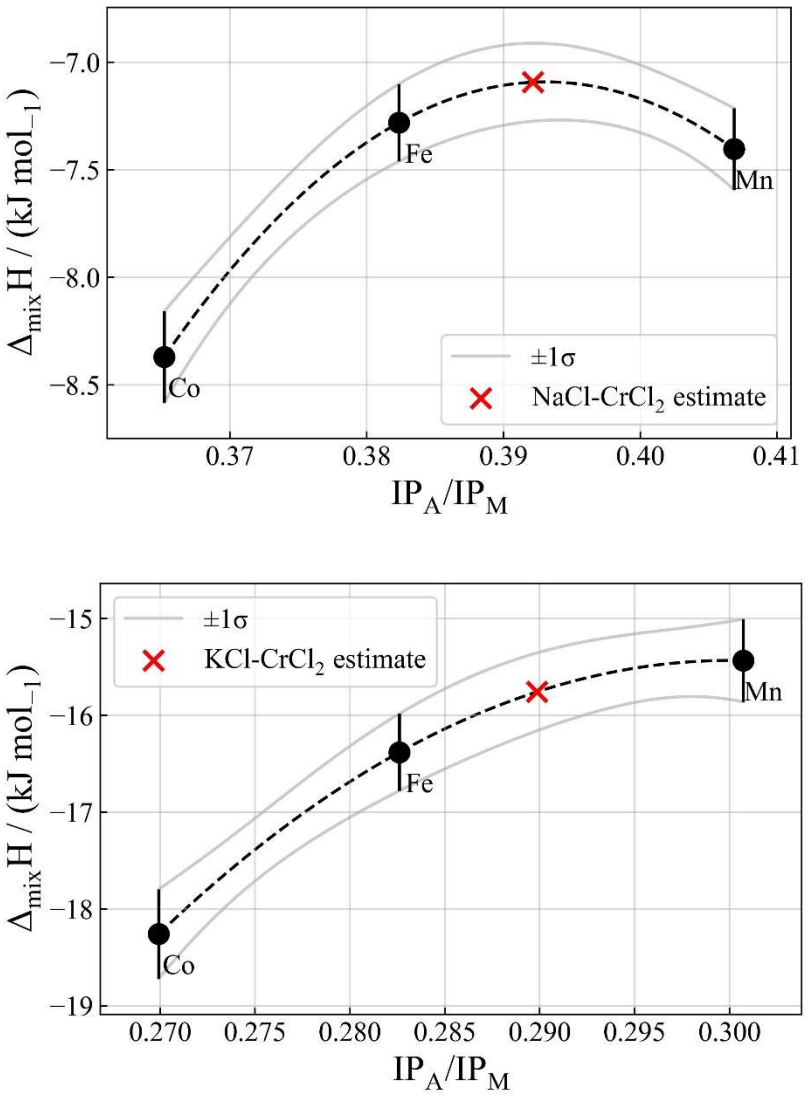

Figure 5.15: Estimated $\Delta_{mix}H$ at 1083K, a) NaCl-$CrCl_2$, b) KCl-$CrCl_2$.

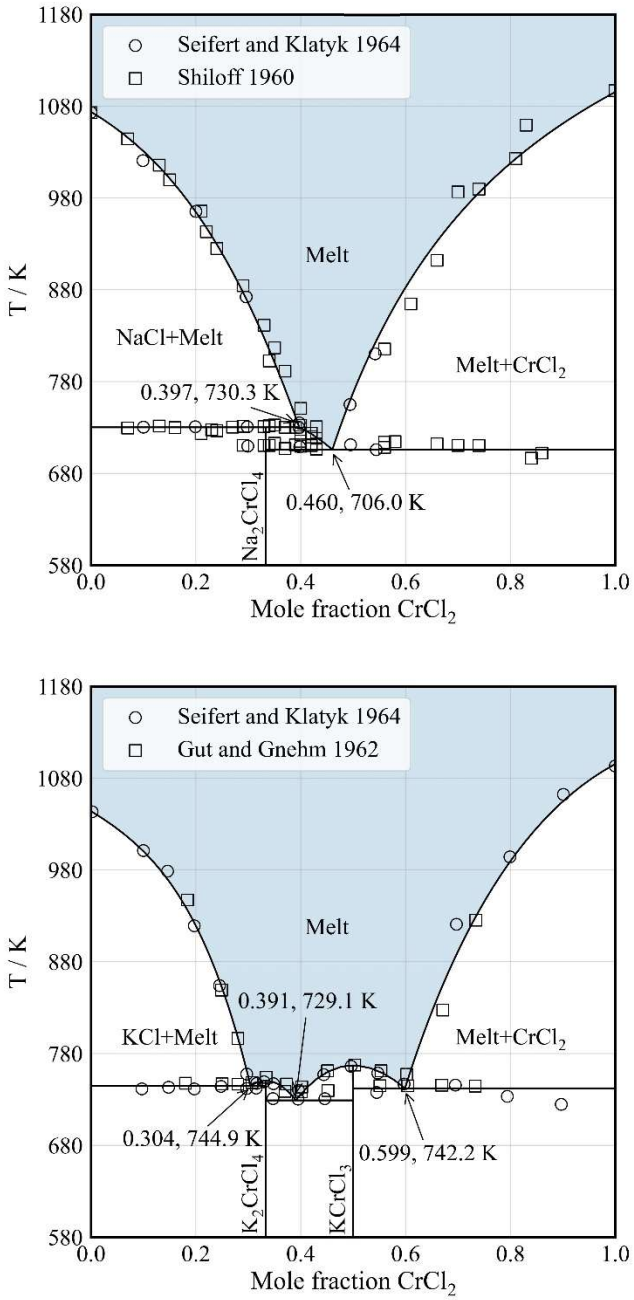

Figure 5.16: Calculated phase diagrams of the a) $NaCl\text{-}CrCl_2$ and b) $KCl\text{-}CrCl_2$ systems.

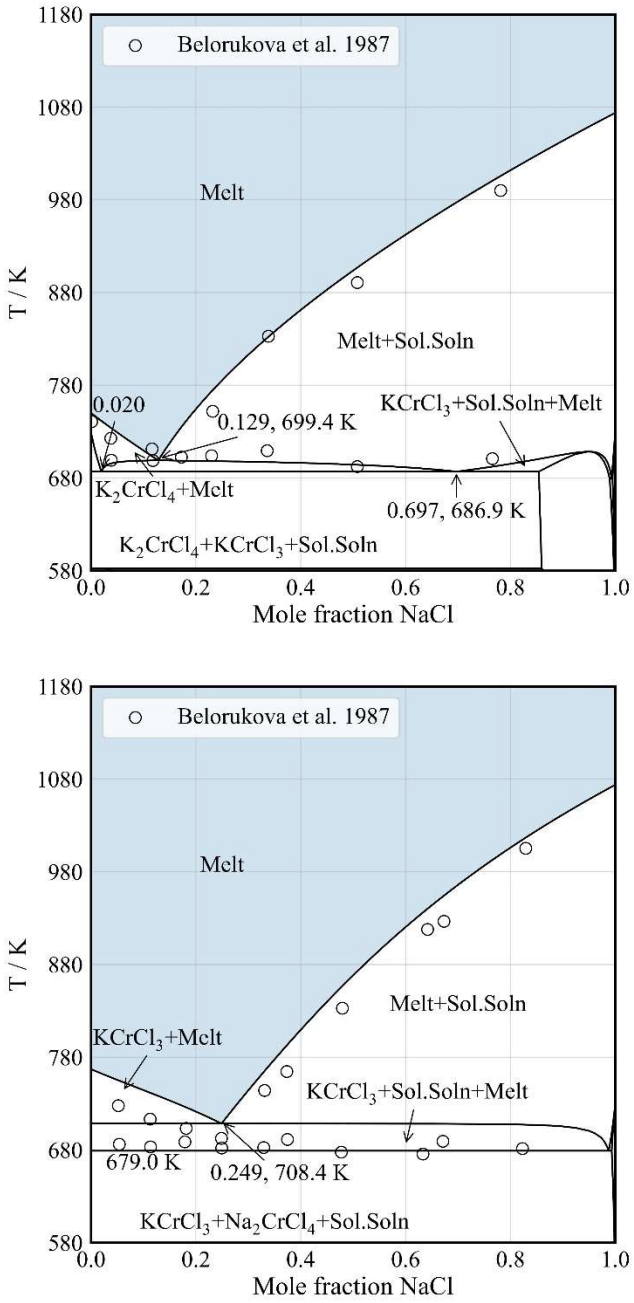

Figure 5.17: Calculated phase diagrams in the NaCl-KCl-$CrCl_2$ system, a) K_2CrCl_4-NaCl, b) $KCrCl_3$-NaCl, where experimental points from Belorukova et al. [36] were recalculated to represent pseudo-ternary mole fractions.

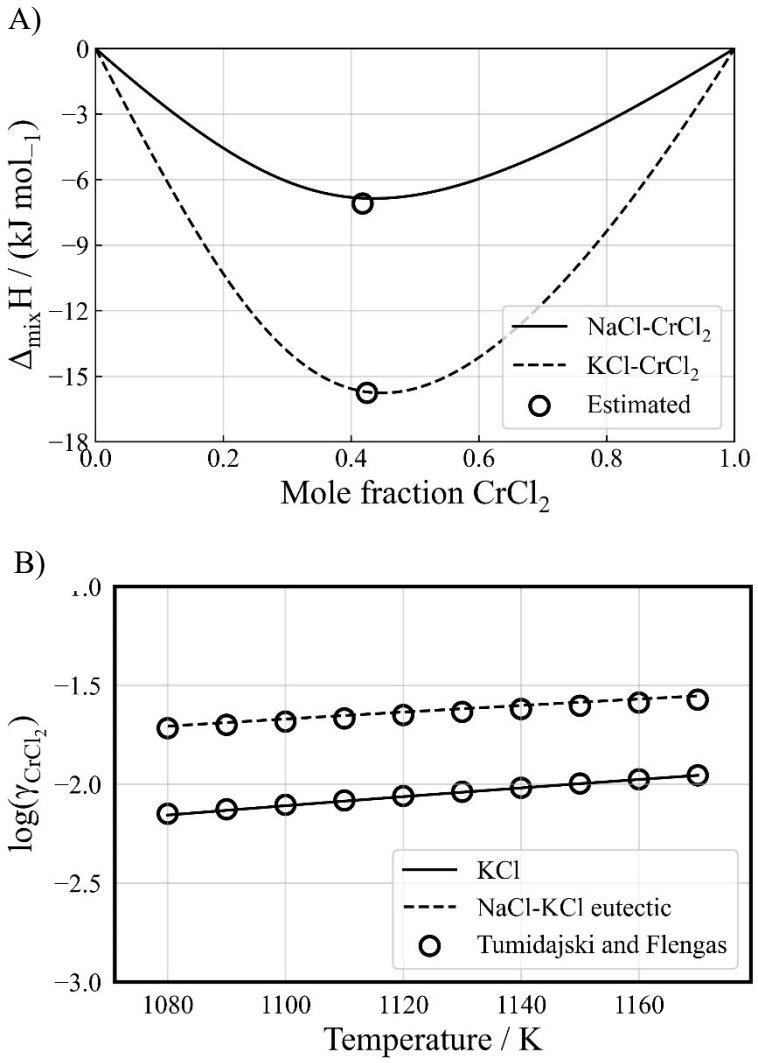

Figure 5.18: a) Estimated and model calculated $\Delta_{mix}H$ at 1083K for NaCl-$CrCl_2$ and KCl-$CrCl_2$ systems. b) Calculated and experimental [245] dilute $CrCl_2$ liquid activity coefficient in the NaCl-KCl-$CrCl_2$ system.

$$\Delta G_{NaCr/Cl} = -8550 - 0.2T\chi_{NaCr/Cl} \quad (5.20)$$

$$\Delta G_{KCr/Cl/Cl} = -18670 + 2.9T - 12500\chi_{CrK/Cl} + 680\chi^2_{KCr/Cl} \quad (5.21)$$

$$Z^{Na}_{NaCr/Cl} = 4.2\ ;\ Z^{Cr}_{NaCr/Cl} = 6 \quad (5.22)$$

$$Z^{K}_{KCr/Cl} = 3;\ Z^{Cr}_{KCr/Cl} = 6 \quad (5.23)$$

NaCl-KCl-$MgCl_2$-$CrCl_2$

The pseudo-binary and pseudo-ternary systems assessed in this work together with the models of Robelin et al. [185] only lack solution models of the $MgCl_2$-$CrCl_2$, NaCl-$MgCl_2$-$CrCl_2$, and KCl-$MgCl_2$-$CrCl_2$ systems for a complete pseudo-quaternary description. We have developed this first-time pseudo-quaternary model from the joint assessment of the phase equilibria [28] of $MgCl_2$-$CrCl_2$, and the EMF measurements for dilute $CrCl_2$ in the NaCl-$MgCl_2$ [219], KCl-$MgCl_2$ [220] and NaCl-KCl-$MgCl_2$ systems [221].

The experimental phase diagram [28] of the $MgCl_2$-$CrCl_2$ system indicates a eutectic resulting from the equilibrium between the melt and two solid solutions. Since an additional assessment parameter for each solid solution must be unambiguously determined in addition to the liquid interaction parameter and liquid SNN coordination number ratio, there are four DOF that must be constrained in the assessment. As $MgCl_2$-MCl_2 data [249] for Mn, Fe, and Co are available, the composition and magnitude of the $\Delta_{mix}H$ in the $MgCl_2$-$CrCl_2$ system may be estimated by the previously described procedure (Figure 5.19), thus providing the needed constraint for the liquid SNN coordination number. The $\Delta_{mix}H$ estimation may also be used jointly with the EMF of dilute $CrCl_2$ in NaCl-KCl-$MgCl_2$ to specify the pseudo-binary liquid interaction parameter. The remaining two DOF are resolved using the liquidus reaction of the $MgCl_2$ and $CrCl_2$ rich regions to specify the $MgCl_2$ and $CrCl_2$ rich solid solution interaction parameters, respectively.

A)

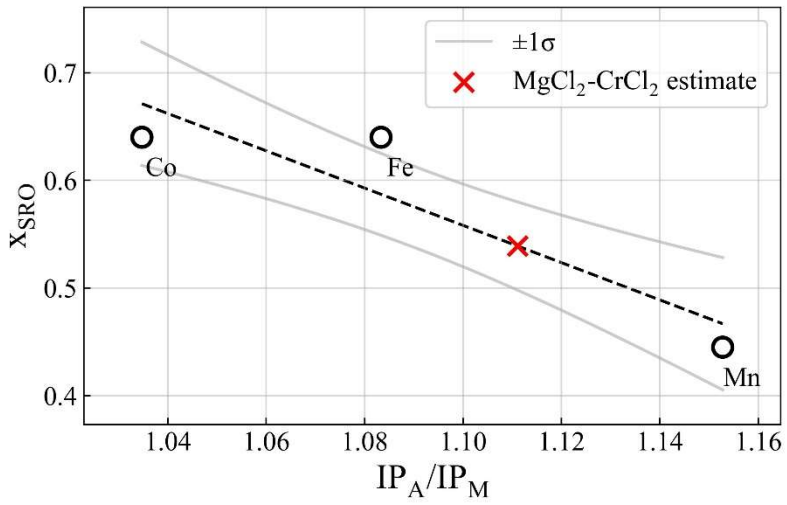

B)

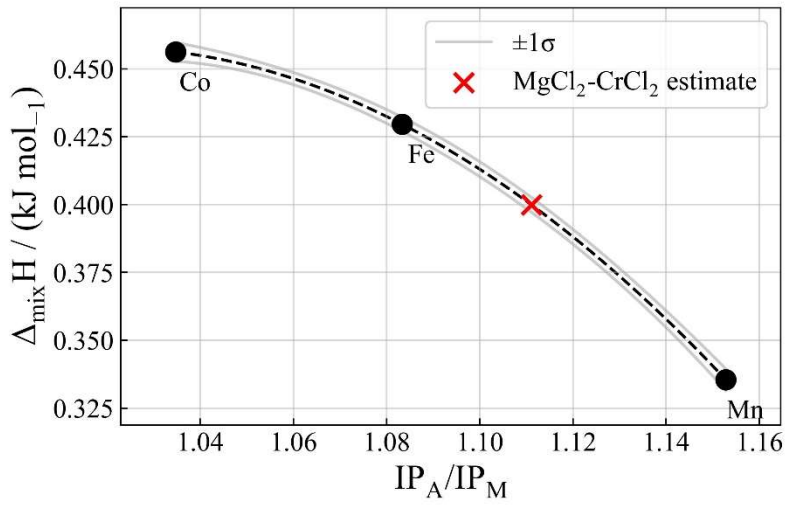

Figure 5.19: $MgCl_2$-$CrCl_2$ system estimates at 1083K, a) $x_{SRO} = 0.54$ and b) $\Delta_{mix}H = 0.399\ \text{kJ mol}^{-1}$.

The phase diagram, Figure 5.20, is calculated following Equations (5.24)-(5.26) and provides a good description of the liquid phase behavior. The calculated liquid γ_{CrCl_2} also agrees well with the EMF measurements of Zhang et al. [221], Figure 5.21, which we have recalculated from the original data to account for the composition dependence of the liquid $CrCl_2$ activity in the NaCl-KCl-$MgCl_2$ system which Zhang et al. assumed to be negligible.

$$\Delta G_{MgCr/Cl} = 545 \quad (5.24)$$

$$G^{xs}_{MgCr/Cl} = 700 Y_{Cr} \quad (5.25)$$

$$G^{xs}_{CrMg/Cl} = 850 Y_{Mg} \quad (5.26)$$

The experimental γ_{CrCl_2} values of the pseudo-quaternary system [221], Figure 5.21, indicate small negative solution interactions, which is contrary to the positive deviations found in the γ_{CrCl_2} values of the pseudo-ternary systems. For example, the value in the NaCl-$MgCl_2$-$CrCl_2$ system at 748.2K is slightly positive, $\log(\gamma_{Cr\ _2}) = 0.166$ [219], which contrasts with our model calculated value of -0.479. Furthermore, the values in the KCl-$MgCl_2$-$CrCl_2$ system are $\log(\gamma_{CrCl_2}) = -0.401$ and 0.168 for two separate measurements at 748.2K [220], which contrast with the model calculated value of -1.427. Since the calculated values in the pseudo-ternary systems are only known at a single temperature, the temperature dependent pseudo-quaternary data of Zhang et al. [221] were preferred for the fit of Equation (5.24).

Equilibrium $CrCl_2$ formation from Hastelloy-N

To characterize the thermodynamic driving forces for alloy corrosion via $CrCl_2$ formation as a function of temperature, salt composition, and redox condition, we examined the equilibrium between Hastelloy-N (Ni-5.7Cr-24.0Mo-4.4Fe molar basis), modeled with the Factsage™ [120] SGTE database, with NaCl-KCl-$MgCl_2$-$UCl_{3,4}$ molten

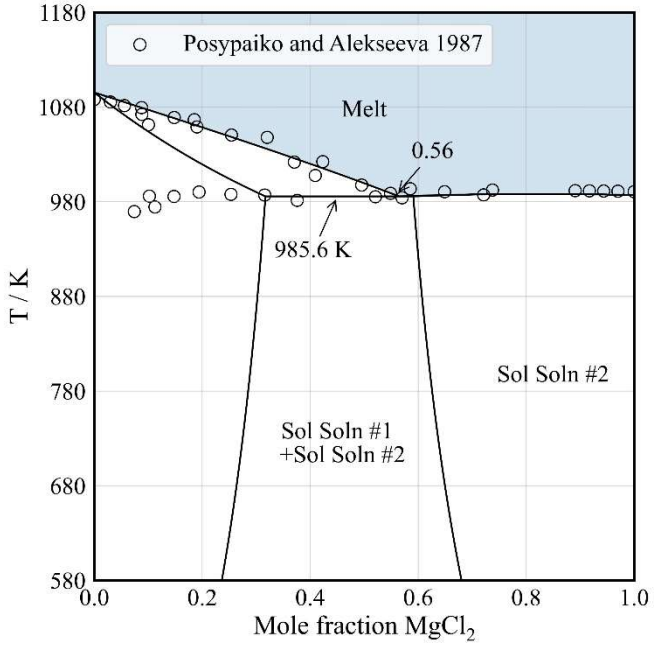

Figure 5.20: Calculated phase diagram of the $MgCl_2$-$CrCl_2$ system.

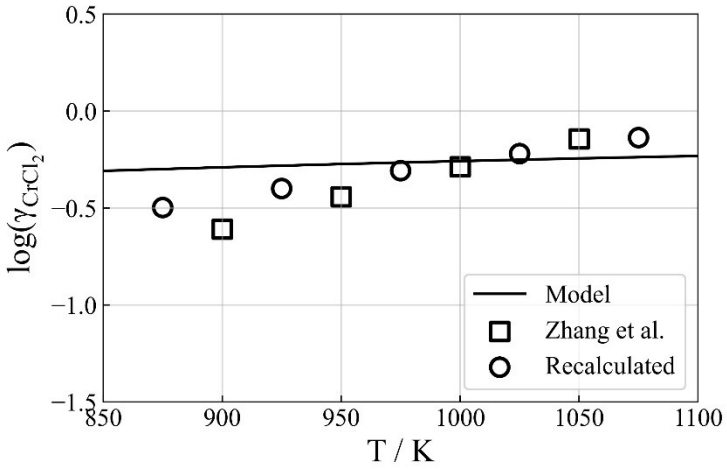

Figure 5.21: Calculated and experimental [221] activity coefficients of dilute $CrCl_2$ in NaCl-KCl-$MgCl_2$ eutectic.

salt. The nominal salt composition was $10UCl_3$-30NaCl-30KCl-$30MgCl_2$ and variations in composition maintained a constant total molar content and a 1:1 NaCl to KCl ratio. The total uranium content also remained fixed with variations in the U^{4+}/U^{3+} ratio to explore corrosion potential as a function of the overall salt redox state, as indicated by the equilibrium molar fraction of $CrCl_2$ (x_{CrCl_2}). The result at 1000K and the calculated difference in x_{CrCl_2} between 1300K and 1000K are provided in Figure 5.22a and Figure 5.22b, respectively.

It is well known that highly reactive metals like K, Li, Na, and Mg can promote a reducing environment [17], and thus, decrease the amount of corrosion in molten salts [207,250]. However, metallic K and Na would be problematic in a MSR melt, and Li softens the neutron spectrum, which may be undesirable. Thus, for our nominal salt composition, we have examined the impact of trace magnesium additions on the corrosion potential at 1000K (Figure 5.23). The equilibrium x_{CrCl_2} calculations are consistent with the experimental results of Sankar and Singh [250] for Li additions in alkali fluoride salt, showing that a very small amount of reactive metal can significantly decrease corrosion potential.

Discussion

The need for well-specified Gibbs energy relations has been recognized since the earliest days of CALPHAD modeling and is essential to proper thermodynamic assessments [39]. Therefore, we limited the parameterization of the thermodynamic assessments in this work commensurate with the quantity and quality of available thermodynamic data, and thus allowed the creation of well-conditioned solution models. In some cases, such as the systems involving UCl_4, the models are informed solely by phase equilibria, thus necessitating the MQMQA parameterization to be restricted to a single

A)

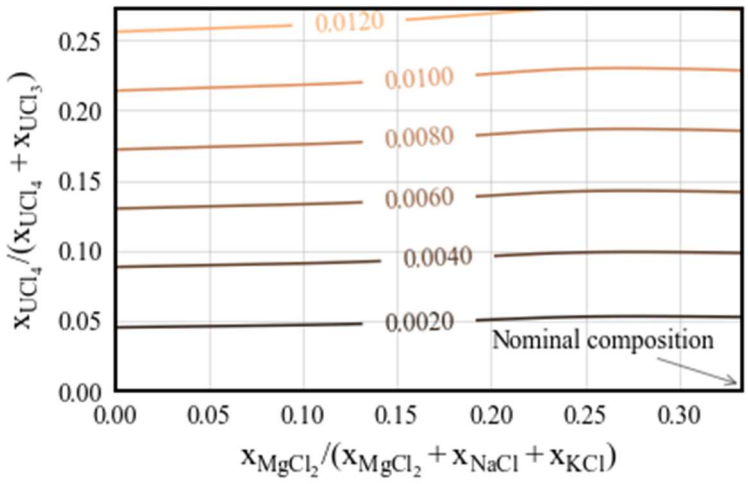

B)

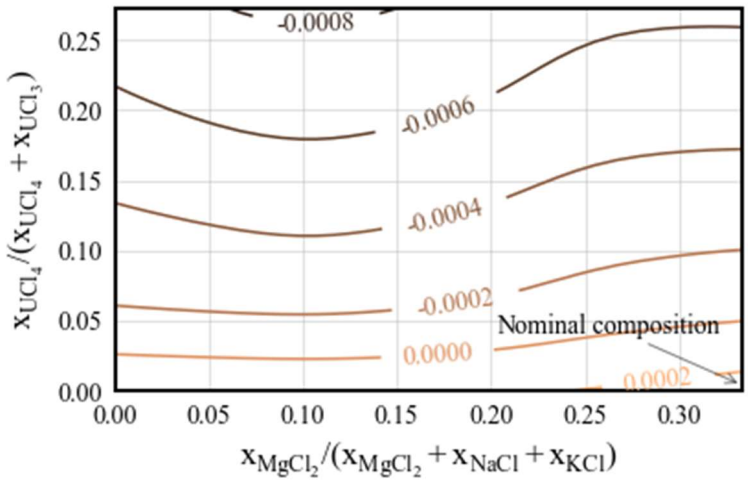

Figure 5.22: a) Calculated x_{CrCl_2} isocontours at 1000K. b) Difference at 1300K, $x_{CrCl_2}(1300\text{K}) - x_{CrCl_2}(1000\text{K})$.

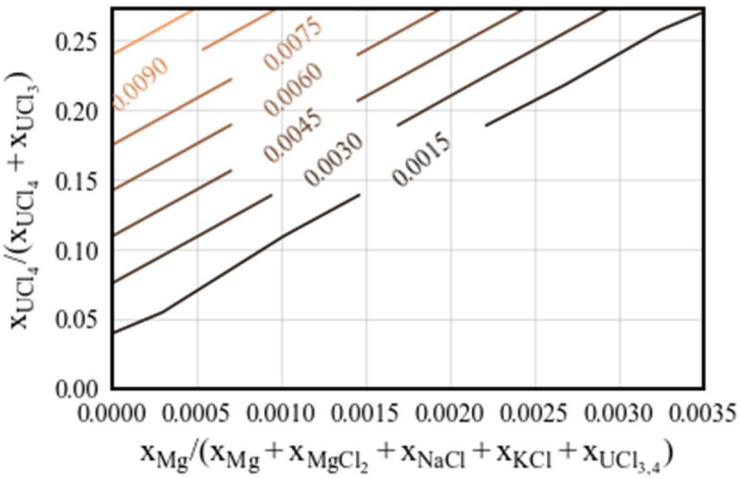

Figure 5.23: Effect of trace magnesium additions on Hastelloy-N $CrCl_2$ formation in NaCl-KCl-$MgCl_2$-$UCl_{3,4}$ salt at 1000K.

parameter. In doing so, the calculated phase diagram of Figure 5.7, for example, does not well reproduce the experimental liquidus in a limited range of compositions near K_2UCl_6, a worthwhile trade-off in exchange for a well-conditioned MQMQA model capable of returning reliable $\Delta_{\mathrm{mix}}H$ and thermodynamic activity estimates.

The need for this concession in the modeled phase equilibria is due to the tendency of UCl_4 to form monomer complexes of varying coordination [243,251,252] when mixed with heavy secondary cations [253]. Pure species exhibiting complex speciation in mixtures of alkali chlorides have been successfully modeled in the MQMQA using multiple endmembers. This approach was applied to $AlCl_3$ [254], $BeCl_2$ [122], and UCl_3 [126], to improve phase equilibria descriptions over all compositions by modeling multiple species which each contribute to the overall SRO, thus allowing a more complex melt coordination environment as a function of temperature and composition. Similarly, UCl_4 requires such treatment in a MQMQA description based on spectrophotometric observations which found composition-dependent complexes of type $UCl_n^{(n-4)-}$, though predominantly UCl_6^{2-} [243]. Molecular dynamics simulations have also described polymeric linking between complexes of type $UCl_n^{(n-4)-}$ [251]. Additionally, electrical conductivities of UCl_4 melts in alkali chlorides indicate structural variations related to complex formation, with peak deviations from the theoretical values of Markov's equation occurring near the A_2UCl_6 composition [255].

We have previously explored MQMQA descriptions that utilized multiple UCl_4 endmembers, which allowed very accurate representations of the ACl-UCl_4 phase equilibria at any composition. However, we have elected not to model these complexes in the present work because each additional endmember in the thermodynamic description

requires the definition of a unique Gibbs energy function. Since these functions are not known for the UCl_4 complexes, doing so would further underspecify the solution models, and create difficulty in estimating the experimentally unknown $\Delta_{mix}H$ from the phase diagrams. Thus, a single endmember description of UCl_4 was chosen despite the experimental evidence justifying the modeling of its complexes. Doing so has allowed the systems involving UCl_4 to be developed with fully specified MQMQA functions to produce improved results in $\Delta_{mix}H$ and thermodynamic activity for the MSR relevant compositions of <20mol% UCl_4.

The solution models of the NaCl-KCl system were previously assessed [185] and are compatible with a large number of systems in *MSTDB-TC*. However, our earlier thermodynamic assessment of the LiCl-NaCl-KCl-UCl_3 pseudo-quaternary system [206] reported the NaCl-KCl solid solution as requiring reassessment due to being overly stable in the pseudo-ternary systems involving UCl_3. We have found the same to be true in this work on the NaCl-KCl-UCl_4 system. Thus, in Figure 5.9, the NaCl-KCl solid solution was excluded from the calculation where the NaCl-KCl solid solution is known not to be stable [35]. This approach allowed accurate reproduction of the experimental pseudo-ternary liquidus determined by Desyatnik et al. [35].

From the mole fraction isocontours of Figure 5.22, it is obvious that the $CrCl_2$ concentration in the melt is very small overall and driven almost entirely by the U^{4+}/U^{3+} ratio. Not surprisingly then, at a constant U^{4+}/U^{3+} ratio, increasing concentrations of $MgCl_2$ is seen to have a small negative effect on $CrCl_2$ formation up to a ~3:1 NaCl+KCl to $MgCl_2$ ratio. On the other hand, the effect of temperature on $CrCl_2$ formation is composition-dependent, with the concentration increasing with the U^{4+}/U^{3+} ratio, particularly near the

~2.3:1 NaCl+KCl to $MgCl_2$ composition. This compositionally dependent inverse relationship between temperature and $CrCl_2$ formation merits further investigation with the objective of possibly limiting temperature-driven $CrCl_2$ transport from regions of high to low temperature in molten chloride MSRs.

Conclusions

Several novel thermodynamic assessments were performed in this work, including those for $CrCl_2$-UCl_3, UCl_3-UCl_4, NaCl-UCl_4, KCl-UCl_4, $MgCl_2$-UCl_4, NaCl-$CrCl_2$, and KCl-$CrCl_2$ pseudo-binary systems. As well, first-time DSC measurements in the $CrCl_2$-UCl_3 system and confirming measurements of the $MgCl_2$-UCl_3 system were obtained. The high-order systems described for the first time include the NaCl-KCl-UCl_4 and NaCl-KCl-$CrCl_2$ pseudo-ternary systems, and these culminated in the development of a set of models and values for the pseudo-quaternary NaCl-KCl-$MgCl_2$-$CrCl_2$ system that agree well with observations and thus are appropriate for corrosion-related calculations in chloride MSRs. In this work, these system assessments were incorporated into *MSTDB-TC* and used to demonstrate the equilibrium formation of $CrCl_2$ from Hastelloy-N, using a range of NaCl-KCl-$MgCl_2$ compositions in addition to variations in the U^{4+}/U^{3+} redox state together with a model for the alloy.

In the course of this work, correlational approaches were used to obtain reliable estimations of $\Delta_f H_{298}$ values for Na_2CoCl_4, Na_2MnCl_4, Na_2CrCl_4, Rb_2CrCl_4, and Cs_2CrCl_4 as well as $\Delta_{mix}H$ values at the compositions of the maximum $\Delta_{mix}H$ for the NaCl-$CrCl_2$ and KCl-$CrCl_2$ systems. Knowledge of these values, in addition to a constrained thermodynamic assessment methodology, allowed full specification of solution model interaction parameters, which ensures that the developed Gibbs energy descriptions provide good representations of $\Delta_{mix}H$ and thermodynamic activity. Thus, the assessments

represent a reliable high-order set of thermodynamic models and values for the NaCl-KCl-$MgCl_2$-UCl_3-UCl_4-$CrCl_2$ system, developed using high-order system electrochemical and phase equilibria data, that will find direct application in multi-physics simulations of MSRs.

Example calculations using the results of this work indicate that corrosion of chromium in Hastelloy-N is driven primarily by the U^{4+}/U^{3+} redox ratio, however, even for relatively high UCl_4 content, the equilibrium concentration of $CrCl_2$ in the melt is low. Interestingly, an overall lower thermodynamic potential for $CrCl_2$ formation occurs at higher temperatures, although the effect is very small. Additionally, only very small amounts of the reactive metal magnesium are needed to establish a reducing environment and minimize $CrCl_2$ formation, again, even for relatively high concentrations of UCl_4. The salt thermodynamic models and values are available in *MSTDB-TC* Ver. 2.0 and higher, which is publicly available.

Author Contributions

J.A.Y. was responsible for manuscript conceptualization, critical analysis of experimental data, and thermodynamic assessments. M.A performed XRD sample preparation, measurement, and analysis. J.S.P aided in the critical analysis of the assessments. J.C.A. curated the database implementation. M.A, J.P.S.P., R.E.B., C.M.D, and T.M.B advised J.A.Y. in various matters including graphical design, document structure, methodology, and statistical analysis. T.M.B. directed the research.

Acknowledgments

This research was supported by the U.S. Department of Energy Office of Nuclear Energy, Nuclear Energy University Programs under award DE-NE0008985 and by the DOE Nuclear Energy Advanced Modeling and Simulation Program administered by Oak

Ridge National Laboratory, which is operated by UT-Battelle, LLC, for the U.S. Department of Energy.

The authors are grateful to Prof. Hans-Conrad zur Loye for use of the XRD facilities, Hunter Tisdale for assistance in performing the XRD measurements, and Dr. Gregory Morrison for assistance in preparing XRD specimens.

Supplemental Material

Endmember characterization

The DSC of the $MgCl_2$ and $CrCl_2$ endmembers on heating and cooling are provided in Figure 5.24 and Figure 5.25, having heating profiles that are smooth and sharp. $MgCl_2$ doesn't have any indications of impurity on cooling, and the determined melting point of 986.8±2.0K agrees very well with the reference melting point of 987.2±1K [194,197]. On the other hand, the DSC profile of $CrCl_2$ has some aberrations below the melting point, and the melting point is 1090.5±2.1K which is lower than the reference value of 1097.2±2K [194,197], moreover, the uncertainty limits do not overlap by ~2.6K.

Powder XRD patterns were measured as described in the main manuscript and are shown here in Figure 5.26 and Figure 5.27. The patterns of $MgCl_2$ and $CrCl_2$ do not indicate any major impurities, and together with the DSC profiles, may be used to provide a qualitative assessment of their respective purity. For $MgCl_2$, we estimated a fractional purity of 0.99±0.01 molar basis due to lack of impurities in the XRD pattern and no appreciable melting point depression. For $CrCl_2$, although the XRD pattern of does not indicate the presence of impurities, the depressed melting point cannot be explained by random error.

To estimate the fractional purity of $CrCl_2$, we used an ideal solution model of the $CrCl_2$ and $CrCl_3$ endmembers in *MSTDB-TC* to calculate the mole fraction of $CrCl_2$ that

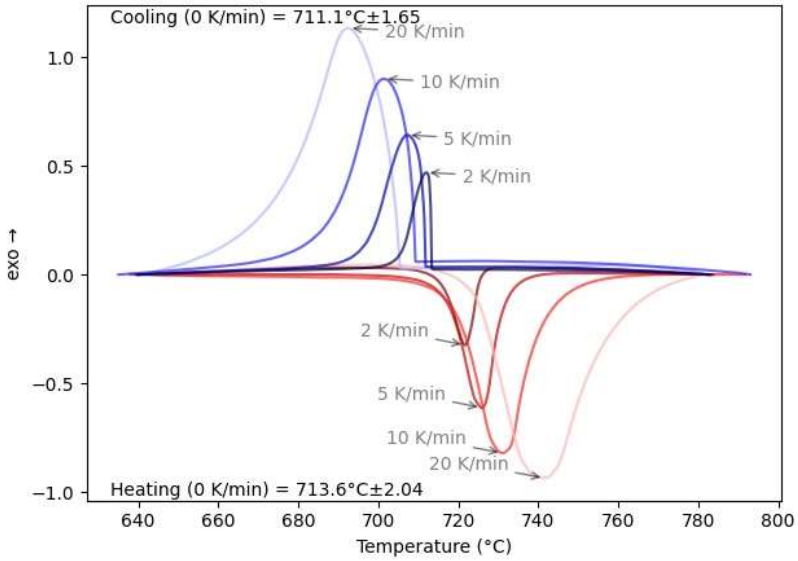

Figure 5.24: DSC measurement of $MgCl_2$ on heating and cooling at 2, 5, 10, and 20 K/min.

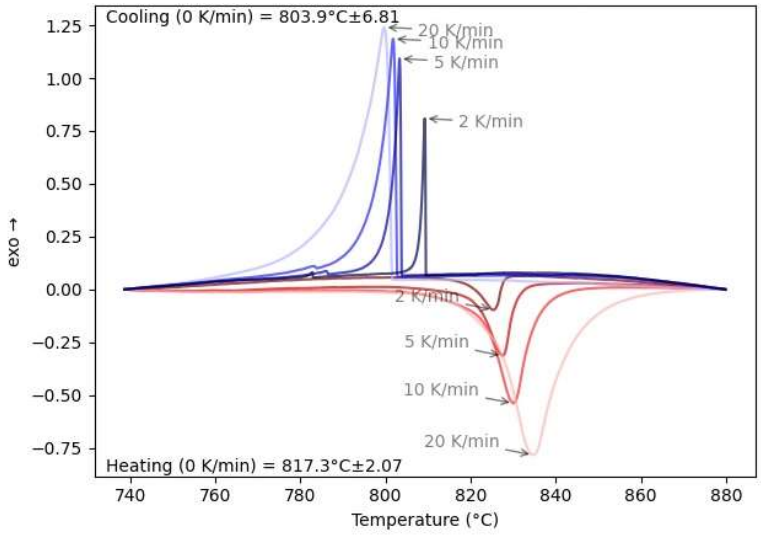

Figure 5.25: DSC measurement of $CrCl_2$ on heating and cooling at 2, 5, 10, and 20 K/min.

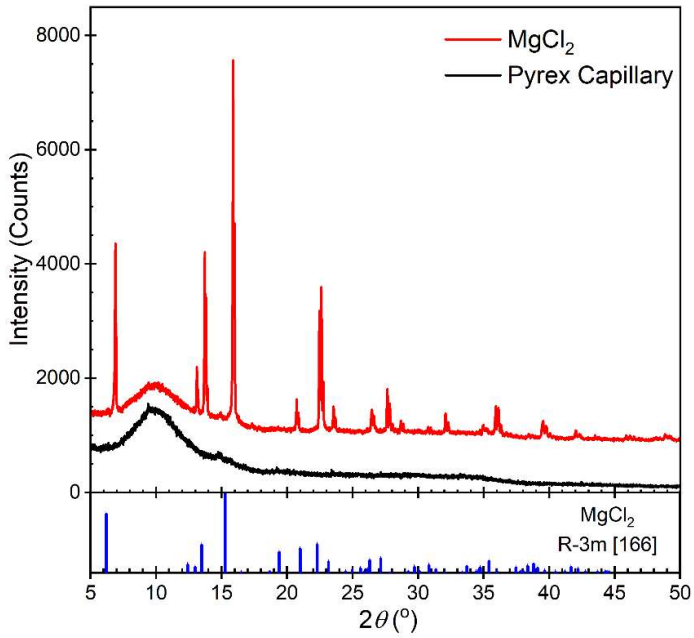

Figure 5.26: Room temperature powder XRD of $MgCl_2$.

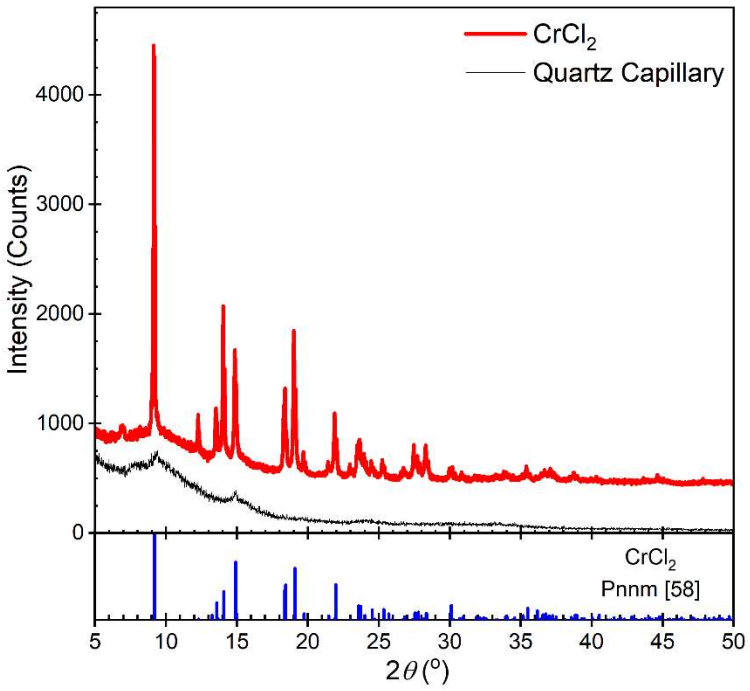

Figure 5.27: Room temperature powder XRD of $CrCl_2$.

reproduces the observed melting point. Thus, a purity of 0.98±0.02 was determined for $CrCl_2$. This estimation is imprecise, however, our experience from measuring XRD patterns of other divalent metal halides has shown that higher oxidation state impurities are common. Furthermore, at low temperature the first heating of $CrCl_2$ was completely absent of additional DSC peaks that would be indicative of hydration.

Approach to constrained thermodynamic assessments using the MQMQA

The Gibbs energy of a single anion ionic liquid is described by the modified quasi-chemical model in quadruplet approximation (MQMQA) [121] as a function of the endmember standard state thermodynamic values of formation enthalpy, entropy, and isobaric heat capacity $\Delta_f H^o_{298}, S^o_{298}, C_p$, respectively. The FNN coordination numbers ($Z^A_{A/X}$), SNN coordination numbers ($Z^A_{AB/X}$), FNN to SNN correlation factors ($\zeta_{A/X}$), and the quadruplet formation energy functions ($\Delta G_{AB/X}$), Equation (5.27), which are dependent on temperature and quadruplet fractions ($\chi_{AB/X}$).

$$\Delta G_{AB/X} = \sum_{i,j} G^{i,j}_{AB/X}\, \chi^{i}{}_{AB/X} \chi^{j}{}_{BA/X}\ (i \geq 0, j \geq 0) \tag{5.27}$$

Provided the endmember Gibb's energy functions are well-described, the $\Delta G_{AB/X}$ functions and $Z^A_{AB/X}$ values are the primary means of fitting thermodynamic data. This is true when $Z^A_{A/X} = 6$, a common practice for molten salts [41,42,254,256], and $\zeta_{A/X}$ is defined as Equation (5.28), as previously established by Wang et al. [122].

$$\zeta_{A/X} = \frac{2 Z^A_{A/X} Z^X_{A/X}}{Z^A_{A/X} + Z^X_{A/X}} \tag{5.28}$$

However, as Equation (5.27) may take the form of i and j expanded quadruplet fraction functions of varying order, also including one or more temperature terms, the MQMQA is unlimited in its available model fitting degrees of freedom (DOF). This can be problematic when relatively little thermodynamic information is available and the

system assessment is unrestricted in the use of fitting parameters. In such cases, it is easy to develop a model containing more $\Delta G_{AB/X}$ parameters than may be justified by the available data (over-parameterization), demonstrated in Figure 5.28a, and attain a correctly valued Gibbs energy function that is nevertheless underspecified, and therefore, may be incorrect in terms of excess values in H, C_p, and/or S due to the ambiguities of parameter selection.

Some of the systems considered in this work lack experimental values for the enthalpy of mixing ($\Delta_{mix}H$) in the liquid phase of the endmembers, which are desirable to the development of well-informed thermodynamic models. In some cases these values may be estimated from those of similar systems [142], however, these are not always available. To overcome the resulting under-specification of the solution models, we utilize an approach that constrains the DOF in the MQMQA relative to the available thermodynamic information, Figure 5.28b, and allows succinct thermodynamic assessments that well-predict $\Delta_{mix}H$ and species activities, especially in the limit of low molar mixing ratios ($x[1-x]/0.25$).

Due to its incorporation short-range ordering (SRO) between ionic species, the MQMQA is capable of good performance in ionic liquids [121,257,258]. Thus, using only the phase diagram, the MQMQA may be used to infer approximate values of $\Delta_{mix}H$ by limiting the number of model parameters to reflect the available number of distinct features in the phase diagram. For example, as shown in Figure 5.29, this is possible using only phase equilibria for a simple eutectic pseudo-binary system since the eutectic composition constrains the choice of the SNN coordination number ratio, and the eutectic temperature

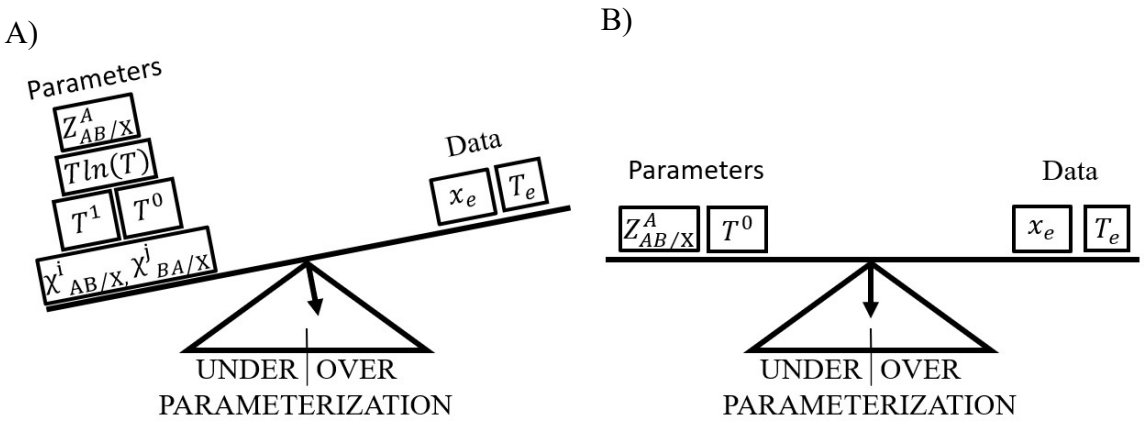

Figure 5.28: Examples of MQMQA parameters and potential available datasets, indicating a) over parameterization, and b) data constrained model development, where x_e and T_e are the eutectic composition and temperature, respectively.

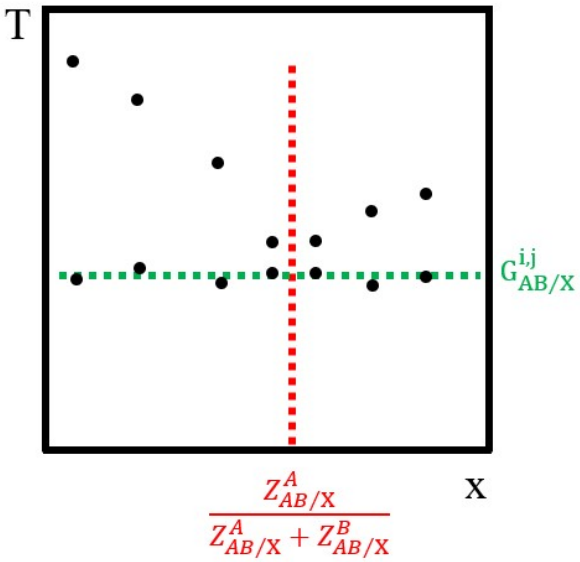

Figure 5.29: Example of MQMQA constraints in a simple eutectic pseudo-binary system.

constrains the value of a single parameter $\mathrm{G_{AB/X}}$ that is independent of composition and temperature.

Even though intermediate compounds often lack known thermodynamic values, these pseudo-binary systems may also be described by a fully constrained MQMQA since the compounds add additional equilibrium reactions, and thus, may resolve additional DOF in the model. For instance, since C_{p} may be reliably estimated by the Neumann-Kopp method [239], if each additional intermediate compound has experimentally known $\Delta_{\mathrm{f}}H^{\mathrm{o}}_{298}$, then the compound adds one additional DOF due to the unknown S^{o}_{298}. However, since each compound also adds an additional invariant equilibrium reaction with the liquid, the Gibbs energy model remains well-specified. Thus, the SNN coordination number ratio, $\mathrm{G_{AB/X}}$, and S^{o}_{298} may be selected simultaneously to best reproduce the eutectic temperatures, compositions, and intermediate compound melting points of highest relevance to the model.

Not only does this assessment approach provide a useful methodology for avoiding model over parameterization, it can also help avoid under-specification caused by disagreements in the thermodynamic datasets. For example, it may be impossible to adequately constrain a pseudo-binary system with only the available low-order data. However, by including the pseudo-ternary thermodynamic values in the pseudo-binary assessment, the parameters of the under-specified pseudo-binary system may be fully constrained. In some cases, doing so allows the assessment of higher order systems without the use of pseudo-ternary interaction parameters. Thus, potential issues may be avoided in the high-order systems that are caused by under-specification in the related lower-order systems.

Demonstration of constrained MQMQA assessments

The predictive capability of the MQMQA for molten salts is exemplified in a simple reassessment of the NaCl-$CoCl_2$ system, previously reported by Robelin et al. [185], from which the endmember Gibbs energy functions were taken. The sole quadruplet fraction independent $\Delta G_{AB/X}$ term, Equation (5.29), was regressed from the eutectic temperature and the SNN coordination numbers, Equation (5.30), were selected to match the eutectic composition.

$$\Delta G_{NaCo/Cl} = -11730 \tag{5.29}$$

$$Z^{Na}_{NaCo/Cl} = 3.2;\ Z^{Co}_{NaCo/Cl} = 6 \tag{5.30}$$

Not only are such assessments simple to undertake, the agreement between the calculated and experimental $\Delta_{mix}H$ values is excellent (Figure 5.30a) especially in the limit of low mole fraction $CoCl_2$. Since the well-described NaCl and $CoCl_2$ endmember Gibbs energy functions leave only two DOF in the eutectic system, the MQMQA functions are fully constrained by the eutectic temperature and composition, which define the sole interaction parameter and the ratio of the SNN coordination numbers, respectively. Consequently, values derived from Gibbs energy, i.e. phase equilibria, enthalpic data, and as shown in Figure 5.30b, even liquid activities (a_{liq}) are well-represented.

Systems that include one or more compounds may also be described using only phase equilibria provided care is taken to ensure the available data are sufficient to constrain the available DOF in the model. The approach is demonstrated in a simple assessment of the KCl-$MnCl_2$ system, which includes two incongruent melting compounds, K_4MnCl_6 and K_3MnCl_7, and a congruently melting compound, $KMnCl_3$.

A)

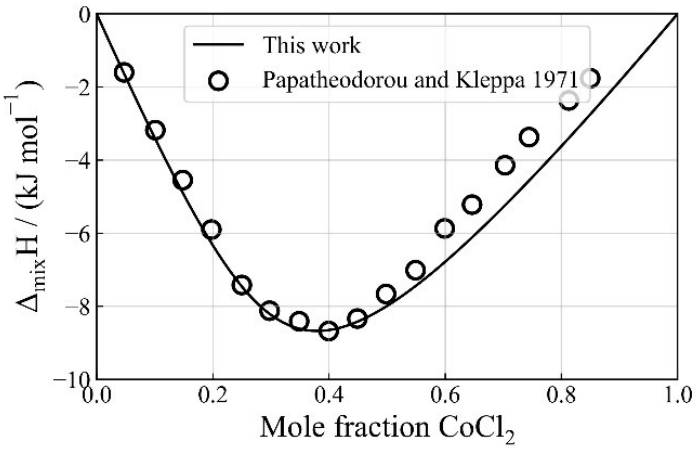

B)

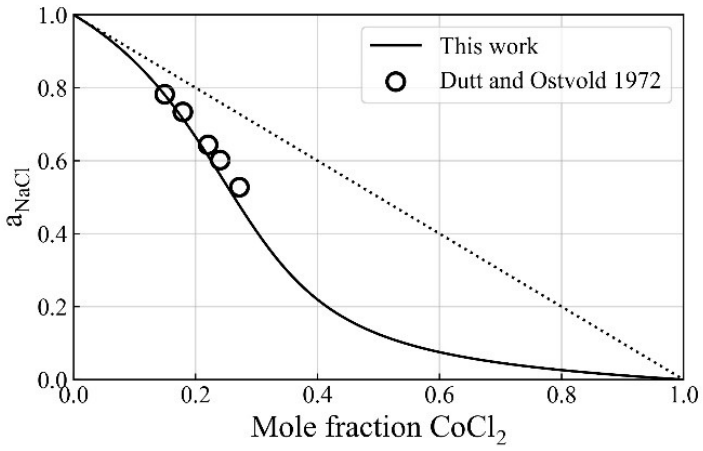

Figure 5.30: a) Calculated $\Delta_{mix}H$ at 1083.2K [248] and b) a_{NaCl} relative to pure liquid reference [259] at 998.2K of the NaCl-$CoCl_2$ system, data extracted graphically from [185].

The endmembers KCl and MnCl2 were previously described by Robelin et al. [185,260], and the intermediate compounds have experimental $\Delta_f H^o_{298}$ [197]. C_p may be estimated via stoichiometric mixing of the endmembers KCl and $MnCl_2$ [239], but S^o_{298} is unknown for each intermediate compound which contribute an additional three DOF to this system. The melting points of the intermediate compounds allow the additional DOF from S^o_{298} to be overcome. The selection of values for Equations (5.31)-(5.32) and the compound S^o_{298} are done simultaneously to match the eutectic temperature and composition in the region of highest practical importance, as well as the incongruent and congruent melting points.

$$\Delta G_{KMn/Cl} = -16330 \quad (5.31)$$

$$Z^{K}_{KMn/Cl} = 3.9;\ Z^{Mn}_{KMn/Cl} = 6 \quad (5.32)$$

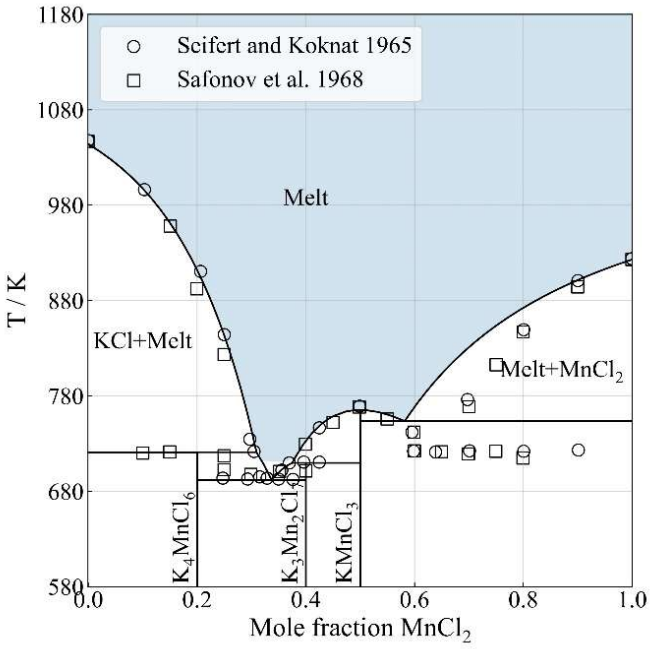

Figure 5.31: Calculated phase diagram of the KCl-$MnCl_2$ system. Experimental points extracted graphically from [185].

A)

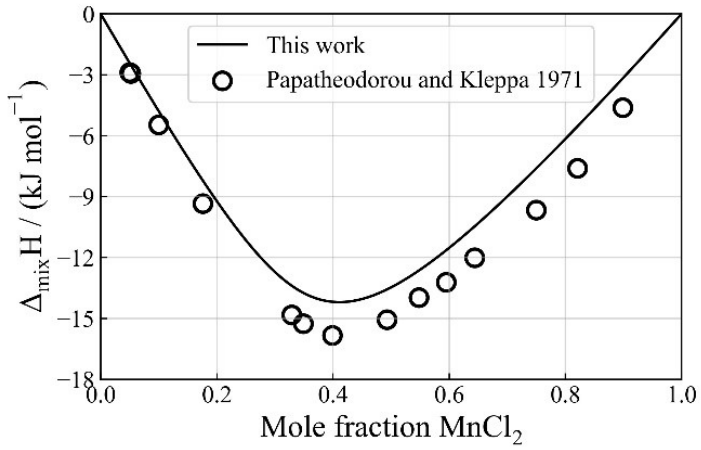

B)

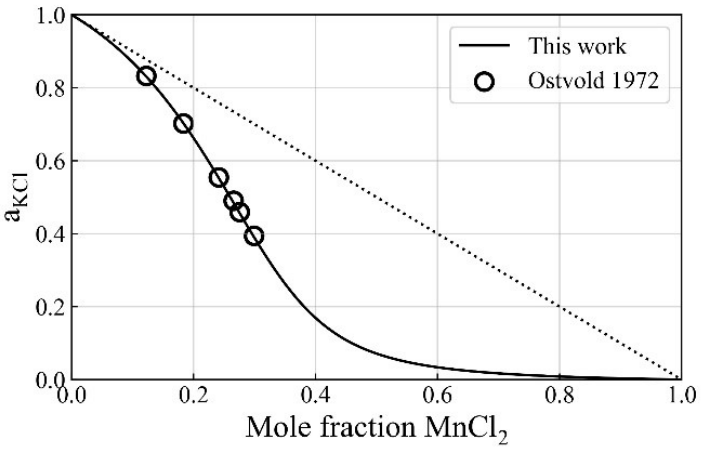

Figure 5.32 a) Calculated $\Delta_{mix}H$ at 1083.2K [248] and b) a_{KCl} relative to pure liquid reference [261] at 1063.2K

REFERENCES

[1] B.L. Welch, Nuclear Power Risks: Challenge to the Credibility of Science, Int. J. Health Serv. 10 (1980) 5–36. https://doi.org/10.2190/NN0J-3X9Q-167L-UR7G.

[2] R.J. Duffy, Nuclear politics in America: A history and theory of government regulation, University Press of Kansas, 1997.

[3] C. Gennaioli, M. Tavoni, Clean or dirty energy: evidence of corruption in the renewable energy sector, Public Choice. 166 (2016) 261–290. https://doi.org/10.1007/s11127-016-0322-y.

[4] J. Richards, P. Sabharwall, M. Memmott, Economic comparison of current electricity generating technologies and advanced nuclear options, Electr. J. 30 (2017) 73–79. https://doi.org/10.1016/j.tej.2017.11.005.

[5] M.G. Morgan, A. Abdulla, M.J. Ford, M. Rath, US nuclear power: The vanishing low-carbon wedge, Proc. Natl. Acad. Sci. U. S. A. 115 (2018) 7184–7189. https://doi.org/10.1073/pnas.1804655115.

[6] B. Mignacca, G. Locatelli, Economics and finance of Molten Salt Reactors, Prog. Nucl. Energy. 129 (2020) 103503. https://doi.org/10.1016/j.pnucene.2020.103503.

[7] J. Serp, M. Allibert, O. Beneš, S. Delpech, O. Feynberg, V. Ghetta, D. Heuer, D. Holcomb, V. Ignatiev, J.L. Kloosterman, L. Luzzi, E. Merle-Lucotte, J. Uhlíř, R. Yoshioka, D. Zhimin, The molten salt reactor (MSR) in generation IV: Overview and perspectives, Prog. Nucl. Energy. 77 (2014) 308–319. https://doi.org/10.1016/j.pnucene.2014.02.014.

[8] B.M. Elsheikh, Safety assessment of molten salt reactors in comparison with light water reactors, J. Radiat. Res. Appl. Sci. 6 (2013) 63–70. https://doi.org/10.1016/j.jrras.2013.10.008.

[9] V. Raffuzzi, J. Krepel, SIMULATION OF BREED AND BURN FUEL CYCLE OPERATION OF MOLTEN SALT REACTOR IN BATCH-WISE REFUELING MODE, EPJ Web Conf. 247 (2021) 13003. https://doi.org/10.1051/epjconf/202124713003.

[10] D.C.W. Forsberg, P.O. Box, Molten Salt Reactors (MSRs): Coupling Spent Fuel Processing and Actinide Burning, (n.d.) 21.

[11] L. Burris, M. Steindler, W. Miller, Proposed pyrometallurgical process for rapid recycle of discharged fuel materials from the integral fast reactor. [Metal fuel], (1984). https://www.osti.gov/biblio/6624028.

[12] S.S. Raiman, R.T. Mayes, J.M. Kurley, R. Parrish, E. Vogli, Amorphous and partially-amorphous metal coatings for corrosion resistance in molten chloride salt,

Sol. Energy Mater. Sol. Cells. 201 (2019) 110028. https://doi.org/10.1016/j.solmat.2019.110028.

[13] P.D. Myers, D.Y. Goswami, Thermal energy storage using chloride salts and their eutectics, Appl. Therm. Eng. 109 (2016) 889–900. https://doi.org/10.1016/j.applthermaleng.2016.07.046.

[14] A. Graham, R. Pillai, B. Collins, J. Mcmurray, Engineering scale molten salt corrosion and chemistry code development, 2020. https://doi.org/10.2172/1649062.

[15] J.A. Ocadiz-Flores, E. Capelli, P.E. Raison, R.J.M. Konings, A.L. Smith, Thermodynamic assessment of the LiF-NiF2 , NaF-NiF2 and KF-NiF2 systems, J. Chem. Thermodyn. 121 (2018) 17–26. https://doi.org/10.1016/j.jct.2018.01.023.

[16] C. Robelin, P. Chartrand, A.D. Pelton, Thermodynamic evaluation and optimization of the (MgCl2+CaCl2+MnCl2+FeCl2+CoCl2+NiCl2) system, J. Chem. Thermodyn. 36 (2004) 793–808. https://doi.org/10.1016/j.jct.2004.05.004.

[17] S. Guo, J. Zhang, W. Wu, W. Zhou, Corrosion in the molten fluoride and chloride salts and materials development for nuclear applications, Prog. Mater. Sci. 97 (2018) 448–487. https://doi.org/10.1016/j.pmatsci.2018.05.003.

[18] G. Zheng, K. Sridharan, Corrosion of Structural Alloys in High-Temperature Molten Fluoride Salts for Applications in Molten Salt Reactors, JOM. 70 (2018). https://doi.org/10.1007/s11837-018-2981-2.

[19] J. Zhang, C.W. Forsberg, M.F. Simpson, S. Guo, S.T. Lam, R.O. Scarlat, F. Carotti, K.J. Chan, P.M. Singh, W. Doniger, K. Sridharan, J.R. Keiser, Redox potential control in molten salt systems for corrosion mitigation, Corros. Sci. 144 (2018) 44–53. https://doi.org/10.1016/j.corsci.2018.08.035.

[20] D.E. Holcomb, G.F. Flanagan, B.W. Patton, J.C. Gehin, R.L. Howard, T.J. Harrison, Fast Spectrum Molten Salt Reactor Options, 2011. https://doi.org/10.2172/1018987.

[21] D. Olander, Redox condition in molten fluoride salts: Definition and control, J. Nucl. Mater. 300 (2002) 270–272. https://doi.org/10.1016/S0022-3115(01)00742-5.

[22] S.S. Raiman, S. Lee, Aggregation and data analysis of corrosion studies in molten chloride and fluoride salts, J. Nucl. Mater. 511 (2018) 523–535. https://doi.org/10.1016/j.jnucmat.2018.07.036.

[23] V. Ignatiev, A. Surenkov, Corrosion phenomena induced by molten salts in Generation IV nuclear reactors, in: Struct. Mater. Gener. IV Nucl. React., Elsevier, 2017: pp. 153–189. https://doi.org/10.1016/B978-0-08-100906-2.00005-7.

[24] P. Chartrand, A.D. Pelton, Thermodynamic evaluation and optimization of the LiCl-NaCl-KCl-RbCl-CsCl-MgCl2-CaCl2 system using the modified quasi-chemical model, Metall. Mater. Trans. A. 32A (2001) 23.

[25] O. Beneš, R.J.M. Konings, Thermodynamic evaluation of the NaCl–MgCl2–UCl3–PuCl3 system, J. Nucl. Mater. 375 (2008) 202–208. https://doi.org/10.1016/j.jnucmat.2008.01.007.

[26] R.E. ed. Thoma, Phase diagrams of nuclear reactor materials, 1959. https://doi.org/10.2172/4234144.

[27] C. Kraus, Phase Diagram of Some Complex Salts of Uranium with Halides of the Alkali and Alkaline Earth Metals, 1943. https://doi.org/10.2172/12687930.

[28] V.I. Posypaiko, E.A. Alekseeva, eds., Phase Equilibria in Binary Halides, Springer US, 1987. https://www.springer.com/gp/book/9781468490268 (accessed February 23, 2021).

[29] H.-J. Seifert, K. Klatyk, Uber die Systeme Alkalimetallchlorid/Chrom(II)-chlorid, Z. Anorg. Allg. Chem. 334 (1964) 113–124. https://doi.org/10.1002/zaac.19643340302.

[30] S. Ghosh, B.P. Reddy, K. Nagarajan, K.C.H. Kumar, Experimental investigations and thermodynamic modeling of KCl-LiCl-UCl3 system, CALPHAD Comput. Coupling Phase Diagr. Thermochem. 45 (2014) 11–26.

[31] I.G. Suglobova, D.E. Chirkst, Phase diagrams of uranium trichloride-alkali metal chloride systems, Koord. Khimia. 7 (1981) 97–102.

[32] V.N. Desyatnik, Yu.A. Izmodenov, Yu.T. Mel'nikov, I.F. Nichkov, S.P. Raspopin, Fusibility diagrams of systems based on magnesium and uranium chlorides, Sov. At. Energy. 26 (1969) 634–635. https://doi.org/10.1007/BF01218787.

[33] Ya.M. Sterlin, V.V. Artamonov, Phase diagrams of the systems UCl4−UO2, UCl4−PbCl2, and UCl4−MgCl2, Sov. At. Energy. 22 (1967) 589–593. https://doi.org/10.1007/BF01121992.

[34] V.N. Desyatnik, B.V. Dubinin, S.P. Raspopin, Phase diagrams of the NaCl-KCl-UCl3 system, Izv. Vysshikh Uchebnykh Zaved. Tsvetnaya Metall. (1974) 61–62.

[35] V.N. Desyatnik, B.V. Dubinin, S.P. Raspopin, Phase diagram of the system NaCl–KCl–UCl4, J Appl Chem USSR Engl Transl V 46 No 8 Pp 1953-1954. (1973). https://www.osti.gov/biblio/4309718.

[36] L. Belorukova, I. Vasilkova, A. Yefimov, E. Kostenko, The Melting-Point Diagram of the System NaCl-KCl-CrCl2, Vestn. Leningr. Univ. Seriya Fiz. Khimiya. (1987) 107–109.

[37] B.J. Thamer, Freezing points of some ternary mixtures derived from 55 mole percent UCl3–45 mole percent KCl., (1966). https://www.osti.gov/biblio/4474451.

[38] A.D. Pelton, Thermodynamics and Phase Diagrams, Centre de Recherche en Calcul Thermodynamique, Montréal, Canada, 2011.

[39] K.C. Hari Kumar, P. Wollants, Some guidelines for thermodynamic optimisation of phase diagrams, J. Alloys Compd. 320 (2001) 189–198. https://doi.org/10.1016/S0925-8388(00)01491-2.

[40] M. Blander, A.D. Pelton, Thermodynamic analysis of binary liquid silicates and prediction of ternary solution properties by modified quasichemical equations, Geochim. Cosmochim. Acta. 51 (1987) 85–95. https://doi.org/10.1016/0016-7037(87)90009-3.

[41] A.D. Pelton, S.A. Degterov, G. Eriksson, C. Robelin, Y. Dessureault, The modified quasichemical model I - Binary solutions, Metall. Mater. Trans. B-Process Metall. Mater. Process. Sci. 31 (2000) 651–659. https://doi.org/10.1007/s11663-000-0103-2.

[42] A.D. Pelton, P. Chartrand, The modified quasi-chemical model: Part II. Multicomponent solutions, Matallic Mater. Trans. 32A (2001) 1355–1360.

[43] P. Chartrand, A.D. Pelton, The modified quasi-chemical model: Part III. Two sublattices, Metall. Mater. Trans. A. 32 (2001) 1397–1407. https://doi.org/10.1007/s11661-001-0229-0.

[44] L.B. Pankratz, Thermodynamic Properties of Halides, United States Department of the Interior, Bureau of Mines, 1984. https://books.google.com/books?id=92QIDx0NlG8C.

[45] H. Landolt, R. Börnstein, W. Martienssen, O. Madelung, RWTH Aachen, Scientific Group Thermodata Europe, eds., Numerical data and functional relationships in science and technology: new series. Group 4 Vol. 19 Subvol. a, Pt. 1: Physical chemistry Thermodynamic properties of inorganic materials Pure substances: heat capacities, enthalpies, entropies and Gibbs energies, phase transition data ; Pt. 1. Elements and compounds from AgBR to Ba3N2, Springer, Berlin, 1999.

[46] N.Q. Minh, Extraction of Metals by Molten Salt Electrolysis: Chemical Fundamentals and Design Factors, JOM. 37 (1985) 28–33. https://doi.org/10.1007/BF03257510.

[47] M. Lizuka, T. Koyama, N. Kondo, R. Fujita, H. Tanaka, Actinides recovery from molten salt/liquid metal system by electrochemical methods, J. Nucl. Mater. 247 (1997) 183–190. https://doi.org/10.1016/S0022-3115(97)00096-2.

[48] S. Jiao, H. Zhu, An investigation into the electrochemical recovery of rare earth ions in a CsCl-based molten salt, J. Hazard. Mater. 189 (2011) 821–826. https://doi.org/10.1016/j.jhazmat.2011.03.027.

[49] S.A. Kuznetsov, M. Gaune-Escard, Redox electrochemistry and formal standard redox potentials of the Eu(III)/Eu(II) redox couple in an equimolar mixture of molten NaCl□KCl, Electrochimica Acta. 46 (2001) 1101–1111. https://doi.org/10.1016/S0013-4686(00)00708-8.

[50] O. Takeda, T.H. Okabe, Current Status on Resource and Recycling Technology for Rare Earths, Metall. Mater. Trans. E. 1 (2014) 160–173. https://doi.org/10.1007/s40553-014-0016-7.

[51] R. Schulze, A. Abbasalizadeh, W. Bulach, L. Schebek, M. Buchert, An Ex-ante LCA Study of Rare Earth Extraction from NdFeB Magnet Scrap Using Molten Salt Electrolysis, J. Sustain. Metall. 4 (2018) 493–505. https://doi.org/10.1007/s40831-018-0198-9.

[52] T.H. Okabe, O. Takeda, K. Fukuda, Y. Umetsu, Direct Extraction and Recovery of Neodymium Metal from Magnet Scrap, Mater. Trans. 44 (2003) 798–801. https://doi.org/10.2320/matertrans.44.798.

[53] M. Xu, V. Smolenski, Q. Liu, A. Novoselova, K. Jiang, J. Yu, J. Liu, R. Chen, H. Zhang, M. Zhang, J. Wang, Thermodynamics, Solubility and the Separation of Uranium from Cerium in Molten In/3LiCl-2KCl System, J. Electrochem. Soc. 167 (2020) 136506. https://doi.org/10.1149/1945-7111/abb7f2.

[54] J. Claquesin, O. Lemoine, M. Gibilaro, L. Massot, P. Chamelot, G. Bourges, Electrochemical behavior of plutonium fluoride species in LiF-CaF2 eutectic melt, Electrochimica Acta. 301 (2019) 80–86. https://doi.org/10.1016/j.electacta.2019.01.169.

[55] GIF, A technology roadmap for generation IV nuclear energy systems, 2002.

[56] D.F. Williams, P.F. Britt, Technology and Applied R&D Needs For Molten Salt Chemistry, (2017).

[57] T.M. Besmann, J. Schorne-Pinto, Developing Practical Models of Complex Salts for Molten Salt Reactors, Thermo. 1 (2021) 168–178. https://doi.org/10.3390/thermo1020012.

[58] Y.A. Chang, S. Chen, F. Zhang, X. Yan, F. Xie, R. Schmid-Fetzer, W.A. Oates, Phase diagram calculation: past, present and future, Prog. Mater. Sci. 49 (2004) 313–345. https://doi.org/10.1016/S0079-6425(03)00025-2.

[59] A. Pelton, Phase Diagrams and Thermodynamic Modeling of Solutions, Elsevier, 2018.

[60] J. Ard, K. Johnson, M. Christian, J. Schorne-Pinto, J. Yingling, T. Besmann, J. McMurray, J. Peng, FY20 Status report on the Molten Salt Thermodynamic Database (MSTDB) development, 2020.

[61] G.N. Papatheodorou, O.J. Kleppa, Thermodynamic studies of binary charge unsymmetrical fused salt systems. Cerium(III) chloride-alkali chloride mixtures, J. Phys. Chem. 78 (1974) 178–181. https://doi.org/10.1021/j100595a018.

[62] S.N. Flengas, A.S. Kucharski, Theory of Enthalpy of Mixing in Reactive Charge Asymmetrical Molten Salt Systems. Part I. Binary Solutions, Can. J. Chem. 49 (1971) 3971–3985. https://doi.org/10.1139/v71-664.

[63] K.C. Hong, O.J. Kleppa, Thermochemistry of the liquid mixtures of the alkaline earth fluorides with alkali fluorides, J. Phys. Chem. 82 (1978) 1596–1603. https://doi.org/10.1021/j100503a005.

[64] H.T. Davis, Theory of Heats of Mixing of Certain Charge-Unsymmetrical Fused Salts, J. Chem. Phys. 41 (1964) 2761–2766. https://doi.org/10.1063/1.1726349.

[65] H.T. Davis, Theory of heats of mixing of certain charge-unsymmetrical molten salts, J. Phys. Chem. 76 (1972) 1629–1631. https://doi.org/10.1021/j100655a024.

[66] H. Reiss, J.L. Katz, O.J. Kleppa, Theory of the Heats of Mixing of Certain Fused Salts, J. Chem. Phys. 36 (1962) 144–148. https://doi.org/10.1063/1.1732285.

[67] T. Østvold, O.J. Kleppa, M.S. Sood, B.E. Nielsen, H. Ljunggren, L. Ehrenberg, Enthalpies of Mixing in Binary Liquid Alkali Sulfate Mixtures., Acta Chem. Scand. 25 (1971) 919–929. https://doi.org/10.3891/acta.chem.scand.25-0919.

[68] R.D. Shannon, Revised effective ionic radii and systematic studies of interatomic distances in halides and chalcogenides, Acta Crystallogr. Sect. A. 32 (1976) 751–767. https://doi.org/10.1107/S0567739476001551.

[69] G.N. Papatheodorou, T. Ostvold, Thermodynamic studies of binary charge unsymmetrical fused salt systems. Calorimetric and electromotive force measurements of liquid lanthanum(III) chloride-alkali chloride mixtures, J. Phys. Chem. 78 (1974) 181–185. https://doi.org/10.1021/j100595a019.

[70] F. Dienstbach, R. Blachnik, Mischungsenthalpien von geschmolzenen Alkalihalogenid-Lanthanoidenhalogenidsystemen, Z. Anorg. Allg. Chem. 412 (1975) 97–109. https://doi.org/10.1002/zaac.19754120202.

[71] L. Rycerz, Y. Okamotoc, M. Gaune-Escard, Enthalpy of Mixing of the PrCl3-LiCl and NdCl3-LiCl Molten Salt Systems, Z. Für Naturforschung A. 60 (2005) 196–200. https://doi.org/10.1515/zna-2005-0312.

[72] G. Hatem, Semi-emperical dependance of the excess functions of asymmetrical molten salt systems, Thermochim. Acta. 338 (1999) 95–102. https://doi.org/10.1016/S0040-6031(99)00194-X.

[73] G. Hatem, M. Gaune-Escard, A.D. Pelton, Calorimetric measurements and coupled thermodynamic phase-diagram analysis in the sodium, potassium/fluoride, sulfate system, J. Phys. Chem. 86 (1982) 3039–3046. https://doi.org/10.1021/j100212a044.

[74] M. Gaune-Escard, Thermodynamic models of molten salt mixtures, Pure Appl. Chem. 55 (1983) 505–514. https://doi.org/10.1351/pac198855030505.

[75] M. Gaune-Escard, J.-C. Mathieu, P. Desré, Y. Doucet, Modèle statistique de solution binaire de sels fondus à cation ou anion commun: II. — X Conséquences du choix de deux formes particulières des énergies potentielle et de vibration sur les grandeurs thermodynamiques de mélange, J. Chim. Phys. 69 (1972) 1397–1401. https://doi.org/10.1051/jcp/1972691397.

[76] M. Gaune-Escard, J.-C. Mathieu, P. Desré, Y. Doucet, Modèle statistique de solution binaire de sels fondus à cation ou anion commun: I. — Traitement général d'un système AB — A'B, J. Chim. Phys. 69 (1972) 1390–1396. https://doi.org/10.1051/jcp/1972691390.

[77] G.N. Papatheodorou, O.J. Kleppa, Enthalpies of mixing in the liquid mixtures of the alkali chlorides with MnCl2, FeCl2 and CoCl2, J. Inorg. Nucl. Chem. 33 (1971) 1249–1278. https://doi.org/10.1016/0022-1902(71)80419-0.

[78] G.N. Papatheodorou, O. Wærnes, T. Østvold, A. Holm, N.H. Toubro, A. Krantz, J. Laureni, Thermodynamic Studies of Binary Charged Unsymmetrical Fused Salt Systems. Calorimetric and Electromotive Force Measurements of Yttrium(III) Chloride - Alkali Chloride Mixtures., Acta Chem. Scand. 33a (1979) 173–178. https://doi.org/10.3891/acta.chem.scand.33a-0173.

[79] A.A. Redkin, Y.P. Zaikov, I.V. Korzun, O.G. Reznitskikh, T.V. Yaroslavtseva, S.I. Kumkov, Heat Capacity of Molten Halides, J. Phys. Chem. B. 119 (2015) 509–512. https://doi.org/10.1021/jp509932e.

[80] O.J. Kleppa, A new twin high-temperature reaction calorimeter. The heats of mixing in liquid sodium-potassium nitrates, J. Phys. Chem. 64 (1960) 1937–1940. https://doi.org/10.1021/j100841a032.

[81] G.N. Papatheodorou, O.J. Kleppa, Enthalpies of mixing of charge unsymmetrical binary fused salt systems: ZnX2-AX (A = Li, Cs, Ag; X = Cl, Br), Z. Für Anorg. Allg. Chem. 401 (1973) 132–144. https://doi.org/10.1002/zaac.19734010203.

[82] K.C. Hong, O.J. Kleppa, Thermochemistry of the liquid mixtures of aluminum fluoride with alkali fluorides and with zinc fluoride, J. Phys. Chem. 82 (1978) 176–182. https://doi.org/10.1021/j100491a010.

[83] H. Matsuura, R. Takagi, L. Rycerz, M. Gaune-Escard, Enthalpies of mixing in molten UCl3-NaCl system, J. Nucl. Sci. Technol. 39 (2002) 632–634. https://doi.org/10.1080/00223131.2002.10875547.

[84] L. Rycerz, M. Gaune-Escard, Mixing enthalpy of TbCl3-MCl liquid mixtures (M = Li, Na, K, Rb, Cs), High Temp. Mater. Process. Int. Q. High-Technol. Plasma Process. 2 (1998) 483–496. https://doi.org/10.1615/HighTempMatProc.v2.i4.40.

[85] I. Chojnacka, L. Rycerz, J. Kapala, M. Gaune-Escard, Calorimetric investigation of TmCl3-MCl liquid mixtures (M = Li, Na, K, Rb), J. Mol. Liq. (2020) 113935. https://doi.org/10.1016/j.molliq.2020.113935.

[86] M. Gaune-Escard, L. Rycerz, W. Szczepaniak, A. Bogacz, Calorimetric investigation of PrCl3-NaCl and PrCl3-KCl liquid mixtures, Thermochim. Acta. 236 (1994) 59–66.

[87] M. Gaune-Escard, A. Bogacz, L. Rycerz, W. Szczepaniak, Calorimetric investigation of NdCl3-MCl liquid mixtures (where M is Na, K, Rb, Cs), Thermochim. Acta. 236 (1994) 67–80. https://doi.org/10.1016/0040-6031(94)80256-4.

[88] M. Gaune-Escard, L. Rycerz, A. Bogacz, Enthalpies of mixing in the DyCl3-NaCl, DyCl3-KCl and DyCl3-PrCl3 liquid systems, J. Alloys Compd. 204 (1994) 185–188. https://doi.org/10.1016/0925-8388(94)90089-2.

[89] W. Lukas, M. Gaune-Escard, J.P. Bros, Enthalpy of mixing of {(1−x)KCl+xBiCl3} at 690 K, J. Chem. Thermodyn. 19 (1987) 717–720. https://doi.org/10.1016/0021-9614(87)90093-0.

[90] L. Rycerz, J. Kapala, M. Gaune-Escard, Experimental mixing enthalpy and thermodynamic modelling of UCl3-KCl system, J. Mol. Liq. (2021) 116963. https://doi.org/10.1016/j.molliq.2021.116963.

[91] G. Hatem, T. Østvold, Enthalpies of mixing of KCl-AlCl3 melts, Berichte Bunsenges. Für Phys. Chem. 93 (1989) 546–548. https://doi.org/10.1002/bbpc.19890930504.

[92] C.M. Cook, W.E. Dunn, The reaction of ferric chloride with sodium and potassium chlorides, J. Phys. Chem. 65 (1961) 1505–1511. https://doi.org/10.1021/j100905a008.

[93] C.R. Harris, K.J. Millman, S.J. van der Walt, R. Gommers, P. Virtanen, D. Cournapeau, E. Wieser, J. Taylor, S. Berg, N.J. Smith, R. Kern, M. Picus, S. Hoyer, M.H. van Kerkwijk, M. Brett, A. Haldane, J.F. del Río, M. Wiebe, P. Peterson, P. Gérard-Marchant, K. Sheppard, T. Reddy, W. Weckesser, H. Abbasi, C. Gohlke, T.E. Oliphant, Array programming with NumPy, Nature. 585 (2020) 357–362. https://doi.org/10.1038/s41586-020-2649-2.

[94] J.J. Moré, The Levenberg-Marquardt algorithm: Implementation and theory, in: G.A. Watson (Ed.), Numer. Anal., Springer, Berlin, Heidelberg, 1978: pp. 105–116. https://doi.org/10.1007/BFb0067700.

[95] P. Virtanen, R. Gommers, T.E. Oliphant, M. Haberland, T. Reddy, D. Cournapeau, E. Burovski, P. Peterson, W. Weckesser, J. Bright, S.J. van der Walt, M. Brett, J. Wilson, K.J. Millman, N. Mayorov, A.R.J. Nelson, E. Jones, R. Kern, E. Larson, C.J. Carey, İ. Polat, Y. Feng, E.W. Moore, J. VanderPlas, D. Laxalde, J. Perktold, R. Cimrman, I. Henriksen, E.A. Quintero, C.R. Harris, A.M. Archibald, A.H. Ribeiro, F. Pedregosa, P. van Mulbregt, SciPy 1.0: fundamental algorithms for scientific computing in Python, Nat. Methods. 17 (2020) 261–272. https://doi.org/10.1038/s41592-019-0686-2.

[96] J. Tellinghuisen, Statistical Error Propagation, J. Phys. Chem. A. 105 (2001) 3917–3921. https://doi.org/10.1021/jp003484u.

[97] H. Yin, J. Lin, B. Hu, W. Liu, X. Guo, Q. Liu, Z. Tang, Thermodynamic description of the constitutive binaries of the NaCl-KCl-UCl3-PuCl3 system, Calphad. 70 (2020) 101783. https://doi.org/10.1016/j.calphad.2020.101783.

[98] H. Yin, P. Zhang, X. An, J. Cheng, X. Li, S. Wu, X. Wu, W. Liu, L. Xie, Thermodynamic modeling of LiF-NaF-KF-CrF3 system, J. Fluor. Chem. 209 (2018) 6–13. https://doi.org/10.1016/j.jfluchem.2018.02.005.

[99] K. Wang, Z. Fei, J. Wang, Z. Wu, C. Li, L. Xie, Thermodynamic description of the AgCl–CoCl2–InCl3–KCl system, Mater. Chem. Phys. 163 (2015) 73–87. https://doi.org/10.1016/j.matchemphys.2015.07.017.

[100] K. Wang, C. Robelin, Z. Wu, C. Li, L. Xie, P. Chartrand, Thermodynamic description of the AgCl–CoCl2–InCl3–NaCl system, J. Alloys Compd. 663 (2016) 885–898. https://doi.org/10.1016/j.jallcom.2015.12.104.

[101] X. Li, K. Wang, L. Xie, Thermodynamic modeling of the GdF 3 -MF (M: Li, K, Rb, Cs) systems, Fluid Phase Equilibria. 449 (2017) 18–27. https://doi.org/10.1016/j.fluid.2017.06.007.

[102] C. Robelin, P. Chartrand, Thermodynamic evaluation and optimization of the (NaCl+KCl+MgCl2+CaCl2+ZnCl2) system, J. Chem. Thermodyn. 43 (2011) 377–391. https://doi.org/10.1016/j.jct.2010.10.013.

[103] G. Lu, C. Robelin, P. Chartrand, M. He, K. Wang, Thermodynamic evaluation and optimization of the (LiCl + NaCl + KCl + MgCl2 + CaCl2 + CeCl3) system, Fluid Phase Equilibria. 487 (2019) 83–97. https://doi.org/10.1016/j.fluid.2018.11.031.

[104] C.W. Bjorklund, J.G. Reavis, J.A. Leary, K.A. Walsh, Phase Equilibria in the Binary Systems PuCl3–NaCl and PuCl3–LiCl, J. Phys. Chem. 63 (1959) 1774–1777. https://doi.org/10.1021/j150580a049.

[105] A.D. Pelton, S.A. Degterov, G. Eriksson, C. Robelin, Y. Dessureault, The modified quasichemical model I—Binary solutions, Metall. Mater. Trans. B. 31 (2000) 651–659. https://doi.org/10.1007/s11663-000-0103-2.

[106] A.D. Pelton, P. Chartrand, G. Eriksson, The modified quasi-chemical model: Part IV. Two-sublattice quadruplet approximation, Metall. Mater. Trans. A. 32 (2001) 1409–1416. https://doi.org/10.1007/s11661-001-0230-7.

[107] D.E. Chirkst, Energetics of complex uranium halides in the light of D. I. Mendeleev Periodic System, Radiokhimiya USSR. 24:6 (1982). https://www.osti.gov/etdeweb/biblio/5134299 (accessed July 15, 2021).

[108] O. Beneš, R.J.M. Konings, Thermodynamic evaluation of the NaCl–MgCl2–UCl3–PuCl3 system, J. Nucl. Mater. 375 (2008) 202–208. https://doi.org/10.1016/j.jnucmat.2008.01.007.

[109] I. Barin, Thermochemical Data of Pure Substances, 3rd edn, VCH Publishers, 1995.

[110] J. Ard, K. Johnson, M. Christian, J. Schorne pinto, J. Yingling, T.M. Besmann, J.W. Mcmurray, J. Peng, FY20 Status report on the Molten Salt Thermodynamic Database (MSTDB) development, Oak Ridge National Lab. (ORNL), Oak Ridge, TN (United States), 2020. https://doi.org/10.2172/1778080.

[111] J.C. Ard, J.A. Yingling, K.E. Johnson, J. Schorne-Pinto, M. Aziziha, C.M. Dixon, M.S. Christian, J.W. McMurray, T.M. Besmann, Development of the Molten Salt Thermal Properties Database − Thermochemical (MSTDB−TC), Example Applications, and LiCl−RbCl and UF3−UF4 System Assessments, J. Nucl. Mater. 563 (2022) 153631. https://doi.org/10.1016/j.jnucmat.2022.153631.

[112] T.M. Besmann, J. Schorne-Pinto, Developing Practical Models of Complex Salts for Molten Salt Reactors, Thermo. 1 (2021) 168–178. https://doi.org/10.3390/thermo1020012.

[113] J.J. Laidler, J.E. Battles, W.E. Miller, J.P. Ackerman, E.L. Carls, Development of pyroprocessing technology, Prog. Nucl. Energy. 31 (1997) 131–140. https://doi.org/10.1016/0149-1970(96)00007-8.

[114] A.L. Hames, A. Paulenova, J.L. Willit, M.A. Williamson, Phase Equilibria Studies of the LiCl-KCl-UCl3 System, Nucl. Technol. 203 (2018) 272–281. https://doi.org/10.1080/00295450.2018.1448673.

[115] G.-Y. Kim, J. Shin, S.-H. Kim, D.-H. Ahn, S. Paek, Recovery of uranium using electrorefining with an anode-liquid cathode module (ALCM) in molten LiCl–KCl–UCl3–NdCl3 and cadmium distillation, J. Radioanal. Nucl. Chem. 307 (2016) 1551–1557. https://doi.org/10.1007/s10967-015-4292-1.

[116] D. Yoon, S. Phongikaroon, Electrochemical Studies of Uranium in LiCl–KCl Eutectic Salt for an Application of Pyroprocessing Technology, in: Mod. Nucl.

Energy Anal. Methods, WORLD SCIENTIFIC, 2018: pp. 55–79. https://doi.org/10.1142/9789813271371_0003.

[117] J. McMurray, K. Johnson, C. Agca, B. Betzler, D. Kropaczek, T. Besmann, D. Andersson, N. Ezell, Roadmap for thermal property measurements of Molten Salt Reactor systems, (n.d.) 29.

[118] C. Agca, K. Johnson, J.W. McMurray, J. Yingling, T.M. Besmann, FY21 status report on the Molten Salt Thermal Properties Database (MSTDB) development, Oak Ridge National Lab. (ORNL), Oak Ridge, TN (United States), 2021. https://doi.org/10.2172/1814280.

[119] H. Lukas, S.G. Fries, B. Sundman, Computational thermodynamics: The calphad method, (2007).

[120] C.W. Bale, E. Bélisle, P. Chartrand, S.A. Decterov, G. Eriksson, K. Hack, I.-H. Jung, Y.-B. Kang, J. Melançon, A.D. Pelton, C. Robelin, S. Petersen, FactSage thermochemical software and databases — recent developments, Calphad. 33 (2009) 295–311. https://doi.org/10.1016/j.calphad.2008.09.009.

[121] A.D. Pelton, P. Chartrand, G. Eriksson, The modified quasi-chemical model: Part IV. Two-sublattice quadruplet approximation, Metall. Mater. Trans. A. 32 (2001) 1409–1416. https://doi.org/10.1007/s11661-001-0230-7.

[122] K. Wang, C. Robelin, L. Jin, X. Zeng, P. Chartrand, Thermodynamic description of the K, Be//F, Cl salt system with first-principles calculations, J. Mol. Liq. 292 (2019) 111384. https://doi.org/10.1016/j.molliq.2019.111384.

[123] M. Poulain, Halide glasses, J. Non-Cryst. Solids. 56 (1983) 1–14. https://doi.org/10.1016/0022-3093(83)90439-8.

[124] C. Robelin, P. Chartrand, A viscosity model for the (NaF+AlF3+CaF2+Al2O3) electrolyte, J. Chem. Thermodyn. 43 (2011) 764–774. https://doi.org/10.1016/j.jct.2010.12.017.

[125] C. Robelin, A Thermodynamic Database for AlCl3-Based Molten Salt Systems, ECS Proc. Vol. 2004–24 (2004) 108–121. https://doi.org/10.1149/200424.0108PV.

[126] G.I.L. van Oudenaren, J.A. Ocadiz-Flores, A.L. Smith, Coupled structural-thermodynamic modelling of the molten salt system NaCl-UCl3, J. Mol. Liq. (2021) 117470. https://doi.org/10.1016/j.molliq.2021.117470.

[127] A.D. Pelton, A database and sublattice model for molten salts, CALPHAD. 12 (1988) 127–142. https://doi.org/10.1016/0364-5916(88)90015-6.

[128] Evaluation of Measurement data - Guide to the expression of uncertainty in measurement, 2008. https://www.bipm.org/documents/20126/2071204/JCGM_100_2008_E.pdf/cb0ef43f-baa5-11cf-3f85-4dcd86f77bd6 (accessed March 7, 2022).

[129] S.S. Parker, A. Long, C. Lhermitte, S. Vogel, M. Monreal, J.M. Jackson, Thermophysical properties of liquid chlorides from 600 to 1600 K: Melt point, enthalpy of fusion, and volumetric expansion, J. Mol. Liq. 346 (2022) 118147. https://doi.org/10.1016/j.molliq.2021.118147.

[130] M.H.A. Piro, K. Lipkina, D. Hallatt, Exploring crucible designs for differential scanning calorimetry measurements of fluoride salts, Thermochim. Acta. 699 (2021) 178860. https://doi.org/10.1016/j.tca.2021.178860.

[131] G. Della Gatta, M.J. Richardson, S.M. Sarge, S. Stølen, Standards, calibration, and guidelines in microcalorimetry. Part 2. Calibration standards for differential scanning calorimetry* (IUPAC Technical Report), Pure Appl. Chem. 78 (2006) 1455–1476. https://doi.org/10.1351/pac200678071455.

[132] P. Fedorov, Glass Formation Criteria for Fluoride Systems, Inorg. Mater. 33 (1997) 1197–1205.

[133] I. Gutzow, I. Avramov, K. Kästner, Glass formation and crystallization, J. Non-Cryst. Solids. 123 (1990) 97–113. https://doi.org/10.1016/0022-3093(90)90777-J.

[134] Z.V. Dobrokhotova, B. Zakharova, Studies of LiF-BeF 2 and KF-BeF 2 glasses by differential scanning calorimetry, Inorg. Mater. 36 (2000) 191–196.

[135] Zh.V. Dobrokhotova, A.L. Emelina, B.S. Zakharova, Studies of RbF-BeF2 glasses by differential scanning calorimetry, Inorg. Mater. 36 (2000) 839–841. https://doi.org/10.1007/BF02758608.

[136] Y. Okamoto, F. Kobayashi, T. Ogawa, Structure and dynamic properties of molten uranium trichloride, J. Alloys Compd. 271 (1998) 355–358. https://doi.org/10.1016/S0925-8388(98)00087-5.

[137] G. W. Neilson, A. K. Adya, S. Ansell, 8 Neutron and X-ray diffraction studies on complex liquids, Annu. Rep. Sect. C Phys. Chem. 98 (2002) 273–322. https://doi.org/10.1039/B111168J.

[138] A.K. Adya, Structural and Thermodynamic Properties of Molten UCl3 and UCl3-MCl (M = Li, Na, K, and Cs) Systems, ECS Proc. Vol. 1999–41 (1999) 341–355. https://doi.org/10.1149/199941.0341PV.

[139] X. Li, J. Song, S. Shi, L. Yan, Z. Zhang, T. Jiang, S. Peng, Dynamic Fluctuation of U (3+) Coordination Structure in the Molten LiCl–KCl Eutectic via First Principles Molecular Dynamics Simulations, J. Phys. Chem. A. 121 (2017) 571–578. https://doi.org/10.1021/acs.jpca.6b10193.

[140] B. Li, S. Dai, D. Jiang, Molecular dynamics simulations of structural and transport properties of molten NaCl-UCl3 using the polarizable-ion model, J. Mol. Liq. 299 (2020) 112184. https://doi.org/10.1016/j.molliq.2019.112184.

[141] D.M. Gruen, R.L. McBeth, Oxidation states and complex ions of uranium in fused chlorides and nitrates, J. Inorg. Nucl. Chem. 9 (1959) 290–301. https://doi.org/10.1016/0022-1902(59)80233-5.

[142] J. Schorne-Pinto, J.A. Yingling, M.S. Christian, A.M. Mofrad, M.A.A. Aslani, T.M. Besmann, Correlational Approach to Predict the Enthalpy of Mixing for Chloride Melt Systems, ACS Omega. 7 (2022) 362–371. https://doi.org/10.1021/acsomega.1c04755.

[143] A.A. Redkin, Y.P. Zaikov, I.V. Korzun, O.G. Reznitskikh, T.V. Yaroslavtseva, S.I. Kumkov, Heat Capacity of Molten Halides, J. Phys. Chem. B. 119 (2015) 509–512. https://doi.org/10.1021/jp509932e.

[144] L.S. Hersh, O.J. Kleppa, Enthalpies of Mixing in Some Binary Liquid Halide Mixtures, J. Chem. Phys. 42 (1965) 1309.

[145] H. Matsuura, R. Takagi, L. Rycerz, M. Gaune-Escard, Enthalpies of mixing in molten UCl3-NaCl system, J. Nucl. Sci. Technol. 39 (2002) 632–634. https://doi.org/10.1080/00223131.2002.10875547.

[146] L. Rycerz, J. Kapala, M. Gaune-Escard, Experimental mixing enthalpy and thermodynamic modelling of UCl3-KCl system, J. Mol. Liq. (2021) 116963. https://doi.org/10.1016/j.molliq.2021.116963.

[147] G. Lu, T. Lai, M. He, X. Liu, Experimental measurement and thermodynamic optimization of the phase diagram of LiCl-NaCl-KCl system, Chin. Sci. Bull. 65 (2020) 641–648. https://doi.org/10.1360/TB-2019-0416.

[148] A. Redkin, I. Korzun, T. Yaroslavtseva, O. Reznitskikh, Yu. Zaikov, Isobaric heat capacity of molten halide eutectics, J. Therm. Anal. Calorim. 128 (2017) 621–626. https://doi.org/10.1007/s10973-016-5869-9.

[149] M. Beilmann, Thermodynamic assessment of the (LiF+UF3) and (NaF+UF3) systems, (2013) 10.

[150] R.J.M. Konings, L.R. Morss, J. Fuger, Thermodynamic properties of actinides and actinide compounds, in: Chem. Actin. Trans. Elem. Vol 4, n.d.: p. 112.

[151] R.J.M. Konings, A. Kovács, Thermodynamic properties of the lanthanide(III) halides, in: Handb. Phys. Chem. Rare Earths, Elsevier, 2003: pp. 147–247. https://doi.org/10.1016/S0168-1273(02)33003-4.

[152] E. Capelli, R.J.M. Konings, Halides of the Actinides and Fission Products Relevant for Molten Salt Reactors, in: Compr. Nucl. Mater., Elsevier, 2020: pp. 256–283. https://doi.org/10.1016/B978-0-12-803581-8.11794-1.

[153] D.A. Andersson, B.W. Beeler, Ab initio molecular dynamics (AIMD) simulations of NaCl, UCl3 and NaCl-UCl3 molten salts, J. Nucl. Mater. (2022) 153836. https://doi.org/10.1016/j.jnucmat.2022.153836.

[154] I. Grenthe, X. Gaona, A.V. Plyasunov, L. Rao, W.H. Runde, B. Gambow, R.J.M. Konings, A.L. Smith, E.E. Moore, Second Update on the Chemical Thermodynamics of U, Np, Pu, Am and Tc, NEA, 2020. https://www.oecd-nea.org/jcms/pl_46643/second-update-on-the-chemical-thermodynamics-of-u-np-pu-am-and-tc?details=true (accessed September 4, 2021).

[155] A. Kovacs, A.S. Booij, E.H.P. Cordfunke, A. Kok-Scheele, R.J.M. Konings, On the fusion and vaporisation behaviour of UCl3, J. Alloys Compd. 241 (1996) 95–97. https://doi.org/10.1016/0925-8388(96)02315-8.

[156] F. Abdoun, AT. Gaune-Escard, G. Hatem, Calorimetric and thermal analysis investigations of the MF-LaF3 mixtures (m = alkali metal), J. Phase Equilibria. 18 (1997) 6–20. https://doi.org/10.1007/BF02646755.

[157] M. Gaune-Escard, Y. Fouque, J.P. Bros, M. Wisniowski, A. Bogacz, Li2UCl6, Na2UCl6 and Cs2UCl6 compounds: Enthalpies of phase transitions and electrical conductivity in the solid and liquid states, Berichte Bunsenges. Für Phys. Chem. 93 (1989) 128–135. https://doi.org/10.1002/bbpc.19890930206.

[158] E.S. Sooby, A.T. Nelson, J.T. White, P.M. McIntyre, Measurements of the liquidus surface and solidus transitions of the NaCl–UCl3 and NaCl–UCl3–CeCl3 phase diagrams, J. Nucl. Mater. 466 (2015) 280–285. https://doi.org/10.1016/j.jnucmat.2015.07.050.

[159] L. Martinot, Some thermodynamic properties of dilute solutions of actinide chlorides in (Li-K)Cl and in (Na-K)CI eutectics, J. Inorg. Nucl. Chem. 37 (1975) 2525–2528.

[160] J. Sangster, A.D. Pelton, Phase diagrams and thermodynamic properties of the 70 binary alkali halide systems having common ions, J. Phys. Chem. Ref. Data. 16 (1987) 509–561.

[161] M.W. Chase, JANAF THERMOCHEMICAL TABLES Fourth Edition, J. Phys. Chem. Ref. Data. 9 (1998) 775–778.

[162] I.G. Suglobova, D.Eh. Chirkst, Formation enthalpies of alkali metal chlorouranates (3), Radiokhimiya. 23 (1981) 387–391.

[163] A.S. Basin, A.B. Kaplun, A.B. Meshalkin, N.F. Uvarov, The LiCl-KCl binary system, Russ. J. Inorg. Chem. 53 (2008) 1509–1511. https://doi.org/10.1134/S003602360809026X.

[164] T.W. Richards, W.B. Meldrum, The melting points of the chlorides of lithium, rubidium and caesium, and the freezing points of binary and ternary mixtures of these salts, including also potassium and sodium chloride., J. Am. Chem. Soc. 39 (1917) 1816–1828. https://doi.org/10.1021/ja02254a004.

[165] L.G. Murgulescu, S. Sternberg, Über die thermodynamischen Überschußgrößen binärer geschmolzener Salzgemische, Z. Für Phys. Chem. 219O (1962) 114–133. https://doi.org/10.1515/zpch-1962-21912.

[166] E. Korin, L. Soifer, Thermal analysis of the system KCL-LiCI by differential scanning calorimetry, J. Therm. Anal. 50 (1997) 347–354. https://doi.org/10.1007/BF01980495.

[167] L. Thulin, O. Waernes, T. Ostvold, Determination of partial Gibb's energies of mixing of LiCl in AlkCl-LiCl mixtures from concentration cell measurements, Acta Chem. Scand. Ser. -Phys. Inorg. Chem. 30 (1976) 731–734. https://doi.org/10.3891/acta.chem.scand.30a-0731.

[168] H. Yin, J. Lin, B. Hu, W. Liu, X. Guo, Q. Liu, Z. Tang, Thermodynamic description of the constitutive binaries of the NaCl-KCl-UCl3-PuCl3 system, Calphad. 70 (2020) 101783. https://doi.org/10.1016/j.calphad.2020.101783.

[169] D. Sergeev, D. Kobertz, M. Müller, Thermodynamics of the NaCl–KCl system, Thermochim. Acta. 606 (2015) 25–33. https://doi.org/10.1016/j.tca.2015.03.003.

[170] V.N. Desyatnik, N.N. Kurbatov, S.P. Raspopin, I.I. Trifonov, Fusibility diagrams of systems involving lithium chloride, uranium trichloride, and uranium tetrachloride, Sov. At. Energy. 32 (1972) 563–564. https://doi.org/10.1007/BF01279535.

[171] A. Nakayoshi, S. Kitawaki, M. Fukushima, T. Murakami, M. Kurata, Investigation of a LiCl–KCl–UCl3 system using a combination of X-ray diffraction and differential thermal analyses, J. Nucl. Mater. 441 (2013) 468–472. https://doi.org/10.1016/j.jnucmat.2013.06.019.

[172] L. Rycerz, Practical remarks concerning phase diagrams determination on the basis of differential scanning calorimetry measurements, J. Therm. Anal. Calorim. 113 (2013) 231–238. https://doi.org/10.1007/s10973-013-3097-0.

[173] V.N. Desyatnik, B.V. Dubinin, S.P. Raspopin, Interaction of uranium trichloride with alkali metal chlorides, Zhurnal Fiz. Khimii. 47 (1973) 2726.

[174] M. Taube, Fast Reactors Using Molten Chloride Salts as Fuel, Swiss federal Institute for Reactor Research, 1978. https://inis.iaea.org/collection/NCLCollectionStore/_Public/13/648/13648304.pdf (accessed May 24, 2021).

[175] W. Gawel, Ionic Potentials of Cations and Types of Phase-Equilibria in MeCln-UCl4 Systems, Rocz. Chem. 49 (1975) 699–704.

[176] R.D. Shannon, Revised effective ionic radii and systematic studies of interatomic distances in halides and chalcogenides, Acta Crystallogr. Sect. A. 32 (1976) 751–767. https://doi.org/10.1107/S0567739476001551.

[177] M. Gaune-Escard, L. Rycerz, E. Ingier-Stocka, S. Gadzuric, Compound formation in lanthanide–alkali metal halide systems, Miner. Process. Extr. Metall. 123 (2014) 35–42. https://doi.org/10.1179/0371955313Z.00000000066.

[178] H.-J. Seifert, H. Fink, J. Uebach, Properties of double chlorides in the systems ACl/NdCl3 (ANa-Cs), J. Therm. Anal. 33 (1988) 625–632. https://doi.org/10.1007/BF02138565.

[179] T. Sato, T. Ogawa, Phase diagram of the neodymium chloride-sodium chloride system, J. Therm. Anal. Calorim. 52 (1998) 363–371. https://doi.org/10.1023/A:1010157809182.

[180] H.J. Seifert, Ternary chlorides of the trivalent late lanthanides, J. Therm. Anal. Calorim. 83 (2006) 479–505.

[181] Y. Sun, X. Ye, Y. Wang, J. Tan, Optimization and calculation of the NdCl3–MCl (M=Li, Na, K, Rb, Cs) phase diagrams, Calphad. 28 (2004) 109–114. https://doi.org/10.1016/j.calphad.2004.07.004.

[182] M. Rose, S. Thomas, Production and Chemical Analysis of NaCl-KCl-UCl3 Salts, Argonne National Lab. (ANL), Argonne, IL (United States), 2021. https://doi.org/10.2172/1773495.

[183] D. Lexa, L. Leibowitz, J. Kropf, On the reactive occlusion of the (uranium trichloride + lithium chloride + potassium chloride) eutectic salt in zeolite 4A, J. Nucl. Mater. 279 (2000) 57–64. https://doi.org/10.1016/S0022-3115(99)00279-2.

[184] W.R. Grimes, Reactor chemistry division annual progress report for period ending January 31, 1965, Oak Ridge, TN, n.d.

[185] C. Robelin, P. Chartrand, A.D. Pelton, Thermodynamic evaluation and optimization of the (NaCl+KCl+MgCl2+CaCl2+MnCl2+FeCl2+CoCl2+NiCl2) system, J. Chem. Thermodyn. 36 (2004) 809–828. https://doi.org/10.1016/j.jct.2004.05.005.

[186] V.N. Desyatnik, G.V. Dubinin, The LiCl-NaCl-UCl3 ternary system, Izv. Vysshikh Uchebnykh Zaved. Tsvetnaya Metall. (1973) 84–85.

[187] V.N. Desyatnik, B.V. Dubinin, Thermographic study of the ternary systems formed by lithium chloride, sodium chloride, potassium chloride, uranium trichloride, and uranium tetrachloride, Zhurnal Prikl. Khimii. 48 (1975) 885–887.

[188] F. Caligara, L. Martinot, G. Duyckaerts, Contribution to the knowledge of the electrochemistry of uranium in molten LiCl-KCl eutectic: IV. The potential of the couple U(III)/U(0), Bull. Sociétés Chim. Belg. 76 (1967) 211–220. https://doi.org/10.1002/bscb.19670760305.

[189] C.G. Zoski, ed., Handbook of electrochemistry, 1st ed, Elsevier, Amsterdam ; Boston, 2007.

[190] O. Knacke, J. Krahe, F. Muller, Aktivitat von UCl3 in der eutektischen schmelze LiCl-KCl, Z. Phys. Chem.-Frankf. 50 (1966) 91-+. https://doi.org/10.1524/zpch.1966.50.1_2.091.

[191] F. Caligara, L. Martinot, G. Duyckaerts, Contribution to the knowledge of the electrochemistry of uranium in molten LiCl-KCl eutectic: I. The redox potential of the couple U(IV)/U(III), Bull. Sociétés Chim. Belg. 76 (1967) 5–14. https://doi.org/10.1002/bscb.19670760102.

[192] M.V. Smirnov, O.V. Skiba, Oxidation-reduction potential of U3+/U4+ in a NaCl-KCl melt, Dokl. Akad Nauk SSSR. Vol: 141 (1961). https://www.osti.gov/biblio/4810389 (accessed February 8, 2022).

[193] S.N. Flengas, Electrode potentials of the uranium chlorides in fused alkali chloride solutions, Can. J. Chem. 39 (1961) 773–784. https://doi.org/10.1139/v61-094.

[194] W.M. Haynes, CRC Handbook of Chemistry and Physics, (n.d.) 2643.

[195] G.J. Janz, J.J. Slowick, Investigations of CsCl, K2SO4, and K2CrO4 as high temperature calibrants for differential scanning calorimetry, Z. Für Anorg. Allg. Chem. 586 (1990) 166–174. https://doi.org/10.1002/zaac.19905860122.

[196] H.T. Fullam, Physical property measurements on cesium chloride and cesium chloride-- alkali metal chloride systems, Inf. Orig Receipt Date 30-JUN-75. (1971). https://doi.org/10.2172/4249367.

[197] V.P. Glushko, L.V. Gurvich, G.A. Bergman, I.V. Weitz, V.A. Medvedev, G.A. Khachkuruzov, V.S. Jungman, Thermodynamic Properties of Pure Substances., Russian Academy of Science, 1982.

[198] C.A. Nieto de Castro, M.J.V. Lourenço, M.O. Sampaio, Calibration of a DSC: its importance for the traceability and uncertainty of thermal measurements,

Thermochim. Acta. 347 (2000) 85–91. https://doi.org/10.1016/S0040-6031(99)00420-7.

[199] G.W.H. Höhne, H.K. Cammenga, W. Eysel, E. Gmelin, W. Hemminger, The temperature calibration of scanning calorimeters, Thermochim. Acta. 160 (1990) 1–12. https://doi.org/10.1016/0040-6031(90)80235-Q.

[200] S.M. Sarge, G.W.H. Höhne, H.K. Cammenga, W. Eysel, E. Gmelin, Temperature, heat and heat flow rate calibration of scanning calorimeters in the cooling mode, Thermochim. Acta. 361 (2000) 1–20. https://doi.org/10.1016/S0040-6031(00)00543-8.

[201] H.K. Cammenga, A.G. Steer, Experimental investigations on factors influencing the calibration of heat flux calorimeters, Thermochim. Acta. 229 (1993) 15–25. https://doi.org/10.1016/0040-6031(93)80311-W.

[202] K.S. Mohandas, N. Sanil, P. Rodriguez, Development of a high temperature conductance cell and electrical conductivity measurements of $MAlCl_4$ (M = Li, Na and K) melts, Miner. Process. Extr. Metall. 115 (2006) 25–30. https://doi.org/10.1179/174328506X91284.

[203] Jiaxin Chen, On the interaction between fuel crud and water chemistry in nuclear power plants, Sweden, 2000. http://inis.iaea.org/search/search.aspx?orig_q=RN:31025623.

[204] C. Falconer, M. Elbakhshwan, W. Doniger, M. Weinstein, K. Sridharan, A. Couet, Activity gradient driven mass transport in molten fluoride salt medium, Npj Mater. Degrad. 6 (2022) 1–10. https://doi.org/10.1038/s41529-022-00239-z.

[205] J.A. Wesselingh, R. Krishna, R. Krishna, Mass transfer in multicomponent mixtures, 1. ed, VSSD, Delft, 2006.

[206] J.A. Yingling, J. Schorne-Pinto, M. Aziziha, J.C. Ard, A.M. Mofrad, M.S. Christian, C.M. Dixon, T.M. Besmann, Thermodynamic measurements and assessments for LiCl-NaCl-KCl-UCl3 systems, J. Chem. Thermodyn. Revision pending review (2022).

[207] K. Hanson, K.M. Sankar, P.F. Weck, J.K. Startt, R. Dingreville, C.S. Deo, J.D. Sugar, P.M. Singh, Effect of excess Mg to control corrosion in molten MgCl2 and KCl eutectic salt mixture, Corros. Sci. 194 (2022) 109914. https://doi.org/10.1016/j.corsci.2021.109914.

[208] G.L. Fredrickson, G. Cao, R. Gakhar, T.-S. Yoo, Molten Salt Reactor Salt Processing – Technology Status, 2018. https://doi.org/10.2172/1484689.

[209] P.A. Nelson, D.K. Butler, M.G. Chasanov, D. Meneghetti, Fuel Properties and Nuclear Performance of Fast Reactors Fueled with Molten Chlorides, Nucl. Appl. 3 (1967) 540–547. https://doi.org/10.13182/NT67-A27935.

[210] Z. Mausolff, M. DeHart, S. Goluoglu, Design and assessment of a molten chloride fast reactor, Nucl. Eng. Des. 379 (2021) 111181. https://doi.org/10.1016/j.nucengdes.2021.111181.

[211] A. Bogacz, W. Trzebiatowski, THERMODYAMIC CHARACTERISTICS OF URANIUM(IV) CHLORIDE IN MELTS WITH ALKALI CHLORIDES BASED ON PHASE DIAGRAMS, Rocz. Chem. Vol: 38 (1964). https://www.osti.gov/biblio/4039081 (accessed June 30, 2021).

[212] T. Kuroda, T. Suzuki, The Equilibrium State Diagrams of UCl4-NaCl, UCl4-KCl, UCl4-CaCl2 and UCl4-BaCl2 Systems, J. Electrochem. Soc. Jpn. 26 (1958) E140–E141. https://doi.org/10.5796/jesj.26.7-9.E140.

[213] G. Gopienko, S.N. Shkolnik, E.F. Klyuchni, Microstructure and Phase Composition of NaCl-CrCl2 System, Zhurnal Prikl. Khimii. 46 (1973) 1123–1124.

[214] J.C. Shiloff, THERMAL ANALYSIS OF THE CHROMOUS CHLORIDE—SODIUM CHLORIDE SYSTEM, J. Phys. Chem. 64 (1960) 1566–1567. https://doi.org/10.1021/j100839a056.

[215] R. Kanno, Y. Takeda, K. Murata, O. Yamamoto, Crystal structure of double chlorides, Na2MCl4 (M=Mg, Cr, Cd): Correlation with ionic conductivity, Solid State Ion. 39 (1990) 233–244. https://doi.org/10.1016/0167-2738(90)90402-D.

[216] R. Gut, R. Gnehm, Die Binaren Phasendiagramme KCl-CrCl2 Und CsCl-CrCl2, Chimia. 16 (1962) 289-.

[217] P. Tumidajski, S. Flengas, Electrode-Potentials of Metal Chlorides in Binary and Ternary Fused Salt-Solutions with Alkali Chlorides, J. Electrochem. Soc. 132 (1985) C374–C374.

[218] V. Desyatnik, D. Vn, K. Nn, R. Sp, C.Y. F, DIAGRAMMES DE FUSION DES SYSTEMES BINAIRES CONTENANT UCL4 ET DES CHLORURES ALCALINS, (1972). http://pascal-francis.inist.fr/vibad/index.php?action=getRecordDetail&idt=PASCAL7317008353 (accessed June 30, 2021).

[219] D. Lewis, Studies on the thermodynamic of the oxidation of metals in high-temperature milieu, 1971. https://inis.iaea.org/collection/NCLCollectionStore/_Public/02/013/2013724.pdf#page=192 (accessed January 19, 2022).

[220] H.C. Gaur, H.L. Jindal, Standard electrode potentials in molten chlorides—II, Electrochimica Acta. 15 (1970) 1113–1126. https://doi.org/10.1016/0013-4686(70)85004-6.

[221] M. Zhang, J. Ge, T. Yin, J. Zhang, Redox Potential Measurements of Cr(II)/Cr Ni(II)/Ni and Mg(II)/Mg in Molten MgCl2–KCl–NaCl Mixture, J. Electrochem. Soc. 167 (2020) 116505. https://doi.org/10.1149/1945-7111/aba15a.

[222] Y. Fouque, J.P. Bros, M. Gaune-Escard, M. Wisaniowski, A. Bogacz, UCl4 Compound: Determination of High Temperature Phase Transitions from Electrical Conductivity and Calorimetric Measurements, Berichte Bunsenges. Für Phys. Chem. 89 (1985) 777–779. https://doi.org/10.1002/bbpc.19850890711.

[223] J.P. Bros, M. Gaune-Escard, W. Szczepaniak, A. Bogacz, A.W. Hewat, Structural transitions in UCl4 anticipating melting, Acta Crystallogr. B. 43 (1987) 113–116. https://doi.org/10.1107/S0108768187098197.

[224] M.M. Popov, G.L. Gal'chenko, M.D. Senin, Specific Heats and Heats of Fusion of UCl4 and UI4 and Heat of Transformation of UI4, Russ. J. Inorg. Chem. 4 (1959) 560–562.

[225] I. Barin, Thermochemical Data of Pure Substances, Wiley, 1995. https://books.google.com/books?id=IUgpAAAAYAAJ.

[226] C.G. Maier, Sponge Chromium, U.S. Department of the Interior, Bureau of Mines, 1942.

[227] V.M. Vdovenko, V.A. Volkov, I.G. Suglobova, Complexing in systems of uranium halogenide-alkali metal halogenide, Radiokhimiya. 16 (1974) 363–368.

[228] J.W. Stout, R.C. Chisholm, Heat Capacity and Entropy of CuCl2 and CrCl2 from 11° to 300°K. Magnetic Ordering in Linear Chain Crystals, J. Chem. Phys. 36 (1962) 979–991. https://doi.org/10.1063/1.1732699.

[229] B.B. Ebbinghaus, Thermodynamics of gas phase chromium species: the chromium chlorides, oxychlorides, fluorides, oxyfluorides, hydroxides, oxyhydroxides, mixed oxyfluorochlorohydroxides, and volatility calculations in waste incineration processes, Combust. Flame. 101 (1995) 311–338. https://doi.org/10.1016/0010-2180(94)00215-E.

[230] E. Cordfunke, R. Konings, The Vapor-Pressure of UCl4, J. Chem. Thermodyn. 23 (1991) 1121–1124. https://doi.org/10.1016/S0021-9614(05)80142-9.

[231] C.T. Anderson, The Heat Capacities of Chromium, Chromic Oxide, Chromous Chloride and Chromic Chloride at Low Temperatures, J. Am. Chem. Soc. 59 (1937) 488–491. https://doi.org/10.1021/ja01282a019.

[232] NIST, NIST Chemistry WebBook, (n.d.). https://doi.org/10.18434/T4D303.

[233] H.A. Doerner, Chemistry of the Anhydrous Chlorides of Chromium: A Thermodynamic Investigation, U.S. Department of the Interior, Bureau of Mines, 1937.

[234] R.C. Schoonmaker, A.H. Friedman, R.F. Porter, Mass Spectrometric and Thermodynamic Study of Gaseous Transition Metal (II) Halides, J. Chem. Phys. 31 (1959) 1586–1589. https://doi.org/10.1063/1.1730656.

[235] J.C. Zhao, Methods for Phase Diagram Determination, Elsevier, 2007. https://doi.org/10.1016/B978-0-08-044629-5.X5000-9.

[236] H. Seifert, K. Klatyk, Das System Cscl/Crcl2, Naturwissenschaften. 49 (1962) 539-. https://doi.org/10.1007/BF00626806.

[237] V.N. Desyatnik, N.N. Kurbatov, S.P. Raspopin, Yu.F. Chervinskij, Phase diagrams of binary systems of uranium tetrachloride and alkali metal chlorides, Zhurnal Fiz. Khimii. 46 (1972) 2159.

[238] N.S. Martynova, Z.P. Kudryashova, I.V. Vasil'kova, ENTHALPY OF FORMATION OF K2UCl6, KUCl5, Na2UCl6, AND KNaUCl ., Energ USSR 25 226-7Sep 1968 Pap. No 229. (1970). https://www.osti.gov/biblio/4080352 (accessed July 27, 2021).

[239] J. Leitner, P. Voňka, D. Sedmidubský, P. Svoboda, Application of Neumann–Kopp rule for the estimation of heat capacity of mixed oxides, Thermochim. Acta. 497 (2010) 7–13. https://doi.org/10.1016/j.tca.2009.08.002.

[240] N.S. Martynova, I.V. Vasil'kova, M.P. Susarev, Thermographic investigation of UO2, UCl, and KCl ternary and binary systems, Sov. At. Energy. 18 (1965) 777–783. https://doi.org/10.1007/BF01115330.

[241] N.S. Martynova, I.V. Vasil'kova, M.P. Susarev, S.S. Tolkachev, Thermographic and X-ray Structural Study of the System UCl4-KCl-NaCl, Sov. At. Energy. 25 (1968) 1112–1113.

[242] O.B. Babushkina, S.V. Volkov, Raman spectroscopy of the heteronuclear complexes in the ZnCl2□CdCl2□Li,K/Cl and AlCl3□MgCl2□Li,K/Cl melts, J. Mol. Liq. 83 (1999) 131–140. https://doi.org/10.1016/S0167-7322(99)00080-X.

[243] J.R. Morrey, Fused Salt Spectrophotometry. IV. Uranium(IV) in Chloride Melts, Inorg. Chem. 2 (1963) 163–169. https://doi.org/10.1021/ic50005a042.

[244] O. Beneš, R.J.M. Konings, Thermodynamic study of LiF–BeF2–ZrF4–UF4 system, J. Alloys Compd. 452 (2008) 110–115. https://doi.org/10.1016/j.jallcom.2007.01.184.

[245] P.J. Tumidajski, S.N. Flengas, Potential Measurements of Reactive Metal Chlorides in Alkali Halide Solutions: II . Chromium, J. Electrochem. Soc. 138 (1991) 1659. https://doi.org/10.1149/1.2085850.

[246] H.J. Seifert, G. Thiel, Thermal analysis by EMF-measurements on solid electrolytes, J. Therm. Anal. Calorim. 25 (2005) 291–298. https://doi.org/10.1007/bf01912954.

[247] S. De Gryze, I. Langhans, M. Vandebroek, Using the correct intervals for prediction: A tutorial on tolerance intervals for ordinary least-squares regression, Chemom. Intell. Lab. Syst. 87 (2007) 147–154. https://doi.org/10.1016/j.chemolab.2007.03.002.

[248] G.N. Papatheodorou, O.J. Kleppa, Enthalpies of mixing in the liquid mixtures of the alkali chlorides with MnCl2, FeCl2 and CoCl2, J. Inorg. Nucl. Chem. 33 (1971) 1249–1278. https://doi.org/10.1016/0022-1902(71)80419-0.

[249] G.N. Papatheodorou, O.J. Kleppa, Enthalpies of Mixing of Some Binary Fused-Salt Mixtures Involving the Chlorides of Transition Metals, Calcium, Magnesium, and Cadmium, J. Chem. Phys. 51 (1969) 4624–4632. https://doi.org/10.1063/1.1671835.

[250] K.M. Sankar, P.M. Singh, Effect of Li metal addition on corrosion control of Hastelloy N and stainless steel 316H in molten LiF-NaF-KF, J. Nucl. Mater. 555 (2021) 153098. https://doi.org/10.1016/j.jnucmat.2021.153098.

[251] B. Li, S. Dai, D. Jiang, First-Principles Molecular Dynamics Simulations of UCln–NaCl (n = 3, 4) Molten Salts, ACS Appl. Energy Mater. 2 (2019) 2122–2128. https://doi.org/10.1021/acsaem.8b02157.

[252] L. Martinot, Thermodynamic properties of infinitely dilute solutions of UCl3 and UCl4 in the KCl-NaCl-MgCl2 (30: 20: 50) ternary eutectic, J. Common Met. 86 (1982) 203–210.

[253] M. Poulain, Glass formation in ionic systems, Nature. 293 (1981) 279–280. https://doi.org/10.1038/293279a0.

[254] C. Robelin, P. Chartrand, A.D. Pelton, Thermodynamic evaluation and optimization of the (NaCl+KCl+AlCl3) system, J. Chem. Thermodyn. 36 (2004) 683–699. https://doi.org/10.1016/j.jct.2004.04.011.

[255] A. Bogacz, B. Ziolek, Electrical Conductivities and Densities of Molten Salts in Systems Mcl-UCl4 (m=na, K, Rb, Cs), Rocz. Chem. 44 (1970) 665-.

[256] E. Renaud, C. Robelin, M. Heyrman, P. Chartrand, Thermodynamic evaluation and optimization of the (LiF+NaF+KF+MgF2+CaF2+SrF2) system, J. Chem. Thermodyn. 41 (2009) 666–682. https://doi.org/10.1016/j.jct.2008.12.013.

[257] J.P.S. Palma, R. Gong, B.J. Bocklund, R. Otis, M. Poschmann, M. Piro, Y. Wang, T.G. Levitskaia, S. Hu, H. Kim, S.-L. Shang, Z.-K. Liu, Thermodynamic modeling with uncertainty quantification using the modified quasichemical model in quadruplet approximation: Implementation into PyCalphad and ESPEI, arXiv, 2022. https://doi.org/10.48550/arXiv.2204.09111.

[258] M. Mirarabrazi, O. Stolarska, M. Smiglak, C. Robelin, Solid–liquid equilibria for a pyrrolidinium-based common-cation ternary ionic liquid system, and for a pyridinium-based ternary reciprocal ionic liquid system: an experimental study and a thermodynamic model, Phys. Chem. Chem. Phys. 20 (2018) 637–657. https://doi.org/10.1039/C7CP04678B.

[259] Y. Dutt, T. Ostvold, Emf measurements for the determination of partial gibbs energies and entropies of mixing of the alkali chlorides in liquid mixtures with CoCl2, Acta Chem. Scand. 26 (1972) 2743–2751.

[260] C. Robelin, P. Chartrand, A.D. Pelton, Thermodynamic evaluation and optimization of the (MgCl2+CaCl2+MnCl2+FeCl2+CoCl2+NiCl2) system, J. Chem. Thermodyn. 36 (2004) 793–808. https://doi.org/10.1016/j.jct.2004.05.004.

[261] T. Østvold, S.R. Johansson, J. Krogh-Moe, Ø. Ra, S. Svensson, Emf Measurements for the Determination of Partial Gibbs Energies and Entropies of Mixing of the Alkali Chlorides in Liquid Mixtures with MnCl2., Acta Chem. Scand. 26 (1972) 2788–2798. https://doi.org/10.3891/acta.chem.scand.26-2788.

APPENDIX A: JOINT FIRST-AUTHORSHIP MEMORANDUM

Memorandum

To: Graduate School, University of South Carolina

Through: Major professor, T. M. Besmann

From: Doctoral candidate, Jacob A. Yingling (B41398714)

We, the committee for doctoral of philosophy candidate Jacob A. Yingling, have received a request to review the enclosed publication titled, "Correlational Approach to Predict the Enthalpy of Mixing for Chloride Melt Systems" for approval to include in his dissertation. It is his original shared first co-authorship work, in which ideas fundamental to the development of thermodynamic models are thoroughly reviewed, expanded upon, and implemented in the course of research essential to the completion of his approved dissertation proposal. We recommend the graduate school approve Jacob's request to include this publication in his doctoral thesis.

Respectfully signed,

4/5/2022
Dr. T.M. Besmann (Major Professor)

4/5/2022
Dr. T.W. Knight (Member)

4/5/2022
Dr. Ming Hu (Member)

4/5/2022
Dr. J.W. McMurray (Outside Member)

APPENDIX B: PERMISSION TO REPRODUCE PUBLISHED MATERIALS

American Chemical Society

Authors may reuse all or part of the Submitted, Accepted or Published Work in a thesis or dissertation that the author writes and is required to submit to satisfy the criteria of degree-granting institutions. Such reuse is permitted subject to the ACS' "Ethical Guidelines to Publication of Chemical Research".

Journal of Chemical Thermodynamics and Journal of Molecular Liquids

Author rights in Elsevier's proprietary journals:
Use and share their works for scholarly purposes (with full acknowledgement of the original article):
1. In their own classroom teaching. Electronic and physical distribution of copies is permitted
2. If an author is speaking at a conference, they can present the article and distribute copies to the attendees
3. Distribute the article, including by email, to their students and to research colleagues who they know for their personal use
4. Share and publicize the article via Share Links, which offers 50 days' free access for anyone, without signup or registration
5. Include in a thesis or dissertation (provided this is not published commercially)
6. Share copies of their article privately as part of an invitation-only work group on commercial sites with which the publisher has a hosting agreement